UNIVERSITA' DI PISA

Dottorato di Ricerca in Ingegneria Industriale

Curriculum in Ingegneria Chimica e dei Materiali

Ciclo XXXIII – Anno 2020

Production of Ceramic Matrix Composites using non-conventional energy sources

Author

Roberto D'Ambrosio

Supervisors

Prof. Ing. Andrea Lazzeri

Dr. Giuseppe Annino

Coordinator of PhD program

Prof. Ing. Giovanni Mengali

Look up at the stars and not down at your feet.

Try to make sense of what you see,

and wonder about what makes the universe exist.

Be curious.

Stephen Hawking

Abstract

This PhD work investigates the use of a Microwave assisted Chemical Vapor Infiltration (MW-CVI) technology as a clean, economic and efficient solution for the production of Ceramic Matrix Composites (CMCs). CMCs combine reinforcing ceramic phases with a ceramic matrix to create materials with new and far superior properties which include high toughness, high-temperature stability, low density, high thermal shock resistance, high hardness, high corrosion resistance, and versatility in providing unique engineering solutions.

Key barriers to the broad application of CMCs include difficulty of processing, high cost, reliability, lack of specifications, databases, in-service repair methodology and scale-up. New and more efficient manufacturing technologies based on a widespread usage of renewable energy sources are needed in order to face the new challenges arising from the climate change emergency while being able to improve material quality, reduce processing time, converge towards near-net shape fabrication, trim energy spent and abate production costs.

Accordingly, the use of microwave radiation is a clean and attractive alternative thanks to its volumetric heating mechanism and is continuously gaining attention at the industrial level. The design of microwave-assisted reactors able to answer the demanding requests of industry as large scale productivity, homogeneous heating of relevant dimension samples, reproducible operating conditions and processing, requires a highly specific procedure where the main target is the achievement of the highest efficiency in the transfer of electromagnetic energy from the source to the material.

In the framework of this PhD an innovative approach has been developed to exploit the benefits of a microwave heating to produce silicon carbide based CMCs through a careful design of the reactor chamber heated by magnetron sources operating around the 2.45 GHz Industrial Scientific and Medical (ISM) frequency band. The procedure has been validated through rigorous numerical modelling using finite element method software COMSOL Multiphysics and experimentally performing several MW-CVI trials on different pilot scale preforms. Research activities have been carried out at an innovative pilot plant, built in the framework of the European HELM project, proving in particular the scalability and great potential of this technology.

Preface

Ceramic Matrix Composites were originally developed to overcome problems associated with the brittle nature of their monolithic ceramic counterparts while today they are increasingly being investigated to be tailored for customized purposes offering new possibilities and perspectives of application for energy-intensive industries, aerospace, automotive as well as power-generation systems.

As a recent category of materials, CMCs present a lot of challenges from many points of view regarding their processing, thermo-mechanical behaviour, innovative design and tailoring of specific properties, non-destructive evaluation and health monitoring, therefore they represent a current and very interesting topic for a young scientist.

Moreover, the use of a microwave-assisted heating requires a multidisciplinary approach to understand the relevant physical and chemical phenomena beneath, which gave me the possibility to achieve a diversified set of useful skills and methodologies.

In particular, a key factor for the success of a microwave assisted process is the adequate interaction among not only material engineers, but also process designers and microwave experts. Generally, commercial microwave systems are already available on the market, but the specific methodology required for their integration, tailored design of the applicator and process control in the material process of interest requires several preliminary considerations.

The research activities regarding this PhD work have been carried out at an innovative hybrid MW-CVI pilot plant, designed and developed in the framework of the European HELM project (FP7/2007-2013 under grant agreement no. 280464). This system has been developed thanks to the cooperation between material scientists, microwave experts both from academy and industry (SAIREM IBERICA SL - now BEMENS, Barcelona Electromagnetic Energy Solutions S.L. - Castellbisbal, Barcelona, Spain), and dedicated chemical plant designers (Archer Technicoat Ltd - ATL, Wycombe, England).

The starting point of the activities related to this PhD thesis was at the end of the HELM project, where I conducted first experimental trials on lab-scale preforms (50 mm diameter, 10 mm of thickness), noticing several critical points both regarding the MW heating and the chemical processing part. Regarding the heating technology, it was soon clear that a detailed knowledge of the electromagnetic behaviour of the overmoded resonant cavity was necessary in order to predict and tune the desired inverse temperature profile inside the preforms of interest as well as the scalability of this technology for bigger samples.

My activities were therefore first dedicated to a detailed understanding of the MW loaded cavity through modelling and experimental MW heating tests, aiming at optimize the energy efficiency in terms of power dissipated in the sample with respect to the walls and the sample-holder. One of the main achievements was the identification of the conditions in which the desired EM mode, having a relevant fraction of energy distributed in the sample (volume mode), can be efficiently excited with the available magnetrons. Following, the MW-CVI trials carried out on different pilot scale preforms (100 mm diameter, 10 mm of thickness) allowed to confirm the good control over the desired EM mode, resulting in a high source-applicator energy coupling and stability along different infiltration runs. These results confirmed some of the expected benefits regarding this technology as the inside-out infiltration mechanism with acceptable deposition

rates, potentially leading to a significant reduction of the processing times. In this framework, great attention was dedicated to the operating conditions granting the best results in terms of chemical efficiency while avoiding thermal degradation of the reinforcement with silica formation, due to plasma establishment using microwaves at low pressures. The latter points have been addressed proposing some optimization of the pilot plant to achieve a finer tuning and control of the operating parameters.

Table of contents

List of Figures

List of Tables

List of Abbreviations and Symbols

The acronyms employed along the thesis are reported below:

CMC	Ceramic Matrix Composite
SiC	Silicon Carbide
MW	Microwave
CVI	Chemical Vapor Infiltration
MW-CVI	Microwave assisted Chemical Vapor Infiltration
I-CVI	Isothermal Isobaric Chemical Vapor Infiltration
CVD	Chemical Vapor Deposition
C	Carbon
SiC	Silicon Carbide
ISM	Industrial, Scientific and Medical
EM	Electro-magnetic
PIP	Polymer Infiltration and Pyrolysis
RMI	Reactive Melt Infiltration
LSI	Liquid Silicon Infiltration
EBC	Environmental Barrier Coating
PyC	Pyrolytic carbon
MTS	Methyltrichlorosilane
PMC	Polymer Matrix Composite
MMC	Metal Matrix Composite
TEM	Transverse Electro Magnetic
TE	Transverse Electric
TM	Transverse Magnetic
FEM	Finite Element Method
S-parameters	Scattering parameters
VNA	Vector Network Analyzer

The mathematical quantities with their International System (SI) units are reported below:

E_f $[GPa]$	Fibre elastic modulus
E_m $[GPa]$	Matrix elastic modulus
ε_f^R [%]	Fibre failure strain
ε_m^R [%]	Matrix failure strain
λ $[m]$	Wavelength
ν $[Hz]$	Frequency
ω $[Hz]$	Angular frequency
H $\left[\frac{A}{m}\right]$	Magnetic field

$\boldsymbol{E}\ \left[\frac{\boldsymbol{V}}{\boldsymbol{m}}\right]$	Electric field
$\boldsymbol{\sigma}\ \left[\frac{\boldsymbol{S}}{\boldsymbol{m}}\right]$	Electrical conductivity
$\boldsymbol{\varepsilon}\ \left[\frac{\boldsymbol{F}}{\boldsymbol{m}}\right]$	Dielectric permittivity
$\boldsymbol{\varepsilon_0}\ \left[\frac{\boldsymbol{F}}{\boldsymbol{m}}\right]$	Dielectric permittivity of free space
$\boldsymbol{\mu_0}\ \left[\frac{\boldsymbol{H}}{\boldsymbol{m}}\right]$	Magnetic permeability of free space
$\boldsymbol{q}\ \left[\frac{\boldsymbol{C}}{\boldsymbol{m^3}}\right]$	Charge density
$\boldsymbol{D}\ \left[\frac{\boldsymbol{C}}{\boldsymbol{m^2}}\right]$	Electric induction field
$\boldsymbol{B}\ \left[\frac{\boldsymbol{T}}{\boldsymbol{m^2}}\right]$	Magnetic induction field
$\boldsymbol{J}\ \left[\frac{\boldsymbol{A}}{\boldsymbol{m^2}}\right]$	Free conduction current density
$\boldsymbol{\varepsilon'}\ \left[\frac{\boldsymbol{F}}{\boldsymbol{m}}\right]$	Relative dielectric constant
$\boldsymbol{\varepsilon''}\ \left[\frac{\boldsymbol{F}}{\boldsymbol{m}}\right]$	Dielectric loss factor
$\boldsymbol{\tan\delta}\ [\boldsymbol{1}]$	Loss tangent
$\boldsymbol{k}\ [\boldsymbol{1}]$	Propagation constant
$\boldsymbol{\beta}\ \left[\frac{\boldsymbol{rad}}{\boldsymbol{m}}\right]$	Phase constant
$\boldsymbol{\alpha}\ [\boldsymbol{m^{-1}}]$	Attenuation constant
$\boldsymbol{\delta}\ [\boldsymbol{m}]$	Penetration depth
$\boldsymbol{\rho}\ \left[\frac{\boldsymbol{\Omega}}{\boldsymbol{m}}\right]$	Electrical resistivity
$\boldsymbol{\zeta}\ [\boldsymbol{\Omega}]$	Characteristic impedance
$\boldsymbol{s}\ \left[\frac{\boldsymbol{W}}{\boldsymbol{m^2}}\right]$	Poynting vector
$\boldsymbol{d}\ \left[\frac{\boldsymbol{g}}{\boldsymbol{cm^3}}\right]$	Material density
$\boldsymbol{c_p}\ \left[\frac{\boldsymbol{J}}{\boldsymbol{kg*K}}\right]$	Specific heat
$\boldsymbol{k}\ \left[\frac{\boldsymbol{W}}{\boldsymbol{m^2*K}}\right]$	Thermal conductivity
$\boldsymbol{P_d}\ \left[\frac{\boldsymbol{W}}{\boldsymbol{m^3}}\right]$	Power loss density per unit volume
$\boldsymbol{P_{loss}}\ [\boldsymbol{W}]$	Power losses
$\boldsymbol{P_{conv}}\ [\boldsymbol{W}]$	Convective power losses
$\boldsymbol{P_h}\ [\boldsymbol{W}]$	Radiative power losses
$\boldsymbol{\epsilon}\ [\boldsymbol{1}]$	Emissivity
$\boldsymbol{\sigma_{SB}}\ \left[\frac{\boldsymbol{g}}{\boldsymbol{s^{-3}*K^{-4}}}\right]$	Stefan-Boltzmann constant
$\boldsymbol{h}\ \left[\frac{\boldsymbol{W}}{\boldsymbol{m^2*K}}\right]$	Mean heat transfer coefficient
$\boldsymbol{S_{11}}\ [\boldsymbol{dB}]$	Reflection coefficient
$\boldsymbol{S_{21}}\ [\boldsymbol{dB}]$	Transmission coefficient
$\boldsymbol{Q}\ [\boldsymbol{1}]$	Quality factor
$\boldsymbol{P_c}\ [\boldsymbol{W}]$	Cavity walls power dissipations
$\boldsymbol{P_s}\ [\boldsymbol{W}]$	Sample power dissipations

$\boldsymbol{Q_0}$ [1]	Unloaded quality factor
$\boldsymbol{Q_{ex}}$ [1]	External quality factor
$\boldsymbol{Q_L}$ [1]	Loaded quality factor
$\boldsymbol{c}$ $\left[\frac{\boldsymbol{m}}{\boldsymbol{s}}\right]$	Light speed in vacuum
$\boldsymbol{\eta}$ [1]	Electric energy filling factor
$\boldsymbol{V_{SiC}}$ $\left[\boldsymbol{s^{-1}}\right]$	Deposition rate

Chapter 1

1. Introduction

This Chapter aims to give a general introduction to the research activity focusing on different relevant aspects, clarifying background field and motivation. Particular attention will be dedicated to the building of the relationship between Ceramic Matrix Composites (CMCs) and Industrial Microwave Heating. The goal, inside this specific multidisciplinary environment, is to develop a connection among those two topics which will be increasingly reinforced and detailed along the thesis.

As for any other multidisciplinary field, in this case it becomes immediately evident that it is important not only to have a knowledge of the related material industrial process but also an understanding of the principles of microwave heating. Only thanks to the convergence between those two different cross-cultural fields it is possible to develop a successful application.

Accordingly, first an introduction on CMCs has been given, without entering on detail on their thermo-mechanical behaviour and manufacturing technologies, focusing on current main market applications followed by the barriers to their widened use and future research perspectives.

Next, some of the issues emerged from the short economic analysis performed previously will be addressed using microwave assisted technologies. Thus, a suitable introduction has been carried out focusing on industrial applications of microwaves and identifying the main issues and solutions.

A final short paragraph has been inserted on the main topic of this research activity, which is the usage of a MW-CVI process for CMCs production, highlighting the expected benefits and challenges that will be faced.

Finally, an overview of thesis structure has been provided including details on the participation to national and international conferences, papers, academic collaborations, and projects born during these three years of work.

1.1 Motivation

There is an increasing need in the twenty-first century to develop stronger, tougher and more chemically resistant structural materials in order to meet the challenges arising from the rapid increase in demanding requirements across a wide and diverse range of applications, from construction to transportation, health to energy [1].

In 2018 the European Commission set the strategy "A Clean Planet for all", a long-term vision for a European climate neutral economy [2]. In December 2019 the European Green Deal (COM (2019) 640) was published, setting new ambitious priorities and aiming at Europe to become the first climate-neutral continent by 2050. Considerable effort is being made towards reaching this objective, such as research and innovation on technologies that will allow an intense exploitation of renewable energy, improvement of energy efficiency and development of clean, new low-carbon technologies.

Novel materials able to sustain variable and harsh conditions (high temperature, corrosive environments, etc.) are needed to optimise the shift to renewable energy sources and, at the same time, guarantee high-energy efficiency and high-performance.

Ceramic Matrix Composites (CMCs) represent one of the latest and most promising solutions for high temperature applications in strategic industrial sectors, such as transport and energy. Specifically, CMCs are a class of materials that show considerable promise providing fracture-toughness values like the one needed for metals such as cast iron. They display the distinguishable property of being as strong as metal yet are lighter and can withstand higher temperatures.

For those reasons, CMCs are also designed to substitute refractory metals and other materials in high temperature applications. Excellent structural performance, high thermal shock resistance, low thermal conductivity and density make their design and functional configuration suitable for several applications in severe environments. Moreover, erosion and oxidation resistance provided at high temperatures and improved, due to the use of specifically designed environmental barrier coatings (EBC), are only some of the added features of CMCs.

Much development work has been done on non-oxide CMCs [3], particularly carbon (C) or silicon carbide (SiC) fibre-reinforced SiC-based materials (SiC_f/SiC, C_f/SiC and C_f/C-SiC composites). This is because non-oxide CMCs have attractive high temperature properties, such as creep resistance, microstructural stability and excellent thermal stress resistance due to their high thermal conductivity and low thermal expansion.

Depending on the different methods for developing the C or SiC-matrix, the resulting SiC_f/SiC, C_f/C, C_f/SiC and C_f/C-SiC materials present different properties and manufacturing costs. Specifically, among all infiltration techniques, the Chemical Vapor Infiltration (CVI) best meets the quality requirements for the industrial production of CMCs [4–6].

However, the potential for this type of materials is still hindered by several factors such as: high cost, difficulty of processing and materials reliability. Thus, this calls for major research efforts to develop adequate industrial solutions and novel manufacturing processes for CMCs that can lead to significant reduction of the processing times, possibly continuous manufacturing processes and near to net-shaped products. In addition, improved control of temperature and thermal gradients can deliver renewed material microstructures and morphologies with enhanced technical performance and/or creation of unexpected new features. Moreover, a better

release of heating energy will lead to subsequent reduction of losses and will enable moving towards more sustainable manufacturing industry while reducing environmental impacts [7].

Non-conventional energy sources, such as microwave (MW), plasma, ultra-sound and laser, as well as electrochemical and photochemical processes, have already proved their high potential for process intensification thanks to the benefits obtained in terms of energy efficiency. The processes powered by non-conventional energy sources are suitable for connection to the electricity grid. They allow variable throughputs to better follow market demand and enable leaner production paradigms (e.g. decreased stock, production on demand). Such technologies are suitable for downscaling and continuous processing, where they can also be coupled with real time monitoring allowing a finer control of the process.

Specifically, processing materials using high-frequency electromagnetic (EM) fields, such as microwave (MW), presents great possibilities from an industrial point of view. In fact, between the most common goals of any new manufacturing process, there are the reduction of processing time as well as energy consumption and the improvement of material properties. Different attempts have been made in order to broaden the range of application of MW energy, especially as an alternative heat source for materials manufacturing [8].

Currently, industrial MW heating applications have mainly remained restricted to low temperature materials processes (e.g. food, wood, rubber, plasma). In the latest years a raising interest was developed for high-temperature MW materials processing applications [9]. The latter, involving several energy intensive processes, are among the segments that could benefit more of a MW assisted heating, thus it represents a "non-conventional" and increasingly popular research field [10].

The eco-friendliness of MW processing, in comparison to the standard techniques in which the entire chamber is heated to the temperature at which the processes occur, derives from the important energy savings thanks to the selective and volumetric heat of the material. In addition to the much lower thermal mass to be heated, the MW fields-assisted processes represent a cleaner, faster, and more efficient approach, whose speed is limited only by the available MW power.

The major difficulty preventing wide industrial application of EM-assisted techniques mainly include the lack of proper design methods of MW-assisted reactors that can effectively reproduce the processing of large samples. Moreover, this is exacerbated by the limited and approximated knowledge of the dielectric properties at the operating conditions of interest.

Thus, this PhD work aims to contribute to the development of sustainable and economic production of SiC-based CMCs of industrial interest by means of a MW-CVI process using magnetron sources operating around 2.45 GHz. A specific methodology has been developed to allow the scale up of this technology while keeping the highest energy efficiency. It describes the design of a new hybrid conventional/MW-assisted pilot plant, built in the framework of the European HELM project [11], by using an innovative approach to achieve a reproducible heating pattern and infiltration of relatively large scale samples, in view of further industrial scale-up of this technology.

1.2 Ceramic Matrix Composites: Markets and Future perspectives

CMCs combine reinforcing ceramic phases with a ceramic matrix to create materials with new and superior properties. Their intrinsic ability to be tailored as composites make CMCs highly attractive in a vast array of applications, most notably internal engine components, exhaust systems and other "hot-zone" structures, where CMCs are envisioned as lightweight replacements for metallic superalloys. For those reasons they are primarily used in the aerospace, defense and automotive industries. However, the product is still in the nascent phase in energy and power industries as well as electrical and electronic sectors.

The global CMCs market was valued at US$ 4,857.6 million in 2018 and is projected to reach US$ 11,516.1 million by 2026, growing at a CAGR of 11.4% from 2019 to 2026 [12]. The major factors that are expected to be driving CMCs market are tighter government regulations concerning fuel efficiency, high demand from aerospace, defense, automotive, energy and power end-use industries.

1.2.1. Main market applications

The applications of CMCs are on the rise in the aerospace industry. In fact, the demand for CMCs is expected to increase tenfold over the next decade, according to jet engine and aircraft systems manufacturer GE Aviation[1] (Newark, Del.). GE made its intentions clear regarding CMCs when it announced plans to build a $125 million, 125,000-ft^2 (11,613 m^2) manufacturing plant in Asheville, N.C., to produce CMC engine components [13,14].

Specifically, thanks to their high-temperature resistance (up to 1316°C) and reduced weight (one-third the weight of nickel superalloys) SiC-based CMCs became increasingly more attractive to engine manufacturers that are looking for weight reduction in engine hot zones in pursuit of greater fuel efficiency, making them as the largest product segment in terms of demand (accounted for 35.24% of market share by volume in 2018), as shown in **Figure 1.1**.

First applications into the aerospace sector date back to the birth of CMCs with the development of C$_f$/C segment during 1960s [15–17], which were originally customised for military uses as rocket nozzles and re-entry parts for missiles due to their high cost [18,19]. R&D activities related to C$_f$/C were initially aimed at improving the reliability and performance of solid propellant rocket nozzles [20]. Nowadays, C$_f$/C are considered high-performance engineering materials with several high-temperature applications under inert gas or vacuum atmospheres as hot pressing dies, heating elements, high-temperature fasteners, liners and protection tubes [21], although the biggest market share is dedicated to military and civil aircraft brakes.

[1] https://www.geaviation.com/

***Figure 1.1** - CMCs main market segments* [12]

The development of carbon fibre reinforced SiC composites, as C_f/SiC materials started during 1970s, being also mainly driven by aerospace applications, which still remain one of the main application fields for these materials. Their high temperature and thermal shock stability coupled with the high abrasive resistance was exploited for the development of lightweight hot structures as thermal protection systems (TPS) of reusable spacecraft (nose caps, wing-leading edges). Regarding aeronautic applications, C_f/SiC nozzle flaps production started in 1996 for the Snecma (today Safran[2], after a joint-venture with Sagem in 2005) M88-2 jet engine to be used in the Rafale military aircraft [22]. The so-called "Sepcarbinox" outer flaps for military aircraft propulsion devices allowed a total weight saving of 40%, overcoming the typical drawbacks of Inconel 718 pendants as the reduced creep resistance and excessive cracking [20].

The appealing high-temperature properties of CMCs attracted also the attention of NASA for space vehicles applications [23]. A pair of body flaps made entirely of coated high performance ceramic composite and joined with C_f/SiC screws, were manufactured for NASA's X-38 experimental re-entry vehicle V201 [24]. The body flaps were developed within the framework of the German space program TETRA. This vehicle was built as a prototype of the Crew Return Vehicle, the "lifeboat" for the International Space Station.

Today's high-efficiency jet engines emit hotter exhaust gas — hot enough to exceed the limits of traditional materials, such as titanium and conventional superalloys. In jet engine propulsion history, the average rate of technology progress for turbine engine material temperature capability has increased 10°C per decade, according to GE. However, with the introduction of CMCs, GE believes that actual material temperature capability will increase by 66°C in this decade alone [25].

In 2016 LEAP[3] (Leading Edge Aviation Propulsion), a new aircraft engine, became the first widely deployed CMC-containing product, produced by CFM International, a 50/50 joint venture of Safran and GE [26,27]. The engine has one CMC component, a turbine shroud lining in its hottest zone, so it can operate at up to 1316°C. Additionally, CMCs needs less cooling air than nickel-based super-alloys and is part of a suite of technologies that contribute to 15 percent fuel savings over its predecessor, the CFM 56 engine. More recently, in 2019 GE produced the GE9X engine with five CMC parts - two combustor liners, two nozzles, one shroud.

[2] https://www.safran-aircraft-engines.com/
[3] https://www.cfmaeroengines.com/engines/

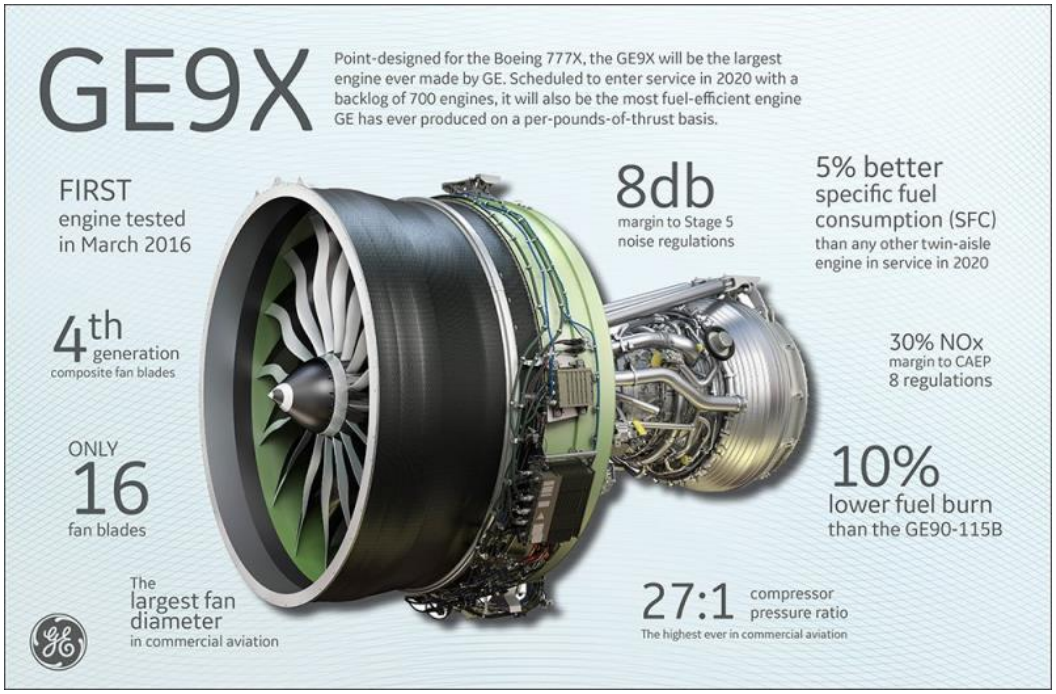

Figure 1.2 *– Advancements achieved with GE9X engine* [28]

As for aerospace applications, gas turbine engine for industrial power generation leverage the higher CMCs operating temperatures with reduced need of cooling air, thus enabling superior fuel efficiency and reduced harmful emissions. Great research efforts have been dedicated to this application based on the experience gained on military engines. SiC- and oxide-based CMCs combustor liners have been evaluated mainly under US government sponsored programs and led by industrial consortiums as Solar Turbines, Inc.[4] and General Electric Power Systems[5].

Solar Turbines, Inc. tested CMC combustor liners in test rigs and their Solar Centaur 50S engines since 1992, accumulating over 67000 hours of field test experience, to replace respectively Hastelloy X components. Specific EBC (mainly based on barium strontium alumina-silicate, BSAS, and mullite) have been developed to improve oxidation resistance of SiC_f/SiC thus resulting in an extended in-service life by a factor of 2-3 [29]. Additional fuel saving possibilities were investigated through the development of CMC turbine shrouds. GE successfully tested SiC_f/SiC turbine shrouds on its 7FA advanced gas turbine (~170 *MW* in combined cycle) [30].

Aircraft brakes are another important CMCs market segment. Those are key components for aircraft landing and take-off safely, which must perform as friction parts to generate the required stopping torque under various service environmental conditions, as heat sinks to absorb the kinetic energy of the aircraft while keeping lower temperatures, and as structural elements to transfer torque to the tyres. Therefore, the trend in the development of brake materials always focus for higher energy absorptions and brake temperatures may be higher than that could be burdened by traditional materials (organic and steel brake materials).

Compared to steel brakes, C_f/C composites display 2,5 times higher heating capacities, low densities thus enabling weight savings of about 40% and doubling service life. Due to these characteristics during the 1990s, 63% by volume of C_f/C composites produced were employed

[4] https://www.solarturbines.com/en_US/index.html
[5] https://www.ge.com/power/gas/gas-turbines

into aircraft brakes [15]. Their manufacturing process was first licensed by Dunlop[6] in 1970 and employed on the now defunct Concorde supersonic aircraft while today, due to the various technological improvements, are largely applied to several civilian airplanes as the Boeing 747 and C-17 Globe Master III [31]. Several aircraft brakes manufacturing leaders are present on the market as Safran Landing Systems[7], Meggitt Aircraft Braking System[8], Avcorp[9], UTC Aerospace Systems (currently Collins Aerospace[10] after a joint-venture with Rockwell Collins), Honeywell Aerospace[11] and other asian companies.

Modern aircraft brake systems are based on a mechanically closed system consisting in an assembly of static and rotating discs pressed together by a set of hydraulical cylinders at high pressures [31]. The main drawback of C-based materials is the reduced oxidation resistance above 400°C, restricting their use to short time applications or to non-oxidative environments in the absence of a proper protective surface treatment [32,33].

As for C_f/C materials, an important milestone for carbon fibre reinforced SiC composites was their application as high-performance friction systems into the automotive sector. Currently C_f/C represent the state of the art of brake systems for aircrafts as well as racing cars (Formula 1, the 24 Hours of Le Mans racing series) [15], while C_f/SiC brake discs for luxury cars have been successfully commercialised due to their excellent properties such as high and stable friction coefficient, long life and lower sensibility to surroundings and oxidation [34]. Starting from 2009, Brembo SGL Carbon Ceramic Brakes[12] (BSCCB) became the leading producer of carbo-ceramic brake discs and supplies their products for the most exclusive models.

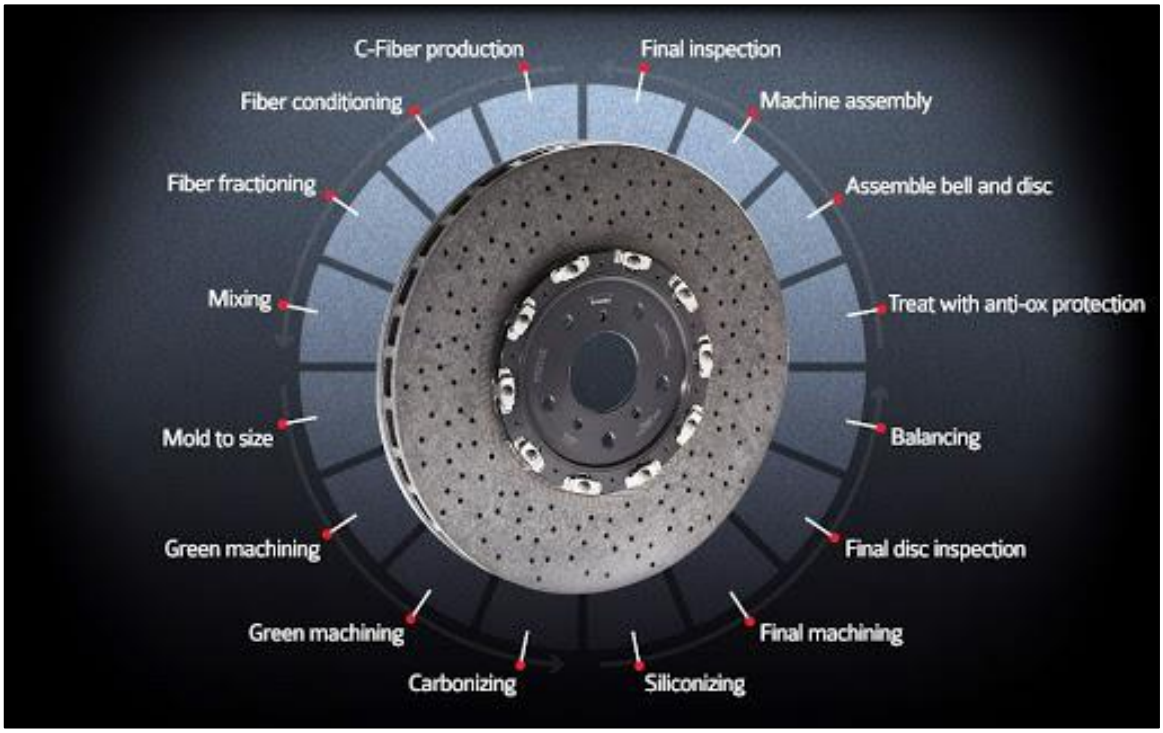

Figure 1.3 *– Production steps of a carbo-ceramic composite brake* [35]

[6] https://www.dunloptires.com/
[7] https://www.safran-landing-systems.com/
[8] https://www.meggitt-mabs.com/
[9] https://www.avcorp.com/2015-07-19-hitco
[10] https://www.collinsaerospace.com/who-we-are/about-us
[11] https://aerospace.honeywell.com/en
[12] http://www.carbonceramicbrakes.com/it/Pages/default.aspx

Some of the constraints discussed are shared also in other fields such as the nuclear one. In this case, besides high operating temperature, resistance under oxidizing and weakly oxidizing conditions and high temperature mechanical strength, there are additional constraints such as the effects of irradiation and containment of radioactive substances.

Currently CMCs are mainly under consideration for use as a cladding material (providing fuel containment and heat exchange) or as structural material, for both fission and fusion reactors [36,37]. High levels of safety as well as long and costly qualification phases are required in nuclear industry which leads to severe and precise choices for the materials employed [38,39]. Thanks to the introduction of the "third generation" SiC fibres [36], various applications have been developed in fission reactors [40].

In the case of fusion reactors, CMCs are under consideration as plasma-facing components (PFCs), both as complete structures and components and would therefore be exposed to both a high heat flux and high energy (14.1 MeV) neutron flux.

SiC_f/SiC composites are the most promising for use in nuclear reactors. In particular, they provide better resistance under neutron flux, even under high doses (>40 dpa) [41] and display better high temperature resistance under weakly oxidizing and oxidizing conditions than C_f/C composites. However, to be compatible with such applications, new concepts need to be developed and the most suitable manufacturing processes chosen.

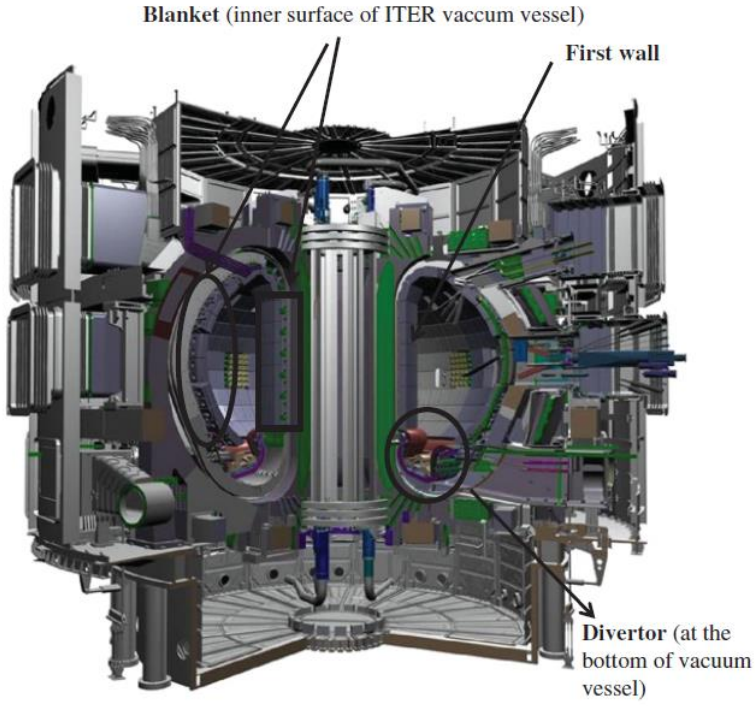

Figure 1.4 *- Schematic illustration of ITER with localization of plasma-facing components* [42]

Meanwhile, significant research into C_f/SiC CMCs is yielding promising materials for hard-use applications, where strength, durability and ductility are every bit as important as heat management. For example, Lancer purchased CeraComp, a C_f/SiC composite developed by Greene, Tweed[13] (Kulpsville, Pa.). This company is now expanding CMCs into the oil and gas, chemical processing and power generation industries.

[13] https://www.gtweed.com/

CeraComp was designed for greater fracture toughness, similar corrosion protection, and wear characteristics equivalent to, monolithic SiC ceramics used in sleeve bearings in magnetic coupled pumps [43]. SiC bearings for stationary and rotating components in pumps have been widely employed from several pump manufacturers for decades. Due to its susceptibility to thermal and mechanical shock fracture, CeraComp was developed as a high-pressure, high-temperature CMC bearing to improve their lifetime. Those bearings are currently undergoing field tests.

1.2.2. Issues and future developments of CMCs

The cost of CMCs has proven to be the main barrier to their spread over the past decade. Mainly the prices of these materials are controlled by two factors: the high cost related to the ceramic fibres and manufacturing processes of the matrix [44]. As was observed for carbon fibres, an increased market demand and subsequent mass production is necessary to significantly reduce ceramic fibres cost.

Especially in the case of SiC and alumina (Al_2O_3), production volumes are too small and the few market leaders, mostly located in East Asia and North America, demand for too high prices. Recently, due to the interest in the development of a European market of SiC fibres, German BJS Ceramics[14] company won an important EU funding for the scale-up of their patented "Silafil" SiC fibre production process to a commercial stage [45].

Regarding matrix manufacturing routes, they usually require expensive batch processes at high temperatures in controlled atmosphere. In addition, finished components require additional processing costs, as well as numerous inspection steps if the component is to be used commercially or where the risk of failure can endanger life. For these reasons many industries consider CMCs just for a limited number of applications with high added value. This high cost represents an important obstacle to the further growth of CMCs market.

The large-scale production of components with simple geometries, such as plates and tubes, would help to eliminate the manual steps involved in the processing. Joining techniques remain a critical tool for reducing assembly time, cost and excessive use of materials. Japan and the USA have intensive activity on joining and testing of dissimilar materials; the Joining and Welding Research Institute[15] in Japan, Pacific Northwest National Laboratory[16] and NASA Glenn Research Center[17] in USA are specialized in joining technologies and testing of advanced materials.

If the issues related to joining CMCs to themselves and to dissimilar materials are solved, they will be much more extensively used to produce both new components and 'hybrid' structures, the latter constructed of two or more different types of materials where each one contributes with its own unique properties complementing the properties of the other(s) [46].

Some of the manufacturers are using computer-based design tools for new components. The standardization of CMCs using simple shapes and computer-based design will be another important tool for the rapid growth of those material markets [1].

---

[14] https://www.bjsceramics.com/
[15] http://www.jwri.osaka-u.ac.jp/en/index_e.jsp
[16] https://www.pnnl.gov/
[17] https://www.nasa.gov/centers/glenn/home/index.html

CMCs can degrade through different kinds of mechanisms: transverse matrix microcracks, interlaminar cracks or delamination, oxidation ingress, oxidation/corrosion recession, fibre breakage, unbridged crack growth, and so on. Moreover, the flaw-sensitive nature of CMCs results in the necessity of understanding composite damage development which can lead to different end of life scenarios. Non-destructive evaluation (NDE) and in-situ health-monitoring techniques are then other important ways to improve the reliability of CMCs resulting in their safer and broadened use [47].

A plethora of CMCs development programs abound worldwide; some of them reached the commercial application while others are still under development. The introduction of a new material in a well-consolidated application meets always several difficulties. When customers consider the high cost and increased time associated with CMCs production, their adoption will consequently slow down.

For these reasons, it is of fundamental importance researching on new manufacturing technologies that can reduce processing time leading to the opening of a greater number of applications.

1.3 Industrial Microwave Heating

Processing of materials using high-frequency EM fields, such as MW and radiofrequency (RF), is gaining more and more attention at the industrial level [48]. Its potential in heating applications has been known and exploited since the early '50s, when the first MW ovens were introduced to the marketplace by Raytheon [49,50]. Since then, many different attempts have been made in order to broaden the range of application of MW energy, especially as an alternative heat source for materials processing.

In the early stages of the evolution of MW-heating the well-known advantages were often difficult to justify against the relative cheapness of fossil fuel heat. Certain countries with reduced fossil fuel sources were instead committed to electricity from hydroelectric or nuclear sources and consequently manufacturing firms tended to select electrical methods, which gives wider opportunities for MW techniques.

However, despite some low-temperature processing applications (e.g. food, wood, rubber, polymers) have achieved industrial maturity in the '80s and are now considered as standard production methods, MW processing has mainly remained restricted to laboratory-scale research as far as most classes of materials are concerned, in particular for high-temperature applications [9]. The use of MW heating in industrial material processes can provide a versatile tool to treat several different categories of materials under a wide range of conditions. Successful applications of MW regard sintering of metals and ceramic powders [51], joining [52], waste processing [53], chemical or electrochemical reactor systems [54], composites technology [55].

Microwaves generate higher power densities, enabling increased production speeds and decreased production costs with the possibility to achieve unique and/or superior properties. However, the widespread application of MW energy has encountered many barriers through years. Some examples are the reduced databases of dielectric properties in the MW range as a function of temperature, the limited presence of industrial equipment for large scale high-temperature manufacturing as well as the reluctance for material manufacturers to change from a proven technology.

Industrial MW heating systems operate within the Industrial, Scientific, and Medical (ISM) frequency bands set aside by the Federal Communications Commission (FCC) for industrial applications, such as around 915 MHz and 2450 MHz, to prevent interference with other frequency bands. The increasing interest of MW energy for industrial applications as heating, drying, pasteurization, sintering, led to the crescent need for in-line design methodologies of specialty applicators.

Single-mode cavities provide high power densities and therefore rapid heat-up rates but, their reduced dimensions (half of the wavelength at the operating frequency) and strict frequency tuning requirements around the narrow ISM bands, are of limited interest for industrial applications. Accordingly, multi-mode cavities, having dimensions of several wavelengths, are the most used at industrial level both for low and high-power applications but, paradoxically, are also the most complex systems to be designed [48].

Being a complex multidisciplinary field, MW processing involves different kinds of topics as EM equipment design, MW materials interaction, dielectric properties measurement, where each one is strongly interconnected with the other. A high degree of technical knowledge is required for determining how, when and where to use MW most effectively.

1.3.1. Market analysis and industrial applications

The global industrial MW heating equipment market size was valued at US$ 890.2 million in 2016. Escalating demand in numerous end-use industries such as paper, food, plastic, wood and derivatives and chemical is projected to boost the market over the forecast period [56]. The market is expected to witness significant growth, which can be attributed to the numerous benefits offered by these products. For instance, selective heating minimizes over-processing, overheating, promotes a pollution-free environment as there are no byproducts of combustion, and provides instantaneous heating control [57].

Increased industrialization and stringent government regulations are expected to boost the industrial MW heating equipment market. Other driving factors include lower maintenance costs, higher operating efficiency, and reduced power consumption. However, increasing prices of electricity could hamper the growth of the market. Moreover, the increasing requirement for even heating while increasing production speeds and reducing production costs drives the demand for these systems.

The industrial MW heating equipment market can be currently segmented into two product categories, namely magnetrons and RF solid state amplifiers. Magnetrons are high-powered vacuum tubes that create energy through interacting electrons in a magnetic field. As magnetrons penetrate an object, the electric dipole molecules rotate and bump into other molecules to align themselves with the alternating electric field, thereby producing heat. The electric dipole molecules in salted liquids react the most, and are therefore more heated, which is one of the main reasons why the typical magnetron-powered MW may produce food with uneven hot and cold spots.

Different kinds of RF power sources are commonly employed to feed cavities which are distinguished depending on the operating frequency range and the required unitary power level. Due to the request of high frequency and phase stability these sources are normally based on amplifiers, which have the function to convert available energy into RF output power whose amplitude and phase is determined by the low-level RF input power [58].

Historically RF power amplifiers for high power applications employed vacuum tube technology, using d.c. voltages from several kilovolts to hundreds of megavolts depending on the type of tube, power level and the frequency. In particular, starting from 1940s, magnetron sources (which are intrinsically oscillators rather than amplifiers) have been the preferred choice to generate microwaves at high RF power levels in the frequency range 1 GHz – 10 GHz for radar and MW oven applications [59].

Modern RF power amplifiers instead use solid-state devices, particularly LDMOS (laterally-diffused metal-oxide semiconductor) transistors due to their superior performance. RF solid state amplifiers are still limited to low power applications but are envisioned to replace magnetron sources in the near future thanks to their reduced form factor, low operating voltage and in particular the ability to precisely control phase and frequency achieving better heat distribution [60].

A potential major trend in MW industrial technology is the insertion of solid-state sources on the market due to its important advantages related to frequency and phase variability and control, low input-voltage requirements, compactness and rigidity, reliability as well as better compatibility with other electronic circuitry, enabling greater efficiency and control than currently possible with conventional magnetrons [61].

Recent studies showed that magnetrons could be replaced by RF solid-state amplifiers over the forecast period, owing to several benefits offered by the latter. As a result, even though the magnetron segment captured the largest market share in 2016, it is anticipated to grow at a slower rate owing to factors such as uneven heating, drop in quality of end-product, limited shelf life, residual temperature differences and slow heat transfer. Moreover, the product has undergone several technological advancements over the past few years, which has led to its increased demand [62].

The Europe Industrial Microwave Heating market generated the highest revenue in 2017 and is expected to lead the global market throughout the forecast period. The European market is expected to witness steady growth over the forecast period, registering a CAGR of over 6.0% [56]. This can be attributed to rapid industrialization and favorable government regulations for the usage of MW/RF equipment for industrial processing. Europe, being a technology-driven nation, is anticipated to adopt RF solid-state amplifiers at a faster pace. The global market includes large-scale and small-scale industrial microwave heating equipment manufacturers.

Key market players focus on inorganic growth strategies, such as joint ventures and mergers and acquisitions, to sustain the competition and capture a larger market share. These companies launch new products and collaborate with other market leaders to meet the increasing needs and requirements of consumers.

In the last decades several industrial applications raised interest on the market taking full advantage of the unique mechanism of MW heating, while other applications are still in a prototype industrial stage or under laboratory work. Specifically, some of those applications were successfully scaled up developing MW heating systems up to 100 kW. Nevertheless, the ultimate power levels required cannot be used as a good discriminant between different processes since a laboratory scale process could require powers higher than those of a pilot scale one, depending on the final application.

One of the well-known and most successful industrial application of MW regards food industry, where power consumption and material processing are the key operating parameters toward minimization of the process cost. Microwave heating/drying systems uses only a small percentage of the energy required by other comparable systems per liter of water evaporated from the processed material with reduced thermal processing time.

Figure 1.5 *- Industrial Microwave Tunnel Conveyor Machine developed by Max Industrial Microwave* [63]

The baking industry was one of the first successful food industry sectors where a combination of MW energy and deep frying, used for proving doughnuts raised with yeast, leaded to unique quality results with 15% reduction in ingredients and 20% increase of market sales, transforming a clumsy batch process into an efficient continuous one [64].

MW drying is another well-established industrial application employed in several fields as chemical, ceramic, pharmaceutical and biotech industries. Quick drying of active pharmaceutical ingredients (API) at low temperatures is achieved thanks to MW freeze drying devices. Additionally, the use of MW flow heaters for pasteurization in the food industry or sterilization in the pharmaceutical industry resulted as well in important energy savings using more compact units, environmentally friendly processes and obtaining high-quality products.

Figure 1.6 *– Microwave drying system developed by Püschner Microwave Power Systems* [65]

Industrial MW drying has established itself in recent years also in production processes of technical ceramics. The conventional drying process with hot air caused too high costs for the required moulds and took too long to prevent cracking and inhomogeneous surfaces, while the use of MW drying significantly reduces the number of moulds required and the total drying time.

Figure 1.7 *- Microwave hybrid continuous dryer for fast and homogeneous drying of technical ceramics developed by Fricke und Mallah Microwave Technology* [66]

Rubber vulcanization was one of the first successful MW industrial applications which, together with the food segment, covered more than 90% of the market up to 1980s [67]. For rubber manufacturers, vulcanization is a very critical process as it gives the strength and durability that is required for any application. Due to its low thermal conductivity, long curing times are required for rubber vulcanization using conventional ovens while, the application of MW energy, led to a quick and uniform heating significantly shortening processing times. Kerone's[18] Microwave based vulcanization systems have proven their superior efficiency with respect to conventional hot air heating processes.

[18] http://www.kerone.com/microwave-heating-for-rubber.php

High-power MW plasma processing is another raising industrial application that offers great benefits to produce several kinds of materials, including semiconductor wafers. MW plasma processing has been employed in semiconductor manufacturing for such operations as material deposition, etching and photoresist removal. It allows dry etching of photoresist materials at high etch rates and with no ionic damage to the material samples [68]. Moreover, non-oxide ceramic materials such as silicon nitride and tungsten carbide have been fabricated at sintering temperatures to 1700 °C with fine-detail, high-quality microstructures using MW plasma ovens. Muegge Gmbh[19] is the leading international manufacturer and supplier of Microwave Power Systems for advanced Industrial Microwave Heating and Plasma–Applications.

From the above described applications, it is worth noticing that usual preliminary considerations to be made, before the purchase of any industrial MW system, regards energy savings, increased throughput, improved quality for the materials produced as well as high compactness, which strongly reduces space requirements using lighter equipment with respect to conventional one employed.

Especially for those processes where energy will be the major voice of cost, the shift to a MW heated system is likely to become much faster. The widespread diffusion of MW equipment could be another important factor leading to the reduction in their purchase prices.

1.3.2. Issues and Future perspectives

Industrial MW heating systems are powerful devices that can provide important advantages related to new ways to treat materials or improve their properties. However, the complexity of MW interactions with materials requires different skills and competences to guarantee the achievement of the most efficient application.

MW present some distinctive characteristics with respect to other conventional processing technologies:

- Rapid heating;
- Reversed thermal gradients;
- Controllable electric field distribution;
- Selective heating of materials through differential absorption;
- Self-limiting reactions;

Each one of those properties, considered singularly or in combination, gives important benefits and opportunities for treating a large variety of materials including ceramics, polymers, rubbers and composites. The different MW absorption properties of materials leads also to different approaches to be able of properly process them.

The development of a hybrid heated system represents another promising area of research that could be required for the full realization of the expected MW heating benefits.

In order to realize the full potential of MW much research efforts are needed to develop methodologies allowing process scale-up to large batch or preferentially continuous routes. Currently, most of the research activities on high temperature MW processing of materials have been dealt on a laboratory scale due to unfavourable bias and preconceptions, since the interaction between the electrical field and the matter may cause some unbeneficial effects such

[19] https://www.muegge.de/en/

as thermal runaway, cut-off phenomena or heterogeneous heating but also due to the limited knowledge of the basic principles and the potential of MW heating in the industrial sector.

An interesting approach which is always more employed for a quick and efficient MW system design is the use of numerical techniques. Provided to have a precise knowledge of the dependence of dielectric and thermal properties with temperature and other operating parameters, computer modelling can be used to optimize applicator design, determine the best operating conditions for the specific sample dimension and geometry desired.

The current high cost for MW generators requires that also other factors need to be considered to justify their use, namely process time savings, increased process yield and environmental compatibility, making the future of MW applications particularly significant for specialty applications where its usage is not simply limited to the production of process heat.

1.4 MW-CVI processing of CMCs

Specialty applications, as the CVI of CMCs, is a highly promising candidate that can take full advantage of the unique characteristics of microwaves for future production scale applications [69]. The main advantages of conventional CVI techniques are the possibility to manufacture complex near-net-shape components at relatively low temperatures and pressures, deposition of a stoichiometric matrix with fine control of the related microstructure, leading to the best combination in terms of thermo-mechanical properties with respect to other common CMCs manufacturing routes. Despite of those advantages, the long manufacturing times (of the order of several weeks) and the run-to-run reproducibility severely limits the usage of this technology [4].

The main solutions currently derived to overcome those issues generally are based on the application of systems developing temperature or pressure gradients in the preform to be infiltrated to reduce processing times thus increasing mass transport. Each one of these solutions requires the addition of complex devices for temperature and flow control which further increase the capital equipment cost, making the scale-up difficult [6,70].

In this PhD work, the above cited drawbacks have been addressed using a MW-assisted CVI (MW-CVI) process exploiting benefits like the inverse temperature profile as well as the fast and selective heating mechanism, to achieve a clean and efficient solution for the sustainable production of CMCs. Well-known CVI issues, as the premature pore closure due to crusting, is completely avoided allowing densification to occur an order of magnitude faster with an inside-out densification pattern, particularly suited for the manufacturing of CMCs using infiltration techniques.

Nevertheless, the use of a MW heating generally leads to additional problems and challenges for the effective processing of materials [55]. Inadequate design of MW heated cavities usually results from the lack of knowledge of the dielectric properties with temperature and processing state of the treated materials, inappropriate MW systems (generators, applicators, transmission lines, coupling devices) choice and their integration applied to the specific manufacturing process.

A general trend in the development of new industrial MW systems is the achievement of the highest power density [71]. The use of a high-quality overmoded resonant cavity provides an interesting solution to reach this goal, provided to design the MW heated reactor being able of properly heating the desired large scale samples along the whole manufacturing process while keeping the highest energy efficiency, thus reducing dissipations in other components rather than in the sample.

Accordingly, the design of the MW-CVI pilot plant in Pisa used along this PhD activity, unlike other existing lab-scale equipment, has been carried out with the idea of a further industrial scale-up using an innovative approach to achieve the highest energy efficiency for a large variety of CMC samples with dimensions of industrial interest. This new approach has faced some complex engineering problems which have been tackled in an original way and will be discussed along the thesis.

1.5 Thesis overview

The thesis is structured into 6 chapters (including the current), with someone being based on original papers. The thesis has been written maintaining a logical order about the research activities carried out along these three years. Each chapter begins with an abstract, a short introduction and ends with conclusions, thus having the same structure of a general paper. Due to the structure employed, the thesis might unavoidably contain some repetition among the various chapters.

Besides the current chapter, the content of the others is as follows:

- **Chapter 2:** It is presented as a review about general CMCs properties with a focus on non-oxide segment components and manufacturing technologies. Particular attention is dedicated to the conventional CVI process and its variants in order to highlight the main disadvantages and limits which will be addressed using the MW-CVI process.
- **Chapter 3:** It outlines the main principles and parameters of MW heating, as applied to industrial processes and the basic design of applicators for material processing. A brief paragraph on EM theory is inserted to understand MW generation, propagation and material interaction mechanisms related to the main MW system components. Among the various applicator designs, the overmoded resonant solution was highlighted due to its potential for industrial applications.
- **Chapter 4:** It is focused on the core of the system, namely the design of a high-quality overmoded resonant cavity for high-temperature MW materials processing, to achieve optimal performance both in terms of MW heating efficiency and reproducibility. The resulting performance, as applied for the production of CMCs, is proved both in terms of fraction of EM energy dissipated into the material of interest at critical coupling conditions and the expected MW heating benefits (rapid heating, inverse temperature profile). Another element of robustness highlighted about the MW cavity designed is given by the high versatility in treating a wide and diverse range of materials along the heating and infiltration process, with a good level of predictability and stability.
- **Chapter 5:** It follows the results of the previous chapter addressing the design of all the other parts of the pilot plant and their integration with the MW heated cavity. Based on the first results on lab scale samples, the main parameters controlling the MW-CVI process are identified and, after a targeted optimization procedure, the final results obtained about the infiltration on pilot scale preforms are presented. The inside-out densification profile expected, due to the reversed temperature profile, as well as the fast and reproducible heating pattern of different 1°gen SiC-Nicalon reinforced preforms are analyzed showing the potential reduction of the total processing time of about one order of magnitude.
- **Chapter 6:** It reports further steps ahead made about this technology from the trials on a Hi-Nicalon Type S™ fibre reinforced preform, previously coated with a PyC interphase in order to achieve a pseudo-ductile fracture behavior, and slightly densified with a slurry infiltration process. Despite of the presence of the highly conductive PyC coating, critical coupling conditions were obtained also for this preform, using almost the same operating conditions previously employed with good results in terms of reaction efficiency. Finally, future developments and conclusions are outlined showing possible improvements and outcomes of the MW-CVI technology.

1.5.1. PhD research activity outcomes

Parts of the research activity carried out during these three years have been presented at national and international conferences:

- *Poster presentation* (AIMAT 2019): "Development and Optimization of new methodologies for high temperature microwave processing of SiC-based Ceramic Matrix Composites"
- *Oral talk* (AMPERE 2019): "Design of an Overmoded Resonant Cavity based Reactor for SiC-based Ceramic Matrix Composites production"
- *Oral talk* (HT-CMC10 2019): "Design of a pilot-scale Microwave Heated Chemical Vapor Infiltration plant: An innovative approach"

In particular, some of the chapters above described have been published on international journals (some others will be instead published asap):

- **Chapter 4**: D'Ambrosio R, Cintio A, Lazzeri A, et al. Design of an Overmoded Resonant Cavity-based Reactor for Ceramic Matrix Composites Production. Chem. Eng. J. [Internet]. 2020;405. Available from: https://doi.org/10.1016/j.cej.2020.126609;
- **Chapter 5**: D'Ambrosio R, Aliotta L, Gigante V, et al. Design of a pilot-scale microwave heated chemical vapor infiltration plant: An innovative approach. J. Eur. Ceram. Soc. [Internet]. 2020; Available from: https://doi.org/10.1016/j.jeurceramsoc.2020.05.073;
- **Chapter 4-5**: "*High temperature dielectric characterization of SiC-based Ceramic Matrix Composites*", to be published as soon as possible;
- **Chapter 6**: "*Production of SiC_f/PyC/SiC composites by hybrid slurry infiltration and MW-CVI process*", to be published as soon as possible;

During these years some academic collaborations have been established leading to significant results related to the research activity and improving my knowledge about both CMCs materials and MW heating technology. The first, which is still underway, was carried out with the Department of Metallurgy and Materials of the University of Birmingham leaded by Prof. Binner, and the main results have been collected and described into **Chapter 6**.

A research internship of six months was conducted along the third year (February 2020 – August 2020) at the Department of Ceramic Materials Engineering of the University of Bayreuth leaded by Prof. Krenkel, to deepen the aspects related to one of the industrial benchmark among CMCs manufacturing technologies, namely the Liquid Silicon Infiltration (LSI) process. In addition to that topic, part of the research stay was dedicated to the improvement of the reliability of SiC-based CMCs through the study and development of an innovative tensile testing device, whose results will be soon published as follows:

- "*Development and evaluation of a tensile testing device for C_f/C-SiC materials*";

The experimental research activities were carried out at the pilot plant designed, built and setup during the European project HELM, into the joint labs of the University of Pisa (UNIPI) and the Institute for chemical and physical processes (IPCF), located into the National Research Council (CNR) area of Pisa. The collaboration with the IPCF-CNR carried out in these years allowed me to investigate various issues concerning microwave heating technologies, leading to the results published in the articles reported.

Moreover, the results achieved along all the PhD research activity have been exploited writing a proposal for a recently funded European project (1/10/2020 – 31/03/2024) named "Novel CEramic Matrix Composites produced with MicroWAVE assisted Chemical Vapour Infiltration process for energy-intensive industries" (**CEM-WAVE**, Grant Agreement n°958170). The project derives from the establishment of a multidisciplinary team with some of the main players on the European scene among which several are part, as the University of Pisa, of the A.SPIRE network such as ENEA, Fraunhofer ISC, Arcelor Mittal and Politecnico di Torino.

1.6 References

[1] Low IM. Advances in ceramic matrix composites: Introduction. In: Low IM, editor. Adv. Ceram. Matrix Compos. 2nd ed. Cambridge, UK: Woodhead Publishing; 2018. p. 1–7.

[2] High-Level Group on Energy-intensive Industries. Masterplan for a Competitive Transformation of EU Energy-intensive Industries. Enabling a Climate-neutral, Circular Economy by 2050. 2019.

[3] Clauß B. Fibers for Ceramic Matrix Composites. In: Krenkel W, editor. Ceram. Matrix Compos. Fiber Reinf. Ceram. their Appl. Weinheim, Deutschland: Wiley- VCH; 2008. p. 1–19.

[4] Lazzeri A. Cvi Processing of Ceramic Matrix Composites. In: Bansal NP, Boccaccini AR, editors. Ceram. Compos. Process. methods. Hoboken, NJ, USA: John Wiley & Sons; 2012. p. 313–349.

[5] Coltelli M-B, Lazzeri A. Chemical vapour infiltration of composites and their applications. In: Choy K-L, editor. Chem. Vap. Depos. Adv. Technol. Appl. CRC Press; 2019.

[6] Naslain R, Langlais F, Fedou R. The CVI processing of Ceramic Matrix Composites. J. Phys. Colloq. 1989;50.

[7] Ibn-Mohammed T, Randall CA, Mustapha KB, et al. Decarbonising ceramic manufacturing: A techno-economic analysis of energy efficient sintering technologies in the functional materials sector. J. Eur. Ceram. Soc. [Internet]. 2019;39:5213–5235. Available from: https://doi.org/10.1016/j.jeurceramsoc.2019.08.011.

[8] Clark DE, Folz DC, West JK. Processing materials with microwave energy. Mater. Sci. Eng. A. 2000;287:153–158.

[9] Bykov Y V., Rybakov KI, Semenov VE. High-temperature microwave processing of materials. J. Phys. D. Appl. Phys. 2001;34:R55.

[10] Agrawal D, Cheng J, Peng H, et al. Microwave energy applied to processing of high-temperature materials. Am. Ceram. Soc. Bull. 2008;87:39–43.

[11] High-frequency ELectro-Magnetic technologies for advanced processing of ceramic matrix composites and graphite expansion" (HELM), FP7-NMP.2011.4.0-1, GA n°. 280464 [Internet]. Available from: http://www.helm-project.eu/.

[12] Allied Market Research. Ceramic Matrix Composites Market Outlook - 2026 [Internet]. Available from: https://www.alliedmarketresearch.com/ceramic-matrix-composites-market.

[13] American Ceramic Society Bulletin. Ceramic matrix composites taking flight at GE Aviation. 2019; Available from: www.ceramics.org.

[14] Tomas Kellner. Space Age Ceramics Are Aviation's New Cup Of Tea [Internet]. 2016. Available from: https://www.ge.com/reports/space-age-cmcs-aviations-new-cup-of-tea/.

[15] Savage G. Applications of Carbon-Carbon composites. Carbon-Carbon Compos. Heidelberg: Springer Netherlands; 1993. p. 323–357.

[16] Roland W. Carbon/Carbon and Their Industrial Applications. In: Krenkel W, editor. Ceram. Matrix Compos. Fiber Reinf. Ceram. their Appl. Weinheim, Deutschland: Wiley-VCH; 2008.

[17] Fitzer E, Manocha LM. Carbon Reinforcements and Carbon/Carbon Composites. Berlin: Springer-Verlag; 1988.

[18] Adams DF. Applications in Aerospace, Especially in the USA. In: Fitzer E, editor. Carbon Fibres Their Compos. Berlin: Springer; 1985.

[19] Appleyard SP, Rand B. Carbon-Carbon Composites. In: Rand B, Appleyard SP, Yardim MF, editors. Des. Control Struct. Adv. Carbon Mater. Enhanc. Perform. NATO Scien. Dordrecht: Springer; 2001.

[20] Christin F. Application of Thermostructural Composites (TSC) like C / C , C / SiC , and SiC / SiC Composites. Adv. Eng. Mater. 2002;4:903–912.

[21] Scarponi C. Carbon–carbon composites in aerospace engineering [Internet]. Adv. Compos. Mater. Aerosp. Eng. Elsevier Ltd; 2016. Available from: http://dx.doi.org/10.1016/B978-0-08-100037-3.00013-4.

[22] Christin F. Design, Fabrication and Applications of C/C, C/Si and SiC/SiC Composites. In: Krenkel W, Naslain R, Schneider H, editors. High Temp. Ceram. Matrix Compos. Berlin: Wiley-VCH; 2001.

[23] Hurst JB, Lee K, Harder B. Overview of NASA Transformational Tools and Technologies Project ' s 2700 ° F CMC / EBC Technology Challenge Acknowledgements : Transformational Tools and Technologies Project ' s. 2019;

[24] Mühlratzer A and HP. CMC Body Flaps for the X-38 Experimental Space Vehicle. In: Wiley Online Library, editor. 26th Annu. Conf. Compos. Adv. Ceram. Mater. Struct. A Ceram. Eng. Sci. Proc. 2002. p. 331–338.

[25] Composites world. Ceramic-matrix composites heat up [Internet]. Available from: https://www.compositesworld.com/articles/ceramic-matrix-composites-heat-up.

[26] Levy D. Ceramic matrix composites take flight in LEAP jet engine [Internet]. ScienceDaily. 2017. Available from: https://www.ornl.gov/news/ceramic-matrix-composites-take-flight-leap-jet-engine.

[27] CFM. CFM LEAP engine [Internet]. Available from: https://www.cfmaeroengines.com/engines/leap/.

[28] GE Aviation hits Farnborough at full throttle; $7.5B in R&D investments since 2010; ceramic matrix composites and 3D printing [Internet]. Available from: https://www.greencarcongress.com/2016/07/20160710-geav.html.

[29] van Roode M, Price J, Kimmel J, et al. Ceramic matrix composite combustor liners: A summary of field evaluations. J. Eng. Gas Turbines Power. 2007;129:21–30.

[30] Dicarlo JA, Roode M Van. Ceramic Composite Development for Gas Turbine Engine Hot Section Components. ASME Turbo Expo 2006 Power Land, Sea, Air. Barcelona, Spain; 2008.

[31] Gadow R, Jiménez M. Carbon fiber-reinforced carbon composites for aircraft brakes. Am. Ceram. Soc. Bull. 2019;98:28–34.

[32] Windhorst T, Blount G. Carbon-carbon composites: A summary of recent developments and applications. Mater. Des. 1997;18:11–15.

[33] Devi GR, Rao KR. Carbon-carbon composites - an overview. Def. Sci. J. 1993;43:369–383.

[34] Krenkel W. Carbon Fibre Reinforced Silicon Carbide Composites. In: Bansal NP, editor. Handb. Ceram. Compos. Boston: Springer; 2005. p. 117–148.

[35] Brembo SGL Carbon Ceramic Brakes. Production of Carbon ceramic brakes [Internet]. Available from: http://www.carbonceramicbrakes.com/en/technology/Pages/production-steps.aspx.

[36] Katoh Y, Snead LL, Henager CH, et al. Current status and critical issues for development of SiC composites for fusion applications. J. Nucl. Mater. 2007;367-370 A:659–671.

[37] Katoh Y, Snead LL, Nozawa T, et al. Advanced Radiation-Resistant Ceramic Composites. Adv. Sci. Technol. 2006;45:1915–1924.

[38] Snead LL, Nozawa T, Ferraris M, et al. Silicon carbide composites as fusion power reactor structural materials. J. Nucl. Mater. [Internet]. 2011;417:330–339. Available from: http://dx.doi.org/10.1016/j.jnucmat.2011.03.005.

[39] Katoh Y, Ozawa K, Shih C, et al. Continuous SiC fiber, CVI SiC matrix composites for nuclear applications: Properties and irradiation effects. J. Nucl. Mater. [Internet]. 2014;448:448–476. Available from: http://dx.doi.org/10.1016/j.jnucmat.2013.06.040.

[40] Bonal JP, Kohyama A, Van Der Laan J, et al. Graphite, ceramics, and ceramic composites for high-temperature nuclear power systems. MRS Bull. 2009;34:28–34.

[41] Katoh Y, Nozawa T, Snead LL, et al. Stability of SiC and its composites at high neutron fluence. J. Nucl. Mater. [Internet]. 2011;417:400–405. Available from: http://dx.doi.org/10.1016/j.jnucmat.2010.12.088.

[42] ITER ORGANIZATION. The ITER Tokamak [Internet]. 2020. Available from: https://www.iter.org/fr/mach.

[43] Tweed G. New Ceracomp material virtually eliminates catastrophic failure in sealless pumps [Internet]. 2011. Available from: http://www.jeccomposites.com/knowledge/international-composites-news/new-ceracomp-material-virtually-eliminates-catastrophic.

[44] National Research Council. Ceramic Fibers and Coatings: Advanced Materials for the Twenty-First Century [Internet]. Washington, DC: National Academies Press; 1998. Available from: https://doi.org/10.17226/6042.

[45] BJS Ceramics. Silicon-Carbide-Fiber Pilot-Production in Europe, SPE-Project [Internet]. 2019. Available from: https://www.bjsceramics.com/bjs-ceramics/eu-horizon-2020/.

[46] Asthana R, Singh M. Active metal brazing of advanced ceramic composites to metallic systems. Adv. Brazing [Internet]. Elsevier; 2013 [cited 2018 Mar 12]. p. 323–360. Available from: http://linkinghub.elsevier.com/retrieve/pii/B9780857094230500110.

[47] Sun J, Deemer C, Ellingson W, et al. NDE technologies for ceramic matrix composites: Oxide and nonoxide. Mater. Eval. 2006;64:52–60.

[48] Metaxas AC, Meredith RJ. Industrial applications and economics. Ind. Microw. Heat. London, United Kingdom: IET; 2008. p. 296–319.

[49] Meredith RJ. Introduction and fundamental concepts. Eng. Handb. Ind. Microw. Heat. [Internet]. Stevenage, United Kingdom: IET; 1998. p. 1–16. Available from: https://doi.org/10.1049/PBPO025E.

[50] Collin RE. Introduction. Found. Microw. Eng. 2nd ed. New York: Wiley-IEEE Press; 2001. p. 1–16.

[51] Oghbaei M, Mirzaee O. Microwave versus conventional sintering: A review of fundamentals, advantages and applications. J. Alloys Compd. Elsevier B.V.; 2010. p. 175–189.

[52] Rosa R, Veronesi P, Han S, et al. Microwave assisted combustion synthesis in the system Ti – Si – C for the joining of SiC : Experimental and numerical simulation results. J. Eur. Ceram. Soc. [Internet]. 2013;33:1707–1719. Available from: http://dx.doi.org/10.1016/j.jeurceramsoc.2013.03.005.

[53] Jones DA, Lelyveld TP, Mavrofidis SD, et al. Microwave heating applications in environmental engineering - A review. Resour. Conserv. Recycl. 2002;34:75–90.

[54] Marken F. Chemical and electro-chemical applications of in situ microwave heating. Annu. Reports Prog. Chem. - Sect. C. 2008;104:124–141.

[55] Singh S, Gupta D, Jain V, et al. Microwave processing of materials and applications in manufacturing industries: A Review. Mater. Manuf. Process. 2015;30:1–29.

[56] Polaris Market Research. Industrial Microwave Heating Market [Internet]. Available from: https://www.polarismarketresearch.com/press-releases/industrial-microwave-heating-market.

[57] Thostenson ET, Chou T. Microwave processing : fundamentals and applications. Compos. Part A Appl. Sci. Manuf. 1999;30:1055–1071.

[58] Carter RG. Radio-frequency power generation. Cern Accel. Sch. Course High Power Hadron Mach. [Internet]. 2013;45–70. Available from: https://arxiv.org/abs/1303.1355.

[59] Jacob J. Radio frequency solid state amplifiers. Cern Accel. Sch. Power Convert. CAS 2014 - Proc. 2014;197–216.

[60] Wesson R, Jerby E, Schwartz E, et al. Ampere newsletter: Trends in RF and Microwave Heating. Electr. Eng. 2016;

[61] Gregory S. Introduction to RF Solid State Microwave Heating [Internet]. Available from: https://www.slipstream-design.co.uk/introduction-rf-solid-state-microwave-heating/.

[62] Machiels M. Ampere newsletter. Electr. Eng. 2006;1–6.

[63] Microwave Max Industrial. Industrial Microwave Tunnel Conveyor Machine [Internet]. Available from: https://www.maxindustrialmicrowave.com/.

[64] Schiffmann RF. Microwave technology in baking. Adv. Bak. Technol. [Internet]. Boston, MA: Springer US; 1993. p. 292–315. Available from: https://doi.org/10.1007/978-1-4899-7256-9_11.

[65] Püschner. Püschner Microwave Power Systems [Internet]. Available from: https://www.pueschner.com/en/.

[66] Mallah F und, GmbH MT. Fricke und Mallah Microwave Technology GmbH - Solid State Microwave Generator [Internet]. Available from: https://www.microwaveheating.net/en/home.html.

[67] Clark DE, Sutton WH. Microwave Processing of Materials. Annu. Rev. Mater. Sci. [Internet]. 1996;26:299–331. Available from: https://doi.org/10.1146/annurev.ms.26.080196.001503.

[68] Jack B. Microwave Energy Powers Many Industrial Applications [Internet]. 2017. Available from: https://www.mwrf.com/technologies/systems/article/21848252/microwave-energy-powers-many-industrial-applications.

[69] National Research Council. Microwave processing of materials. Met. Mater. Bury St Edmunds. Washington, DC: National Academies Press; 1994.

[70] Langlais F, Vignoles GL. Chemical vapor infiltration processing of ceramic matrix composites. In: Peter W.R. B, Carl H. Z, editors. Compr. Compos. Mater. II. Oxford: Elsevier; 2018. p. 86–129.

[71] Sun J, Wang W, Yue Q. Review on microwave-matter interaction fundamentals and efficient microwave-associated heating strategies. Materials (Basel). 2016;9.

Chapter 2

2. Ceramic Matrix Composites: Properties and Manufacturing technologies

Ceramic materials are characterized by high temperature resistance, high specific mass properties, resistance to oxidation, wear and corrosion. This attractive package is generally marred by one deadly flaw, namely an utter lack of toughness (except for toughened ceramics as zirconia). However, by embedding long/short fibres or fabrics, the toughness of the material can be increased and a damage-tolerant ceramic with all its positive properties can be produced, obtaining the so-called Ceramic Matrix Composites (CMCs).

Fibre composite materials, as CMCs, are not modern inventions but are gaining increasing influence in the field of lightweight construction as "best material". It will be the principle of nature to embed fibres in a matrix, such as for wood, increasingly refined and perfected, so that modern fibre composite materials have outstanding mechanical properties with low density. The weight reduction achieved in this way enables for example important fuel savings to be made, which are both an economic and an increasingly ecological goal today. In particular, CMCs show some distinctive properties related to their components and peculiar manufacturing routes.

In this Chapter a panoramic of CMCs will be given focusing on:

- Main components: Fibres, Matrix and Interface/Interphase;
- Processing technologies: advantages/disadvantages;

Due to the enormous literature in merit and target of this PhD thesis, special attention will be dedicated to SiC-based CMCs reinforced with SiC fibres and produced by Chemical Vapor Infiltration (CVI).

2.1 Introduction

Ceramic Matrix Composites represent one of the latest and most promising solutions for high temperature applications in strategic industrial sectors, such as transport and energy. CMCs are extremely valuable for applications with demanding thermal and mechanical requirements and they have been developed to achieve a damage tolerant quasi-ductile fracture behaviour while maintaining all other advantages of monolithic ceramics at high temperatures.

The distinctive lack of toughness displayed by their monolithic counterpart is overcome reinforcing the otherwise brittle matrix with high-strength ceramic fibres:

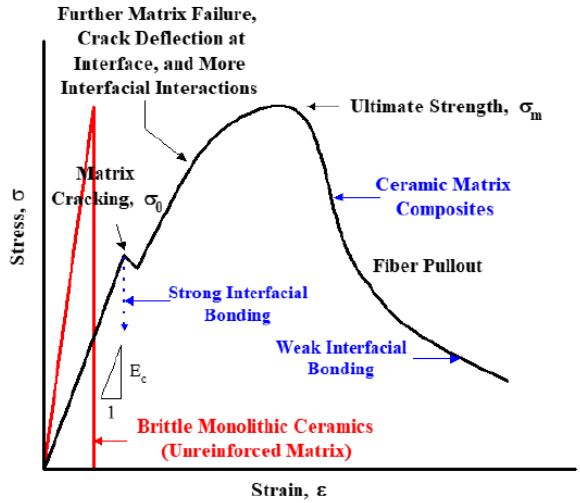

Figure 2.1 *- The stress–strain behaviour in ceramic matrix composites as compared with monolithic ceramics* [1]

Various ceramic materials, oxide or non-oxide based, are used for the fibres and the matrix. Non-oxide CMCs offer the better high-temperature performances in terms of thermo-mechanical properties and low density, while oxide CMCs are increasingly gaining attention due to their considerably lower cost and intrinsic oxidation resistance, albeit their maximum use temperature is generally around $1000 - 1100\ °C$ [2].

There are some distinctive properties which distinguish CMCs from other composites. It is common approach, inside a composite material, the use of fibres bearing most part of the applied load, resulting in very high ratios between the elastic modulus of the fibres E_f with respect to that of the matrix E_m, while CMCs presents values of E_f/E_m close to the unity. These materials are usually referred as "inverse composites", namely that the failure strain of the matrix ε_m^R is lower than the failure strain of the fibres ε_f^R (hence, under load, it is the matrix which fails first). Moreover, due to the limited ductility of the matrix at the high fabrication temperature, thermal mismatch among components presents great importance on CMC overall performance with respect to the foreseen application [3].

The great potential of CMCs is directly linked to the use of high strength and modulus reinforcement fibres (typically of diameters of the order of 10 μm). Non-oxide fibres used in CMC are mainly made of carbon (C) or silicon carbide (SiC) while oxide fibres are based on alumina (Al_2O_3), mullite (Al_2O_3-SiO_2) or silica (SiO_2). Non-oxide matrices are mostly based on SiC, C or mixtures of SiC and silicon (Si), while oxide matrices consist of Al_2O_3, zirconia (ZrO_2), Al_2O_3-SiO_2 or other alumino-silicates. Usually oxide fibres are combined with oxide matrices and non-oxide fibres with non-oxide matrices.

Most conventional ceramic materials are prepared from powders of appropriate purity and size to then be formed and densified until the desired density and microstructure is reached [4]. Those methods of processing the powders with temporary addition of organic binders followed by grinding, pressing and densification, are generally not compatible for the production of CMCs, which require gentle handling of the fibres in order to avoid introduction of defects as well as good dispersion in the matrix to be effective.

It is worth noticing that reinforcing a composite using low aspect ratio particulates is easier with respect to the use of fibres. Moreover, the dispersion in the matrix results simplified since common grinding/mixing through slurry or granulation paths can still be employed because pressures involved does not result in damage or degradation of the reinforcement and there is much less impediment during matrix sintering. Albeit the increase in toughness, following this approach, is highly disadvantaged [5] and therefore alternative methods are needed to produce such composites.

Key characteristic to prevent an early brittle failure of the material is the control of the fibre-matrix bonding along processing. The latter must be sufficiently weak to allow debonding and the bridging of the matrix cracks by the fibres and consequently the relaxation of the stress field at the crack tip [6].

There are two methods of achieving this: for dense matrix CMCs (e.g. SiC-based composites) a low cohesion interface/interphase coating (e.g. pyrolytic carbon or boron nitride) is applied to the fibres before the matrix is infiltrated. CMCs of this type are called "Weak Interface Composites" (WICs) and toughening mechanisms such as crack deflection at the fiber/matrix interface, crack-bridging by fibres and fibre pullout at the crack plane are operative. An alternative approach (e.g. for oxide-based composites) is to ensure that the matrix is weak. Such "Weak Matrix Composites" (WMCs) are characterized by the matrix being porous; the reduced matrix stiffness and strength allows damage-tolerant behaviour, even in the case of a strong fiber-matrix interface. Whilst both approaches work, for WICs the interface coatings may oxidize at high temperatures in air leading to brittle failure, whilst WMCs typically display a low overall strength or, if used at excessively high temperatures, the matrix can further densify leading to brittle behaviour.

Manufacturing technologies of CMCs constitute an additional point of importance, where the main requirement is that the degradation of the reinforcement must be absolutely avoided. For this reason, processes that employ relatively low temperatures and pressures are favoured. This is the case for the CVI and the Polymer Infiltration and Pyrolysis (PIP) processes, where the precursor of the matrix is gaseous or liquid respectively. Both routes are carried out under vacuum and at temperatures of the order of $900 - 1200\ °C$, and can be used for the production of near-net-shape components with complex shape but they also generally result in high residual porosity ($10 - 15\%$). An important milestone, regarding CMCs manufacturing routes, was the development at plant level of Reactive Melt Infiltration (RMI) technologies, where the matrix is formed by chemical reaction between a liquid precursor and a pre-consolidated fibre preform. The latter allow to reach degree of residual porosity close to zero with reduced processing times but leads to unreacted precursor presence and, due to the high matrix manufacturing temperature ($1400 - 1600\ °C$), high-quality reinforcements or carbon-based ones needs to be employed to minimize fibre degradation risks.

Despite their remarkable suitability for high-temperature lightweight applications, non-oxide CMCs components suffer from rapid recession when used in combustion environments above $1100\ °C$. This is because volatile $Si(OH)_x$ species are formed when the superficial SiO_2-layer is

in contact with hot water vapor, which is formed during the combustion of hydrocarbons and/or hydrogen. Therefore, it is important to improve the oxidation resistance through the use of one or more strategies: use of highly crystallized fibres with reduced oxygen and amorphous carbon content (higher creep resistance), multi-layered interphase or self-healing coatings, addition of Environmental Barrier Coatings (EBCs). The latter generally comprise multiple layers, usually one bond-coat layer up to several intermediate layers and one top layer. The respective materials have to be carefully selected regarding their coefficient of thermal expansion (in order to have a high thermo-mechanical stability), chemical compatibility (in order to have a good bonding to the substrate and each other and to avoid contact corrosion) and phase stability.

The final costs of CMCs strongly depend on composition and manufacturing route. They vary between some hundred and some thousands of EUR/kg. So, CMCs are expensive compared to other materials and the high price must pay off by longer service life and by a unique performance in value-added products.

2.2 CMCs components

The mechanical performance and design of a CMCs are closely related to the properties of the components chosen for the respective application, which are:

- ***Reinforcement***: based on long fibres, short fibres, whiskers or particles. The use of long fibres as reinforcements allows to obtain composites with high temperature mechanical properties, able of arrest crack propagation through deflection at fiber/matrix interface, characteristics which cannot be obtained with other types of reinforcements [7]. Additionally, only ceramic fibres able of withstanding the high temperatures required by matrix processing can be employed. Other requirements to be met include long-term stability, creep and oxidation resistance. CMCs are further classified according to their fibre structure, which has a large impact on final material properties.
- ***Interface/Interphase***: depending on the characteristics of this domain, the composite will be either a brittle ceramic or a damage tolerant composite, thus it must fulfil several requirements. In particular, a good fibre/matrix bonding is necessary to ensure material integrity; once the matrix cracks, the load needs to be efficiently transferred through the interface while a small amount is still carried by the matrix, avoiding exposure of the fibres to aggressive environments [8].
- ***Matrix***: provides rigidity to the otherwise compliant mass of fibres, protecting them from mechanical and chemical damage and supplying thermo-mechanical restraint to the reinforcement to control the interface properties, and hence the mechanical behaviour under load. It is important that the processing temperature of the matrix should not exceed that at which degradation of the reinforcement occurs and a suitable method, able to uniformly disperse the precursor of the matrix, must be chosen depending on matrix type [5].

Due to the anisotropy and broad range of qualities, CMCs can be designed and tailored displaying a wide range of thermo-mechanical properties. **Table 2.1** reports the mechanical properties for different categories of CMCs:

***Table 2.1** - Material properties of typical CMC at ambient temperature, the range reflects minimum and maximum of the respective property in different directions or for different CMC qualities (Ox/Ox covers CMC with alumina fibers and alumina or alumino-silicate matrix)* [9–11]

Property	Unit	SiC_f/SiC	C_f/SiC	C_f/C	$C_f/C\text{-}SiC$	Ox/Ox
Fibre content	*vol.-%*	40-60	10-70	40-60	55-65	30-50
Porosity	*vol.-%*	10-15	1-20	8-23	2-5	10-40
Density	g/cm^3	2,3-2,5	1,8-2,8	1,4-1,7	1,9-2,0	2,1-2,8
Tensile strength	*Mpa*	150-360	80-540	14-1100	80-190	70-280
Bending strength	*Mpa*	280-550	80-700	120-1200	160-300	80-630
Strain to failure	*%*	0,1-0,7	0,5-1,1	0,1-0,8	0,15-0,35	0,12-0,4
Young's Modulus	*GPa*	70-270	30-150	10-480	50-70	50-210
Fracture Toughness	$Mpa*m^{0,5}$	25-32	25-30	5,7-7,8	-	58-69
Thermal conductivity	$W/m*K$	6-20	10-130	10-70	7,5-22,6	1-4
Coefficient of thermal expansion	ppm/K	2,8-5,2	0-7	0,6-8,4	0-7	2-7,5
Maximum service temperature	*°C*	1100-1600	1350-2100	2000-2100	1750	1000-1100

2.2.1. Non-oxide fibres for CMCs

The term "ceramic fibres" is continuously being updated; currently it refers to all non-metallic inorganic fibres (oxide and non-oxide), except for fibres produced via solidification of glass melts [12]. **Figure 2.2** reports a general classification for different types of ceramic fibres. These are characterized by a tensile strength between $1000\,MPa$ and $7000\,MPa$ (about an order of magnitude higher than the strength of the matrix) and an elastic modulus typically between $200\,GPa$ and $900\,GPa$. Fiber degradation occurs between $1000\,°C$ and $2100\,°C$ depending on fiber material and quality, then the maximum service temperature of the CMC depends on this choice.

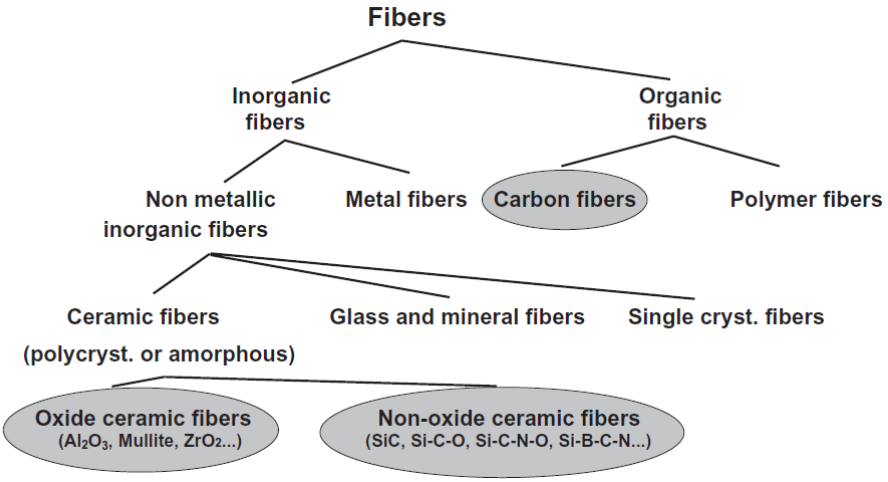

***Figure 2.2** - Classification of different fiber types* [12]

The distinction among ceramic and glass fibres has also become more difficult during last years since ceramics produced by preceramic precursors or sol-gel route display a "glassy" amorphous phase (especially considering first generation SiC fibres), meaning that ceramic fibres can be either polycrystalline, partially crystalline or amorphous. Specifically, the expression "glass

fibres" is generally applied to fibres produced via solidification of typical glass melts based on silicate systems. If these melts are produced by using minerals such as basalt, then the fibres should be called "mineral fibres".

The physical structure of ceramic fibres determines its thermo-mechanical behaviour. Fibre morphology instead influence the properties at the macroscopic level. Related important parameters are the cross-section, uniformity of diameter along the fibre, porosity and surface defects and properties such as surface energy and roughness, from which depends the adhesion of the matrix during the infiltration step.

Due to the importance for high temperature applications, a great effort has been made to improve creep behaviour [13]. The latter is particularly influenced by the oxygen content and grain size, besides being dependent on the structure and morphology of the fibre. For these reasons, specific and expensive treatments at high temperatures and controlled atmospheres are used to eliminate the amorphous phase, reorganizing the carbon-based structure, and reducing the oxygen content [14].

Manufacturing processes of fibres can be divided in [15]:

- *Indirect processes*: when the fibres are not obtained directly from a spinning process but by pyrolysis of a preceramic precursor previously soaked or deposited on inorganic fibre surfaces acting as carriers;
- *Direct processes*: when inorganic precursors (based on salt, sols or precursor melts) are directly spun to so called "green fibres";

Continuous or short fibres are used for CMC manufacture. Fibres can be oriented unidirectional or planar to achieve special anisotropic properties. Woven or unwoven fabrics can be used, whereby textile techniques like breading allow for 3D structures with complex load characteristics.

A wide spectrum of ceramic fibres is currently available on the market. Due to the higher temperature resistance, non-oxide ceramic fibres (carbon or silicon carbide based) are particularly considered for related demanding applications. However, carbon fibres degrade in oxidizing environments starting from $450\,°C$, whereas SiC-based fibres present much higher resistance to oxidation depending on their quality. Anyway, due to the high cost-performance ratio and high-temperature resistance in non-oxidizing atmosphere (up to $2800\,°C$), carbon fibres have been widely used for CMCs manufacture. Therefore, the importance of the research on protective coatings to extend the range of usage of CMCs.

Since the research activities conducted during this thesis are based on SiC fibre reinforced CMCs, more detailed information will be given about their manufacturing, thermo-mechanical behaviour and properties.

2.2.1.1. SiC-based fibres

Since the production of the first SiC fibres during the 1970s, three generations of SiC-based fibres were manufactured essentially by three companies: Nippon Carbon Co. Ltd[20], Ube

[20] http://www.carbon.co.jp/english/

Industries Ltd[21] and COI Ceramics[22]. The most important commercial trademarks are reported in **Figure 2.3** and differ by composition and properties as a result of the organo-siliced precursors and manufacturing processes used.

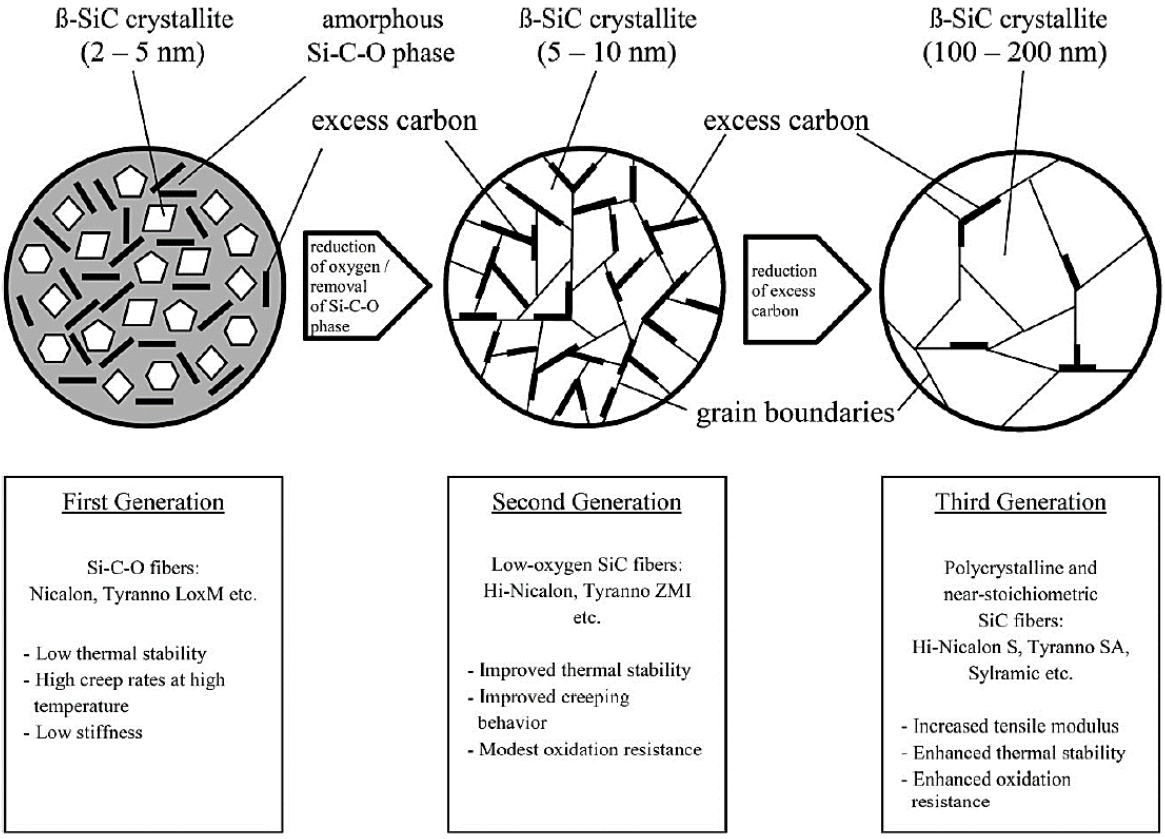

***Figure 2.3** - Three generations of commercial SiC fibres* [15]

First generation SiC fibres were produced by melt spinning from polycarbosilanes (PCS), followed by curing in oxygen atmosphere and subsequent pyrolysis achieving a fine diameter fibre [16]. Due to the residual large amount of oxygen in a silicon oxycarbide phase, they tend to decompose up to $> 1100\ °C$ with evolution of $SiO_{(g)}$ and $CO_{(g)}$ with consequent degradation of their strength [17,18].

Second generation SiC fibres were developed to reduce the thermal instability deriving from the silicon oxycarbide phase drastically abating the oxygen content through specific curing steps [18,19]. As a result, those fibres present a higher thermal stability than first generation. Still the high turbostratic carbon content affects the resistance to oxidation and creep [14,20,21].

Finally, third generation SiC fibres production processes aimed to reduce the free carbon content and improve high temperature properties achieving a nearly stoichiometric SiC fibre. The main difference in the manufacturing route is in the thermal treatment which is made under hydrogen atmosphere [22]. The resulting fibre exhibit high Young modulus, creep and oxidation resistance and excellent thermal stability up to $1600\ °C$ [23–25].

The main approaches to produce SiC fibres are based on:

[21] https://www.ube-ind.co.jp/ube/en/index.html
[22] http://www.coiceramics.com/

- *Chemical Vapor Deposition (CVD)*: used to produce the first ceramic fibres introduced on the market during the mid-1960s for metal matrix composites (MMCs), where a preceramic gaseous precursor containing carbon or silicon species are continuously deposited on a continuous core monofilament (based on carbon or tungsten). Reactant gas species, carrier, and/or reducing gases, deposition pressure, temperature and gas phase concentration are the parameters which needs to be adjusted and tuned to achieve a homogeneous ceramic filament with the desired microstructure [26]. The resulting product present low flexibility with diameters $> 75\ \mu m$, which makes them suitable to make unidirectional or cross-ply reinforced MMCs but not to be woven for complex shaped parts.
- *Preceramic polymer processing*: based on the pyrolysis of organosilicon precursor filaments (similar to the production of carbon fibres from PAN or pitch through dry/melt-spinning), SiC fibres obtained using this method are used to reinforce lightweight thermo-structural composite materials thanks to their higher flexibility and reduced diameter ($< 30\ \mu m$); several organosilicon polymers have been investigated in the last years including PCS, polysilazanes, polycarbosilazanes (PCSZ), polyborosilazanes and polysiloxanes [27]. **Figure 2.4** shows the main steps for the manufacturing of ceramic fibres from precursor route as well as important parameters for a controllable processing of ceramic fibres.

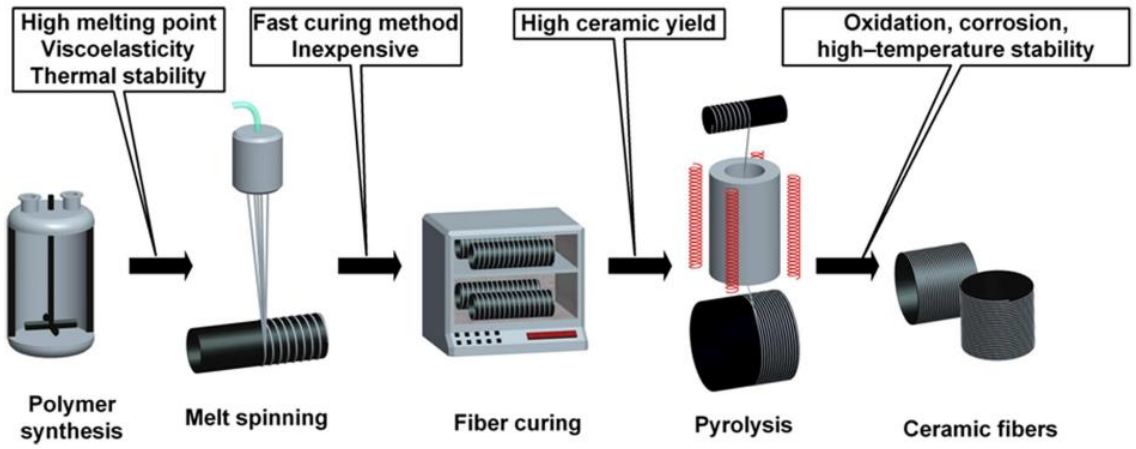

***Figure 2.4** - Manufacturing steps for ceramic fibres from precursor route* [28]

Particular attention is dedicated to the "curing step", necessary to avoid the re-melting of the fibres during the last stage, namely the conversion of the polymer to the ceramic fibre by pyrolysis. Two are the methods followed in this stage: physical and chemical.

The first approach consists in the formation of radicals leading to cross-linked molecules in radical recombination reactions. Examples of those methodologies are gamma-ray treatment or electron beam irradiation [15,29]. Commercial fibres cured by electron beam irradiation are Hi-Nicalon™ and Hi-Nicalon type S™.

Chemical curing methods are instead based on the exposure of the green fibres to a reactive atmosphere where the gaseous species interacts with the precursor on fibres surface leading to cross-linking. First generation SiC fibres as Nicalon™, Tyranno LoxM™, Tyranno SA™, Tyranno S™ and Sylramic™ are cured in oxygen although it reduces their high temperature stability, therefore different curing agents have been tested during last years.

Table 2.2 reports some of the main commercial trademarks of SiC fibres.

Table 2.2 *– Physical properties, composition of commercial small-diameter non-oxide ceramic fibres, adapted from* [15,28,30]

	Trademark	Manufacturer	Elemental composition [wt%]	Curing	Max production temperature [°C]	Average fibre diameter [µm]	Tensile strength [GPa]	Tensile modulus [GPa]	Electrical conductivity [S m^{-1}]	Coefficient of thermal expansion [10^{-6} °C^{-1}]	Cost [€ kg^{-1}]
First generation	Nicalon 202	Nippon Carbon	Si: 56,5 C: 31,2 O: 12,3	Oxygen	1200	14	3,0	220	0,006	3,2	1000
	Tyranno Lox M	Ube Industries	Si: 55,4 C: 32,4 O: 10,2	Oxygen	1200	11	3,3	187	2,6	3,1	1200
	Tyranno S	Ube Industries	Si: 50,4 C: 29,7 O: 17,9 Ti: 2,0	Oxygen	1200	8,5/11	3,3	170	0,9	3,1	1000
Second generation	Hi-Nicalon	Nippon Carbon	Si: 63,7 C: 35,8 O: 0,5	Electron irradiation	1300	14	2,8	270	23	3,5	3250
	Tyranno ZMI	Ube Industries	Si: 56 C: 34 O: 9 Zr: 1	Oxygen	1300	11	3,4	200	16	3,1	1400
Third generation	Hi-Nicalon S	Nippon Carbon	Si: 68,9 C: 31,3 O: 0,3	Electron irradiation	>1500	12	2,6	420	0,14	3,1	7000
	Tyranno SA3	Ube Industries	Si: 67,8 C: 35,8 O: 0,5 Al: 0,6	Oxygen	>1700	10	2,8	380	80	4,5	6500
	Sylramic	COI Ceramics	SiC: 95,7 TiB_2: 3 B_4C: 1 O: 0,3	Oxygen	>1700	7,5/10	2,7	310	100	5,4	8500

2.2.1.2. *Woven semi-finished products*

There are usually three reasons why textile fabrics are used for composite materials. Their adoption can reduce production costs, enable complex structures to be manufactured easily and increases the strength of the composite in several spatial directions. Unidirectional composite materials have a strong anisotropy and can only achieve their maximum damage tolerance in the direction of the fibres. For this reason, in most cases either fleeces, scrims, fabrics, knitted fabrics, braids or complex 3D structures are used to set up a quasi-isotropic behaviour in the component. The fabric structures show great popularity with fibre-reinforced composites due to their high strength and good drapability.

Conventional 2D fabrics consist of at least two thread systems that are crossed at right angles. The threads running in the production direction are referred to as "warp" threads and the threads running transversely thereto are referred to as "weft" threads. By crossing the warp thread with the weft thread, the two thread systems are connected to one another, and the textile fabric is held together. The final pattern obtained strongly influence fabric properties like the drapability or the shear strength. The three basic weaves are *plain*, *twill* and *satin* weave.

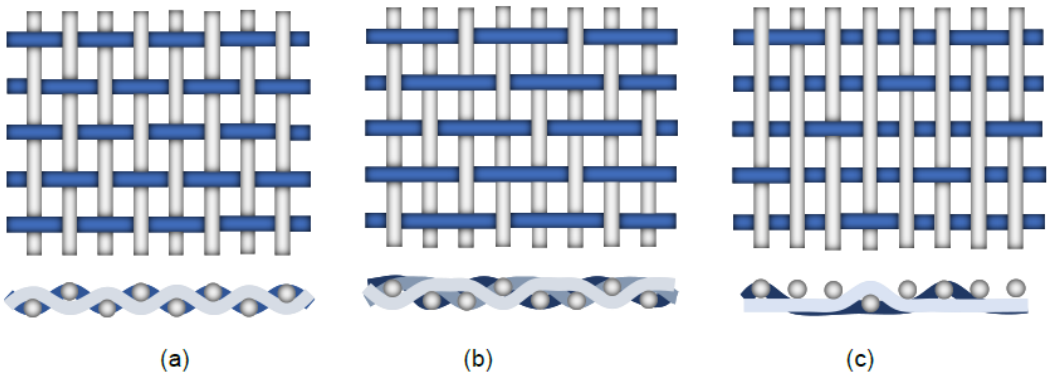

Figure 2.5 *- The three basic weaves (a) plain weave (b) twill weave (2-1 weave) (c) satin weave* [31]

The plain weave is the most used basic weave. Here each warp thread runs alternately over and under each weft thread and each weft thread under and over each warp thread. It has the highest cross density but also the strongest fibre undulations. Although this leads to a high stability of the fabric, it also leads to high losses in stiffness and strength, since full strength can be achieved as a result of the non-elongated fibre (**Figure 2.5-a**) [31].

In the twill weave, each weft thread passes under one warp thread and then over at least two weft threads, which is then repeated. The next weft shifts this rhythm by one to the side (usually to the right) and one to the top. Twill weaves come in a wide variety of designs and differ in the number of warp threads that go under one weft thread. **Figure 2.5-b** shows twill in a 2-1 weave. Depending on whether more warp or weft threads can be seen on the top, we differentiate between warp and weft twill.

The third basic weave is the satin weave. Satin bindings have a largely uniform surface and few undulations. With the atlas weave the weaving rhythm is as follows: under one warp thread, then over more than two, again under one and so on. In the next row, the pattern is shifted to the side by at least two warp threads (**Figure 2.5-c**).

2.2.2. Interface

In CMCs, the fiber-matrix interfacial domain is a decisive component affecting the ceramic matrix and fracture behaviour [6,8]. This domain may consist of an interface or an interphase, whereas the first is a surface between two phases while the latter is a film of one or several layers bonded between the fibre and the matrix through chemical or mechanical type of bonding. The fibre/matrix interfacial domain occupies an extremely large area I_A in the composite:

$$I_A = 4V_f\left(\frac{V}{d}\right) \qquad (1)$$

Where V_f is the fibre volume fraction, V is the volume of the composite and d is fibre diameter.

In the case of non-oxide CMCs, the favoured damage-tolerant fracture behaviour and high fracture toughness are achieved by a weak bonding between the fibre and the matrix [32], while this weak interface needs to be strong enough to have sufficient load sharing between fibre and matrix. This load sharing is of importance to achieve a high strength of the CMC material [33].

In non-oxide CMCs the interfacial domain is adjusted by applying coatings on the fibre [34]. Although many materials have been tested as fiber coatings, long-term stable damage-tolerant fracture behaviour in non-oxide CMCs has only been achieved by using boron nitride (BN) or pyrolytic carbon (PyC) as interphases [35]. A drawback of both materials is their limited oxidation and corrosion resistance; if the interphase corrodes via oxidation, the performance of the CMC degrades. To overcome this issue, additional layers are applied on top of the BN or PyC layers [36]. These additional layers (e.g. SiC, Si_3N_4, etc.), protect the underlying BN or PyC layer during further CMC processing and, to a limited degree, also during use of the CMC [30]. Moreover, these layers provide an additional possibility to adjust the bonding of the interface coating system to the matrix [34].

The fibre-matrix bonding must be sufficiently weak to allow the beginning of toughening mechanisms such as debonding at the interface, crack deflection, crack bridging, fibre fracture and finally fibre pullout. All these energy-absorbing phenomena leads to an enhanced fracture toughness and a pseudo-ductile behaviour of the CMC (as shown in **Figure 2.1**).

Applying the coatings on every single filament of a tow consisting of several hundreds of filaments with high quality is a great challenge. The coatings need to be homogeneous with a high degree of coverage. At the same time, bridging between the filaments needs to be avoided in order to be able to further process the coated tows by techniques such as filament winding. The fiber coatings can be applied by various techniques, among which Chemical Vapor Deposition (CVD) and Wet-chemical deposition are the most common. Advantages and disadvantages of both CVD and wet-chemical coating technologies are compared in **Table 2.3**:

***Table 2.3** - Comparison of advantages and disadvantages of coating ceramic fibres by CVD and wet-chemical coatings technology*

	CVD route	**Wet-chemical route**
Advantages	Doping of coatings relatively simple No additional pyrolysis steps necessary Relatively low thermal load on fiber No synthesis of precursors needed	High variety of material systems can be deposited Low investment costs Coating set-up simple to modify High degree of flexibility for process design High process speed and through-put possible Low maintenance costs Technology easy to upscale and to implement in industrial production
Disadvantages	Limitations in material systems that can be deposited Raw materials often expensive High investment costs for the technology Low process speeds, low through-put Complex infrastructure needed Use of corrosive gases Shrinkage, crystallization or phase transformations of the coatings during CMC processing or use possible	Modification of coating materials needs modification of synthesis of precursors Higher thermal load on fibres during pyrolysis of the coatings Limited coating thickness

2.2.3. Matrix for CMCs

One of the major voices of cost for CMCs is the generation of the matrix. The constraints, detailed in **Section 2.1** and **Section 2.2**, showed that matrices for fibre reinforced ceramics need to be specifically tailored to fulfill their role and the processing routes to achieve that goal are rather different than those employed for conventional ceramics. The latter manufacturing routes have been successfully employed to reinforce ceramic matrices using discontinuous phase (particulates, short fibres). However, those methods are rarely used when reinforcing with continuous long fibres due to mechanical damages and degradation of the reinforcement at the high sintering temperatures.

The aim of all manufacturing processes is to produce the most damage-tolerant ceramic with good mechanical properties and ideally over a wide temperature range. In contrast to polymeric composite materials, in which the matrix has a significantly lower modulus of elasticity than the fibre, these components have approximately the same stiffness in ceramic composite materials. If a crack were to arise in a component due to heavy loads, it would move smoothly

through the component with a strong fibre-matrix bond without energy-dissipative mechanisms and brittle fracture behavior would be observed.

Generally, the generation of a rigidized or densified matrix can be done following different approaches:

a) *Powder dispersion*: impregnating the long fibre reinforced preform with a suspension of matrix precursor in powder form (usually based on a slurry in the case of non-oxide CMCs), which is dried and sintered at high pressure;
b) *Infiltration processes*: where the long fibre reinforced preform is infiltrated by a fluid (gaseous or liquid) which is subsequently converted to a ceramic matrix through pyrolysis or chemical reactions;

The first approach is common of conventional fabrication of monolithic ceramics. Once the matrix powdered material is mixed with the reinforcing phase, it follows a high temperature processing step which is generally based on sintering or hot pressing.

Sintering is always accompanied by a high amount of shrinkage resulting in the subsequent formation of cracks inside the composite. This problem is even enhanced when high aspect ratio reinforcements are used since, depending on the differences among fibre/matrix thermal expansion coefficients, a hydrostatic tensile stress may develop on cooling countering the driving force of sintering (surface energy minimization) and increasing densification times [37].

Hot pressing is another of the most conventional manufacturing routes for ceramics, where the densification of the material is achieved through a simultaneous application of pressure (uniaxial or hydrostatic) and temperature. Regarding CMCs, hot pressing is particularly employed for the consolidation stage, albeit it is not suitable for the manufacturing of complex shapes. Moreover, temperatures and pressures need to be precisely balanced to avoid respectively degradation of the fibres due to possible reactions with the matrix and fibre damage.

Another variant of the latter process is the *slurry infiltration*, which is one of the most employed approaches for the production of fibre glass reinforced ceramic composites. This process is based on the impregnation of the reinforcement with a slurry, consisting on the matrix powder, a liquid carrier and an organic binder that is burnt prior to the consolidation stage. The impregnated preforms or "prepregs" are then dried, cutted to be stacked with specific arrangements depending on the final application and sintered at high pressure. The disadvantages of slurry infiltration are related to the limited range of matrix materials usable, which must be characterized by low softening temperatures with good flow properties to achieve a uniform impregnation with final low or absent residual porosity. Sintering conditions employed for SiC powders are particularly harsh ($T = 1800°C$ and $P = 10 - 50\ MPa$) which limits the use of the slurry infiltration process to high strength stoichiometric SiC fibres (Hi-Nicalon type S™ or Tyranno SA3™). Albeit this process leads to almost no residual porosity it is not suitable for volume productions.

The most employed strategy to overcome fibre degradation risks as well as damage tolerant CMC are based on infiltration processes, where the fibre structure is either impregnated with a liquid or a gas phase and then converted into a ceramic by high temperatures.

Infiltrating a porous structure by a liquid, generally based on an aqueous sol or an organometallic polymeric precursor, represents a fast and reliable way to reach nearly zero values of residual porosity also for complex CMCs shapes. The main disadvantage is that this approach is not very efficient because the subsequent volume occupied by the converted solid is

much lower than the volume occupied by the liquid, leading to multiple cycles (7 to 10) of impregnation/decomposition, thus increasing the cost.

The insertion of a porous preform inside a gaseous reactive atmosphere is another interesting approach to generate the matrix in a CMC. Even this route allows for deposition of the ceramic matrix into complex shapes with high mechanical properties but requires very low pressures to avoid premature closure of surface pores, which further increases processing times and hence the final cost. Several variants have been developed during last years based on the application of temperature or pressure gradients to favor the deposition of the matrix in the inner parts of the composite. All those strategies have the advantages of shorter infiltration times and capability to infiltrate thicker structures but are limited to simple shape components production due to the complex equipment required.

Each infiltration process presents interesting advantages/disadvantages depending on the CMC system to be treated, therefore the main manufacturing routes of industrial interest will be treated in the following section, with particular attention to CVI processing of CMCs.

2.3 Infiltration processes

CMCs reinforced with long fibers are commonly fabricated by infiltration methods, in which the ceramic matrix is formed from a fluid infiltrating into the fibre structure. These techniques differ from each other in the types of fluids and of the processes for converting the fluid into a ceramic:

- *Polymer Infiltration and Pyrolysis* (PIP): infiltration with a low viscosity preceramic organo-metallic polymer followed by pyrolysis where the polymer converts into a ceramic;
- *Reactive melt infiltration* (RMI): infiltration with a liquid metal, which converts into a ceramic by reacting with a surrounding substance;
- *Chemical vapor infiltration* (CVI): infiltration using a preceramic gaseous precursor, which yields a ceramic as a result of chemical decomposition at elevated temperature;

Some of the main advantages/disadvantages related with the various infiltration methods are summarized in **Table 2.4**:

***Table 2.4** - Advantages/disadvantages of non-oxide CMC infiltration technologies*

	CVI	PIP	LSI
Advantages	High purity matrices Low temperature (prevents fiber damage) Excellent mechanical properties	Low temperature (prevents fiber damage) Good control of microstructure and composition No free silicon in the matrix	Low cost Short production time Low residual porosity
Disadvantages	Very slow process (~ several weeks) High residual porosity (10-15%) High capital and production costs	Multiple infiltration-pyrolysis cycles High production cost High residual porosity (10-15%)	High temperature and highly corrosive metal melt (may damage fibers) Residual free silicon Lower mechanical properties Rough surfaces need machining with diamond tools

2.3.1. Polymer Infiltration and Pyrolysis (PIP)

Liquid polymer infiltration is a multi-stage process. The starting materials are a fibre preform and a preceramic polymer precursor, which is converted into a ceramic by means of a shaping process and pyrolisis. The fibre preform is infiltrated by the liquid polymer and later cooled or crosslinked under pressure depending on the matrix material. Both organic silicon polymers as

well as thermoplastic or thermoset polymers (e.g. phenolic resins, pitches) are used as the matrix. Organometallic precursors based on silicon attracted great interest during last years thanks to the possibility to be converted into a ceramic with tailored properties [38–40] for several purposes such as matrices for CMCs [41–43], ceramic fibres [15,27,44,45] and coatings [46–48].

The various precursor systems can be distinguished in terms of chemical composition into oxygen or non-oxygen containing materials. Albeit the lower cost of oxygen containing precursors as silicones (Si-C-O systems), their reduced thermal stability made them less attractive with respect to non-oxygen precursors. The latter are based on polysilanes and polycarbosilanes, which are used to produce SiC matrix, while polysilazanes and carbosilazanes reacting with boron lead respectively to SiN and SiBCN ceramics. The different chemical composition influences high temperature stability, oxidation and corrosion behavior as well as the tendency to crystallize of the resulting ceramic, while the structure and the side groups present influence the processability of the polymeric precursor. Other fundamental parameters for the choice of the precursor are the viscosity, cross-linking behavior and ceramic yield.

The most important advantages related to preceramic precursors are the low processing temperatures ($800 - 1000\,°C$) and the possibility to use the well-known polymeric working techniques. The Resin Transfer Molding (RTM), the autoclave process and hot pressing have established themselves in the PIP process due to the low curing and melting temperatures of over $180\,°C$ for the shaping step. Widely and recent used high-performance silicon-derived polymer precursors available on the market are polysilazane from KiO.N. Corp.[23] or polycarbosilanes from Starfire[24].

Following, the impregnated reinforced preform is “ceramized”, which is usually referred to as pyrolysis. In this stage the bonds of the polymer are broken at high temperatures and in the absence of oxygen, splitting off the organic side groups. As a result, there is a considerable loss of mass and volume compared to the green body with a high porosity, therefore further cycles of infiltration/pyrolysis are necessary until the desired density is achieved.

Today, the carbon fibre reinforced silicon carbide (C_f/SiC) is mainly produced via the PIP process, due to its excellent thermal and mechanical properties at high temperature, fast and low near-net-shaping cost for a limited lifetime [11].

2.3.2. Reactive melt infiltration (RMI)

The RMI process, commonly addressed as Liquid Silicon Infiltration (LSI), derived from industrial processing technologies developed for the manufacturing of SiSiC materials during 1960s. The concept was to infiltrate porous preforms made by SiC particles held together by some organic binder which were then infiltrated with molten silicon to obtain SiSiC ceramics [49]. Following, C-fibre fabrics or felts were infiltrated with the same approach to be fully converted into SiC fibres [50], but soon it was also noted that C-fibre could resist the siliconization process under inert environment achieving a composite with a pseudo-ductile fracture behavior [51,52]. Further research activities aimed at protecting the C or SiC fibres from molten silicon, ensuring a weak fibre/matrix bonding, led to several successful commercial

[23] https://www.clariant.com/en/Corporate
[24] https://www.starfiresystems.com/ceramic-forming-polymers/

applications from companies as Sigri Great Lakes Group[25] (SGL Group) and Schunk Kohlenstofftechnik[26] (SKT).

Compared to other CMC manufacturing processes, the LSI process has the shortest manufacturing time and allows a high degree of design freedom. First steps are similar to PIP with the difference that the pyrolyzed composite is subjected to a siliconization process until the final density is reached. As already mentioned, pyrolysis leads to decomposition of the polymer matrix, which results in a large decrease in volume and mass. The resulting shrinkage puts the fibres under pressure in the longitudinal direction, thus resulting in micro-cracking of the composite.

In the last process step, siliconization ($T > 1420\,°C$ under vacuum) takes place through the infiltration of liquid silicon. Here, the good properties such as low viscosity, high surface tension and good wettability of the SiC or C fibre by liquid silicon are used. The pores and cracks in the pyrolyzed body act as capillaries. As soon as the liquid silicon penetrates the capillaries, the carbon is converted to SiC. In order to implement further SiC, the free Si atoms must diffuse through the layer along the grain boundaries, while the silicon that does not react with the carbon remains in the capillary as pure silicon.

The microstructure or the SiC content in the microstructure is dependent on the open porosity and the fibre volume content. Fibre pre-treatment plays a major influence on the later microstructure of the CMC, since SiC content can be greatly increased depending on the related temperature, hence tailoring the final properties of the material.

After the presentation of the so-called Toughened Silcomp material based on coated SiC fibres [53] in 1993, General Electric (GE) continued its research on MI-SiC$_f$/SiC composites for aerospace applications producing several commercial components as combustion chamber liners, turbine shrouds and even turbine blades.

Figure 2.6 shows GE's MI main process steps. First SiC fibres are coated with CVD-BN and slurry impregnated with SiC and C particles to be wounded on a drum obtaining a unidirectional prepreg. The prepreg sheets are then stacked, compacted and densified in autoclave followed by pyrolysis to remove the organic additives and binders, and finally infiltrated with molten silicon, thus filling the pores resulting in a SiSiC matrix. Generally, it follows an additional step of coating with an EBC to enhance oxidation resistance properties.

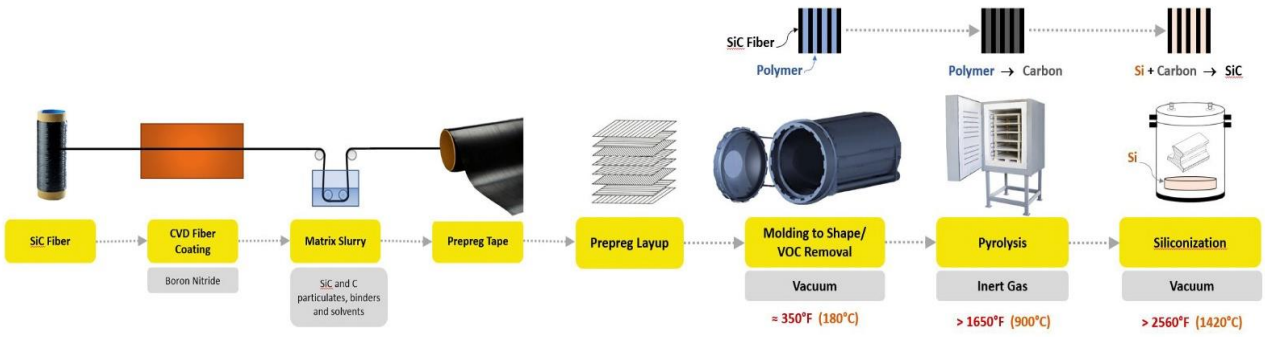

***Figure 2.6** - Process chain for SiC fiber-reinforced SiC matrix composites. The final step is melt infiltration (MI) of liquid silicon into the carbonized composite preform to form the densified SiC$_f$/SiC ceramic composite* [54]

[25] https://www.sglcarbon.com/en/
[26] https://www.schunk-group.com/en/schunk

2.4 Chemical Vapor Infiltration (CVI)

The Chemical Vapor Infiltration (CVI) is a process where a porous preform is infiltrated by a ceramic gaseous precursor which is then thermally decomposed to a ceramic material through chemical reactions on fibre surfaces, thus filling the pore network and densifying the composite. The main advantages of the CVI are the possibility to manufacture complex near-net-shape components at relatively low temperatures and pressures, deposition of a stoichiometric matrix with fine control of the related microstructure, leading to tough and strong composites with good erosion, corrosion and wear resistance properties. Despite of those advantages, the main drawbacks are the long manufacturing times, of the order of several weeks, and the run-to-run reproducibility which severely limits the usage of this technology [55].

First studies on CVI started during 1960s by Bickerdyke [56] aiming at densifying porous carbon structures, while first industrial and commercial applications were achieved during 1980s by Societé Europeènne de Propulsion (SEP, now SNECMA[27]) and Du Pont (USA), thanks to the possibility to manufacture several complex shape components simultaneously through the development of the Isothermal-Isobaric CVI (I-CVI) process. The CVI technology derived from the Chemical Vapor Deposition (CVD) process, used for several applications to deposit thin layers on different substrates (metals, ceramics, semiconductors). In fact, along the CVI process the interphase and the matrix can be successively deposited on the fibre network of the preform.

The importance of the deposition of interphase for CMCs, as SiC_f/SiC composites, was explained in the previous sections. Despite the reduced oxidation resistance of PyC interphases [57], which degrade above 500 °C, previous studies have shown that SiC_f/SiC composites coated with single/multi-layer PyC interphases exhibited increased lifetime with respect to BN coatings produced by CVD/CVI [58,59].

Different hydrocarbons can be used for PyC deposition, which can be distinguished in order of increasing reactivity as: CH_4, C_2H_6, C_2H_4, C_3H_8, C_3H_6, C_2H_2 [60–62]. The surface area is shown to decisively influence the chemistry and kinetics of deposition reactions and thus also the major growth species of PyC [63].

As well as the other infiltration processes described, the main purpose of the CVI process is to increase the density to a factor going from 2-10, depending on the final application. Regarding the deposition of ceramic materials different related precursors, generally based on halides or organometallic species are available, whose overall chemical reactions are reported in **Table 2.5**:

Table 2.5 *- Examples of overall chemical reactions commonly used for the formation of ceramics by CVD/CVI* [64]

$$CH_{4(g)} \rightarrow C_{(s)} + 2H_{2(g)}$$

$$CH_3SiCl_{3(g)} \xrightarrow{H_2} SiC_{(s)} + 3HCl$$

$$CH_{4(g)} + 4BCl_{3(g)} + 4H_{2(g)} \rightarrow B_4C_{(s)} + 12HCl_{(g)}$$

$$BCl_{3(g)} + \frac{3}{2}H_{2(g)} \rightarrow B_{(s)} + 3HCl_{(g)}$$

$$2AlCl_{3(g)} + 3CO_{2(g)} + 3H_{2(g)} \rightarrow Al_2O_{3(s)} + 6HCl_{(g)} + 3CO_{(g)}$$

[27] https://www.safran-group.com/media/20121001_snecma-preparing-engines-tomorrows-aircraft

$$ZrCl_{4(g)} + 2CO_{2(g)} + 2H_{2(g)} \rightarrow ZrO_{2(s)} + 4HCl_{(g)} + 2CO_{(g)}$$
$$CH_{4(g)} + TiCl_{4(g)} \xrightarrow{H_2} TiC_{(s)} + 4HCl_{(g)}$$
$$BCl_{3(g)} + NH_{3(g)} \rightarrow BN_{(s)} + 3HF_{(g)}$$
$$3SiCl_{4(g)} + 4NH_{3(g)} \rightarrow Si_3N_{4(s)} + 12HCl_{(g)}$$
$$TiCl_{4(g)} + 2SiCl_{4(g)} + 6H_{2(g)} \rightarrow TiSi_{2(s)} + 12HCl_{(g)}$$
$$TiCl_{4(g)} + 2BCl_{3(g)} + 5H_{2(g)} \rightarrow TiB_{2(s)} + 10HCl_{(g)}$$

The chemical reactions leading to the deposition of the desired ceramic species usually are not that simple, due to the formation of several reaction intermediates and by-products which could reduce the yield of the solid deposited. A thermodynamic approach allow for a first selection of the operating parameters, assuming that equilibrium is reached, resulting in conditions as those shown in **Figure 2.7** for the H_2/CH_3SiCl_3 (methyltrichlorosilane – MTS) system, used for the deposition of SiC:

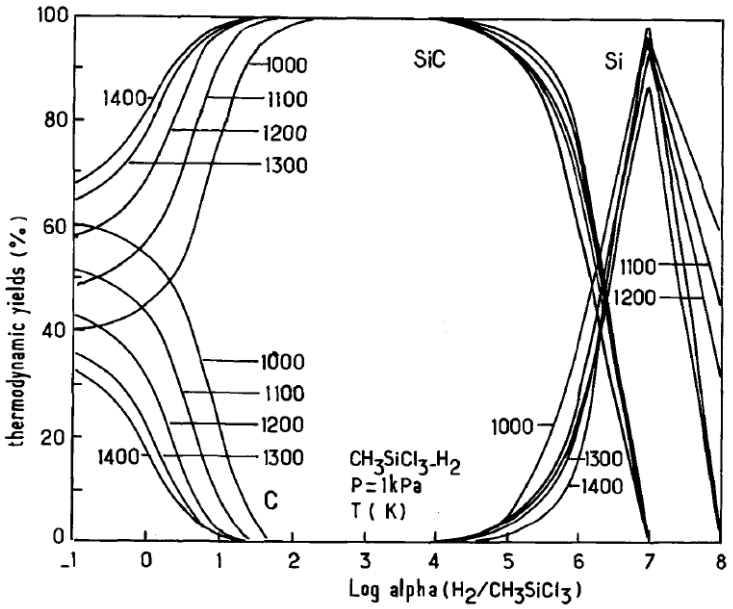

***Figure 2.7** - CH_3SiCl_3/H_2 CVD/CVI system. Calculated thermodynamic yields for the solid phases, as a function of $a = [H_2]/[MTS]$ for various temperatures* [65]

CVI could ideally be able of infiltrating any porous system but some requirements need to be previously fulfilled:

- The pores need to be interconnected with a sufficient diameter;
- Operating conditions must be chosen avoiding both thermal and chemical instabilities of the reinforcement during CVI;

Moreover, the experimental conditions must be chosen to favour in-depth deposition avoiding premature occlusion of surface pores. Preforms used for the CVI process are usually based on cloths or 2D-fabric layers stacked and kept together by using specific tools to achieve the desired shape. Two ranges of porosity are present inside a typical CVI preform, which influence the gas diffusion mechanism:

- Intratow porosity: located between single fibres, with dimensions going from $1 - 10\ \mu m$;
- Intertow porosity: located between fibre bundles and cloth layers, characterized by larger dimensions going from $50 - 500\ \mu m$;

Along the I-CVI process there are not any pressure or temperature gradients, therefore the deposition of the ceramic layer can be described according to five different steps, reproduced in **Figure 2.8**:

i. Diffusion of the source species through a boundary layer surrounding the substrates;
ii. Diffusion of the reactants along the pore length to reach the inner parts of the preform;
iii. Adsorption of the reagents on the surface and reaction leading to the deposition of the desired ceramic layer on the surface;
iv. Desorption of the gaseous by-products from the surface along the pore length;
v. Diffusion of the gaseous by-products through the external boundary layer;

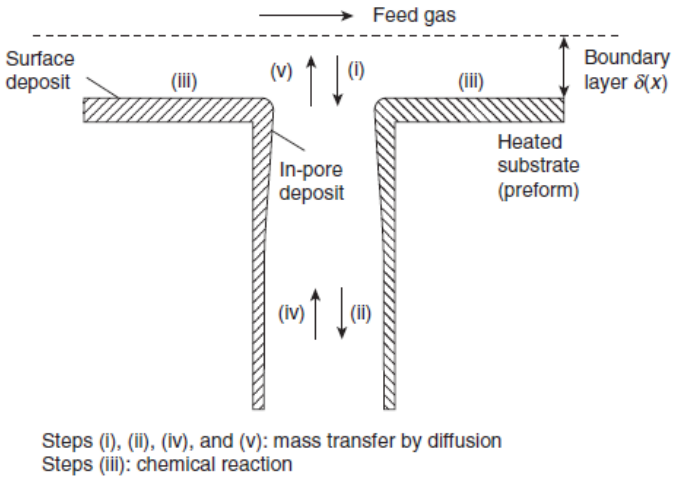

***Figure 2.8** - The different steps in the I-CVI process* [55] *(adapted from* [64]*)*

Differently from CVD processes, two additional steps have been considered to illustrate the I-CVI technology, namely 2) and 4). While steps 1), 2), 4) and 5) are mass-diffusion controlled, step 3) is a surface-controlled phenomenon hence, to favour in-depth deposition, operating parameters must be properly chosen in a way that the latter should be the rate-limiting step. The missing fulfilment of this condition will result in the preferential deposition of the ceramic layer on external pore surfaces resulting in their premature sealing and not being able of further densify the material.

The activation of chemical reactions on the inner preform surfaces rely on heating mechanisms, but also plasma or laser induced approaches are reported in literature [66]. For the majority of inorganic species, preforms are heated to temperatures around $900 - 1200\,°C$. Many studies have dealt with the modelling of surface phenomena to describe the dynamic of the CVI layer deposition inside the porous network of the preform. Three different scales need to be considered:

- Macroscale: where all the reactor filled with a homogeneous preform is considered;
- Mesoscale: where the preform structure (texture, stacking) is precisely defined to describe its evolution along the infiltration process;
- Microscale: being characteristic of chemical phenomena;

Early modelling activities reduced preform porous domain to a 1-D or 2-D single-pore problem without considering any complex reaction mechanism, temperature gradient, evolution of the porous medium and so on. Optimized temperature and pressure programs yielding the highest in-depth deposition rates have been suggested giving important hints on the influence of processing parameters on the process efficiency [67,68].

Realistic models need to account for diffusion and surface mechanisms along with preform structure change and evolution during the densification process, which further complicates the underlying modelling since it requires the application of a multi-scale approach from process to atomic scale [69,70]. Complex 3-D porous structures can be investigated by X-ray computerized microtomography, obtaining useful information that can be employed to compute effective transport properties [71].

Regarding the deposition of SiC matrix, the ceramic precursor commonly adopted is the MTS, whose overall chemical reaction was previously shown in **Table 2.5**:

$$CH_3SiCl_{3(g)} \overset{H_2}{\rightarrow} SiC_{(s)} + 3HCl \qquad (2)$$

Previous studies reported that MTS is an ideal precursor for the deposition of high-quality beta-silicon carbide ($\beta - SiC$) [72]. The reasons behind this are [73]:

- The Si:C ratio in MTS is the same as the Si:C ratio of the SiC deposit;
- The by-product HCl derived using MTS as a precursor might contribute suppressing the deposition of pure Si crystal during the growth of SiC films or crystals;
- The H_2 carrier gas may favour the reduction of the Si – Cl bonds on the growing surface of SiC, thus resulting in an increase in deposition rate;

The deposition quality of SiC depends on three parameters, namely the pressure, temperature and volume ratio of reactants $\alpha = P_{H_2}/P_{MTS} = Q_{H_2}/Q_{MTS}$ [74]. Preferential deposition of SiC, with respect to C, occurs when using values of $\alpha > 20$ [75]. Lower values of the latter lead to carbon-rich deposits while higher values lead to silicon-rich deposits, therefore values of $\alpha = 5 - 10$ are commonly employed due to kinetic factors [76].

Regarding operating conditions, the use of high temperatures and pressures allow to achieve higher deposition rates but lead to a reduction of the penetration depth of the products with crusting phenomena. In-depth deposition is instead favoured by lower temperatures and pressures, whose effects on the resulting thickness of the ceramic layer deposited are shown in **Figure 2.9**:

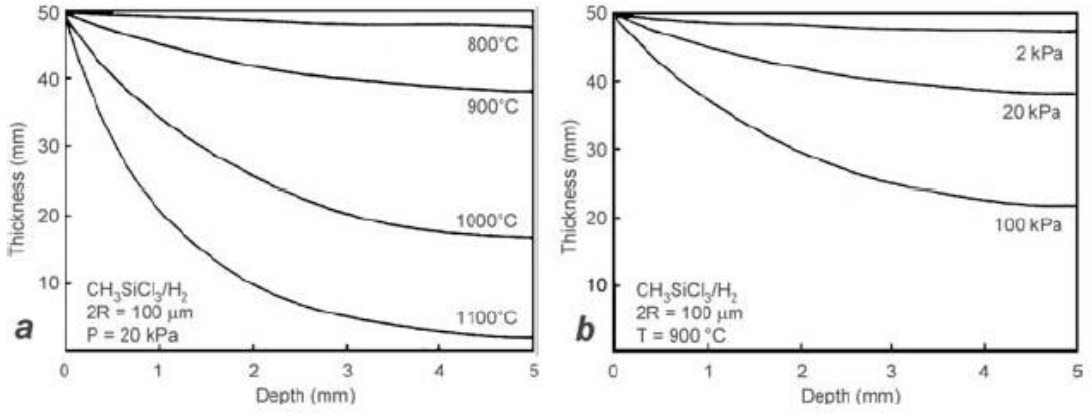

***Figure 2.9** - (a) Thickness of SiC deposition in a pore with a diameter of 100 microns for different temperatures at 20 kPa pressure; (b) for different pressures at 900 °C* [74] *(adapted from* [64]*)*

Lower temperatures and pressures increase the mean free path of gaseous species which can reach easily the inner parts of the preform. Moreover, the use of low pressures eliminates the hydrodynamic boundary layer (see **Figure 2.8**), thus making surface reactants decomposition phenomena the deposition rate determining factor [77].

2.4.1. Variants of the CVI process

Commonly CVI processes can be distinguished depending on the heating method (inductive, radiative, plasma or MW-assisted) and the presence/absence of temperature or pressure gradients inside the reactor. All of those methods are at different levels of technological and industrial maturity [78]; usually data on particular processes are also unpublished or unavailable.

Thanks to its capacity to infiltrate simultaneously several complex shaped preforms, the I-CVI was the first industrially well-established CVI process. In this process the preform is placed inside a special isothermal-isobaric reactor with the gaseous precursors which flows outside the preform by convection and inside by diffusion [79] (see **Figure 2.10**); operating parameter values are chosen in order to avoid the premature occlusion of surface pores which generally leads to temperatures around $1000\,°C$ and pressures below $100\,mbar$, thus resulting in an uneconomically slow process with reduced deposition yield rates. Moreover, sample thickness is limited to $\sim 5\,mm$ otherwise two or more infiltration steps are required to be able to densify higher thicknesses preforms.

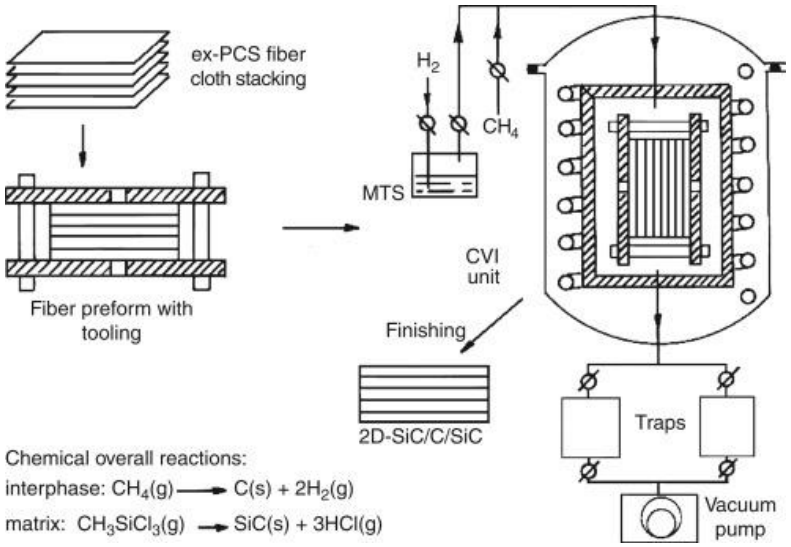

***Figure 2.10** - Principle of I-CVI processing of 2D fiber SiC matrix composites* [79]

Fitzer and Gadow [80] conducted a study to determine the optimal infiltration condition for a SiC_f/SiC Nicalon™ based preform of $4 * 5 * 50\,mm$ with a fibre volume fraction around $40 - 50\,vol\%$. The above mentioned preform was infiltrated at a temperature of $1047\,°C$ and a pressure of $30\,mbar$, resulting in a total infiltration time of 14 days.

Currently the I-CVI process is used mostly for the production of SiC_f/SiC as aerospace components [10] and C_f/C composites as aircraft brakes [81]. Other matrices commonly deposited by this process are [64]: SiC, C, Si_3N_4, BN, Al_2O_3, B_4C, TiC and ZrO_2.

The other variants of the CVI process were born with the idea of overcoming the drawbacks discussed as the long manufacturing times and premature pore closure. The use of a gradient or forced CVI (F-CVI) process [82] allows for the penetration of the gaseous precursors not only by diffusion but also by the development of pressure gradients inside the preforms (see **Figure 2.11**). This process has been studied both in isothermal and thermal gradient conditions to enhance material quality and processing time.

The application of a thermal gradient through the wall thickness was applied to avoid a faster deposition on the external surface. Following this approach, the SiC deposition rate starts from the hotter outlet side to the colder inlet side and proceeds with this profile along the infiltration process due to the increased thermal conductivity. When the densification on the hotter outlet side is completed the infiltration proceeds to completion as it can now penetrate in the preform only on the colder inlet side. In this way the total infiltration time can be reduced to few days.

The temperature difference is one of the most important controlling parameters for the F-CVI process since its tailoring results in the desired deposition profile inside the preform [83], however the control of the densification front is not trivial and could result in undesired density gradients. Another determining parameter is the total flow rate which must be balanced to achieve a uniform deposition of the matrix [84]. The pressure difference, necessary to achieve the required forced flow inside the preform, depends on the pore geometry and spectrum.

Modelling investigations showed how the densification front depends from the established temperature gradient [85,86]. Analytical results suggested that an initial minimal heat flux is necessary in order to start the infiltration reaction which then needs to be finely controlled until it settles to reduce energy wastes and achieve maximal uniform density.

As a result, total infiltration times for F-CVI processes the order of 10-24 hours for SiC matrixes and few hours for C matrixes [87] have been achieved. Additionally, this method allows the infiltration of preforms with dimensions of the order of 30 cm in width and 2,5 cm in thickness [88]. The maximum temperature values limit the choice of the most suited fibres to avoid their thermal and subsequently mechanical properties degradation.

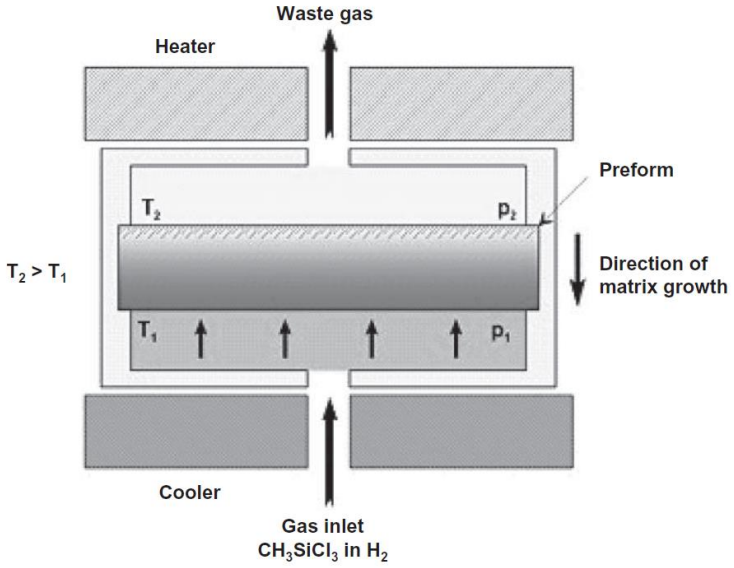

Figure 2.11 *- Scheme of a gradient CVI process* [74]

Another variant of the CVI process is the Pulsed flow CVI (P-CVI) [89], where the reactor loaded with the preform is first evacuated by pumping and then the reactants are quickly injected into the reaction chamber. This approach was investigated to overcome the above described drawbacks of the I-CVI and to obtain newly engineered CMCs. The P-CVI process is based on a cyclical feed of fresh reactants to be introduced when the reaction products are removed, thus allowing a simple way to control the residence time of the reactants inside the preform. Moreover, this method allows for the deposition of multi-layered ceramic deposits changing the precursors along the process. The usage of big furnaces as well as the pumping of large amounts

of gases are the liabilities which resulted in technical problems in the industrial transfer of this technology.

Other interesting solutions are the so-called "Rapid-CVI" routes which can be distinguished into two different methods. The first variant is the film-boiling technique where a porous fiber preform, acting as susceptor, is immersed into the liquid state precursor which is then inductively heated to infiltrate in the vapour phase the material. This method is particularly suited for C_f/C due to the high carbon yield of the precursors usually employed (cyclohexane or toluene) which results in a single densification cycle of few hours [90]. Among the main drawbacks of this process there are the strong energy consumption, due to the usage of extreme temperature gradients, and the requirement of handling flammable liquids together with a strong energy source.

The second technique is the rapid vapor-phase densification, developed and patented by CVT[28], where the porous preform is placed in a furnace, isothermally heated through an outer graphite tool which imposes also a forced flow of the gaseous precursor between them [61,91].

Both Rapid-CVI methods, being in a kinetic regime where the rate-limiting step is not the diffusion of gaseous species inside the preform (as in conventional CVI) but the kinetics of surface reactions, display some distinctive advantages in terms of higher conversion efficiency and good product quality.

The use of CVI methods employing pressure/temperature gradients leads to significant processing time reductions but also inhomogeneous densification patterns and more complex setup [78,92]. Therefore, great research efforts have been dedicated in the last years to the development of improved variants of the CVI process to yield rapid and complete densification of CMCs.

2.4.2. Microwave-assisted CVI process

In microwave-assisted CVI (MW-CVI) process, the sample heating is obtained by means of a high-power MW irradiation, which releases energy in the sample through its dielectric absorption. This approach enables a volumetric heating of the sample, whose speed is basically limited only by the available MW power. Moreover, the combination of volumetric heating with the thermal irradiation of the sample surface towards the colder walls of the reactor, results in an inverse temperature profile in the sample. The fast and selective heating mechanism coupled with the inverse temperature profile was exploited in order to overcome some of the main technological issues of conventional CVI, as the premature pore closure, in order to decrease processing times with reduced residual porosities.

First research activities on MW-CVI started during the 1990s, where a 700 W multimode cavity operating around 2,45 GHz was employed to infiltrate preforms based on 10 circular SiC-Nicalon stacked cloths, each having a diameter of 7 cm [93]. SiC inside-out deposition was confirmed, according to the expected inverse temperature profile, although with an inhomogeneous heating pattern and thus different degrees of matrix infiltration into the preform. In addition, silicon (Si) co-deposition was observed showing the importance in the precise control of the established

[28] https://www.cv-technology.com/en/chemical-vapor-infiltration/

temperature profile while the relatively low operating pressures ($< 400\ mbar$) led to plasma formation phenomena, depending on the MW power density and gaseous reaction environment.

Further works proved the applicability of MW-CVI process for the densification of different ceramic systems. Based on previous results, infiltration tests of SiC-Nicalon cloths (stack of 10 circular laminae with 5 cm diameter) with a Si_3N_4 matrix have been carried out using a 1300 W multimode cavity operating around 2,45 GHz [94]. Processing conditions (operating pressure, infiltration temperature and flow reagents) have been adjusted obtaining the desired inverse densification pattern. In this work the influence of a PyC interphase ($10 - 20\ \mu m$ thick) on SiC-Nicalon fibres was investigated as well showing a small impact on the effective preform MW energy absorption, although more detailed analysis had been scheduled.

More recent investigations on SiC_f/SiC components (50 mm diameter, 10 mm thick) have been carried out using a F-CVI system with MW heating, thus showing that fabrication times can be reduced from hundreds of hours to around 100 hours [95]. In this work a 5 kW multimode applicator operating around 2,45 GHz, equipped with a mode-stirrer to minimize hotspots formation, was employed. The treated samples analysis showed an efficient filling of intratow porosity although intertow infiltration flattened out after few hours as the densification front moved outward from the centre of the preform. The latter issue was dealt with by pre-impregnating the preforms with SiC slurries through a vacuum bagging or electrophoretic impregnation technique [96]. The effectiveness of those solutions was proved by the higher infiltration levels reached, although non-uniform matrix deposition was observed due to the inhomogeneous SiC powder distribution into the preform.

Experimental MW-CVI activities on $Al_2O_3/\alpha - Al_2O_3$ systems yielded the same inside-out densification profile [97]. In this case, a 3 kW single mode cavity operating around 2,45 GHz was used to infiltrate uniaxial fibre reinforced preforms having a diameter of 16 mm and a length between $80 - 120\ mm$. A carbon coating was applied to the preform in order to help initial MW heating. The starting operating frequency was set to excite a perturbed TM_{012} in order to obtain a radial thermal gradient in the preform, showing the possibility to tune a specific matrix deposition pattern by manipulation of the heating and flow parameters.

Alumina MW transparency at low temperature presented more difficulties to be properly heated. Therefore, hybrid MW heating approaches implementing conventional systems or surrounding the sample of interest with a lossy susceptor material have been investigated. Skamser et al. [98] employed an external Sr-doped lanthanum chromite layer to heat alumina-based preforms at 1100°C, due to its higher electrical conductivity and oxidation resistance at high temperatures, thus avoiding the development of thermal instabilities (thermal runaway) typically displayed by low loss dielectric materials.

The above cited works showed the importance of tuning suitable thermal gradients into the preforms to be infiltrated in order to control matrix composition and microstructure as well as the deposition profile. In fact, the temperature difference between the centre and the surface of the component can be up to several hundred degrees centigrade, taking into account the high efficiency of the thermal irradiation, governed by a T^4 dependence.

Accordingly, Day et al. [99] reported a decrease of SiC deposition rates with increasing temperature during MW-CVI processing of SiC_f/SiC; optical micrographs at an infiltration temperature of 975°C displayed a higher degree of closed porosity, with respect to a similar sample treated at 900°C, due to the faster deposition kinetics which resulted in a lower accessible preform surface area.

Several modelling activities have been carried out to highlight the physicochemical phenomena governing the MW-CVI process and to provide useful guidelines for the design of the reactor. Gupta and Evans [100] investigated first the impact of a volumetric heating with external cooling on the CVI of SiC-based composites, by using a simplified model of the sample structure based on a one dimensional single-pore slab-like preform. The heat generation rate has been computed from the electric power density deposited by solving the electromagnetic equations coupled with appropriate boundary conditions (e.g. continuity of tangential component of electric and magnetic field). The resulting temperature profile was then employed to solve transport and chemical reaction equations considering an initial uniform pore radius.

Computed results confirmed the expected inverse temperature profile and its sensitivity from preform thickness and position into the cavity. The usage of a MW heating with external cooling resulted in a quicker infiltration rate with lower residual porosity values with respect to the isothermal case. The weak temperature dependence of Knudsen diffusive regime for a pore radius of 1 μm resulted in a higher residual porosity. Moreover, for an initial pore radius of 3 μm, the deposition rate was also influenced by the heat transfer coefficient (which includes both the radiative and convective components). Nevertheless, the above mentioned model did not account for the transient nature of composite temperature along the densification and it assumed that the thermal and dielectric properties were independent from the degree of infiltration in order to uncouple heat generation/transport equations from mass diffusion/reaction relations.

Differently, Morell et al. [101] developed a mathematical model to analyse the MW-CVI process of a carbon-based cylindrical preform reinforced with carbon fibres, where the change of all material properties along the densification with temperature, pressure, composition and porosity have been accounted. In addition, since among the critical aspects necessary to provide a comprehensive description of any CVI process there is the need to incorporate fibre architecture and its evolution into the mathematical model, effective Knudsen diffusion coefficient, permeability coefficient and accessible porosity, as a function of the total porosity (obtained from previous studies [102,103]), have been used to characterize the composite structure where each of these parameters depended on temperature, pressure and gaseous mixture. Specifically, in this work the authors focused more on the effect of novel preform heating methods as by microwaves, therefore a simplified chemical kinetic was considered.

The results suggested that the MW power level had a significant influence on the densification uniformity and processing time showing the appearance of a minimum in the porosity profile beyond a critical amount, thus hindering the further penetration of gaseous reagents into the preform. This outcome can be mitigated by the usage of lower operating pressures, since they lead to higher gas diffusivities and therefore higher mass-transport rates, or through the application of specific power-modulation schemes.

Accordingly, two follow-up studies have been subsequently published by Morell et al. [104,105] proposing the usage of a pulsed power MW-CVI process to improve the matrix deposition uniformity while reducing processing times. The development of thermal stresses due to temperature gradients was also considered in those works assuming a plane stress problem (the width of the sample is considered much smaller than its height and length). As a result, the inverse temperature profile led to the development of tensile stresses on the external surface (larger in magnitude) and compressive stresses in the core. Furthermore, stress distribution was affected by preform thickness due to the decrease of MW power density closer to the external surface, thus resulting in an opposite temperature profile.

A different approach was followed by Tilley et al. [106] that modelled the MW-CVI process as a moving-boundary problem using asymptotic techniques in order to account for the variation of

processing parameters along the infiltration. A one-dimensional model was employed for SiC-CVI of an Al_2O_3 fibre-reinforced preform, due to the disparate electrical and thermal conductivities which allowed to decouple the respective physical problems. The latter hypothesis was introduced based on previous works by Pelesko et al. which investigated the heating of the respective preform and substrate, in the absence of chemical reactions, verifying that, when the square ratio of the thermal conductivities are proportional to the ratio of the electrical conductivities, the thermal and electrical problems decouple [107]. The boundary was represented by the interface between the unreacted and the processed region, which changes its position as a function of time, and it stops simultaneously when the model loses its asymptotic validity and the gas inlet pore closes. Specifically, a threshold power level necessary to reach the critical temperature where reactions occur was identified. It was also observed that increasing the preform thickness the skin depth decreases thus reducing the MW power level necessary although at the expense of the dimension of the heated region.

The above reported works proved that by means of the MW-CVI process matrices of high purity and density can be obtained and preforms of complex geometry can be successfully infiltrated at operating temperatures between 900 and 1200°C. Since the pressure required by the process is low (1-100 kPa), the damaging of fibres and their reactions with the matrix are limited and the processing times can be significantly reduced as for the other CVI variants discussed in the previous paragraph.

2.5 Conclusions

CMCs are designed to overcome the main drawbacks of brittle monolithic ceramics while displaying all their benefits as their high temperature mechanical properties in severe environments. The high fixed cost of ceramic fibres, in particular for SiC-based ones, always demands for the development of more cost-efficient matrix manufacturing routes.

In this chapter a general review about CMCs materials has been carried out discussing their properties and manufacturing technologies to highlight the related advantages and disadvantages.

Besides the well-established CVI, PIP, RMI infiltration technologies, other interesting variants as the thermal/pressure gradients or film-boiling routes are being continuously improved and researched. Moreover, hybrid approaches combining at least two manufacturing processes are considered to complement the disadvantages of one technology with the advantages of another, shortening processing times and further improving product quality.

Regarding the CVI process, the I-CVI variant has the advantage of great flexibility with the possibility of infiltrating simultaneously several complex shaped preforms while the main drawbacks are the too long manufacturing times, due to premature pore plugging, and limits in maximum values of thickness that can be infiltrated in one step. Albeit the F-CVI process is characterized by reduced manufacturing times around one order of magnitude with the capability of infiltrating preforms with thickness up to $3\,cm$, the employed reactors required quite complex tools to develop both pressure and temperature gradients inside the preform which limits the infiltration to one simple shaped component (e.g. plates and tubes) at a time.

Especially in the case of new densification technologies, great efforts have been dedicated to develop simpler, economic and more efficient approaches. Even if they exhibit reduced flexibility with respect to conventional industrial technologies (I-CVI, LSI) they could provide important advantages for specific matrix compositions and/or application fields provided to develop methodologies for the scale-up of the technology.

In this framework, the usage of a MW-CVI process can be an interesting solution due to its potential for generating a controllable temperature profile in the preform of interest. Based on the above state-of-the-art analysis, several critical points have been identified:

- MW cavity design quality determines the actual MW power losses in the sample and thus the resulting energy efficiencies. Lab-scale MW cavities considered in the cited works were based on single/multimode cavities using magnetron sources operating around $2{,}45\,GHz$. The latter devices lack of precise frequency and thus excited mode control. As a consequence, the design of the MW cavity should be very carefully conducted in order to provide a sufficiently robust behaviour along the whole infiltration process. Advantages and disadvantages deriving from the choice of a particular cavity will be properly addressed in **Chapter 3**.
- The achievement of an inside-out densification was proved by all works reported, although some samples displayed an inhomogeneous deposition pattern. As for F-CVI processes, matrix infiltration uniformity depends from the temperature front established along the infiltration. Therefore, precise knowledge and control of the EM field is necessary to achieve a high-quality product. MW power coupled to the sample should be enough to guarantee the activation of inside-out SiC deposition reaction while avoiding hotspots formation, which could result in several issues as reinforcement degradation,

plasma formation and co-deposition of silicon, the latter leading to a non-stoichiometric matrix with a different MW absorption behaviour.

- The presence of an interphase coating on the reinforcement influence the resulting MW absorption properties of the preform. Therefore, it needs to be explored in detail due to its influence on the mechanical behaviour characteristic of non-oxide CMCs.
- The results suggested that, in order to control matrix composition and uniformity, precise power modulation or variation schemes can be useful. In particular, the power needed to be continuously increased to maintain the desired heating rate, overcoming in some cases the limitations imposed by the available sources.
- Experimental temperature preform information have been obtained usually by pyrometers, although they provide information limited to the sample surface. On the other hand, numerical modelling can provide important feedbacks on the inverse temperature profile resulting from a certain MW power input, in order to finely control the final matrix composition. The precision of these investigations require a reliable knowledge about dielectric and thermal properties as a function of the temperature and density level. The further integration of those properties into models which consider also the evolution of the porous medium structure along the infiltration will provide additional hints on processing parameters influence and optimization.

2.6 References

[1] Kim J. Tensile fracture behavior and characterization of ceramic matrix composites. Materials (Basel). 2019;12:5–8.

[2] Parlier M, Ritti M-H, Jankowiak a. Potential and Perspectives for Oxide / Oxide Composites. J. AerospaceLab. 2011;1–12.

[3] Chawla KK. Ceramic Matrix Composites. Compos. Mater. Sci. Eng. 4th ed. Birmingham, AL, USA: Springer; 2019. p. 251–295.

[4] Carter CB, Norton MG. Shaping and forming. Ceram. Mater. Sci. Eng. 2nd ed. New York: Springer-Verlag; 2013. p. 423–435.

[5] Ruggles-Wrenn MB. Ceramic and Carbon Matrix Composites. In: Zweben CH, Beaumont P, editors. Compr. Compos. Mater. II. 2nd ed. Ohio, USA: Elsevier; 2017. p. 4288.

[6] Naslain RR. The design of the fibre-matrix interfacial zone in ceramic matrix composites. Compos. Part A Appl. Sci. Manuf. [Internet]. 1998;29:1145–1155. Available from: http://www.sciencedirect.com/science/article/pii/S1359835X97001280.

[7] Majidi AP. Whiskers and Particulates. In: Zweben CH, Beaumont P, editors. Compr. Compos. Mater. II. Elsevier; 2017. p. 175–198.

[8] Lamon J. Influence of Interfaces and Interphases on the Mechanical Behavior of Fiber-Reinforced Ceramic Matrix Composites. Ceram. Matrix Compos. [Internet]. John Wiley & Sons, Ltd; 2014. p. 40–64. Available from: https://onlinelibrary.wiley.com/doi/abs/10.1002/9781118832998.ch3.

[9] Raether F. Ceramic Matrix Composites – an Alternative for Challenging Construction Tasks. Ceram. Appl. 2013;1:45–49.

[10] Lamon J. Chemical Vapor Infiltrated SiC/SiC composites (CVI SiC/SiC). In: Bansal NP, editor. Handb. Ceram. Compos. Boston: Springer; 2005. p. 55–76.

[11] Krenkel W. Carbon Fibre Reinforced Silicon Carbide Composites. In: Bansal NP, editor. Handb. Ceram. Compos. Boston: Springer; 2005. p. 117–148.

[12] Clauß B. Fibers for Ceramic Matrix Composites. In: Prof. Dr.-Ing. Walter Krenkel, editor. Ceram. Matrix Compos. Fiber Reinf. Ceram. their Appl. Weinheim: Wiley-VCH; 2008. p. 1–20.

[13] Lamon J. Review: creep of fibre-reinforced ceramic matrix composites. Int. Mater. Rev. [Internet]. 2020;65:28–62. Available from: https://doi.org/10.1080/09506608.2018.1564182.

[14] Chollon G, Pailler R, Naslain R, et al. Correlation between microstructure and mechanical behaviour at high temperatures of a SiC fibre with a low oxygen content (Hi-Nicalon). J. Mater. Sci. 1997;32:1133–1147.

[15] Schawaller D, Clauß B, Buchmeiser MR. Ceramic filament fibers - A review. Macromol. Mater. Eng. 2012;297:502–522.

[16] Yajima S, Okamura K, Hayashi J, et al. Synthesis of Continuous Sic Fibers with High Tensile Strength. J. Am. Ceram. Soc. 1976;59:324–327.

[17] Simon G, Bunsell AR. Mechanical and structural characterization of the Nicalon silicon carbide fibre. J. Mater. Sci. 1984;19:3649–3657.

[18] Ichikawa H, Hayase T, Nagata Y, et al. Strength and Structure of SiC Fiber after Exposure at High Temperatures. J. Soc. Mater. Sci. Japan. 1987;

[19] Toreki W, Batich CD, Sacks MD, et al. Polymer-derived silicon carbide fibers with low oxygen content and improved thermomechanical stability. Compos. Sci. Technol. 1994;51:145–159.

[20] Chollon G, Pailler R, Naslain R, et al. Thermal stability of a PCS-derived SiC fibre with a low oxygen content (Hi-Nicalon). J. Mater. Sci. 1997;32:327–347.

[21] Pailler R, Lamon J, Guette A, et al. Non-oxide ceramic fibres: relationships between nanostructure or composition and properties. Ann. Chim. des Mater. Paris, France: Elsevier; 2005. p. 565–578.

[22] Shimoo T, Katase Y, Okamura K, et al. Carbon elimination by heat-treatment in hydrogen and its effect on thermal stability of polycarbosilane-derived silicon carbide fibers. J. Mater. Sci. 2004;39:6243–6251.

[23] Bunsell AR, Piant A. A review of the development of three generations of small diameter silicon carbide fibres. J. Mater. Sci. 2006;41:823–839.

[24] Shimoo T, Okamura K, Mutoh W. Oxidation behavior and mechanical properties of low-oxygen SiC fibers prepared by vacuum heat-treatment of electron-beam-cured poly(carbosilane) precursor. J. Mater. Sci. 2003;38:1653–1660.

[25] Takeda M, Urano A, Sakamoto JI, et al. Microstructure and oxidative degradation behavior of silicon carbide fiber Hi-Nicalon type S. J. Nucl. Mater. 1998;258–263:1594–1599.

[26] DiCarlo JA, Yun H-M. Non-oxide (Silicon Carbide) Fibers. In: Bansal NP, editor. Handb. Ceram. Compos. Boston, MA: Springer US; 2005. p. 33–52.

[27] Colombo P, Mera G, Riedel R, et al. Polymer-derived ceramics: 40 Years of research and innovation in advanced ceramics. J. Am. Ceram. Soc. 2010. p. 1805–1837.

[28] Flores O, Bordia RK, Nestler D, et al. Ceramic fibers based on SiC and SiCN systems: Current research, development, and commercial status. Adv. Eng. Mater. 2014;16:621–636.

[29] Peuckert M, Vaahs T, Brück M. Ceramics from organometallic polymers. Adv. Mater. 1990;2:398–404.

[30] Dicarlo JA. Advances in SiC/SiC composites for aero-propulsion. In: Bansal NP, Lamon J, editors. Ceram. Matrix Compos. Mater. Model. Technol. Hoboken, New York: John Wiley & Sons; 2014. p. 217–233.

[31] Cherif C. Textile Werkstoffe für den Leichtbau. Berlin: Springer; 2011.

[32] Lamon J. Interfaces and Interphases. Ceram. Matrix Compos. [Internet]. John Wiley & Sons, Ltd; 2008. p. 49–68. Available from: https://onlinelibrary.wiley.com/doi/abs/10.1002/9783527622412.ch3.

[33] Rebillat F, Lamon J, Guette A. Concept of a strong interface applied to SiC/SiC composites with a BN interphase. Acta Mater. 2000;48:4609–4618.

[34] Naslain R. Design, preparation and properties of non-oxide CMCs for application in engines and nuclear reactors: An overview. Compos. Sci. Technol. 2004. p. 155–170.

[35] Kerans RJ, Hay RS, Parthasarathy TA, et al. Interface Design for Oxidation-Resistant Ceramic Composites. J. Am. Ceram. Soc. 2004;85:2599–2632.

[36] Naslain R, Pailler R, Bourrat X, et al. Non-oxide ceramic composites with multilayered interphase and matrix for improved oxidation resistance. Key Eng. Mater. 2001;213:2189–2192.

[37] Rahaman MN. Science of sintering ceramic matrix composites. Int. Symp. Adv. Process. Ceram. Met. Matrix Compos. Halifax, UK: Elsevier; 1989.

[38] Birot M, Pillot J-P, Dunogues J. Comprehensive chemistry of polycarbosilanes, polysilazanes, and polycarbosilazanes as precursors of ceramics. Chem. Rev. 1995;95:1443--1477.

[39] Motz G, Hacker J, Ziegler G. Design of SICN - Precursors for Various Applications. Ceram. Mater. Components Engines. 2007;581–585.

[40] Lukacs A. Polysilazane precursors to advanced ceramics. Am. Ceram. Soc. Bull. 2007;86:9301--9306.

[41] Rak ZS. A Process for Cf/SiC Composites Using Liquid Polymer Infiltration. J. Am. Ceram. Soc. 2004;84:2235–2239.

[42] Miller D V, Pommell DL, Schiroky GH. Fabrication and Properties of SiC/SiC Composites Derived from Ceraset™ SN Preceramic Polymer. 21st Annu. Conf. Compos. Adv. Ceram. Mater. Struct. John Wiley & Sons; 2009. p. 409.

[43] Ziegler G, Richter I, Suttor D. Fiber-reinforced composites with polymer-derived matrix: processing, matrix formation and properties. Compos. Part A Appl. Sci. Manuf. 1999;30:411–417.

[44] Baldus P, Jansen M, Sporn D. Ceramic fibers for matrix composites in high-temperature engine applications. Science (80-.). 1999;285:699–703.

[45] Hacker J, Motz G, Ziegler G. Novel Ceramic SiCN-Fibers from the Polycarbosilazane ABSE. High Temp. Ceram. Matrix Compos. 2006;52–55.

[46] Mucalo MR, Milestone NB, Vickridge IC, et al. Preparation of ceramic coatings from pre-ceramic precursors - Part I SiC and “Si3N4/Si2N2O” coatings on alumina substrates. J. Mater. Sci. 1994;29:4487–4499.

[47] Cross TJ, Raj R, Prasad S V., et al. Synthesis and tribological behavior of silicon oxycarbonitride thin films derived from poly(Urea)methyl vinyl silazane. Int. J. Appl. Ceram. Technol. 2006;3:113–126.

[48] Motz G, Ziegler G. Simple processibility of precursor-derived SiCN coatings by optimised precursors. Key Eng. Mater. 2001;206–213:475–478.

[49] D’Amico G. Si-SiC based materials obtained by infiltration of silicon: study and applications. Politecnico di Torino; 2015.

[50] Hillig WB, Wb H, Cr M, et al. Silicon/silicon carbide composites. Am. Ceram. Soc. Bull. 1975;54:1054–1056.

[51] Krenkel W, Hald H. Liquid Infiltrated C/SiC: An Alternative Material for Hot Space Structures. Spacecr. Struct. Mech. Test. 1988;

[52] Singh M, Levine SR. Low cost fabrication of silicon carbide based ceramics and fiber reinforced composites. Mater. Sci. 1995;

[53] Luthra K, Singh R, Brun M. Toughened silcomp composites--process and preliminary properties. Am. Ceram. Soc. Bull. [Internet]. 1993;72. Available from: https://www.osti.gov/biblio/6325332.

[54] Gardiner G. Commercialization of CMCs and developments for next-gen performance [Internet]. CompositesWorld. 2017. Available from: https://www.compositesworld.com/blog/post/the-next-generation-of-ceramic-matrix-composites.

[55] Lazzeri A. Cvi Processing of Ceramic Matrix Composites. In: Bansal NP, Boccaccini AR, editors. Ceram. Compos. Process. methods. Hoboken, NJ, USA: John Wiley & Sons; 2012. p. 313–349.

[56] Bickerdike RL, Brown ARG, Hughes G, et al. The deposition of pyrolytic carbon in the pores of bonded and unbonded carbon powders. In: Mrosowski S, Studebaker MC, Walker PL, editors. Fifth Conf. Carbon. New York: Pergamon Press; 1962.

[57] Kotlensky WV. Deposition of pyrolytic carbon in porous solids. Chem. Phys. carbon. 1973;9:173–262.

[58] Bertrand S, Pailler R, Lamon J. Influence of Strong Fiber/Coating Interfaces on the Mechanical Behavior and Lifetime of Hi-Nicalon/(PyC/SiC)n/SiC Minicomposites. J. Am. Ceram. Soc. 2001. p. 787–794.

[59] Bertrand S, Droillard C, Pailler R, et al. TEM structure of (PyC/SiC)n multilayered interphases in SiC/SiC composites. J. Eur. Ceram. Soc. 2000;20:1–13.

[60] Becker A, Huttinger K. Chemistry and kinetics of chemical vapor deposition of pyrocarbon—II pyrocarbon deposition from ethylene, acetylene and 1,3-butadiene in the low temperature regime. Carbon N. Y. [Internet]. 1998;36:177–199. Available from: https://doi.org/10.1016/S0008-6223(97)00175-9.

[61] Becker A, Hüttinger KJ. Chemistry and kinetics of chemical vapor deposition of pyrocarbon - III pyrocarbon deposition from propylene and benzene in the low temperature regime. Carbon N. Y. 1998;36:201–211.

[62] Becker A, Hüttinger KJ. Chemistry and kinetics of chemical vapor deposition of pyrocarbon - IV pyrocarbon deposition from methane in the low temperature regime. Carbon N. Y. 1998;36:213–224.

[63] Becker A, Hüttinger KJ. Chemistry and kinetics of chemical vapor deposition of pyrocarbon - V influence of reactor volume/deposition surface area ratio. Carbon N. Y. 1998;36:225–232.

[64] Naslain R, Langlais F, Fedou R. The CVI processing of Ceramic Matrix Composites. J. Phys. Colloq. 1989;50.

[65] Langlais F, Prebende C, Tarride B, et al. On the kinetics of the CVD of Si from SiH2Cl2/H2 and SiC from CH3SiCl3/H2 in a vertical tubular hot-wall reactor. J. Phys. Colloq. 1989;

[66] Upadhya K, Hoffman WP. Densification of porous articles by plasma enhanced chemical vapor infiltration. 1996.

[67] Fitzer E, Fritz W, Schoch G. Modelling of the chemical vapour impregnation of porous (carbon) substrates with SiC. High Temp. High Press. 1992;24:343–354.

[68] Fedou R, Langlais F, Naslain R. A Model for the Isothermal Isobaric Chemical Vapor Infiltration(CVI) in a Straight Cylindrical Pore. Application to the CVI of SiC. J. Mater. Synth. Process. 1993;1:61–74.

[69] Vignoles GL. Modelling of the CVI Processes. Adv. Sci. Technol. 2006;50:97–106.

[70] Vignoles GL. Modeling of chemical vapor infiltration processes. In: Boisse P, editor. Adv. Compos. Manuf. Process Des. [Internet]. Elsevier Woodhead Scientific; 2016. p. 415–458. Available from: http://dx.doi.org/10.1016/B978-1-78242-307-2.00017-8.

[71] Coindreau O, Mulat C, Germain C, et al. Benefits of X-ray cmt for the modeling of C/C composites. Adv. Eng. Mater. 2011;13:178–185.

[72] Papasouliotis GD, Sotirchos S V. Experimental study of atmospheric pressure chemical vapor deposition of silicon carbide from methyltrichlorosilane. J. Mater. Res. 1999;14:3397–3409.

[73] Coltelli M-B, Lazzeri A. Chemical vapour infiltration of composites and their applications. In: Choy K-L, editor. Chem. Vap. Depos. Adv. Technol. Appl. CRC Press; 2019.

[74] Martin L. Chemical Vapor Infiltration Processes for Ceramic Matrix Composites: Manufacturing, Properties, Applications. In: Krenkel W, editor. Ceram. Matrix Compos. Fiber Reinf. Ceram. their Appl. Wiley-VCH; 2008. p. 141–161.

[75] Fischman GS, Petuskey WT. Thermodynamic Analysis and Kinetic Implications of Chemical Vapor Deposition of Sic from Si-C-C1-H Gas Systems. J. Am. Ceram. Soc. 1985. p. 185–190.

[76] Loumagne F, Langlais F, Naslain R. Kinetic laws of the chemical process in the CVD of SiC ceramics from CH3SiCl3-H2 precursor. J. Phys. IV Colloq. 1993;

[77] Pierson HO. Handbook of Chemical Vapor Deposition. Handb. Chem. Vap. Depos. 1992.

[78] Golecki I. Rapid vapor-phase densification of refractory composites. Mater. Sci. Eng. R Reports. 1997;20:37–124.

[79] Naslain RR, Pomeroy M. Ceramic Matrix Composites: Matrices and Processing. Sci. Technol. Elsevier; 2016. p. 1060–1066.

[80] Fitzer E, Gadow R. Fiber-reinforced silicon carbide. Am. Ceram. Soc. Bull. [Internet]. 1986;65:326 335. Available from: https://pascal-francis.inist.fr/vibad/index.php?action=getRecordDetail&idt=8606468.

[81] Roland W. Carbon/Carbons and Their Industrial Applications. In: Krenkel W, editor. Ceram. Matrix Compos. Fiber Reinf. Ceram. their Appl. Weinheim, Deutschland: Wiley-VCH; 2008. p. 69–111.

[82] Stinton DP, Caputo AJ, Lowden RA. Synthesis of fiber-reinforced SiC composites by chemical vapor infiltration. Am. Ceram. Soc. Bull. 1986;65:347–350.

[83] Roman YG, Stinton DP, Besmann TM. Development of High Density Fiber Reinforced Silicon Carbide F-CVI Composites. Le J. Phys. IV. 1991;02:C2-689-C2-695.

[84] Roman YG, de Croon MHJM, Metselaar R. Analysis of the isothermal forced flow chemical vapour infiltration process. Part II: Experimental study. J. Eur. Ceram. Soc. 1995;15:887–898.

[85] Vignoles GL, Nadeau N, Brauner C, et al. The Notion of Densification Front in CVI Processing with Temperature Gradients. In: Zhu D, Curzio L-, E., Kriven WM, editors. Mech. Prop. Perform. Eng. Ceram. Compos. Ceram. Eng. Sci. Proceedings, Vol. 26. Westerville, OH: The American Ceramic Society; 2005. p. 187–195.

[86] Vignoles GL, Duclous R, Gaillard S. Analytical Stability Study of the Densification Front in Carbon- or Ceramic-Matrix Composites Processing by TG-CVI. Chem. Eng. Sci. 2007;62:6081–6089.

[87] Caputo AJ, Lackey WJ. Fabrication of Fiber-Reinforced Ceramic Composites by Chemical Vapor Infiltration. Proc. 8th Annu. Conf. Compos. Adv. Ceram. Mater. Ceram. Eng. Sci. Proc. 2008. p. 654–667.

[88] Besmann TM, McLaughlin JC, Lin HT. Fabrication of ceramic composites: forced CVI. J. Nucl. Mater. 1995;219:31–35.

[89] Bertrand S, Lavaud JF, El Hadi R, et al. The thermal gradient - pulse flow CVI process: a new chemical vapor infiltration technique for the densification of fibre preforms. J. Eur. Ceram. Soc. 1998;18:857–870.

[90] Delhaes P. Chemical vapor deposition and infiltration processes of carbon materials. Carbon N. Y. 2002;40:641–657.

[91] Benzinger W, Hüttinger KJ. Chemistry and kinetics of chemical vapor infiltration of pyrocarbon-V. Infiltration of carbon fiber felt. Carbon N. Y. 1999;37:941–946.

[92] Probst KJ, Besmann TM, Stinton DP, et al. Recent advances in forced-flow, thermal-gradient CVI for refractory composites. Surf. Coatings Technol. 1999;120–121:250–258.

[93] Devlin DJ, Currier RP, Barbero RS, et al. Microwave assisted chemical vapor infiltration. MRS Proc. 1991;250.

[94] Devlin DJ, Currier RP, Barbero RS, et al. Chemical vapor infiltration with microwave heating. In: Watchman JB, editor. 17th Annu. Conf. Compos. Adv. Ceram. Mater. Part 2 2. Westerville, OH: The American Ceramic Society - John Wiley & Sons; 1993. p. 761–767.

[95] Jaglin D, Binner J, Vaidhyanathan B, et al. Microwave heated chemical vapor infiltration: Densification mechanism of SiCf/SiC composites. J. Am. Ceram. Soc. 2006;89:2710–2717.

[96] Binner J, Vaidhyanathan B, Jaglin D, et al. Use of electrophoretic impregnation and vacuum bagging to impregnate SiC powder into SiC fiber preforms. Int. J. Appl. Ceram. Technol. 2015;12:212–222.

[97] Spotz MS, Skamser DJ, Day PS, et al. Microwave-assisted chemical vapor infiltration. In: Wachtman Jr JB, editor. 17th Annu. Conf. Compos. Adv. Ceram. Mater. Westerville, OH: The American Ceramic Society - John Wiley & Sons; 1993. p. 753–760.

[98] Skamser DJ, Day PS, Jennings HM, et al. Hybrid Microwave-Assisted Chemical Vapor Infiltration of Alumina Fiber Composites. In: Wachtman JB, editor. 18th Annu. Conf. Compos. Adv. Ceram. Mater. Hoboken, NJ, USA: John Wiley & Sons; 1994.

[99] Day PS, Skamser DJ, M. HJ, et al. Fabrication of SiC Matrix Surface Composites by Chemical Vapor Infiltration with Microwave Heating: Temperature Effects. 18th Annu. Conf. Compos. Adv. Ceram. Mater. Hoboken, NJ, USA: John Wiley & Sons, Inc.; 1994.

[100] Gupta D, Evans JW. A mathematical model for chemical vapor infiltration with microwave heating and external cooling. J. Mater. Res. 1991;6:810–818.

[101] Morell JI, Economou DJ, Amundson NR. A Mathematical Model for Chemical Vapor Infiltration with Volume Heating. J. Electrochem. Soc. 1992;139:328–336.

[102] Melkote RR, Jensen KF. Gas diffusion in random-fiber substrates. AIChE J. 1989;35:1942–1952.

[103] Tomadakis M, Sotirchos S. Effective Kundsen diffusivities in structures of randomly overlapping fibers. AIChE J. 1991;37:74–86.

[104] Morell JI, Economou DJ, Amundson NR. Chemical vapor infiltration of SiC with microwave heating. J. Mater. Res. 1992;8:1057–1067.

[105] Morell JI, Economou, Demetre J. Amundson NR. Pulsed-power volume-heating chemical vapor infiltration. J. Mater. Res. 1992;7:2447–2457.

[106] Tilley BS, Kriegsmann GA. Microwave-enhanced chemical vapor infiltration: A sharp interface model. J. Eng. Math. 2001;41:33–54.

[107] Pelesko J, Kriegsmann G. Microwave heating of ceramic laminates. J. Eng. Math. 1997;32:1–18.

Chapter 3

3. MW materials processing: Principles and applicator design

Microwave heating is one of the most rapid and efficient ways of heating materials. Its specificity, with respect to conventional methods, is based on a volumetric heating mechanism where MW energy is directly converted into heat inside the material leading to important energy savings and process time reductions. In addition, the rapid and selective heating mechanism, when properly controlled, can be exploited to achieve improved product quality, increased throughput and important space savings.

Large scale industrial applications of MW heating leverage the benefits of uniform heat distribution which are not achievable by conventional heating methods. The raising interest on MW processing of materials led in the latest years to several successful applications for a wide range of material systems and sectors. In particular, great efforts have been dedicated to the development of new material processes to substitute inefficient conventional methods and transferring the acquired knowledge to the industry.

The achievement of this goal is hindered by several barriers. When a process is scaled up from laboratory to industrial scale, additional elements as the material transport and thermal insulation system and their interaction with the electromagnetic (EM) field needs to be considered to guarantee a reliable design. This issue is even more demanding at high temperatures, where a precise knowledge of material dielectric properties and its behaviour during the heating process is critical.

This Chapter aims to briefly introduce the benefits and peculiarities of MW materials processing and applicator design, identifying some helpful guidelines and parameters for the development of an efficient MW assisted application. Particular attention will be dedicated to overmoded resonant cavities which constitutes the final design choice for the applicator employed in this PhD activity.

3.1 Introduction

The widespread diffusion of domestic MW ovens led to the quick acknowledgment of this technology. The apparent ease of use of this device inside our houses derived from the wide presence of water inside food, which makes them easy to be "coupled" into MW ovens, and by the success of many MW equipment manufacturers in making it a daily "user-friendly" device.

The same phenomenon was not as well observed for MW assisted industrial applications involving different material processes, which require a greater degree of technical complexity to achieve the desired heat distribution and product quality.

Although the advantages of MW material processing are manifold, starting from the improved mechanical properties and specific microstructures (sometimes not achievable through conventional technologies) to the reduction in processing times and energy savings leading to more eco-friendly applications [1], its full potential still need to be exploited and efficiently carried into industrial applications, especially in the case of high temperature processes [2].

During the end of 20th century, 90% of MW industrial applications in the United States were limited to the food industry (meat tempering, bacon cooking) and rubber vulcanization [3]. In the latest years MW heating gained great popularity for processing of ceramics, polymers, metals as well as advanced materials like composites (PMCs, MMCs, CMCs) and into several specific processes related to different areas (see **Figure 3.1**) [4,5].

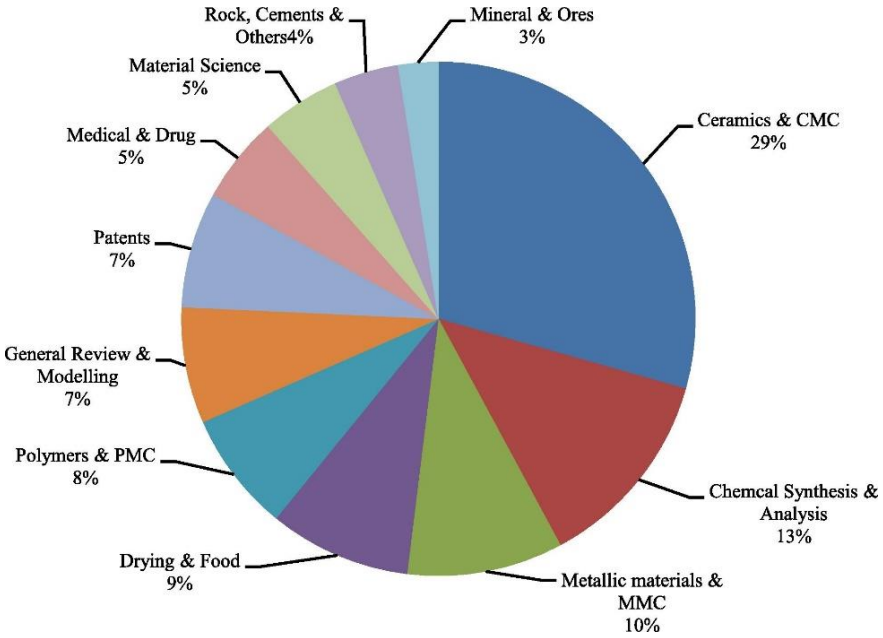

***Figure 3.1** - Published research in the field of Microwave processing of materials* [6]

For instance, distinctive advantages were reported for PMCs with a thermoset/thermoplastic matrix in terms of improved mechanical properties and better fibre/matrix bonding using selective MW heating [7–9]. Extensive past research activities on MW processing of ceramics, first motivated by the high temperatures required using conventional methods, led today to several well-recognized applications, thanks to benefits as the enhanced densification rates, improved materials microstructure and mechanical properties [10,11]. Despite of the various proven advantages related to MW heating, there is still some reluctance for the replacement of existing systems.

In general, a MW system is composed by three main components:

- The MW power source;
- The transmission line, including a coupling structure to guarantee the efficient MW delivery from the source to the applicator;
- The applicator, being a specific section designed to promote effective coupling with MW energy;

Inadequate design of these components, as well as their integration into the process of interest, easily results in the missing exploitation of MW heating benefits and an unsuccessful application. Therefore, a basic knowledge of MW generation, propagation and interaction with the material is fundamental.

Several books have been published about MW heating [12–16], although the most comprehensive still remains the [17] authored by Metaxas and Meredith, which presents the main topics and physical parameters related to MW heating for specific applicator design and components of industrial interest.

Among the different types of applicator, analytical solutions, providing quick ways to assess the suitability and efficiency of a MW system, are available only in the case of single-mode or simple-shape multi-mode cavities [18]. To the best of author knowledge, a widely usable expression for the design and assessment of multi-mode cavities is still not available. For these reasons, a lot of commercial packages are being more and more employed for the simulation of MW heated cavities to increase design reliability [14,19]. Depending on the cavity volume to be modelled, severe computational resources could be required.

Specific measurement techniques are required to retrieve the parameters necessary to have a clearer insight of the MW cavity and evaluate modelling results. High frequency measurement devices, as vector network analysers, are frequently used to measure scattering parameters (S-parameters), which give information in terms of transmitted/reflected waves at each applicator port to control the coupling levels between the different MW components.

Although essential in the design of high temperature MW reactors, there is a lack of data about material dielectric properties owing to the extreme temperature conditions at which they must be determined and the requirement of specific composition and structure of the materials of interest. This situation is complicated by the strong variations showed by these quantities with respect to frequency and temperature, which makes the extrapolation of the available data questionable.

Thus, the material to be treated needs to be considered as an integral part of the system during the design to maximize MW heating efficiency, minimize EM field inhomogeneities and guarantee the highest flexibility in terms of material size, shape and dielectric properties.

Moreover, the achievement of the highest overall MW heating efficiency requires that most of the EM energy needs to be dissipated in the sample than in applicator walls. Specifically, in the case of a MW assisted chemical reactor, other parameters, based on the operating conditions (high temperatures, aggressive environments), will need to be considered for the proper walls material selection.

3.2 MW heating: theory, mechanisms and parameters

Microwaves belongs to the portion of the EM spectrum between frequencies ν from 300 MHz to 300 GHz corresponding to wavelengths λ which respectively go from 1 m to 1 mm [20] (see **Figure 3.2**).

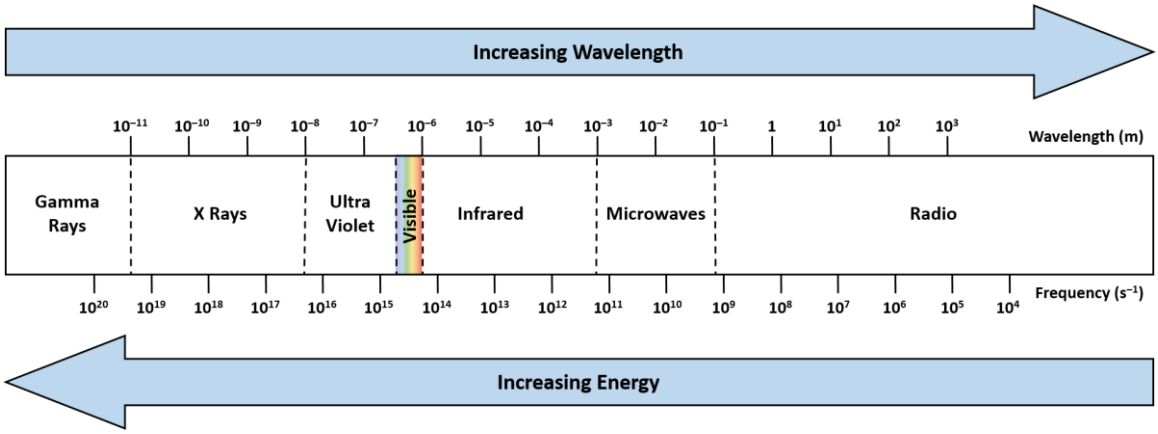

***Figure 3.2** – EM spectrum* [21]

The allocated frequencies, set aside by the International Telecommunications Union (ITU) in Europe for industrial MW heating applications, operate within the Industrial, Scientific and Medical (ISM) frequency bands (commonly centered on 915 MHz or 2450 MHz), reported in **Table 3-1**, to prevent interference with other electronic devices [22].

***Table 3-1** – ISM allocated frequency bands*

Frequency range [MHz]	Central frequency [MHz]
6,765 – 6,795	6,780
13,553 – 13,567	13,560
26,957 – 27,283	27,120
40,66 – 40,70	40,68
433,05 – 434,79	433,92
902 – 928	915
2400 – 2500	2450
5725 – 5875	5800
24000 – 24250	24125
61000 – 61500	61250
122000 – 123000	122500
244000 – 246000	245000

The interaction between an electric field and a dielectric media is originated by the response of the bound charged particles to the applied field. Due to the displacement of these charges from their equilibrium conditions, several induced dipoles arise which are able of interacting with the electric field (dipolar polarization mechanism). In addition, some dielectric materials (named polar dielectrics) display permanent dipoles due to the asymmetric charge distribution of unlike charges which attempt to re-orientate in response to the applied field (orientation polarization mechanism). A final source of polarization derives from the charge build-up in

interfaces between components in heterogeneous systems which is named Maxwell-Wagner polarization.

The heating mechanisms of dielectric materials using high frequency EM fields have been long established and, inside the MW frequency range, are based on two fundamental methods of energy transfer [6]. At the lower frequency end, the transfer of MW energy from the EM field to the material is related to the flowing of conducting currents due to the movement of ionic constituents. With increasing frequency, the energy absorption depends instead on the presence of permanent dipole molecules which tend to re-orientate under the influence of a MW electric field. The inability of those species to follow the rapid changes of the alternating electric field at such high frequencies results in the dissipation of power within the material, an effect known as "dielectric loss". Among the different loss mechanisms, the most significant ones for industrial MW heating applications at frequencies above 1 GHz usually are the dipolar and orientation polarisation.

MW radiation displays the important property of penetrating and simultaneously heating the bulk of the material [23]. This mechanism leads to a quick increase of material bulk temperature with respect to the external surface, resulting in a "reverse" temperature gradient. Thanks to this property, MW heating results in rapid volumetric heating rates where the surface of the material is not overheated (especially in the case of low thermal conductivity materials), leading to applications like the removal of binders or other chemical species from the inner side as well as the heating of reactive gases into the hotter internal areas of porous materials (CVI process). Moreover, the heating of the material is instantaneous, with the possibility to precisely control the temperature only by adjusting the power level.

The differential MW coupling mechanism can be exploited to selectively heat materials made of different constituents. This feature was used for instance in the MW processing of rubber, asphalt and many composite systems [24–26]. Some materials absorb MW only above certain temperatures (as alumina) and can be therefore heated using other materials, acting as susceptors, which are able to absorb more readily MW at room temperature. SiC rods are good susceptors which are usually employed to hybrid heat low-loss materials at room temperature [27]. This self-limiting MW absorption mechanism can be also exploited in other ways, as for the drying of water from wood or chemicals, which is automatically stopped when all the water is removed.

Unfortunately, several materials are characterized by sharp variations of the dielectric properties beyond a critical value, known as "kick-in temperature", which could result in an uncontrolled acceleration of the heating (thermal runaway), that can be exacerbated by non-uniform field distributions. Coupled with the low thermal conductivity of some materials (as many ceramics), this phenomenon leads to the formation of localized overheated surfaces (hotspots), thus requiring great care for the use of a MW heating [10].

Whatever the final application, each one of the characteristics described above can be used singularly or in combination to provide considerable improvements in terms of efficiency and flexibility or to tailor specific properties.

However, the implementation of MW assisted heating into a specific process is not straightforward since the generation and dissipation of heat into the material depends from several factors. The heating pattern developed depends on the EM field distribution inside the cavity, which generally demands for rigorous numerical approaches to be able of predicting and controlling the required parameters for a precise heating.

3.2.1. Electromagnetic theory

The theoretical analysis of MW components is based on the solution of Maxwell equations (with the appropriate boundary conditions) which, in the case of time-harmonic electric and magnetic fields for a linear, non-dispersive, isotropic and conducting medium in the frequency domain (in terms of the angular frequency $\omega = 2\pi\nu$), are given by [28]:

$$\nabla \times \boldsymbol{H} = \sigma \boldsymbol{E} + i\omega\varepsilon_0\varepsilon\boldsymbol{E} \qquad (3.1)$$

$$\nabla \times \boldsymbol{E} = -i\omega\mu_0\boldsymbol{H} \qquad (3.2)$$

$$\nabla * \varepsilon_0\varepsilon\boldsymbol{E} = q \qquad (3.3)$$

$$\nabla * \mu_0\boldsymbol{H} = 0 \qquad (3.4)$$

Where $\boldsymbol{E}$ and $\boldsymbol{H}$ represents the electric and magnetic field respectively. The constitutive relations have been made explicit into **Equations 3.3-3.4**, displaying the electric induction field and the magnetic induction field respectively as $\boldsymbol{D} = \varepsilon_0\varepsilon\boldsymbol{E}$ and $\boldsymbol{B} = \mu_0\boldsymbol{H}$, where ε_0 is the dielectric constant of free space while μ_0 is the magnetic permeability of free space. Other terms employed into Maxwell equations are the free conduction current density into an ohmic medium $\boldsymbol{J} = \sigma\boldsymbol{E}$, where σ is the electric conductivity and q is the charge density. Since in the following paragraphs it will be considered only the MW heating of dielectric materials, only dielectric losses will be accounted (magnetic losses are neglected).

The dielectric permittivity $\varepsilon = \varepsilon' - i * \varepsilon''$ is a measure of the material response to an external electric field, where the real part of the dielectric permittivity ε' (or relative dielectric constant) accounts for the capacitive component, as a measure of the MW energy density stored in the material, while the imaginary part of the dielectric permittivity ε'' (or dielectric loss factor) accounts for all internal loss mechanisms.

The dielectric loss factor gives an idea of how readily a material absorbs microwaves. Accordingly, a material with a high ε'' is a good MW absorber and is quickly heated, provided that it has small dimensions with respect to the penetration depth. Commonly, it is possible to distinguish materials in terms of the different MW absorption properties through ε'' (see **Figure 3.3**) or another parameter called the loss tangent, $\tan\delta = \varepsilon''/\varepsilon'$.

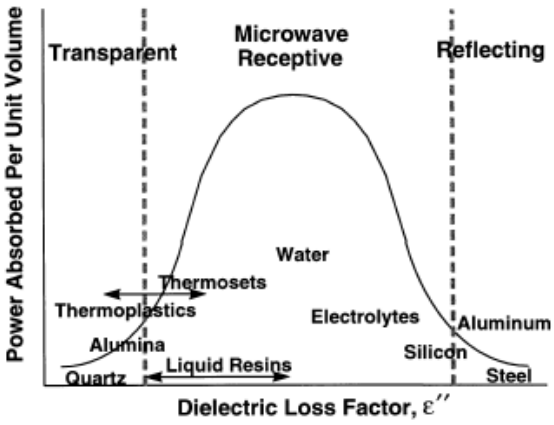

Figure 3.3 *- Relationship between the dielectric loss factor and ability to absorb microwave power for some common materials* [23]

In particular, it is convenient to express Maxwell equations in the frequency domain to account for losses in the material due to the complex nature of the dielectric permittivity. The solution of Maxwell equations for a dispersive medium in the frequency domain results in the following wave (or Helmholtz) equations

$$\nabla^2 \boldsymbol{E} = -\omega^2 \mu_0 \varepsilon_0 \varepsilon \boldsymbol{E} \qquad (3.5)$$

$$\nabla^2 \boldsymbol{H} = -\omega^2 \mu_0 \varepsilon_0 \varepsilon \boldsymbol{H} \qquad (3.6)$$

which are used, under certain boundary conditions, to derive the EM field distribution and related parameters inside MW systems.

Solving these equations for a plane wave propagating along the z-direction, the above expressions are reduced to a one-dimensional wave equation, usually referred as Transverse Electro Magnetic (TEM) wave, with a field distribution given only by the E_x and H_y components, orthogonal to each other and characterized by both the electric and magnetic field components along the direction of propagation E_z, H_z equal to zero (see **Figure 3.4**).

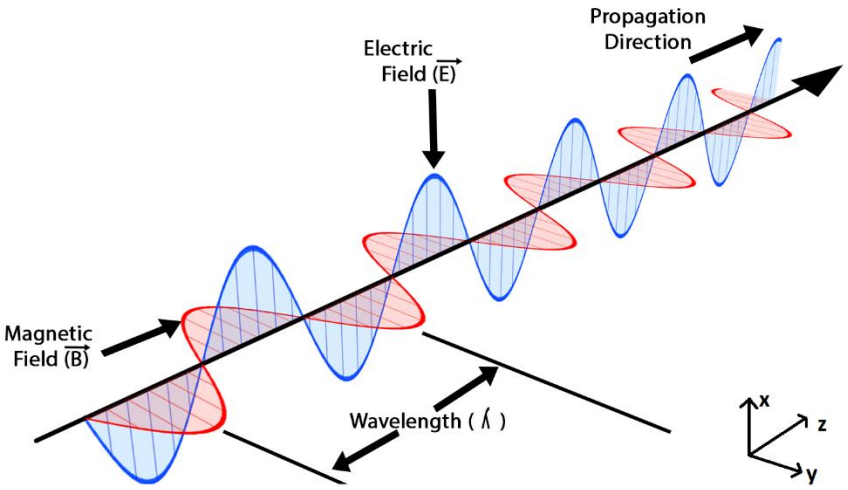

***Figure 3.4** – Representation of an EM wave* [29]

Solving for E_x the following expression is obtained:

$$\frac{\partial^2 E_x}{\partial z^2} = -\omega^2 \mu_0 \varepsilon_0 \varepsilon E_x \rightarrow E_x = E_0 e^{-ikz} \qquad (3.7)$$

Where E_0 is the value of the electric field at $z = 0$, while $k = \omega\sqrt{\mu_0 \varepsilon} = \beta - i * \alpha$ is called propagation constant, expressing the change in terms of amplitude and phase undergone by a wave as it propagates in a given direction. Following, the phase constant β gives the phase of the signal along a transmission line at a constant time, while the attenuation constant α causes the signal amplitude to decrease while propagating through a transmission line. **Equation 3.7** proves that a plane wave can propagate only to the positive z-direction being attenuated along the way, except if the material is without losses ($\alpha = 0$).

Through the attenuation constant it is possible to define the penetration (or skin) depth δ, defined as the distance that a wave must travel before its amplitude has decayed by a factor of $1/e$. In the case of a good conductor the penetration depth can be simplified as:

$$\delta = \frac{1}{\alpha} = \sqrt{\frac{\rho}{\pi \mu_0 \nu}} \qquad (3.8)$$

Applicators usually employed are based on metallic enclosures where MW are reflected on the walls. This mechanism is particularly important in resonant cavities, where MW are reflected multiple times giving rise to power dissipations on the walls and the load, requiring to find a compromise in order to have the highest energy dissipation focused on the load.

Another important parameter is the characteristic impedance ζ of the medium which expresses the ratio of the transverse components of the electric and magnetic fields (equivalent to the low-frequency circuit impedance given by the voltage to current ratio) and it is used for matching purposes among MW systems.

There are some specific MW components where it is not possible to have one or both E_z, H_z terms equal to zero due to the boundary conditions arising from geometrical constraints, thus resulting into specific field distributions. High frequency EM signals propagate along dedicated transmission lines called waveguides, that are hollow metallic tubes with rectangular/cylindrical shape (see **Figure 3.11**).

The waves travelling along those structures are known as Transverse Electric (TE), having only $E_z = 0$, or Transverse Magnetic (TM) where only $H_z = 0$ (see left side of **Figure 3.5**). The field pattern developed inside waveguides are called modes and represent the various solutions of Maxwell equations.

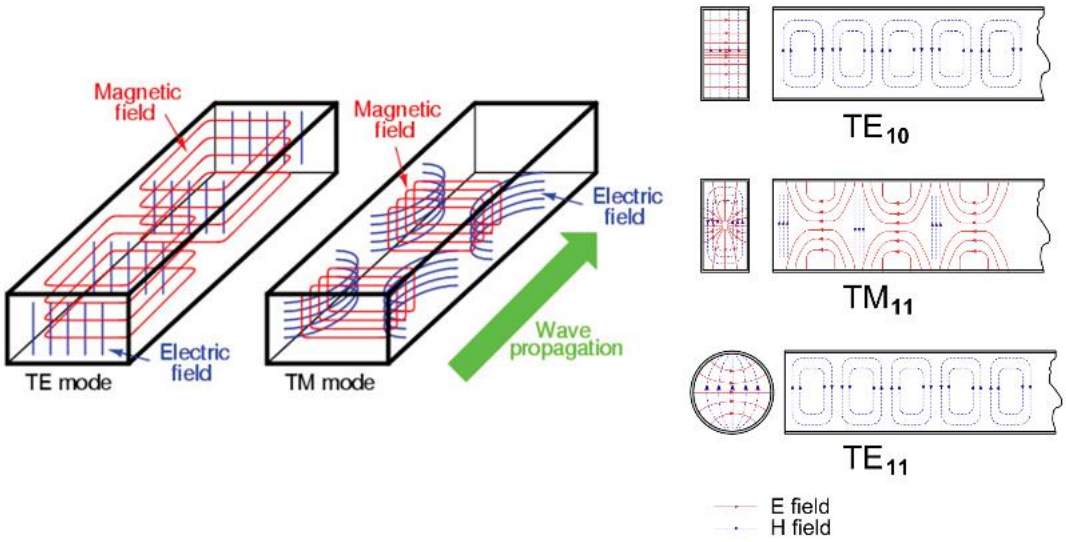

Figure 3.5 *– TE, TM modes field patterns into a rectangular waveguide* [30] *(left) and field patterns of some commonly used waveguide modes (right)* [31]

The wave impedance of these TE_{mn}, TM_{mn} modes is a frequency-dependent parameter, namely there is a lower limiting value, called "cut-off frequency" $(\nu_c)_{mn}$, below which the signal cannot propagate (it is quickly attenuated). The subscripts m, n are positive integers designating half wavelengths of sinusoidal electric field variation along the principal axis of the applicator (see right side of **Figure 3.5**). Regarding rectangular waveguides the cut-off frequency depends from the lateral dimensions a, b and it is given by:

$$(\nu_c)_{mn} = \frac{1}{2\pi\sqrt{\mu_0 \varepsilon}} \sqrt{\left(\frac{m\pi}{a}\right)^2 + \left(\frac{n\pi}{b}\right)^2} \qquad (3.9)$$

The lowest frequency mode possible to transmit the signal is called the dominant mode, and it is usually used to select waveguides dimensions, in order to have only that specific mode propagation into the transmission line.

Regarding whichever MW heating application, we are generally interested into the subsequent material heating profile and maximum/minimum temperatures achieved. Those parameters can be obtained from the EM energy released into the material to be converted as heat. The power loss density per unit volume P_d can be expressed though the integration of the Poynting's vector $\boldsymbol{s} = \boldsymbol{E} \times \boldsymbol{H}^*$, which in the case of constant electric field leads to a simple expression given by:

$$P_d = \omega \varepsilon_0 \varepsilon'' |\boldsymbol{E}|^2 \qquad (3.10)$$

Knowing the power stored inside the material, it is possible to determine the temperature T rise from the heat equation:

$$dc_p \frac{\partial T}{\partial t} = P_d + \nabla * (k \nabla T) + P_{loss} \qquad (3.11)$$

Where d is the material density, c_p is the specific heat and k is the thermal conductivity. The heat losses respectively due to radiation and convective mechanism are included inside the term $P_{loss} = P_h + P_{conv}$:

$$P_h = \epsilon \sigma_{SB} A_s T^4 \qquad (3.12)$$

$$P_{conv} = h A_s \Delta T \qquad (3.13)$$

Where ϵ is the emissivity of the sample, σ_{SB} is the Stefan-Boltzman constant, h is the mean heat transfer coefficient and A_s is the sample surface area.

Most of the analytic expressions reported can be used and solved only in the case of simple-geometry systems. As soon as complex shaped components or cavities containing lossy loads are considered, those equations become impossible to be analytically solved, requiring the use of numerical techniques.

3.2.2. Multiphysics modelling of MW heating problems

During past years, preliminary tests on MW heated cavities usually led to unsatisfactory and non-reproducible results due to the lack of understanding on the EM field distribution inside the applicator. This phenomenon always resulted in the premature discard of new potential MW applications and increased the reluctance from industrial end-users about the usage of these solutions [32].

Currently, several kinds of feasibility studies, based on the usage of numerical techniques, significantly limited those issues highlighting the most important process variables for all cavity configurations (empty and loaded), overcoming eventual issues and improving design reliability [33].

The main parameters that are derived from numerical simulations are based on the EM field distribution inside the cavity, S-parameters and power dissipation within the processed material. It is worth noting that the results obtained need to be validated through experimental measurements, to further improve the physical insight and practical applicator design as well as avoiding inexperience mistakes.

Today, there are a great number of commercial packages which significantly reduce time-consuming tasks as the writing of the code, which is itself a wide research area. One of the

preferred methods for MW heating applications is the Finite Element Method (FEM), being one of the most powerful approaches to solve partial differential equations over irregular shaped regions thanks to its unstructured meshing capability. A detailed analysis on the usage of FEM dedicated to single and multimode cavities can be found in [34].

FEM is based on the discretization of the entire problem domain into a number of sub-regions with simple geometry, where each dependent variable is solved assigning it a specific function and then applying the same approach to all the other elements approximating the overall solution by summation of all contributions.

The main usage of this method, regarding the solution of high frequency EM systems, is related to [34]:

- 2D-3D analysis of waveguides with complex geometries;
- Eigenvalue 3D analysis;
- Determination of power loss inside lossy dielectrics;

The Eigenvalue (source-free) analysis is particularly important for resonant cavities to predict the resonant modes present inside them. This study determines the eigenfrequencies and associated EM field distributions, or eigenmodes, by specifying the cavity geometry, material properties and boundary conditions.

Possible disadvantages about the use of FEM methods regards the high computational cost, which depends on several factors as the number of selected frequencies and excitation ports of the MW system. Large matrixes are usually produced which then needs to be decomposed for each frequency value at the selected port.

After the Eigenvalue analysis, the excited cavity behaviour is checked to analyse resonant modes characteristics in narrow frequency ranges, close to the values determined in the first step, reducing in this way the simulation run-time. Focusing on a single frequency value, it is then possible not only to analyse the corresponding EM field distribution but also to derive variables as the S-parameters and load power dissipations.

Finally, one of the latest and appreciated approaches for the study and design of MW cavities is the simultaneous solution of the coupled equations governing the EM and the thermal problems (multiphysics approach). Commercial finite element method COMSOL software [35] is one of the most recent packages for multiphysics simulations, which solves in a rigorous way the coupled equations governing both the EM and the thermal problem involved in this interaction, taking into account for instance anisotropic, dielectric, magnetic and thermal properties as well as the conductive, convective, and radiative mechanisms for the heat transfer.

Numerical techniques can undoubtedly provide a very powerful tool to orient the design of MW heated cavities, provided that the results obtained in this way will be supported by experimental validations. The synergy between both those results can indeed lead to a successful application, limiting eventual problems and saving money and time to build the desired MW heated cavity.

3.2.3. High frequency properties measurement

The complexity of MW interactions with materials requires several preliminary considerations for the efficient application of MW heating into a dedicated material process. In particular, as

motivated in the previous paragraph, the precision of numerical techniques depends on the availability of reliable data.

One of the high frequency parameters, usually measured for radiofrequency or MW applications, are the S-parameters since, through these quantities, it is possible to derive different kinds of information. Specifically, S-parameters provide complete insight into the linear behaviour of radiofrequency and MW components which are used for cross-coupling purposes as well as dielectric properties measurement. The instrument used for these kinds of measurements is called Vector Network Analyzer (VNA) that, in its simplest form, is a device used for impedance measurements (see **Figure 3.6**).

At lower frequencies, the impedance can be measured with relatively simple tools, including a sine wave generator, a voltmeter, a current meter, and a calculator. Then the impedance is simply derived from the voltage to current ratio. At radiofrequency and MW frequencies, measurements of voltage and current become more complex. As a result, a VNA uses a more complex design to measure incident and reflected waves.

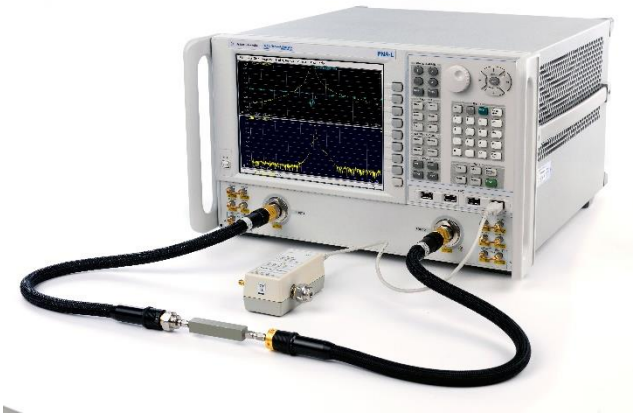

***Figure 3.6** - Agilent's new PNA-L vector network analyzer (VNA)* [36]

When using a VNA to measure the impedance or the reflection factor, a sine generator stimulates the device under test (DUT). In addition, two receivers take the place of the combination of a voltmeter and current meter. These receivers, with the help of signal separation hardware, characterize the response of the device by measuring the phase and amplitude of signals that are both incident to and reflected from the DUT. Finally, calibration capabilities are required to eliminate systematic errors and compute the appropriate ratios (similarly to the impedance) necessary, obtaining the so-called reflection coefficient S_{11} and transmission coefficient S_{21}.

The primary use of a VNA is to determine the S-parameters of a myriad of passive components. In the case of a MW heated cavity the VNA is used to obtain the frequency spectrum of the cavity revealing the number of resonant modes and their coupling level in terms of S_{11} measurements (see **Figure 3.7**):

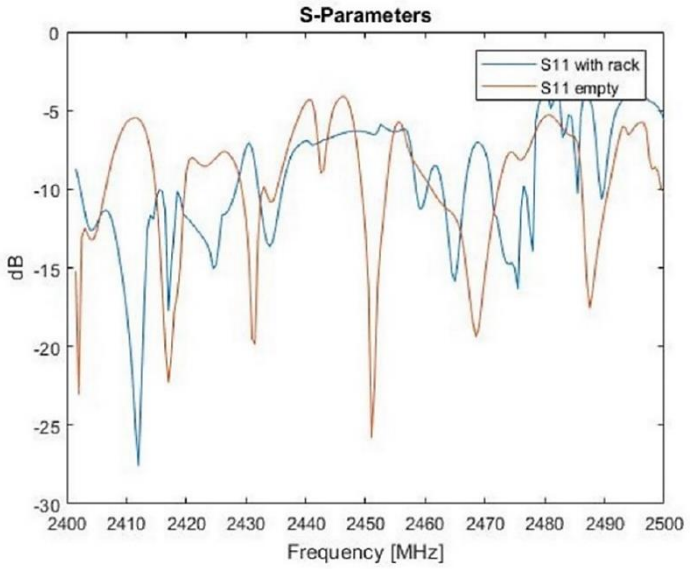

Figure 3.7 *- S-parameters for an oven with and without a rack* [37]

The insertion of a generic lossy load inside the cavity lead to significant changes in the frequency characteristics of resonance curves. Depending on the dimensions and dielectric properties of the load the resonant modes can be shifted becoming wider and maybe increasing in number (case of a small sample with low dielectric loss factor), or the frequency spectrum may even lose its resonant profile (case of big samples with high dielectric loss factor).

The deeper the resonance, the higher the power dissipation in the cavity. Frequency spectrum analysis is fundamental for the selection of the best heating mode that should be possibly centered on the load of interest instead of cavity walls, and with high coupling levels. As shown in **Figure 3.7**, S-parameters are usually expressed in decibels (dB), where a level of 0 dB means that the wave is fully reflected. Regarding practical applications, a coupling level lower than $-10\ dB$ is not acceptable while values close to $-20\ dB$ are considered an excellent match.

Starting from the solutions of Maxwell equations, the expected outcome would have been to have a certain frequency spectrum at the operating frequency range, where a generic load could be heated simply exciting the cavity at the resonance frequency. Usually the process is not that straightforward, but there is instead a certain number of frequency bands where considerable excitation could occur. The reason for the presence of these narrow/large frequency bands derive from the dissipations into the cavity walls and the load. A parameter that can give an insight on those phenomena is the Q-factor or quality-factor, defined as:

$$Q = 2\pi \frac{total\ energy\ stored}{energy\ dissipated\ in\ the\ walls\ and\ dielectric/cycle} = \frac{\omega W}{P_c + P_s} \qquad (3.14)$$

Where W is the energy stored in the cavity per cycle, that could be given by both the electric or magnetic field component since the energy is equally divided between them, while P_c, P_s are respectively the power dissipations into the cavity walls and the sample.

The Q-factor can be also calculated from S_{11} frequency measurements as:

$$Q = \frac{\nu_0}{\Delta\nu} \qquad (3.15)$$

Where ν_0 is the resonance frequency while $\Delta\nu$ is the full-width at half maximum.

Thus, S_{11} measurements reveal the number of operating modes over the analysed frequency range and their coupling levels, but they cannot provide alone complete information on cavity performance. The nature of the operating modes need the correlation of those measurements with analytical or computational calculations.

The different mechanisms of energy transfer into a material depend primarily on its dielectric properties. Theoretical considerations about the interaction of EM waves and materials can give just qualitative information on its dielectric properties and frequency dependence, since the interaction mechanism is strongly connected to the type and strength of the chemical bond between atoms [38]. The first general reference in practice, to understand if a material can be heated by MW, is still based on Von Hippel's enormous work on many organic and inorganic materials related dielectric properties into the $100\ Hz < \nu < 10^{10}\ Hz$ range [39].

Unfortunately, while the material is being processed, it can undergo physical and structural transformations resulting in sharp changes of its MW absorption properties leading to problems as non-uniform heating and difficulties in process control. Due to the large variation of dielectric properties, many applications require special applicator design, resulting in an even more demanding need for precise dielectric data along processing.

Several techniques are available to measure dielectric properties in different frequency ranges. Regarding the frequency range $400\ MHz < \nu < 3000\ MHz$, where are located the two main frequency bands of interest for industrial applications, experimental methods based on coaxial line or waveguide techniques are used. Those techniques are based on the insertion of the material into simple coaxial TEM lines or TE_{01} waveguides and the measurement of S_{11}, S_{21} parameters. From the latter is then possible to derive dielectric properties using simple equation inversion techniques.

Another common method is based on the cavity perturbation technique. The principle of this approach is based on the insertion of a small low loss material into a high Q-factor cavity through a sample holder. The real and imaginary part of the dielectric permittivity are obtained from the change of Q-factor from an unperturbed resonance frequency value ν_0 characteristic of the empty cavity, to the new perturbed resonance frequency value ν_0' after the insertion of the load, which enables an analytical treatment of the data by means of some calibration constants. The validity of the perturbation theory depends on sample dimensions, which need to be small with respect to the cavity in order to observe a small frequency shift [40]. A through calibration process and high standard connections are required to accurately describe material behaviour during the measurement. Anyway, without having a preliminary knowledge of the expected dielectric properties, the use of a calibration procedure leads to a lot of uncertainties.

Additional difficulties in retrieving precise dielectric properties are encountered at high temperatures (above several hundred degrees), due to the increasing radiation losses of the samples which leads also to practical limitations in temperature evaluations. Very quick measurements need to be performed to avoid the cooling of the material on its way to the measurement cell with subsequent loss of dielectric properties temperature relation.

Some of those problems have been dealt changing the heating method from a conventional to a MW assisted type. In the latter case, two are the main approaches employed in literature, depending on the usage of one or two different modes for the heating and dielectric permittivity measurement [41]. The precision of both methodologies relies on the application of a mechanical tracking mechanism in order to tune the response of the measurement cell with the variation of sample dielectric properties, which severely limits the temperature and dielectric permittivity

measurement range. In addition, precise knowledge of the excited mode and control of the resulting sample heating distribution are necessary to precisely measure dielectric properties.

Another approach is based on the "frequency shift technique", based on the measurement of the resonance frequency and Q-factor when a load is introduced into a specifically designed MW cavity, where the above changes are correlated with the dielectric permittivity. A small cylindrical-shape sample (with respect to the characteristic wavelength in the material), previously inserted into a low loss sample holder tube, is conventionally heated and rapidly inserted into the MW cavity, thus avoiding mistakes due to radiation losses contributions and providing great accuracy in the frequency shift calculation without any approximation [42,43].

Beyond the measurement of dielectric properties or the direct application into MW heated cavities, temperature measurements plays an important role into MW heating applications. Basic thermocouples are usually the first choice due to the low cost and temperature range. Unfortunately, when inserted inside MW heated cavities, thermocouples may perturb the field inside leading also to spark formation. Fibre-probes, while being non-metallic are too fragile and expensive for most applications. Thus, although limited to surface temperature measurement, pyrometers (see **Figure 3.8**) are the preferred choice for MW heated cavities since they give real-time and visual information on the temperature distribution.

***Figure 3.8** – Pyrospot DIAS pyrometers* [44]

3.2.4. Associated MW heating phenomena

It is known that high frequency electric field of sufficient intensity applied into gaseous environments may transfer energy to the electrons present leading to breakdown phenomena. The latter is associated to the conversion of the gas into a conducting medium usually addressed as plasma.

This phenomenon is sometimes advantageous, and it was exploited into several industrial applications based on plasma enhanced chemical processes. For istance, plasma enhanced chemical vapor deposition is a well-recognized solution for the processing of flexible and printable electronic devices, due to its high process efficiency, large-scale patternability, lower cost, and environmentally friendly nature [45]. Instead other times, the appearance of breakdown phenomena and plasma discharges into MW heated cavities is a quite undesirable phenomenon since it could result into material/applicator damages or reduced efficiency.

Therefore, it is important to analyse plasma formation conditions during the design phase, especially for continuous industrial applications. This is a quite complex phenomenon that depend from several factors as the pressure range, power levels involved, geometry of system components and specific gaseous environment. In particular, the pressure decreases lower the electric field strengths necessary for gas breakdown.

Vacuum processing presents distinctive advantages for several processes as enhanced material diffusion rates or lower boiling solvent temperatures (vacuum drying processes). The heating of materials by convection or conduction at low pressures is not favoured, thus making the use of a MW heating an interesting solution.

In order to establish a safe operational region for the process of interest, some estimations can be done starting from the associated operating conditions. Based on the cavity volume V for a certain power input P_{in} and unloaded Q-factor Q_0 (see **Section 3.3.2**), it is possible to calculate the maximum electric field inside the cavity from the following relation [17]:

$$E_{max} = 2\left(\frac{(P_{in}/V)Q_0}{\omega\varepsilon_0 * 10^6}\right)^{0,5} \qquad (3.16)$$

It is worth remembering that **Equation 3.16** lack of precision depends from the inhomogeneous EM field distribution at several locations of the cavity as sharp edges, corners or high dielectric loss factor workloads. Thus, applying **Equation 3.10,** the maximum power dissipation can be determined to have a first estimate for a safe operation based on the gaseous environment and operating pressure range, although preliminary experimental testing is the only way to completely assess the loaded cavity EM behaviour.

3.3 MW system components

Typical industrial MW heating systems are based on three main components: the MW power source, the transmission line and the applicator (see **Figure 3.9**).

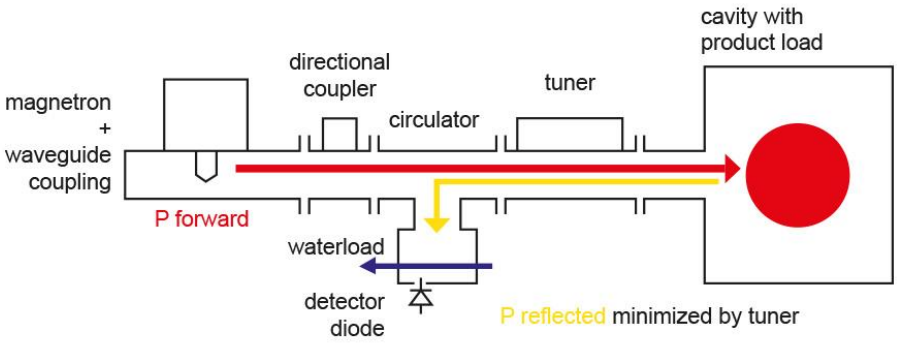

Figure 3.9 *- Schematic Design of an industrial Microwave Plant* [46]

Primarily due to efficiency and cost reasons, magnetrons are the most employed MW sources. The latter is based on a tungsten thoriated cathode at the center of the cavity and a circular hollow metal anode, containing a number of resonant cavities tuned to the operating MW frequency (see **Figure 3.10**).

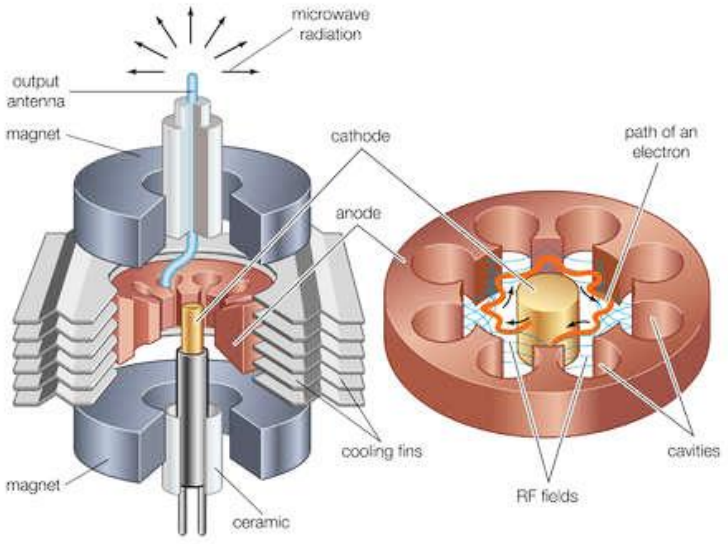

Figure 3.10 *– Magnetron structure* [47]

Through the application of a kV order voltage, an orthogonal electric and magnetic field is produced ejecting electrons from the cathode to the anode. The resonant cavities are equivalent to tuned circuits where its dimension determines the source frequency. The resulting power is extracted by a coupling loop to be sent into the applicator through the transmission line. Significant changes in the load could lead to variations of the emitted power and oscillating frequency of the magnetron.

Magnetron sources are characterised by a not tunable operating frequency and scarce spectral purity (more expensive industrial magnetrons may display an improved spectral purity but lower bandwidth). Those disadvantages are compensated by the low cost, high efficiency and power levels available.

Besides the power source, another important component, generally integrated into the MW generator close to the magnetron head, is the isolator which is based on a circulator (3-port device utilizing ferrite technology to selectively direct microwave energy to a specific port, based on the direction of wave propagation) and an absorbing (dummy) load attached to one port. The purpose of the isolator is to protect the magnetron from eventual MW reflections and to provide a matched load for an efficient energy generation.

Once obtained a good understanding of the MW cavity behaviour it is necessary to know the magnetron output spectrum, in order to have a suitable source-applicator coupling. Usually employed magnetron sources operate under certain bandwidth, as $2450 \pm 50\ MHz$, which needs to be maintained within well specified limits to avoid interferences with other electronic devices.

Another advantage of MW is that they can be transmitted through air for long distances without significant losses in terms of electric field strength, thus resulting in very clean and controlled environments. Datasheets about the various kinds of waveguides are generally differentiated based on their geometrical dimensions with subsequent operating frequency range and cut-off frequencies.

Figure 3.11 *– Waveguides with rectangular to circular transition* [48]

The minimization of the reflected power is usually achieved adding a tuner on the waveguide, being a component used for matching of the load impedance to that of the source, thereby maximizing the coupling with it. A tuner works as an impedance matching device, manipulating the EM field inside the waveguide by adjusting the depth of metal stubs placed at specific guide lengths. Those tuners can be either manual, where the position of the stubs is manually adjusted into the waveguide, or automatic, where the stubs are attached to a motor controlled by specific algorithms for maximum power transfer.

The final critical component is the applicator. Regarding MW heating applications, the latter can either be a reactor volume specifically designed or an integral part of the waveguide. The efficiency in MW transfer is determined from applicator design since the temperature profile developed into the material is directly linked to the EM field distribution inside the cavity.

Depending on whether the heating takes place inside or outside the applicator, it is possible to classify MW applicators as open or closed structures. Regarding the first category, devices as horn antennas or waveguide slotted arrays are employed to irradiate the material of interest, which makes them suitable for treating planar objects [49,50]. Closed structures include

travelling wave applicators or single/multimode resonant cavities, which are characterized by higher field strengths with different degrees of field uniformity.

Cavity walls of a generic MW applicator should display several characteristics. Based on the operating conditions of the process of interest, an ideal material selected for the cavity walls should result in an electrically closed volume where the currents flow, possibly without impediments. A first barrier is represented by the cavity Q-factor value among the various configurations, that should guarantee the best overall MW heating efficiency. Moreover, whereas the applicator is used for high temperature applications in aggressive environments, material walls should be selected to ensure possibly a constant performance with the operating conditions.

The implementation of a MW system is first based on the heating characteristics of the application. Whether the material is to be simply heated or more complex processes are involved, it is necessary to understand if the MW assisted route would be the most effective and economic solution. Some of the basic factors which favour a MW assisted or a traditional heating method are reported in **Table 3-2**:

Table 3-2 *– Factors favouring conventional or MW heating methods*

+ Conventional heating	**+ MW heating**
Large surface area and small volume	Inverse temperature profile
Low specific heat	Higher process speed
High thermal conductivity	Instant on/off processing
Acceptable long heating times	Reduction in equipment footprint
High coefficients of thermal exchange	More compact systems
Possible use of higher surface/bulk temperature	Energy savings

MW heating benefits have been listed above but it is obvious that the opposite of the factors favouring conventional heating methods can be considered as first good discriminants for the choice of a MW assisted process.

Although batch MW processing is still used, the high throughput demands of many industries means that continuous MW processing, as using conveyors or within pipes, is now being used to a greater extent.

Due to the tremendous range of materials and processes that could be treated by MW heating, there is not a specific applicator design which could be directly employed ensuring good performance. Commonly, any applicator design needs to be tailored for the application of interest, although some of the historical types still constitutes the starting point. In the next paragraphs some of the main applicator schemes will be discussed.

3.3.1. Travelling wave applicator

Travelling wave applicators generally consist of a length of a MW transmission line, such as a rectangular waveguide, along which MW energy propagates heating the workload while the residue is absorbed by a matched terminating load.

The material to be heated is introduced directly into the transmission line via a "choked" input and output opening that are positioned at the points of minimum wall current, minimizing eventual power leakages. The advantages of travelling wave applicators are the very good heating uniformity, high coupling levels and the size of the applicator that is small with respect to multimode cavities [51].

Travelling wave applicators are usually used in continuous processing applications and their efficiency is related to the dielectric properties and cross-section of the load. Low loss materials are usually considered for this kind of applicators, to avoid usage of inconvenient long lines. Specifically, the attenuation of the wave propagating through the workload is determined by its cross-section and dielectric loss factor. Practical length travelling wave applicators are characterized by attenuations of the order of $2 - 15\ dB/m$ [12]. The wave attenuation increases with frequency and the waveguide "filling factor" (fraction of electric energy stored in the sample). Therefore, high frequency applicators are characterized by great compactness, but too high attenuations could lead to unacceptable non-uniformities in the EM field distribution.

Travelling wave applicators can be made resonant by substituting the terminating load with an adjustable short circuit and fitting an aperture plate at the generator end [17], with the possibility to efficiently heat also high loss materials. Although, the resonant condition implies additional constraints for the achievement of a reproducible EM field distribution and uniform heating pattern, which is a debated issue in literature [52].

Usual geometries employed for the design of travelling wave applicators are the axial and meander or serpentine type (see **Figure 3.12**).

Figure 3.12 *– Image of a 922 MHz "meander line" travelling wave applicator* [51]

The axial applicator is simply a waveguide operating in the TE_{10} dominant mode, with the workload travelling axially inside it through a conveyor belt. Advantages of this geometry are the high transverse heating uniformity, ease of construction and low cost, while the disadvantages are mostly related to the reduced materials width, which is in turn determined by the acceptable attenuation per unit length that gives the maximum MW heating efficiency.

The limits in terms of width of the materials that can be treated using the first approach have been overcome by using the "meander" travelling wave applicator, which is basically a series of slotted waveguide applicators connected by 180° bends. By use of such an applicator, each pass displays a highly uniform electric field and relatively low attenuation resulting in uniform heating. The number of meander passes, where the MW energy is absorbed, depends from the final MW heating efficiency (low residual power to be absorbed by the terminating load). The

high symmetry of the slotted waveguide avoids leakages, although the introduction of a workload could introduce changes in the field distribution requiring the addition of choking systems or power absorbers at each end for safety reasons.

When the attenuation per pass becomes too low, the number of passes reach uneconomically high values. Specifically, when the attenuation per pass reach values of about 0,5 dB, the wall losses become a critical factor in the overall heating efficiency. Another fundamental element to be considered is the variation of the dielectric loss factor with operating conditions.

The need for a uniform, reproducible and controllable EM field distribution is particularly important in applications involving chemical reactions. The characteristic design of the travelling wave applicator, displaying a MW field travelling only in one direction along the reactor, can avoid inhomogeneities in the resulting heating pattern enabling an easier process scale-up. Some of the critical factors for the design of a travelling wave MW reactor have been recently addressed using a particular coaxial structure [53].

3.3.2. Single mode resonant cavities

Resonators are important components for MW applications. These systems are used into low power communication applications to create, filter and select frequencies for several components as oscillators, tuners and amplifiers. Regarding MW heating applications, resonant cavities are employed thanks to their capacity of high EM energy storage to be dissipated as heat into the material.

Practically, a resonant cavity is based on an insulated chamber with conductive walls where the material is heated thanks to multiple passages of the waves reflected by them. However, this constructive interference leads to an increase in the intensity of the field only if its frequency is close to one of the resonance frequencies of the system. The parameter that determine the performance of a resonant cavity is the Q-factor.

In fact, each resonator is characterized by a discrete number of modes, which depends on the volume and geometry of the system, while each mode is in turn characterized by a specific resonance frequency and Q-factor. Specifically, the amount of EM energy in the resonator, given a constant absorbed power, is higher the larger the Q-factor of the excited mode, where the latter is inversely proportional to the bandwidth.

The increasing interest in energy efficiency and precise process control matters led to several investigations in the usage of single mode resonant cavities. These applicators are able of supporting only one mode at the source frequency, where the superposition of the reflected waves generates a very well-defined and predictable standing wave pattern in the space.

In order to achieve a reliable design, the characteristics of the cavity needs to be considered before. It is normal practice to distinguish between an “unloaded Q-factor” Q_0, where only the dissipation contributions in the walls and the dielectric material have been included, and a “loaded Q-factor” Q_L, where also the dissipation in the external excitation circuit (characterized by an external Q-factor Q_{ex}) have been accounted, based on the following relation:

$$\frac{1}{Q_L} = \frac{1}{Q_0} + \frac{1}{Q_{ex}} \qquad (3.16)$$

In order to achieve the maximum amount of energy transfer from the source to the applicator, the characteristic impedance of the waveguide needs to be matched with the cavity impedance, given by all internal dissipation contributions. This issue usually requires the addition of a matching system between the cavity and the waveguide. It appears immediately that an experimental investigation on the cavity spectrum is of fundamental importance to understand the EM cavity behaviour.

The different spectra derived from the various cavity configurations, allow to determine the variation of the Q-factor simply using **Equation 3.15**. The decrease of the Q-factor from the empty to the loaded configuration allow to determine the order of magnitude of the losses into the system.

Finally, it is important also to consider the variation of dielectric properties with the operating conditions to keep the highest efficiency along the process. Especially in the case of single mode resonant cavities, automatic frequency tuning networks are employed, although they usually lack the desired degree of flexibility and precision required.

The main advantages and disadvantages related to single mode resonant cavities are reported in **Table 3-3**:

Table 3-3 *– Advantages/Disadvantages of single mode resonant cavities*

Advantages	**Disadvantages**
High localized field strength	Reduced sample dimensions (half of the wavelength at the operating frequency)
Well-known EM field distribution	Strict frequency tuning requirements
Heating of both low/high loss materials	Low flexibility of use among different materials
High MW heating efficiency	Not scalable to industrial applications

In particular, the narrow ISM frequency bands and strict tuning requirements strongly limits the dimensions of the material that can be treated, even at frequencies of 915 MHz. For those reasons, single mode resonant cavities are usually employed for lab-scale applications. Furthermore, when processing low loss materials, automatic feedback control systems are necessary to operate within the required resonant frequency band and hence maintain high heating rates.

Some important applications, where the latter applicator design is particularly employed, regards dielectric properties measurement or MW effects analysis. The understanding of the complex EM/material interaction phenomena demands for well-known field patterns inside the cavity to position the sample of interest in the region of higher field strength for optimal performance, provided to keep working in the narrow operating frequency range. If the latter condition is respected, single mode resonant cavities provide the highest power densities of about $10^7\ kW/m^3$, corresponding to heating rates of $30°C/s$, among all applicator schemes.

Another example where the high localized field strength of single mode resonant cavities, which gives the possibility to quickly heat also low-loss materials, can be exploited is related to the joining of selected regions among different substrates [54].

3.4 Overmoded resonant cavities

Overmoded, or multimode, cavities are the most commonly employed applicators for low and high-power industrial MW applications [12,17]. Their wide usage derives from the possibility to process a very wide range of samples with cavities whose overall dimensions are several times the wavelength at the operating frequency.

Although characterised by a simple mechanical design, the analysis of the EM behaviour of these cavities and the approach to achieve a high MW heating efficiency with acceptable uniformity is quite complex and it is the focus of several research activities [55].

Due to the complexity of the procedure required for a proper MW heating of large samples, two different approaches are usually considered, one based on an overmoded resonant cavity and one based on an overmoded non-resonant cavity.

In an overmoded reactor resonant system, the quasi-continuum spectrum of EM modes can be excited combining different techniques as a multi-port excitation scheme.

In an overmoded non-resonant system, the walls of the reactor are covered with a MW absorbing material that damps the EM reflections. This system reproduces the EM behaviour of a sample in free space irradiated by a series of MW sources. A regular series of excitation ports in the reactor can ensure a uniform illumination of all regions of the sample, ensuring in turn its uniform heating.

Crucial points in the theoretical investigation and in the design of both the above-mentioned approaches is the accurate knowledge of the characteristics of the samples and the reliability of numerical simulations.

A careful analysis of the constraints imposed by the typical sample size, shape, and physical properties showed that the overmoded non-resonant solution was not viable for the MW-CVI reactor, since it would require a high number of sources and access ports as well as a large reactor volume and well MW matched reactor walls thus, in the following, only the overmoded resonant approach will be considered.

The main advantages and disadvantages related to the usage of overmoded resonant cavities are reported in **Table 3-4**:

***Table 3-4**: Advantages/Disadvantages of overmoded resonant cavities*

Advantages	**Disadvantages**
Processing of bulky materials	Complex analysis of the EM behaviour
Moderate/High efficiency	Difficult conditions of heating uniformity
Suitable for batch/continuous processes	
Performance independent from the optimal sample positioning or geometry	

Those cavities operate in frequency ranges quite far from their cut-off frequencies, displaying spectra with a high number of modes. Therefore, the achievement of a highly uniform EM field into the loaded cavity depends from the simultaneous excitation of the highest possible number of modes. The larger the cavity the higher the number of modes, although that would be a less practical solution since it would reduce MW heating efficiency. This problem usually leads to a

trade-off between the latter parameters, to find a compromise resulting in optimal performance of the applicator.

The passage from an empty to a loaded cavity configuration generally leads to a widening of the operating frequency bands, which is experimentally displayed as a decrease of modes Q-factor due to an increase in cavity losses. Provided to have a sufficient spectral density, the single resonances will overlap with each other resulting in a continuous coupling with the load. Another effect is the down shifting of the resonances, which could be fully or partially within the source frequency band resulting in different degree of field intensity.

The increase in load size result in a less homogeneous heating pattern with presence of hotspots/coldspots, mostly located close to the feed point. Smaller loads require high dielectric loss factor, in order to compensate for the cavity filling factor decrease, which would lead to a lower efficiency.

It is convenient to distinguish two different operational scenarios [56]:

1. Small load with a low dielectric loss factor: the material will not influence the modal spectrum of the cavity displaying a homogeneous EM field with high penetration depth;
2. Big load with high dielectric loss factor: the modal spectrum is completely different from the empty cavity configuration exhibiting a highly inhomogeneous EM field with low penetration depth;

The upper bound is reached above a certain material dimension and dielectric loss factor, when the cavity will lose its overmoded operational characteristic. In addition, a highly lossy load display very low penetration depths resulting only in a surface heating.

Some additional precaution that could be needed regard the shape of the materials of interest; the presence of sharp edges usually results in localized overheating since the field is more intense in those spots. This situation is exacerbated in the case of highly lossy samples since are less penetrated by MW, sometimes exhibiting spark formation. Another good practice regards the positioning of the samples, which should not be too close to the feed point since it could receive too much energy with respect to the material electrical strength [57]. In the case of a relatively large sample, the latter issue could be mitigated heating the material from multiple ports or adding a rotating system leading to a time-averaged constant EM field distribution.

Starting from the above considerations, different strategies have been industrially adopted to achieve optimal performance with good heating uniformity. Some commercial applicators were developed with a larger cavity and multiple excitation ports using particular geometries to increase the degree of EM field uniformity. Weisstechnik[29] company designed an exagonal cavity excited by 12 magnetrons, where a total of 962 modes were present exhibiting a rather uniform field. Moreover, the usage of curved surfaces on the walls limited the excitation of the same modes. The hexagonal cavity design was employed to cure carbon reinforced ephoxy composites halving the total processing time [58].

Among the main drawbacks of overmoded resonant cavities there is the unpredictable formation of hotspots and coldspots, which results particularly detrimental for the achievement of a uniform heating profile on the sample. Traditional approaches to prevent the occurrence of hotspots consist in the rotation of the object to be heated or in the inclusion of mode stirrers, i.e.

[29] https://www.weiss-technik.com/en/products/heat-technology/

mobile metallic surfaces that dynamically affect the EM field in the reactor. Both of these solutions, however, have severe limitations: they involve moving metal parts, which may get stuck as a consequence of dust accumulation in the environment of the applicator and they provide a limited capability to control the actual field intensity distribution [59].

The usage of higher frequency sources was also investigated in order to exploit advantages as the excitation of a larger number of modes and higher power energy deposited. The next ISM frequency source, after the common 2,45 GHz, is centred at 5,8 GHz where several benefits, as the higher throughputs, were reported in literature [60]. Following, the next ISM frequency source is the 24 GHz or Gyrotron sources, which were successfully employed for ceramic sintering for the production of high-purity alumina [61].

Another approach was to excite more modes widening the source frequency bandwidth, although this task is tough to achieve with magnetron sources. Moreover, in addition to the higher cost there would be also to take into account the expenses for the safe shielding of the applicator if the emission limits were exceeded, which are far more stringent than other safety rules. Thus, the only possibility would be to employ multiple sources operating at different ISM frequencies, exciting a larger number of modes, thus improving heating uniformity.

The latter solution, although displaying the above reported benefits, requires a detailed preliminary analysis to avoid cross-coupling between the various sources, leading to impedance mismatches. Usually this scenario is analysed through numerical techniques in order to predict the EM field distribution inside the applicator. Moreover, the addition of circulators, diverting the power to dummy loads, is crucial in order to avoid magnetron damages.

3.5 Conclusions

In this Chapter some of the main parameters related to MW heated cavities have been introduced and discussed. A short review on EM theory was included in order to facilitate the understanding of EM wave generation, propagation and interaction phenomena with dielectric materials.

A short review of the main approaches, currently employed to improve design reliability of MW applicators, have been included analysing various critical aspects which lagged in the past the passage to an efficient MW assisted process. The latter were mostly based on numerical techniques, where it was clarified in particular the importance of validating the results obtained through experimental evidences. Following this approach, some of the main high frequency and temperature measurement devices and quantities have been shortly detailed, to retrieve the fundamental parameters necessary to achieve a realistic simulation of the MW cavity.

The basic applicator designs were then presented, highlighting the main advantages and disadvantages as well as critical issues which should be first taken into account, based on the process where the MW assisted heating will be implemented. Among those applicators, the overmoded resonant cavity presented important advantages from an industrial point of view both in terms of robustness, versatility and scale-up, provided to have a good understanding of the MW cavity behaviour for a certain sample dimension.

The proficient transfer of knowledge from MW-CVI at lab-scale to industrial level requires a detailed understanding of microwave-material electromagnetic interaction phenomena. An important part of this understanding relies on the dielectric properties of the sample at the conditions at which the infiltrations are conducted. Accordingly, the construction of an efficient reactor based on the MW heating requires a careful design of the applicator *loaded by the typical sample of interest*, since the efficiency in the dissipation of the MW energy in the material of interest is critically dependent on this design. According to the literature, often the design of the MW applicators tends to rely more on empirical information based on the designer experience and on trial and error, instead on a robust and well-defined procedure.

Depending on the dielectric properties of the materials to be treated, very different MW heating results can be obtained, both in terms of energy efficiency and infiltration uniformity, due to the interplay between the dielectric properties of the material and the EM field distribution. In some cases, the MW-assisted processing can lead to the insurgence of thermal instabilities, related to positive feedback mechanisms in which the overheating of a region of the sample corresponds to an increase of the local dielectric losses, which in turn leads to a further overheating phenomenon. This condition is exacerbated in the case of those materials with low thermal conductivities, as often the case of ceramics. Especially in the case of overmoded cavities loaded with large samples, the insurgence of pronounced non-homogeneous heating phenomena can produce experimental results that can be difficult to rationalize, due to the intrinsically unstable nature of these phenomena.

Therefore, in order to achieve a controllable MW heating, it is necessary to carefully investigate the EM behaviour of the reactor loaded by the sample as well as the resulting temperature profile. In the design of overmoded reactors, the situation is made more complex by the high number of EM modes that can be excited in the reactor. The possibility of achieving sufficient predictability and control of the EM behaviour of overmoded reactors loaded by relatively large

samples has been strongly questioned recently. This important issue will be carefully addressed in the next chapters.

A consolidated praxis for the development of industrial MW heated plants is the validation through simple experimental tests in order to determine the efficiency of the process and correlated costs. Specific strategies to improve source-applicator coupling and heating uniformity can be evaluated in this stage. Due to the lack of frequency and phase control of magnetron sources, common approaches to increase power density distribution involve the usage of mode stirrers, mechanical movement of the sample or dual/multi-frequency devices feeding microwaves at different points and polarisations (provided to minimize the cross-coupling between different generators). The application of hybrid heating approaches, based on the simultaneous or subsequent usage of MW and conventional heating methods, is another possibility to enhance the energy efficiency of the system providing improved heating uniformity and process control.

Most of the modern research activities are devoted to lab-scale exploratory efforts, therefore much work is needed to scale-up processes to large batch or continuous process in order to realize full potential of MW assisted applications.

In conclusion, a first roadmap was developed in order to highlight the main aspects necessary to understand, design and control of a cavity for MW-assisted processes, guaranteeing good energy efficiency. Specifically, among the most important information that will need to be considered for the design of an overmoded resonant cavity there are:

- Availability of thermal and dielectric properties of the materials of interest as a function of the temperature and the density, in addition to their shape and dimensions;
- Preliminary evaluation of the cavity spectral density, power efficiency and prediction of the loaded cavity EM behaviour through theoretical analysis and numerical multiphysics models;
- Validation of numerical results with experimental evidences to identify possible sources of error or identifying the insurgence of phenomena which cannot be reliably predicted through modelling (as plasma formation or unexpected microwave effects);
- Development of solutions to monitor and determine internal temperature and thermal profiles within a material during processing;
- Definition of operating conditions providing as much as uniform and stable processing as a function of material properties, specimen size and geometry and strategies to maximize power density distribution within the load;

3.6 References

[1] Das S, Mukhopadhyay AK, Datta S, et al. Prospects of microwave processing: An overview. Bulletin of Materials Science. 2009;32:1–13.

[2] Bykov Y V., Rybakov KI, Semenov VE. High-temperature microwave processing of materials. Journal of Physics D: Applied Physics. 2001;34:R55.

[3] Clark DE, Sutton WH. Microwave Processing of Materials. Annual Review of Materials Science [Internet]. 1996;26:299–331. Available from: https://doi.org/10.1146/annurev.ms.26.080196.001503.

[4] Singh S, Gupta D, Jain V, et al. Microwave processing of materials and applications in manufacturing industries: A Review. Materials and Manufacturing Processes. 2015;30:1–29.

[5] Agrawal D. Latest global developments in microwave materials processing. Materials Research Innovations. 2010;14:3–8.

[6] Mishra RR, Sharma AK. Microwave-material interaction phenomena: Heating mechanisms, challenges and opportunities in material processing. Composites Part A: Applied Science and Manufacturing [Internet]. 2016;81:78–97. Available from: http://dx.doi.org/10.1016/j.compositesa.2015.10.035.

[7] Boey FYC, Lee WL. Microwave radiation curing of a thermosetting composite. Journal of Materials Science Letters. 1990;9:1172–1173.

[8] Yue C, Looi H. Influence of thermal and microwave processing on the mechanical and interfacial properties of a glass/epoxy composite. Composites. 1995;26:767–773.

[9] Nightingale C, Day RJ. Flexural and interlaminar shear strength properties of carbon fibre/epoxy composites cured thermally and with microwave radiation. Composites - Part A: Applied Science and Manufacturing. 2002;33:1021–1030.

[10] Menezes RR, Souto PM, Kiminami RHGA. Microwave Fast Sintering of Ceramics Materials. Sintering of Ceramics - New Emerging Techniques [Internet]. 2012;3–26. Available from: www.intechopen.com.

[11] Agrawal DK. Microwave processing of ceramics. Current Opinion in Solid State and Materials Science. 1998;3:480–485.

[12] Meredith RJ. Engineers' Handbook of Industrial Microwave Heating [Internet]. Stevenage, United Kingdom: IET; 1998. Available from: https://doi.org/10.1049/PBPO025E.

[13] Metaxas AC. Foundation of Electroheat: A Unified Approach. John Wiley & Sons, editor. Chichester, United Kingdom: Wiley; 1996.

[14] Chan TVCT, Reader HC. Understanding Microwave Heating Cavities. Norwood, United States: Artech House Publishers; 2000.

[15] Roussy G, Pearce JA. Foundations and Industrial Applications of Microwave and Radio Frequency Fields: Physical and Chemical Processes. Proceedings of the 6th International Conference on Optimization of Electrical and Electronic Equipments. Brasov, Romania: IEEE; 1998. p. 492.

[16] Mehrdad Mehdizadeh. Microwave/RF Applicators and Probes for Material Heating,

Sensing, and Plasma Generation. 2nd ed. Oxford: William Andrew Publishing; 2015.

[17] Metaxas AC, Meredith RJ. Industrial Microwave Heating. London, United Kingdom: IET; 2008.

[18] Hill DA. Electromagnetic Fields in Cavities: Deterministic and Statistical Theories. Sons JW&, editor. IEEE Press, New York; 2009.

[19] Hill JM, Marchant TR. Modelling microwave heating. Applied Mathematical Modelling. 1996;20:3–15.

[20] Sorrentino R, Bianchi G. Microwave and RF engineering. John Wiley & Sons; 2010.

[21] CEM. Microwave Heating - Mechanism and Theory [Internet]. Available from: https://cem.com/it/microwave-heating-mechanism-and-theory.

[22] W. VL. European Regulations, Safety Issues in RF and Microwave Power. In: M. W-P, editor. Advances in Microwave and Radio Frequency Processing. Heidelberg: Springer-Verlag; 2006.

[23] Thostenson ET, Chou T. Microwave processing: fundamentals and applications. Composites Part A: Applied Science and Manufacturing. 1999;30:1055–1071.

[24] Gallego J, Del Val MA, Contreras V, et al. Heating asphalt mixtures with microwaves to promote self-healing. Construction and Building Materials [Internet]. 2013;42:1–4. Available from: http://dx.doi.org/10.1016/j.conbuildmat.2012.12.007.

[25] Singh VK, Shukla A, Patra MK, et al. Microwave absorbing properties of a thermally reduced graphene oxide/nitrile butadiene rubber composite. Carbon [Internet]. 2012;50:2202–2208. Available from: http://dx.doi.org/10.1016/j.carbon.2012.01.033.

[26] Wei J, Hawley M, Asmussen J. Microwave Power Absorption Model for Composite Processing in a Tunable Resonant Cavity. Journal of Microwave Power and Electromagnetic Energy [Internet]. 1993;28. Available from: https://doi.org/10.1080/08327823.1993.11688225.

[27] Heuguet R, Marinel S, Thuault A, et al. Effects of the susceptor dielectric properties on the microwave sintering of alumina. Journal of the American Ceramic Society. 2013;96:3728–3736.

[28] Balanis CA. Advanced Engineering Electromagnetics. 2nd ed. John Wiley & Sons; 2012.

[29] Dechammakl. Electromagnetic waves [Internet]. 2018. Available from: https://commons.wikimedia.org/wiki/File:Electromagnetic_waves.png.

[30] Creatives AT. TE & TM Modes [Internet]. 2017. Available from: http://www.engineeringdone.com/te-tm-modes/te-tm-modes/.

[31] Wikipedia. Transverse modes [Internet]. Available from: https://en.wikipedia.org/wiki/Transverse_mode.

[32] Veronesi P, Leonelli C, Rivasi MR, et al. The electromagnetic field modeling as a tool in the microwave heating feasibility studies. Materials Research Innovations. 2003;8:9–12.

[33] Yakovlev V V. Examination of Contemporary Electromagnetic Software Capable of Modeling Problems of Microwave Heating. In: Willert-Porada M, editor. Advances in Microwave and Radio Frequency Processing. Berlin: Springer-Verlag; 2006. p. 178–190.

[34] Dibben DC. Numerical and Experimental Modelling of Microwave Applicators [Internet]. University of Cambridge; 1995. Available from: http://www.dspace.cam.ac.uk/handle/1810/237037.

[35] COMSOL Multiphysics. COMSOL Multiphysics [Internet]. Available from: https://www.comsol.it/.

[36] Keysight Technologies. Agilent Technologies' High-Performance Mid-Range VNA [Internet]. Available from: https://about.keysight.com/en/newsroom/imagelibrary/library/PNA-L_images/.

[37] Forrister T. ITW Uses Multiphysics Simulation to Cook Up Smart Microwave Oven Designs [Internet]. 2019. Available from: https://www.comsol.it/story/itw-uses-multiphysics-simulation-to-cook-up-smart-microwave-oven-designs-80551.

[38] Bykov Y V., Rybakov KI, Semenov VE. High-temperature microwave processing of materials. Journal of Physics D: Applied Physics. 2001;34.

[39] Hippel AR von. Dielectric Materials and Applications [Internet]. Cambridge: MIT Press; 1954. Available from: https://doi.org/10.1149%2F1.2430014.

[40] Klein O, Donovan S, Dressel M, et al. Microwave Cavity Perturbation Technique: Part I: Principles. International Journal of Infrared and Millimeter Waves. 1993;14:2423–2457.

[41] Couderc D, Giroux M, Bosisio RG. Dynamic High Temperature Microwave Complex Permittivity Measurements on Samples Heated Via Microwave Absorption. Journal of Microwave Power. 1973;8:69–82.

[42] Hutcheon R, Jong M de, Adams F, et al. A System for Rapid Measurements of RF and Microwave Properties Up to 1400°C. Part 2: Description of Apparatus, Data Collection Techniques and Measurements on Selected Materials. Journal of Microwave Power and Electromagnetic Energy. 1992;27:93–102.

[43] Hutcheon R, Jong M de, Adams F. A System for Rapid Measurements of RF and Microwave Properties Up to 1400°C. Part1: Theoritical Development of the Cavity Frequency-Shift Data Analysis Equations. Journal of Microwave Power and Electromagnetic Energy. 1992;27:87–92.

[44] DIAS Infrared Systems. Pyrometers PYROSPOT – For industry and research [Internet]. Available from: https://www.dias-infrared.com/products/pyrometers.

[45] Hamedani Y, Macha P, Bunning T, et al. Plasma-Enhanced Chemical Vapor Deposition: Where we are and the Outlook for the Future. In: Sudheer Neralla, editor. Chemical Vapor Deposition - Recent Advances and Applications in Optical, Solar Cells and Solid State Devices. Janeza Trdine, Croatia: InTech; 2016.

[46] Püschner. Püschner Microwave Power Systems [Internet]. Available from: https://www.pueschner.com/en/.

[47] Encyclopædia Britannica I. Typical elements of a magnetron [Internet]. Available from: https://kids.britannica.com/students/assembly/view/137.

[48] Flann microwave. Rectangular to circular waveguide transitions [Internet]. Available from: https://flann.com/products/straights/rectangular-to-circular-waveguide-transitions-series-64/.

[49] Castrillo V, D'Ambrosio G, Massa R, et al. Improved design of waveguide slot array applicators for microwave heating. Materials Research Innovations. 2004;8:71–74.

[50] Castrillo VU, Chiadini F, D'Ambrosio G, et al. Waveguide slot applicators for microwave heating. Conference Proceedings - ICECom 2003: 17th International Conference on Applied Electromagnetics and Communications. 2003;49–51.

[51] Microwave New Zealand - Industrial MW and RF technology. Microwave Applicators [Internet]. Available from: https://www.microwavenz.com/mw-applicators.

[52] Sturm GSJ, Stankiewicz AI, Stefanidis GD. Microwave reactor concepts: From resonant cavities to traveling fields. In: Stefanidis G, Stankiewicz A, editors. Alternative Energy Sources for Green Chemistry. Royal Society of Chemistry; 2016. p. 93–125.

[53] Eghbal Sarabi F, Ghorbani M, Stankiewicz A, et al. Coaxial traveling-wave microwave reactors: Design challenges and solutions. Chemical Engineering Research and Design [Internet]. 2020;153:677–683. Available from: https://doi.org/10.1016/j.cherd.2019.11.022.

[54] Rosa R, Veronesi P, Han S, et al. Microwave assisted combustion synthesis in the system Ti – Si – C for the joining of SiC : Experimental and numerical simulation results. Journal of the European Ceramic Society [Internet]. 2013;33:1707–1719. Available from: http://dx.doi.org/10.1016/j.jeurceramsoc.2013.03.005.

[55] Mehrdad Mehdizadeh. Microwave Multimode Cavities for Material Heating. Microwave/RF Applicators and Probes for Material Heating, Sensing, and Plasma Generation. 2nd ed. Oxford: William Andrew Publishing; 2015. p. 153–183.

[56] Bows JR. A classification system for microwave heating of food. International Journal of Food Science and Technology. 2000;35:417–430.

[57] Pedreno-Molina JL, Monzò-Cabrera J, Catala-Civera JM. Sample Movement Optimisation for Uniform Heating in Microwave Heating Ovens. International journal of RF and microwave computer-aided engineering. 2005;17:142–152.

[58] Kwak M, Robinson P, Bismarck A, et al. Curing of composite materials using the recently developed Hephaistos Microwave. 18th International Conference on Composite Materials [Internet]. 2011. Available from: https://www.researchgate.net/publication/285651368_Curing_of_composite_materials_using_the_recently_developed_Hephaistos_Microwave.

[59] Plaza-González P, Monzó-Cabrera J, Catalá-Civera JM, et al. Effect of mode-stirrer configurations on dielectric heating performance in multimode microwave applicators. IEEE Transactions on Microwave Theory and Techniques. 2005;53:1699–1705.

[60] Horikoshi S, Hamamura T, Kajitani M, et al. Green chemistry with a novel 5.8-GHz microwave apparatus. Prompt one-pot solvent-free synthesis of a major ionic liquid: The 1-butyl-3-methylimidazolium tetrafluoroborate system. Organic Process Research and Development. 2008;12:1089–1093.

[61] Bykov Y, Denisov G, Eremeev AG, et al. 3.5 kW 24 GHz Compact Gyrotron System for Microwave Processing of Materials. In: M. W-P, editor. Advances in Microwave and Radio Frequency Processing. Berlin: Springer-Verlag; 2006. p. 24–30.

Chapter 4

4. Design of an Overmoded Resonant Cavity-based Reactor for Ceramic Matrix Composites Production

The use of high-quality resonant cavities in MW-assisted reactors is highly desirable. Thanks to the low losses in the cavity walls and to the possibility to reach critical coupling conditions, high energy efficiency can indeed be achieved. This chapter describes the design, building, and test of a MW assisted Chemical Vapor Infiltration reactor at a pilot scale, based on an overmoded resonant cavity operating at 2.45 GHz.

First, a general design method is proposed, in which the dimensions of the cavity are chosen in order to obtain a defined mode density and a high fraction of MW power dissipated in the sample. Among the modes of this cavity, the most efficient one for the MW heating of the sample is then determined by means of rigorous numerical analysis.

In the graphite reactor cavity built using this approach, the condition of critical coupling is met in a large variety of samples and operating conditions. Moreover, a good agreement between experimental and simulated heating dynamics is obtained, which confirms the validity of the proposed method.

As a result, disc-shaped samples with a diameter of the order of 10 cm and a thickness of the order of 1 cm can be brought to an infiltration temperature of about 900 °C within 5 min, using a MW power of 1000 W, with a well controllable and reproducible temperature variation. In the infiltration of Nicalon™ preforms, more than 60% of the MW power is dissipated in the sample.

4.1 Introduction

Microwave processing of materials presents great possibilities from an industrial point of view. In fact, the reduction of processing time as well as energy consumption and the improvement of material properties, which represent goals of major importance in any manufacturing process, can all be obtained thanks to the MW heating, which is an EM energy transfer into materials with dielectric losses rather than a heat transfer. Advantages taken from MWs as heating technique are that both the heating is volumetric, with heating speed limited only by the available MW power, and the thermal gradients are reversed in the treated sample [1,2]. Moreover, the variability of the dielectric losses among different materials or even different phases of the same material can enable selective heating of internal or surface phases, additives or constituents, with the possibility of self–limiting reactions [3,4].

Processing of materials using high-frequency EM fields, such as MW and radiofrequency, is gaining more and more attention at the industrial level [5]. Its potential in heating applications has been known and exploited since the early '50s, when the first MW ovens were introduced to the marketplace by Raytheon [1]. Since then, many different attempts have been made in order to broaden the range of application of MW energy, especially as an alternative heat source for materials processing. Despite some low-temperature processing applications (e.g. food, wood, rubber, polymers) have achieved industrial maturity in the '80s and are now considered as a standard production methods, MW processing has mainly remained restricted to laboratory-scale research as far as most classes of materials are concerned, in particular for high-temperature applications [6]. Successful applications of MWs regard sintering of metals and ceramics powders [7], joining [8], waste processing [9], chemical or electrochemical reactor systems [10], composites technology [11].

A material processing technology which could highly benefit of the application of MWs is the CVI SiC-based CMCs as the SiC_f/SiC composites [12]. CMCs represent one of the latest and most promising solutions for high-temperature applications in strategic industrial sectors such as aerospace, energy and automotive [13]. In these industrial areas, materials are to be designed for severe environments, usually combining high temperatures, high stress levels, and corrosive atmospheres. Among CMCs, SiC_f/SiC composites attract much industrial consideration for thermally loaded components such as propulsion and thermal protection systems in space applications, and refractory materials for furnaces and energy reactors [14].

Huge market opportunities are expected for CMCs provided that the major identified gaps can be overcome, such as the high cost, the difficulty of processing, and the materials reliability. New and more efficient manufacturing technologies can pave the way to improve material quality, reduce processing time, converge towards near-net-shape fabrication, trimming of spent energy, and cutting of production costs.

The CVI method is a process in which reactant gases diffuse into a porous fibre-reinforced preform and deposit a solid material, as a result of chemical reactions occurring on fibre surface, thus filling the pores inside. In the case of SiC-based CMCs, the ceramic gaseous precursor adopted is Methyltrichlorosilane (MTS), which reacts at high temperatures (900-1100°C) in a hydrogen atmosphere to give SiC and hydrochloridric acid as a byproduct:

$$CH_3SiCl_{3(g)} \overset{H_2}{\leftrightarrow} SiC_{(s)} + 3HCl_{(g)} \qquad (4.1)$$

This process is very slow because the movement of gas molecules is controlled by diffusion only and due to the use of relatively low pressures (100-1000 mbar) to prevent pores on preform surface from being prematurely closed. During the densification process, conditions are required for avoiding pore closure, to prevent macroscopic inter-fibre bundle pores which hamper both mechanical and thermal properties [15].

The use of MW radiation is a clean and attractive alternative due to its potential for generating a controllable inverse temperature profile during the heating of the ceramic fibre preform. In this way the reaction front of the MW-CVI propagates from the centre to the surface of the preform as its dielectric response changes. Previous works carried out by Binner [16], based on SiC_f/SiC components (5 cm diameter, 1 cm thickness), has shown that by using MWs to enhance the CVI process, fabrication times can be reduced from hundreds of hours to around 100 hours.

In the design of applicators for MW-assisted processes, a key element is represented by the efficiency in transferring the EM energy from the source to the sample [17–21]. Ideally, such transfer should be complete, in order to guarantee the highest overall energy efficiency. However, complete absorption of the EM wave in the sample is not trivial, due to the unavoidable impedance mismatch between the wave in the propagating system and that in the sample, which causes a partial wave reflection at its surface.

The coupling of MW radiation to the sample can be enhanced by inserting the sample inside an EM resonator. In this manner, the sample is subject to multiple passages of the wave reflected by the conductive walls of the resonator. Once the proper working conditions are found, the EM energy absorption in the sample can be maximized both by the constructive interference of the waves inside the resonator and by the destructive interference of the waves outside the resonator.

In the particular case of single-port resonators, at the so-called critical coupling condition, the reflected power vanishes and all the incoming power is dissipated in the resonator loaded with the sample, despite the usually low power absorption over the single passage of the wave in the sample. A detailed discussion on the effects of the multiple-wave interference in a resonator and in its excitation circuit can be found in [22,23] and in the references therein.

Whenever the critical coupling condition is reached, all the power available at the excitation port is dissipated in the resonator, partly in its walls and partly in the sample. The efficiency of the sample heating is maximized when the dielectric losses of the sample dominate over the resistive (Ohmic) losses in the resonator walls.

The use of a resonant cavity can thus provide an efficient way to control and optimize the transfer of EM energy from the source to the sample. The MW-assisted processes usually employ sources operating at Industrial, Scientific, and Medical (ISM) bands centred around 915 MHz, 2.45 GHz, and 5.8 GHz [24]. In general, the dimensions of a single-mode resonator are about half of the employed wavelength. Thus, a cavity operating at the frequencies of the above ISM bands can be loaded with a sample with a typical size of few centimetres. Such a solution is of modest relevance for industrial applications, where larger sample sizes are needed. Moreover, the narrow bandwidth allowed by the ISM bands would require a continuous tuning of the single-mode resonator in order to compensate for the variations of the dielectric properties of the sample with the temperature, during the heating stage, and with the density, during the processing [17].

A solution that can overcome the drawbacks of single-mode EM reactors is based on overmoded resonant cavities, having dimensions of several wavelengths. In these cavities, different modes

can be simultaneously excited. The treatment of larger samples and more uniform field distributions, due to the simultaneous excitation of different modes, are benefits expected from using an overmoded reaction chamber in MW-assisted processes [17]. The spectrum of an overmoded reactor should thus appear as a smooth, continuous distribution of EM modes.

Moreover, in the cases of fixed-frequency sources, such a continuous spectrum is necessary to avoid a mismatch between the excitation frequency and the reactor operating frequencies, which change with the dielectric properties of the sample. In this regard, the possibility to achieve a sufficient level of predictability and control on the EM and thermal behaviour of overmoded reactors for the MW processing of relatively large samples was strongly questioned recently [20].

The objective of this work is to illustrate the design, building, and characterization of an efficient and well-controllable MW-CVI reactor chamber for CMCs production at a pilot scale, based on an overmoded resonant cavity operating in the 2.45 GHz ISM band and feed by magnetron sources. The reactor, enabling both MW heating and conventional heating, was built in the framework of the European project HELM [25]. This paper will focus on the core of the reactor, the reaction chamber. Further details on the whole system are provided in **Chapter 5**.

4.2 Materials and Methods

4.2.1. Basic concepts in the design of overmoded resonant cavities

In the design of MW reactors having large dimensions with respect to the employed wavelength, a basic difficulty is the presence of several modes that can be simultaneously excited at the frequency of interest. Furthermore, the process under study is made more complex by the insertion in the cavity of the sample to process since, in general, it causes an increase in the number of modes and a mixing of them.

A general analysis of the EM behaviour of large MW reactors loaded by the sample to process should include a large number of variables, such as the MW frequency, the shape and the dimension of the reactor and the properties of the material forming its walls, the shape and dimension of the sample, and its dielectric properties. In literature, this problem is usually faced assuming simple geometries for both the reactor chamber and the sample to process, in order to obtain analytic approximations for the spectral density of the modes and for the power dissipated in the sample [26].

Aim of this section is to present a general approach to the calculation of both the spectral density of the reactor and its efficiency in dissipating the EM power in samples with arbitrary shape and dielectric properties, without any assumption on the reactor shape. The only assumptions that will be made will concern the dimensions of the reactor, large enough to determine an overmoded behaviour, and the penetration depth of the radiation, which will be considered much larger or much smaller than the sample size.

In the present context, an overmoded resonant cavity can be defined as a resonant system in which consecutive EM modes overlap with each other. This condition can be discussed on the basis of general considerations, independent of its shape.

Consider first the mode density $\partial(\nu)$ at the frequency ν of the EM modes of a cavity with volume V. According to the Weyl law [27], the asymptotical approximation for large frequency of the mode density is given by [28]:

$$\partial(\nu) = 8\pi V \frac{\nu^2}{c^3} \qquad (4.2)$$

Where c is the speed of light in vacuum.

The level of overlap between the modes around the frequency ν is qualitatively determined by both the average mode spacing, whose approximation is $1/\partial(\nu)$, and the average linewidth $\Delta\nu(\nu)$ of the resonance curves of the modes close to ν. Specifically, the property of the modal overlap can be considered to hold if the mode density is large enough that a number of modes greater than one is found in an average linewidth. Actually, the spectrum of the cavity already becomes essentially continuous whenever $1/\partial(\nu)$ is equal to $\Delta\nu(\nu)$. In [29], by applying a Montecarlo method, this condition is found to determine the transition from a single-mode statistics of the field distribution to a multimode one.

Therefore, according to the definition adopted in this study, the reactor cavity can be considered as overmoded when the condition above is verified. The average spacing between the resonance modes can be controlled by changing the volume of the cavity. At a given frequency ν, the larger the resonant cavity, the denser the mode spectrum.

The linewidth $\Delta\nu$, defining the level of the overlap between modes, can be conveniently given as the full-width at half maximum of their resonance curve. This quantity can be expressed in terms of the quality factor Q of the resonance mode, defined as [30]:

$$Q = \frac{\nu_0}{\Delta\nu} = 2\pi\nu_0 \frac{W}{P} \qquad (4.3)$$

where ν_0 is the resonance frequency, W is the stored energy, and P is the dissipated power.

For an empty conducting cavity, the unloaded quality factor $Q_{0,C}$ of a given mode p, obtained neglecting the effect of the coupling to the excitation circuit, can be formulated as [28]:

$$Q_{0,C} = \frac{\iiint_V \boldsymbol{H_p} * \boldsymbol{H_p^*} dV}{\delta \oiint_S \boldsymbol{H_p} * \boldsymbol{H_p^*} dS} \qquad (4.4)$$

where $\delta = \sqrt{\frac{\rho}{\pi\mu\nu}}$ is the skin depth of the EM radiation in the walls of the cavity, having a resistivity ρ and a permeability μ [31], and $\boldsymbol{H_p}$ is the magnetic field of the mode p.

A good approximation of the quality factor $Q_{0,C}$, which is independent on the cavity shape and on the specific mode, is given by [28]:

$$Q_{0,C} \cong \frac{3}{2}\frac{V}{\delta A} \qquad (4.5)$$

Where A is the surface area of the cavity. The basic assumption behind (4.5) is that the EM fields are uniformly distributed in the reactor cavity, except close to its boundaries. A more accurate determination of the average value of the quality factor $Q_{0,C}$ of an ovemoded cavity can be found in [32,33], in which this quantity is obtained with a statistical approach developed for reverberation chambers.

According to (4.2) and (4.5), the knowledge of volume, surface area, and resistivity of a conductive cavity enables the estimation of the mode overlap at a given frequency, under the adopted condition of overmoded cavity. This condition can be expressed as a relationship between the wavelength λ of the EM radiation and the volume δA related to the skin depth:

$$\lambda^3 \cong \frac{16}{3}\pi * \delta A \qquad (4.6)$$

The increase of the cavity surface area A above the value provided by (4.6) reinforces the overlap between modes. However, in general this option is not convenient for the energy efficiency. To elucidate this point, consider a reactor loaded with a sample of volume V_s which is to be processed. The MW power P coupled to the reactor is now partially dissipated in the walls of the reactor (P_C) and partially in the sample (P_s):

$$P = P_c + P_s \qquad (4.7)$$

Equation (4.7) can be reformulated in terms of quality factors taking into account the second part of (4.3), as:

$$\frac{1}{Q_0} = \frac{1}{Q_{0,C}} + \frac{1}{Q_{0,s}} \qquad (4.8)$$

Where Q_0 is the total unloaded quality factor of the cavity and $Q_{0,s}$ is the unloaded quality factor of the cavity which is calculated taking into account only the dielectric losses in the sample. The latter is given by the relation:

$$\frac{1}{Q_{0,s}} = \eta * \tan\delta_\varepsilon \qquad (4.9)$$

Where the loss factor $\tan\delta_\varepsilon = \varepsilon''/\varepsilon'$ is the ratio between the imaginary and real part of the dielectric permittivity ε of the sample, $\varepsilon = \varepsilon' - i * \varepsilon'' = \varepsilon_0(\varepsilon_r' - i * \varepsilon_r'')$, ε_0 is the permittivity of free space, and the pedix r indicates the components of the relative permittivity ε_r [29]. The electric energy filling factor

$$\eta = \frac{\iiint_{V_s} \varepsilon' * \boldsymbol{E_p} * \boldsymbol{E_p^*} dV}{\iiint_{V} \varepsilon' * \boldsymbol{E_p} * \boldsymbol{E_p^*} dV} \qquad (4.10)$$

represents the fraction of electric energy stored in the sample.

In the same spirit of the approximation leading from (4.4) to (4.5), let us assume that the electric energy is distributed in a substantially uniform way in the reactor loaded with the sample. The physical basis of this assumption can be found in the discussions presented in [34]. The condition of constant electric energy density requires, in particular, that the penetration depth of the radiation in the sample is larger than its dimensions. In this case, the electric energy filling factor η can be simply expressed as:

$$\eta \approx \frac{V_s}{V} \qquad (4.11)$$

From the point of view of the MW-assisted process, the MW power dissipated in the walls of the reactor due to ohmic losses represents a reduction in efficiency and should be minimized, in favour of the power dissipated in the sample. From (4.6) to (4.11), one can obtain the ratio between P_s and P_C:

$$\frac{P_s}{P_C} \cong \frac{3}{2}\eta * \tan\delta_\varepsilon \frac{V}{\delta A} \approx \frac{3}{2}\tan\delta_\varepsilon \frac{V_s}{\delta A} \qquad (4.12)$$

The combination of (4.7) and (4.12) enables the determination of the fraction of power dissipated in the sample, which can be written as:

$$\frac{P_s}{P} = \frac{1}{1+\frac{P_C}{P_s}} \approx \frac{1}{1+\frac{2\delta A}{3\tan\delta_\varepsilon V_s}} \qquad (4.13)$$

Finally, from (4.13) it can be concluded that an increase in the surface area of the reactor cavity results in a decrease in the efficiency of the MW heating of the sample, given the characteristics of the materials constituting the cavity and the sample to process. Accordingly, the surface and, ultimately, the volume of the reactor cavity must be set to the minimum value compatible with the other constraints, in the considered case that one of overmoded structure.

A similar conclusion holds for conducting samples. In the case in which the skin depth in the sample, δ_s, is much smaller than the minimum sample dimension, the ratio between P_s and P_C is given by:

$$\frac{P_s}{P_C} \cong \frac{\delta_s * A_s}{\delta_\varepsilon * A} \qquad (4.14)$$

Where A_s is the sample surface area.

In general, the accuracy in the determination of the ratio of Equation (4.12) is strongly related to the accuracy in the determination of the filling factor η. In specific cases, an exact calculation of η is possible, as discussed for instance in [17,35].

Finally, (4.12) and (4.14) provide a quick way to assess how effectively the power is used and thus to decide the convenience of the MW heating of a given sample. Together with (4.7), they represent a vademecum in the design of overmoded cavities of general shape for the MW-assisted processing of arbitrary samples, formulated for the first time to the best of our knowledge.

4.2.2. Materials of interest and dimensions of the reaction chamber

The quantities playing a key role in the design of an efficient MW reactor chamber with overmoded behaviour are those defining (4.7), (4.12), and (4.14). In the case here considered, the MW frequency was set to 2.45 GHz and the typical sample to be infiltrated with the MW-CVI technique was a preform based on polycarbosilane-derived Si–C–O Nicalon NL-202 fibres (Nippon Carbon, Tokyo, Japan), with minimum dimensions of about 10 cm in diameter and 1 cm in thickness.

The determination of the most convenient dimensions of the reactor chamber requires the knowledge of both the dielectric properties of the sample and the resistivity of the chamber walls.

Thanks to its semi-conductivity and good chemical resistance at high temperatures and harsh environments, SiC displayed great potential and practical application at high-temperatures as

a dielectric material by means of its intrinsic electric dipolar polarization. In fact, its electrical conductivity ($\sigma = 10^{-4} - 10^{-2}\ S/cm$) is intermediate in magnitude between that of a conductor and an insulator like alumina [36,37]. The movement of free electrons in semiconductors like SiC is also associated to a good thermal conductivity. Moreover ε'' is relatively constant up to about 1400 °C [38], minimizing the risk of formation of hot spots and thermal runaways. For these reasons SiC is typically used as a susceptor for its ability to absorb MW energy and convert it to heat.

SiC ceramics are produced in a broad and diverse range of structures as wires, whiskers, fibres, tubes with specific morphologies which can be used to enhance even their dielectric absorption properties. It was reported that engineered SiC materials with stacking faults and planes produced extensive polarization under an applied EM field resulting in higher heat dissipation [39]. Improved EM absorption performance of SiC was also achieved through surface modifications with other dielectric or magnetic materials which introduced multiple polarizations thus resulting in higher dielectric properties [40].

In the case of SiC_f/SiC composites the dielectric properties are influenced by each component (i.e. fibre, matrix and interphase). Several papers showed that SiC fibres are good MW absorbers displaying different electrical resistivities (as reported in **Table 2.2**). In particular, the electrical properties of SiC fibres showed a marked dependence from the C/Si ratio [41]. Commonly SiC fibres are employed in the form of woven fabrics therefore detailed investigations are needed for the measurement of the related dielectric properties. Tan et al. examined Tyranno™ fabrics showing how the fibre arrangement and different temperature heat treatments, with eventual oxidation of the reinforcement, affected the MW absorbing properties in the 17-40 GHz frequency range [42]. Further investigations have been carried out on Tyranno ZMI fibres annealed at different temperatures evaluating their composition, tensile strength, degradation mechanisms as well as dielectric properties [43]. The annealing resulted in the decomposition of the low conductive SiC_xO_y phase with an increase of the amount of semiconductive SiC nanocrystals and size of the highly conductive free carbon domains, thus resulting in an enhanced polarization effect. As a result, the complex permittivity of the annealed Tyranno ZMI/ephoxy composites samples increased resulting in an average loss tangent going from 0,93 to 1,02 with good MW attenuation properties in a 2,65 GHz span.

Aside from its contribution on non-oxide CMCs mechanical behaviour, the interphase plays a key role also on the dielectric properties of the composite. An investigation carried out on 2.5D KD-I (China) and Nicalon-202 (Japan) SiC fibre fabrics showed that the carbon-rich outer layer had a strong influence on the higher real and imaginary part of the complex permittivity [37]. Further works proposed that the electrical properties of SiC fibres could be tailored controlling the thickness of the pyrolytic carbon layer on the surface [44]. The commonly adopted PyC interphase is characterized by high electrical conductivity thus resulting inappropriate for MW absorbing applications. A different behaviour was observed in the case of a BN interphase with a layered crystal structure, which showed reduced influence on the electrical resistivity of SiC fibres [45].

In the framework of this PhD activity, the dielectric properties as a function of the temperature T of different Nicalon preforms were determined using a rigorous measurement technique [46], whose detailed description will be published elsewhere. **Figure 4.1** shows the results of the measurements from room T to the usual infiltration temperature of 900 °C.

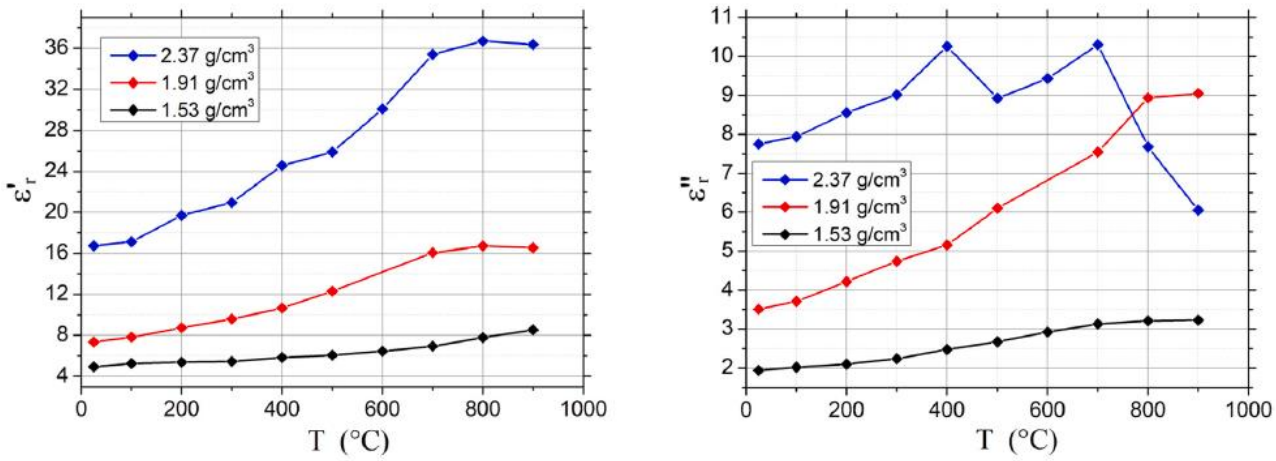

Figure 4.1 *– Relative dielectric permittivity of polycarbosilane-derived Si–C–O Nicalon NL-202 preforms measured at different temperatures and infiltration levels. Left: real part of the permittivity. Right: imaginary part of the permittivity. The samples were provided by ATL* [47]

Another essential point in the building of the reactor cavity is the choice of the material forming its walls, given the conditions it must satisfy. In particular, the electric resistivity of this material must be low to reduce the Ohmic losses in the cavity walls to a level well below the dielectric losses in the sample. Moreover, it must be chemically inert to operate for a long time in a chemically aggressive environment, characterized by a very hot sample and highly reactive chemical species. Finally, its resistivity must remain low enough after many infiltration cycles.

A material that displays these properties is graphite, in particular the FP2584-grade graphite produced by SKT [48]. The choice of the most suited graphite grade was made after a direct determination of its MW resistivity, obtained with a modified version of the Courtney method [49]. In this technique, a MW resonator consists of a low-loss dielectric disc inserted between two metallic plates. Usually, the dielectric properties of the disc can be obtained from the resonance frequency and the quality factor of the resonant system provided that the resistivity of the plates is well known. However, this setup can be also employed to measure the effective MW resistivity of the plates whenever the dielectric properties of the disk are known.

According to the results of these measurements, the MW resistivity of the FP2584-grade graphite at room T was equal to $1400 \pm 1\ \mu\Omega * cm$. The resistivity of the reactor walls was expected to decrease to about $1000\ \mu\Omega * cm$ during an infiltration run, when the walls reach temperatures between $200\ °C$ to $300\ °C$ [50].

At this point it was possible to define the reactor chamber shape and its volume, given all the other quantities involved in (4.7) and (4.12). For the sake of simplicity in the manufacturing, a cylindrical geometry was considered, with a diameter of the order of $50\ cm$ and a height of the order of $30\ cm$. The choice of an elongated cross-section for the cavity depended on the predominant interest in processing flat samples, whose lateral dimensions are much larger than the thickness.

In the given setup, around $2.45\ GHz$ the typical distance between consecutive resonant modes was of the order of $3\ MHz$, and their typical full-width at half maximum was $0.8\ MHz$. The insertion of the sample led to an additional broadening of the resonance lines, owing to the dielectric losses introduced by the sample. This broadening was at least of factor 2, since the target was to have at least 50% of the power dissipated in the sample. A further broadening of the resonance lines was due to the coupling of the cavity to the excitation circuit propagating

the MW radiation. The linewidth of the resonance mode at the critical coupling was double to that at low coupling levels, at which the unloaded quality factor is calculated [17].

Taking into account both the presence of the sample and the critical coupling to the external MW circuit, the proposed graphite cavity behaved as an overmoded resonator around 2.45 GHz. In the system composed by the graphite cavity and the 1.53 g/cm^3 Nicalon sample of **Figure 4.1**, the ratio P_s/P_C was expected to be 1.67 at the beginning of the MW heating process, so about 63% of the EM power coupled to the reactor was dissipated in the sample and about 37% in the reactor walls, as calculated from the second part of (4.12) and (4.13). At the critical coupling, the above fractions refer to the total MW power reaching the reactor.

For the considered sample, a good MW heating efficiency was thus expected with the proposed MW-CVI reactor. In general, the energy efficiency of the reactor is expected to increase with the volume of the sample thank to the increase of the filling factor, provided that the critical coupling condition is still fulfilled.

The above results were obtained with the help of a general approach essentially based on the assumption that the electric energy was equally distributed in the volume of the reactor chamber. A more detailed analysis of the actual EM fields in the cavity, as well as of the resulting efficiency and temperature profile in the sample, requires a rigorous numerical modelling of the reactor, both empty and loaded with sample and sample holder. The aim of the next section is to illustrate this analysis and to present the room temperature tests of the reactor. All the numerical results are based on the Comsol Multiphysics software [51].

4.3 Results and Discussion

4.3.1. Reactor chamber design and room temperature tests

The final structure adopted for the reactor chamber is shown in **Figure 4.2**. It is composed of a cylindrical cavity with a diameter of 49.35 cm and a height of 30.6 cm. The MW radiation can enter the cavity through three identical circular waveguides oriented at 120° to each other and placed in the horizontal median plane of the cavity. Each waveguide is cylindrical with an inner diameter of 9 cm and a length of 27.5 cm and is made by the same graphite material forming the chamber.

The waveguides are connected to the EM sources by means of WR340 rectangular waveguides made of aluminium. A system of moving stubs mounted in a magic T tuner was inserted in each excitation channel, with the aim of controlling and adjusting the coupling level until a nearly critical coupling level is reached. In the heating and infiltration tests, a normalized reflected power lower than -20 dB was considered equivalent to the critical coupling level for all practical purposes.

The main reason behind the choice to excite the reactor by means of different waveguides was the flexibility of use. Switching from one sample to another characterized by different shapes, sizes, and dielectric properties can require very different levels of MW power to reach the desired infiltration temperature, possibly exceeding the maximum power delivered by a single magnetron. Moreover, the combination of several, lower power sources instead of a single source

of high power is advantageous in terms of reduced risk of sparks or plasma generation in the excitation channel. In addition, the concurrent use of different excitation ports enables, in general, a better heating uniformity.

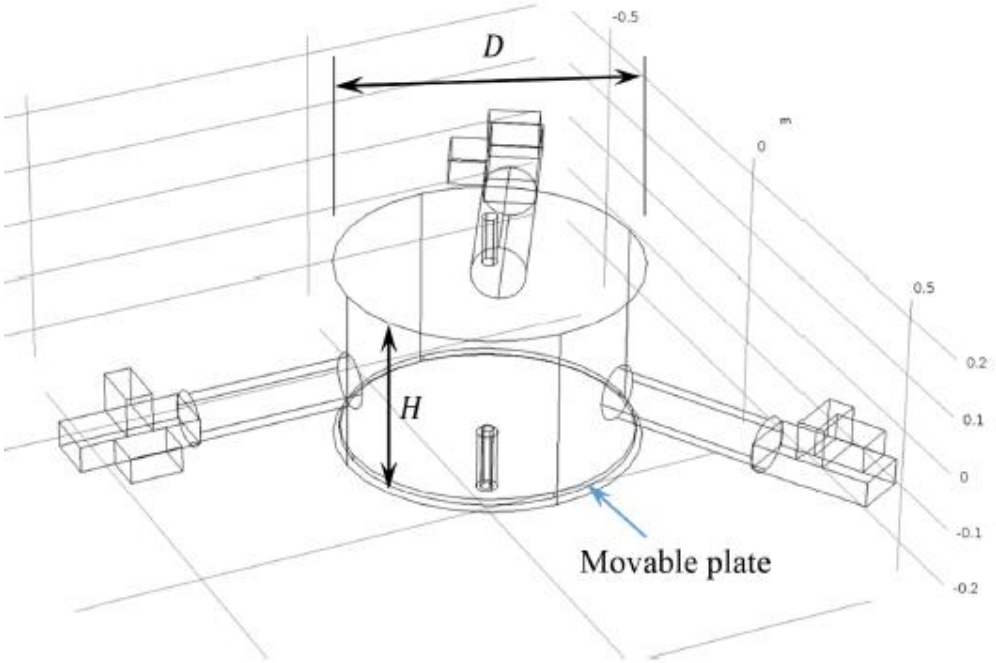

***Figure 4.2** - 3D view of the inner cavity of the reactor, including the excitation waveguides and the gas connections. The diameter D and the height H of the cavity are indicated, as well as the movable plate.*

In the lower part of the chamber, a movable graphite plate was inserted with the purpose of providing a frequency tuning of the resonance modes. This element was necessary in order to match the frequency of the mode of interest with that of the magnetron source, which is fixed. The movable plate is a disc with 47.35 *cm* diameter and 1 *cm* thickness, coaxial to the cylindrical chamber and placed at about 0.6 *cm* from its base. Inlet and outlet gas connections were included in the modeling.

Electromagnetic analysis on a macroscopic level involves solving Maxwell's equations subject to certain boundary conditions. The coupled electromagnetic heating and steady state heat conduction equations, defined over the macroscopic reactor/preform and sample holder domain, are expressed as:

$$\nabla \times (\mu_r^{-1} \nabla \times \boldsymbol{E}) - k_0^2 \left(\varepsilon_r - \frac{j\sigma}{\omega \varepsilon_0}\right) \boldsymbol{E} = 0 \qquad (4.15)$$

$$\rho c_p \frac{\partial T}{\partial t} + \nabla * (-k \nabla T) - P_{loss} = P_d \qquad (4.16)$$

Where P_d and P_{loss} are given by the dielectric losses and the heat losses, respectively, as defined in Section 3.2.1 (**Equation 3.10** and **Equation 3.12).** Among the possible heat losses, in the modelling only the radiative losses $P_h = \epsilon \sigma_{SB} A_s T^4$ have been taken into account, since they dominate over the various possible heat losses due to the high infiltration temperatures.

A "Perfect Electric Conductor" (PEC) boundary condition was applied on the surface of rectangular and cylindrical waveguides as well as the inlet and outlet gas lines:

$$n \times \boldsymbol{E} = 0 \qquad (4.17)$$

Which represents a special case of the electric field boundary condition that sets the tangential component of the electric field to zero. Such a condition is rigorously true only for infinite conductivity surfaces. However, it is a very good approximation for high electric conductivity materials, as aluminium, when the weak residual electromagnetic losses can be neglected.

Such losses cannot be neglected inside the graphite cavity, owing to its much lower electrical conductivity with respect to aluminium and to the intense electromagnetic fields generated by the constructive interference in the cavity volume. In such case, an "Impedance Boundary Condition" (IBC) was applied for the cavity graphite walls:

$$\sqrt{\frac{\mu_0\mu_r}{\varepsilon_r - j\sigma/(\omega\varepsilon_0)}}\, n \times \boldsymbol{H} + \boldsymbol{E} - (n * \boldsymbol{E})n = (n * E_s)n - E_s \qquad (4.18)$$

Where $E_s = 0$ that corresponds to the source electric field, was set equal to zero since we do not have sources in the cavity walls. This condition is representative of the surface of a lossy domain, where the field slightly penetrates outside the boundary, and its application avoids the definition of another domain in the model. The IBC is valid if the skin depth is small compared to the size of the medium and to the wavelength of the radiation.

Finally, a "Port condition" was applied to the inlet of one of the rectangular waveguides simulating where the electromagnetic energy enters or exits, whereas the other two ports were short-ended by applying a PEC condition. Specifically, the excitation port was selected to excite a TE_{10} mode with a certain MW power input, as discussed into Section 4.3.2.

The typical resonance spectrum calculated for the empty reactor excited through one of the three channels is shown in **Figure 4.3**, for a frequency interval corresponding to the ISM band centered around 2.45 GHz. In the simulations, the passive channels were terminated by a short circuit. Among the many modes that can resonate in this interval, the coupling system was efficient in transferring energy to those around 2.441 GHz, 2.45 GHz, and 2.475 GHz. The electric field of these modes, in some representative planes of the reactor, is shown in the insets of **Figure 4.3**.

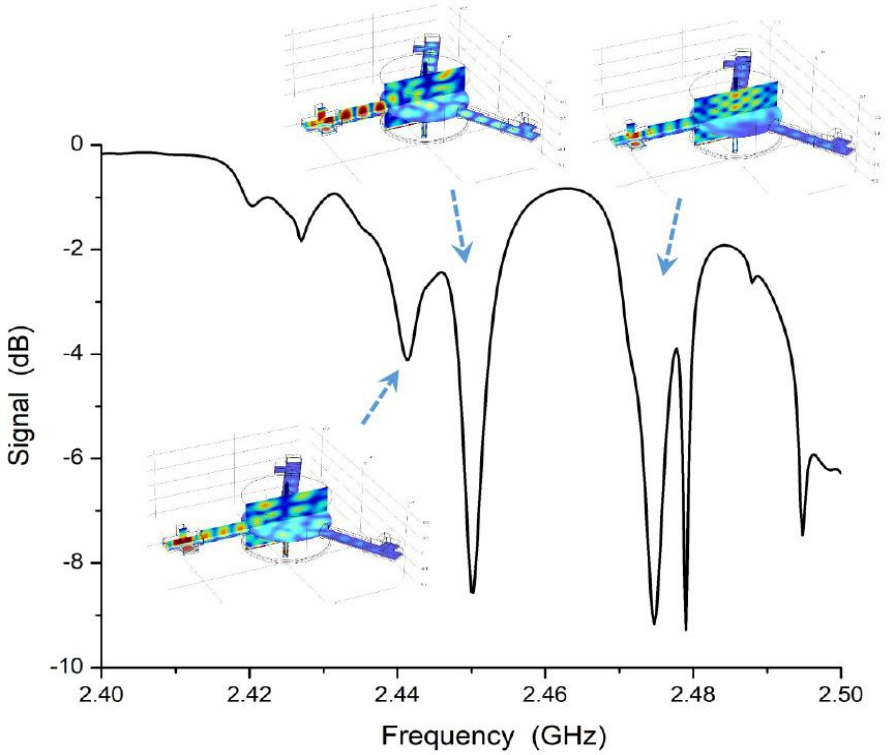

Figure 4.3 *– S_{11} parameter of the EM signal reflected by the cavity shown in Fig. 2, excited through the waveguide on the left of the figure. Data obtained from numerical modeling. The coupling level was not optimized, as the main objective was to determine the frequency of the resonance modes. From left to right, the insets show the electric field distribution for the modes resonating at 2.441 GHz, 2.45 GHz, and 2.475 GHz, respectively*

According to the electric field distribution, the mode with the highest electric energy in the central part of the reactor cavity, where the sample will be placed, was that resonating at 2.475 GHz. A graphite chamber was built following the design of **Figure 4.2**. Its EM spectrum was determined by means of a vector network analyser, connected to the MW channel of interest by means of a coaxial cable-to-waveguide transition. In the measurement of the S_{11} parameter of the reactor, the stubs on the passive channels were adjusted in order to have a short-circuit condition. The reference level in the determination of S_{11} was obtained short-circuiting the end of the coaxial cable-to-waveguide transition.

The experimental and the simulated spectra of this cavity are reported in **Figure 4.4**, for frequencies around the 2.475 GHz mode, together with the spectrum of a magnetron source feeding the reactor. The latter was determined by means of EM compatibility techniques. **Figure 4.4** showed a good agreement between the modelling and the experimental results. The close matching between the resonance frequency of the 2.475 GHz mode and the main emission peak of the magnetron was obtained with proper positioning of the movable graphite plate.

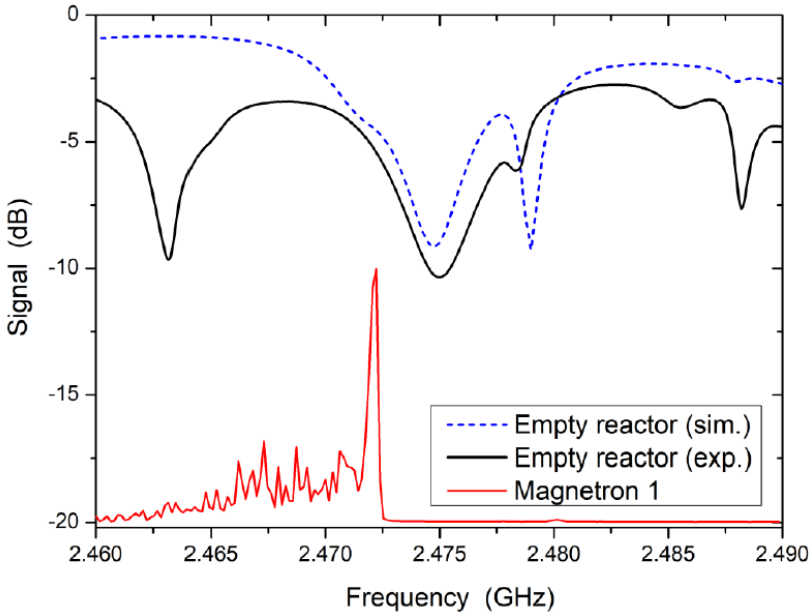

Figure 4.4 *- Comparison between the experimental spectrum of the graphite chamber built following the design of Fig. 2 and its simulated spectrum (left y axis). In the determination of the experimental spectrum of the empty cavity, the coupling level was not optimized. The spectrum of a magnetron source exciting the reactor, with amplitude and baseline arbitrarily normalized, is also shown (right y axis).*

Another important element in the practical use of the reactor is the sample holder, whose function is to keep the sample in the most convenient position inside the reactor cavity. The material forming the sample holder must be again inert with respect to the extremely reactive environment in which it is placed. Moreover, it must be as much as possible transparent to MWs, so as to prevent absorption of a significant fraction of the MW power, which could be detrimental both for its chemical stability and for the efficiency of the infiltration process.

First experimental trials had been carried out using a spider-like shaped sample holder, made of the same graphite employed for the cavity walls, having a structure as showed in **Figure 4.5** and placed on a rotating shaft inserted in the gas exhaust tube.

The dimensions of the sample holder were selected in order to keep the preform at a height corresponding to the median plane of the cavity. The presence of this sample holder had led to a substantial focusing of the electromagnetic fields in the sample, with formation of hot spots around the relatively sharp points of contact. In order to mitigate these drawbacks, a sample holder configuration with vertical elements external to the sample had been first considered, although the presence of sharp edges still resulted in the localized formation of hot spots and possible insurgence of plasma, which resulted detrimental on the material.

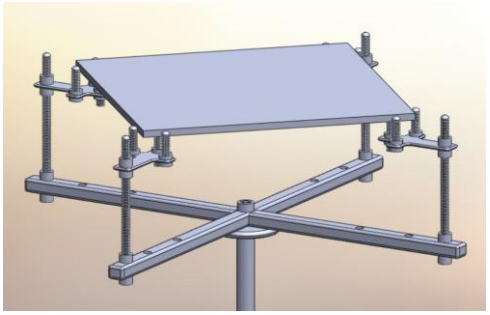

Figure 4.5 *– Spider-like sample holder structure (Courtesy of ATL)*

Based on the above results, a different sample-holder made of a low-loss grade fused quartz (Momentive 214 [42]), whose dielectric permittivity as measured at the infiltration temperature is about $\varepsilon_{qtz} = 3.81 - i * 0.001$, has been tested. A 'chair-like' geometry was adopted for the sample holder with rounded corners in order to minimize the insurgence of hot-spots, as shown in the inset of **Figure 4.6**.

Furthermore, along the infiltration processes, a disc of alumino-silicate fibreboard (Duraboard 1600 [43]), with $10\,cm$ diameter and $1\,cm$ thickness, is usually inserted between the sample holder and the sample, in order to avoid a local overheating of the sample. Moreover, the Duraboard disc reduces the thermal irradiation of the sample, which is thus subject to slower cooling, at a price of a less uniform temperature distribution.

The dielectric permittivity of Duraboard at the infiltration temperature resulted about $\varepsilon_{Dur} = 1.45 - i * 0.009$. Thanks to the high porosity and low dielectric losses, the Duraboard disc did not interfere significantly either with the MW heating and with the flow of the reactant gases.

The effects of the quartz sample holder and the Duraboard disc on the experimental spectrum of the reactor are shown in **Figure 4.6**. As expected, the position and the coupling of the resonance mode are weakly modified by the presence of these elements, characterized by small volume and relatively low dielectric permittivity.

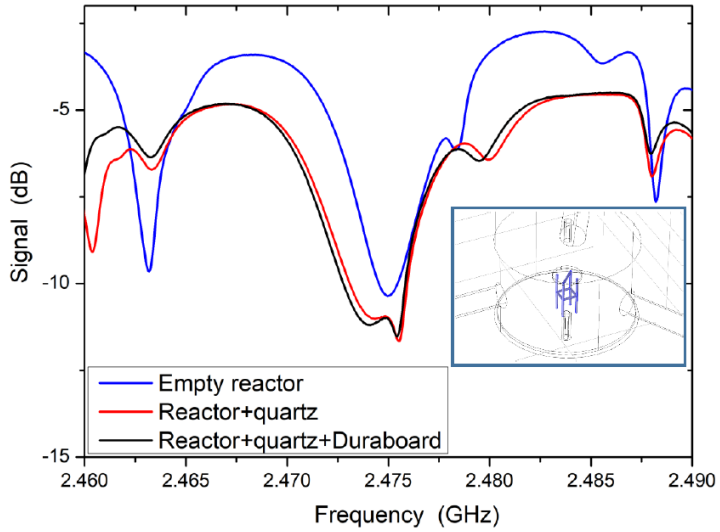

Figure 4.6 *- Comparison among the experimental spectrum of the empty reactor chamber, the spectrum of the reactor loaded with the quartz sample holder, and the spectrum of the reactor loaded with both the quartz sample holder and the Duraboard disc. The inset shows the typical arrangement of the quartz sample holder (shaded region) and of the Duraboard disc*

The experimental spectrum of the reactor loaded with a $1.53\,g/cm^3$ Nicalon disc with $10\,cm$ diameter and $1\,cm$ thickness, placed on top of the sample holder plus the Duraboard disc, is shown in **Figure 4.7**, together with the spectrum of the magnetron.

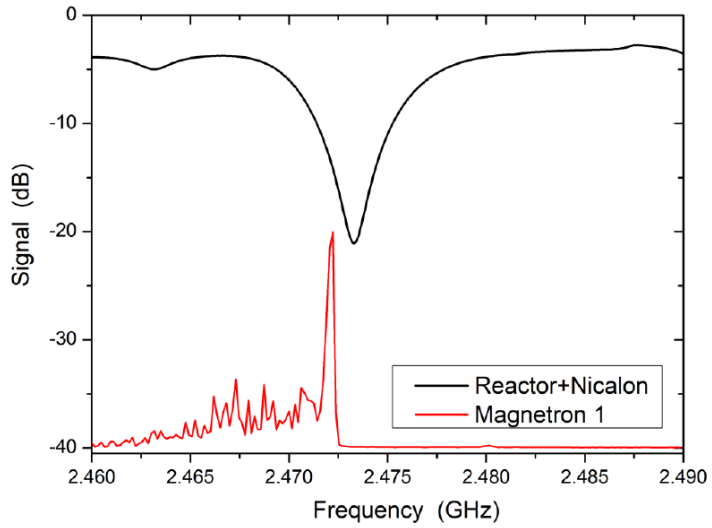

***Figure 4.7** - Experimental spectrum of the reactor loaded with the quartz sample holder, the Duraboard disc, and a Nicalon disc (left y axis), together with the spectrum of a magnetron source exciting the reactor (right y axis). Both the Duraboard disc and the Nicalon disc have a diameter of about 10 cm and a thickness of 1 cm*

The insertion of the Nicalon sample in the reactor gave rise to only a small shift in the resonance frequency of the mode of interest, which remained well superposed to the magnetron emission.

Such behaviour was common to several other materials of interest, as shown by **Figure 4.8**, which reports the spectrum of the reactor loaded with similar disc-shaped specimens made of Tyranno ZMI fibres and carbon fibre cloth. The Tyranno ZMI fibre-based preform was coated with a pyrolytic carbon coating (thickness of 100 nm) and densified through conventional CVI from 1.008 g/cm^3 up to 1.298 g/cm^3.

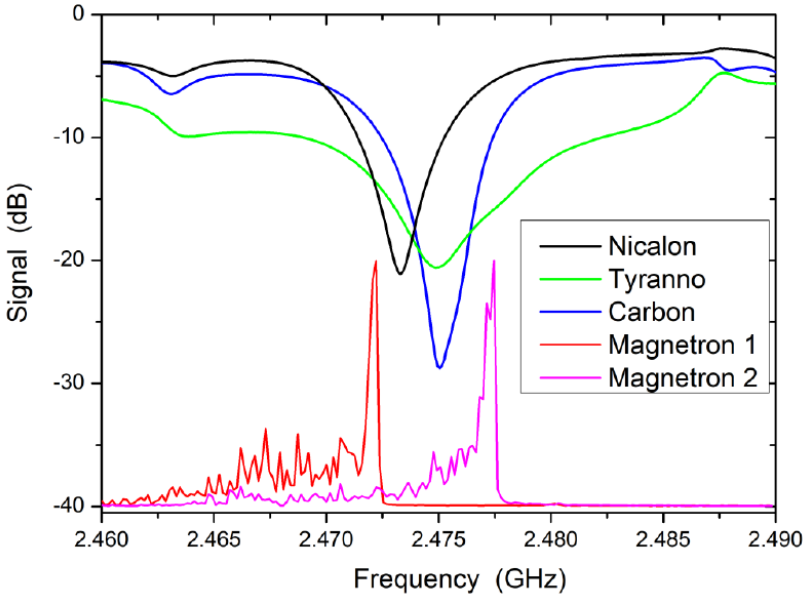

***Figure 4.8** - Comparison among the experimental spectra of the reactor loaded with a Nicalon sample, with a Tyranno ZMI fibres sample, and with a carbon fibres cloth sample (left y axis), all placed on the quartz sample holder and the Duraboard disc. The spectra of two of the available magnetron sources, with amplitude and baseline arbitrarily normalized, are also shown (right y axis)*

The Tyranno fibre sample was representative of high dielectric loss materials, whereas the carbon fibre sample was representative of conducting materials. For all the materials considered in **Figure 4.8** the resonance mode of interest was always well coupled and only slightly shifted with respect to the empty reactor case. In general, a sample that is small with respect to the

resonant system in which is inserted leads to a small frequency shift of the resonance mode, owing to its small filling factor [54,55].

The frequency detuning introduced by different samples can be overcome either by using a second available magnetron, emitting at a higher frequency as shown in **Figure 4.8**, alone or in combination with the first magnetron, or by acting on the movable plate. In the infiltration tests conducted so far, all the investigated samples were processed by using one of the two magnetrons indicated in **Figure 4.8**, without the need to adjust the position of the movable plate.

The coupling level achievable with the investigated samples can easily be brought below $-20\ dB$ at the emission of one of the two magnetrons by optimizing the position of the tuning stubs, as shown by **Figure 4.8**. Accordingly, in practice all the MW power reaching the reactor can be transferred to its EM modes.

The $1.53\ g/cm^3$ Nicalon sample will be taken as a reference in the following. The room temperature spectrum of the reactor loaded with the Nicalon sample is shown in **Figure 4.9**.

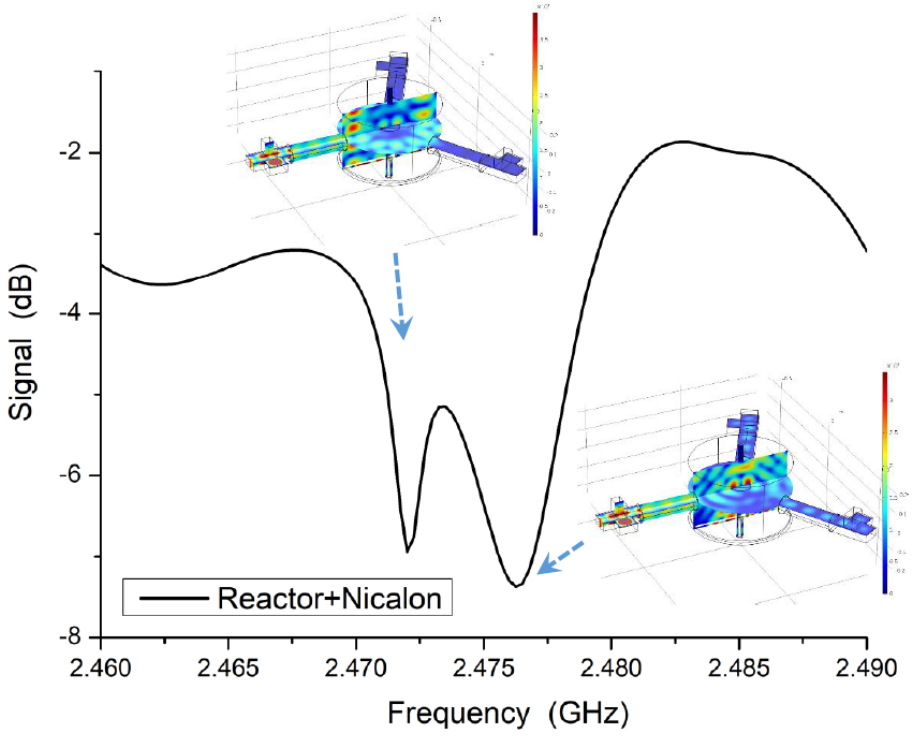

Figure 4.9 *- Calculated resonance spectrum of the reactor loaded with the quartz sample holder, the Duraboard disc, and a Nicalon disc. The position of the stubs was not optimized. From left to right, the insets show the electric field distribution for the modes resonating at 2.472 GHz and 2.4763 GHz, respectively*

Two main modes are visible in **Figure 4.9**, one resonating at 2.472 GHz and one resonating at 2.4763 GHz. The distribution of the electric field of these modes is shown in the insets of the figure. The mode at 2.472 GHz corresponded to a 'surface', Whispering Gallery-like mode [56], in which the EM energy was prevalently confined around the surface of the cavity. On the contrary, the mode at 2.4763 GHz corresponded to the 'volume' mode of interest, in which the EM energy was more evenly distributed in the entire volume of the cavity, in particular in its centre, where the sample is placed. The slight discrepancy between the calculated (2.4763 GHz) and the experimental (2.473 GHz) resonance frequency of the volume mode was mainly due to the irregular shape of the sample.

In the design of the reactor, care must be taken to avoid coupling to the surface modes, which make problematic the heating of samples placed in the centre of the reactor chamber. This aspect is evidenced by the fraction of power dissipated in the sample (P_s/P) and by that in the walls of the reactor (P_C/P), both reported in **Figure 4.10**.

For the surface mode, the majority of the MW power was dissipated in the walls of the reactor. On the contrary, for the mode of interest the 80% of the power coupled to the reactor was dissipated in the sample. This value can be compared with the value provided by the second part of (4.13), given by 54% taking now into account the extra surface introduced by the movable plate. Despite the simplicity of the analysis leading to (4.13), the agreement between the approximate and the rigorous result is still acceptable. A similar agreement has been verified under very different conditions.

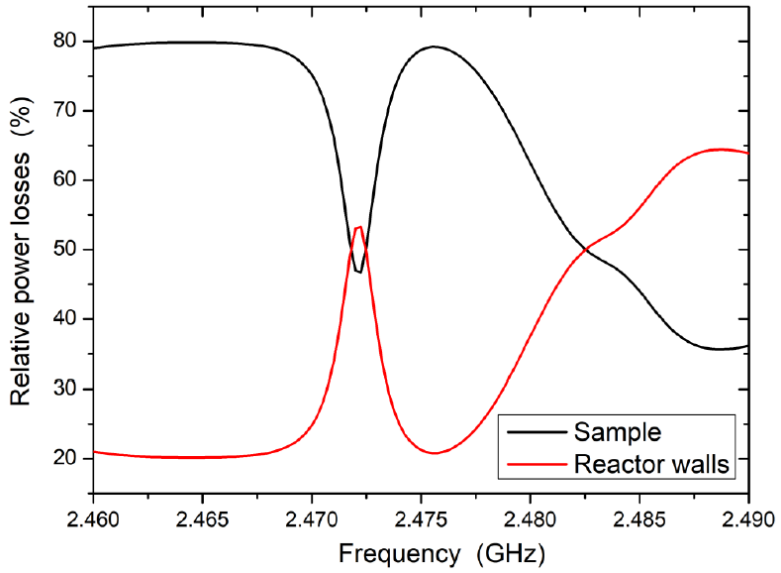

Figure 4.10 *- Calculated fraction of MW power dissipated in the sample and in the walls of the reactor, in the case of reactor loaded with the quartz sample holder, the Duraboard disc, and a Nicalon disc (see also Figure 4.8)*

Through the many infiltration cycles conducted so far, the efficiency of the reactor cavity was continuously monitored to check for a possible deterioration of its characteristics, in particular the resistivity of the graphite walls. This quantity can be directly obtained from the quality factor of a reference resonance mode, according to (4.5). After a marked increase with the initial infiltration processes, the resistivity of the graphite walls stabilized to about 4000 $\mu\Omega * cm$ at the typical temperatures of the reaction chamber. The fraction of MW power currently dissipated in the reference Nicalon sample is $P_s/P \approx 62\%$.

4.3.2. MW heating and infiltration tests

In stationary conditions, all the MW power absorbed by the sample through its dielectric losses is dissipated as heat, assuming no chemical reactions. Under the conditions of high temperatures and low pressures at which the infiltration reactions are usually conducted, the dominant dissipation mechanism is given by the thermal irradiation towards the much colder walls of the reactor. Accordingly, the MW power P_h necessary to keep the sample at the infiltration temperature T can be estimated by means of the Stefan-Boltzmann law:

$$P_h = \epsilon\sigma A_s T^4 \qquad (4.19)$$

Where $\sigma_{SB} = 5.67 * 10^{-8}\, W * m^{-2}\, K^{-4}$, ϵ is the emissivity of the sample, A_s its surface area, and T the surface temperature.

Under the assumption that the sample is homogeneously heated, $\epsilon \approx 1$, and neglecting the thermal irradiation towards the Duraboard disc, the power necessary to heat the reference Nicalon sample to 900 $°C$ is about $P_h = 1200\, W$.

In real process conditions, the spatial variation of the electric field in the sample volume and the limited thermal conductivity of most ceramic materials lead to an inhomogeneous sample heating, characterized by localized domains with much higher temperature (hot spots).

The actual temperature distribution of the sample can be calculated by means of a multiphysics numerical modelling, in which the coupled EM and thermal problems are solved simultaneously and in a self-consistent way. In particular, the multiphysics couplings consider the electromagnetic losses from the electromagnetic waves as a heat source with the dielectric and thermal properties of the preform as a function of the temperature, based on the assumption that the electromagnetic cycle time is short compared to the thermal time scale. The preparation of realistic multiphysics models requires the knowledge, as functions of T, of the dielectric permittivity, the specific heat, the thermal conductivity, and the emissivity of the sample. For the materials of interest, all these quantities were determined in the framework of the project HELM and are reported in **Table 4.1**.

Table 4.1 *– Dielectric and thermal properties characteristic of the Nicalon sample with density of 1,53 g/cm³*

$T\ [°C]$	ε'	ε''	$c_p\ [J/kg * K]$	$k\ [W/m * K]$
25	4,92	1,94	710	0,67
100	5,24	2,02		
200	5,38	2,10	1000	0,78
300	5,45	2,24		
400	5,83	2,48	1190	0,8
500	6,07	2,67		
600	6,46	2,92	1340	0,83
700	6,94	3,13		
800	7,78	3,21	1570	1,00
900	8,53	3,23		
1000			1870	1,21

The thermal conductivity and the specific heat were measured by Petroceramics[30] in the framework of the project HELM. For all the above quantities, a linear function was employed both for the interpolation between consecutive points and for the extrapolation outside the measurement intervals. The emissivity of the sample was fixed to $\epsilon = 0{,}937$ for all temperatures.

The accuracy of the multiphysics models describing the reactor loaded with the sample was first assessed comparing the power P_h obtained from (4.19) with the numerically obtained value, in the same conditions of very high thermal conductivity and thermal emission from the free surfaces of the sample. In the case of the numerical model, the power P_h was directly determined as the MW power released in the sample based on the EM power loss density into its volume domain. The discrepancy between these calculations resulted lower than 1%.

[30] http://www.petroceramics.com/

In the case of the reference Nicalon sample, a multiphysics model was prepared with the aim of determining the sample heating dynamic and the temperature distribution in the typical infiltration conditions. The MW frequency was set to 2.4763 GHz, corresponding to the volume mode of **Figure 4.9**. The MW power coupled to the reactor was fixed to 1000 W at the beginning of the MW heating process, in which the temperature of the reactor walls and that of the sample was set to 200 $°C$.

In stationary conditions, the resulting temperature distribution on the surface of the sample is shown in **Figure 4.11**.

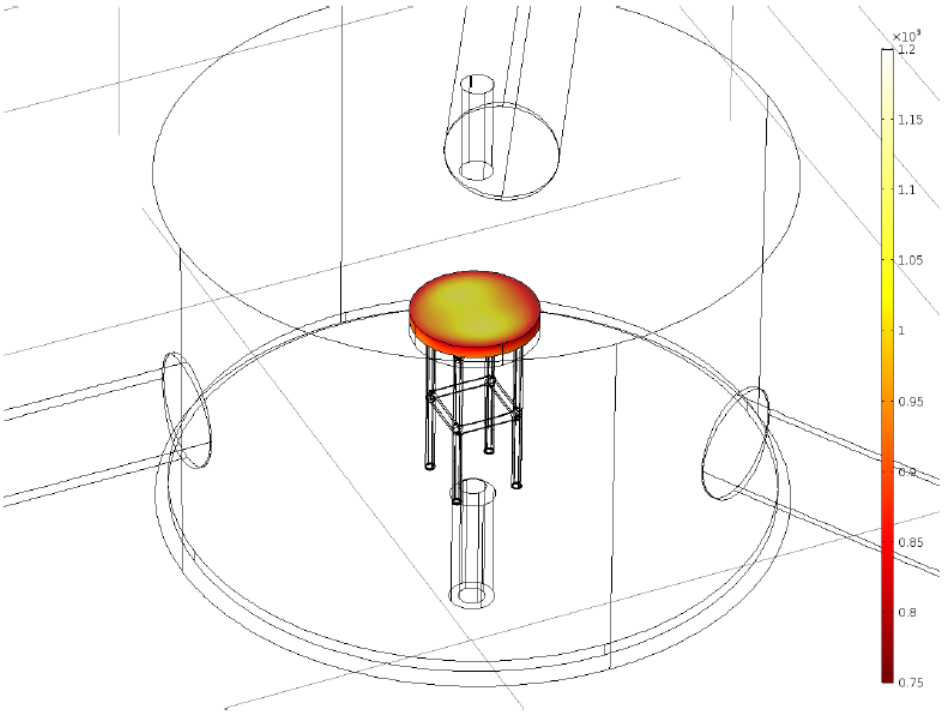

Figure 4.11 *- Temperature distribution of the Nicalon sample, in the same configuration of Figures. 4.8 and 4.9, calculated with Comsol Multiphysics. In the modeling, the reactor is excited at 2.4763 GHz with a power of 1000 W, delivered through the excitation channel on the left of the figure. The initial temperature of the sample and of the reactor walls was fixed to 200 °C. The color legend on the right is in degrees K.*

The evolution of the Nicalon temperature, determined at the hotspot on the upper surface of the sample, is reported in **Figure 4.12**. The characteristic time of the nearly exponential curve describing the sample heating is of the order of 2 min.

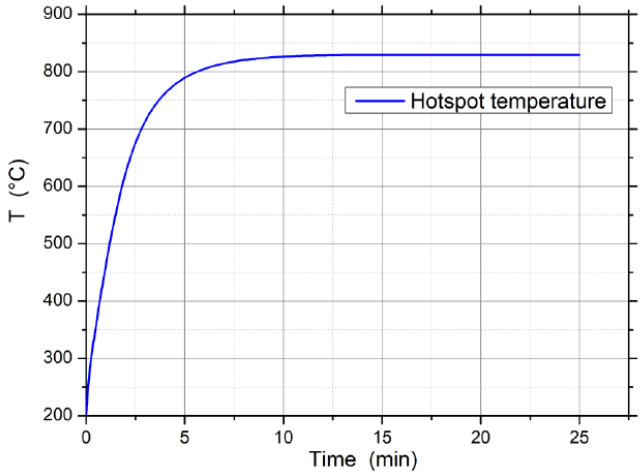

Figure 4.12 *- Time dependence of the temperature of the hot spot of Figure 4.10*

The experimental tests on the reactor were conducted in conditions similar to those considered in the numerical models. The reactor was loaded with the quartz sample holder, the Duraboard disc, and the Nicalon sample, as shown in **Figure 4.11**. A MW power of 1000 W in the heating stage, and of about 850 W in the infiltration stage, was delivered to the reactor by means of a single excitation channel. The level of the reflected power was determined with the help of a high-power circulator mounted just after the magnetron, which conveys the reflected power to a detector. The latter was calibrated short-circuiting the port of the circulator towards the reactor and varying the power emitted by the magnetron. By acting on the tuning stubs, the reflected power was kept close to the detection limit of the system throughout the infiltration process. The temperature of the sample was monitored by means of a digital pyrometer (Dias Pyrospot DSR 10NV), providing also its emissivity.

The evolution of the Nicalon temperature during the heating and the infiltration process is shown in **Figure 4.13**. The inset shows the control panel of the magnetrons, indicating a typical incident power (P_i) and reflected power (P_r) during the infiltration stage.

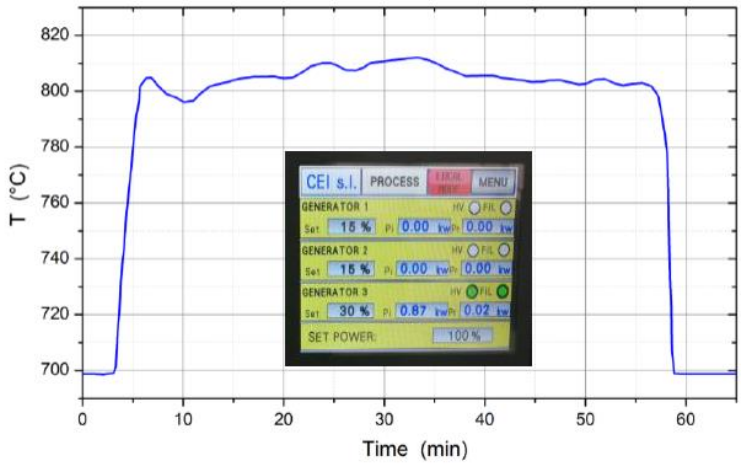

Figure 4.13 *- Experimental Nicalon temperature during the heating and the infiltration process, determined in the central part of its upper surface. The lower limit in the temperature reading of the detector is 700 °C. The inset is a picture of the control panel of the magnetrons, reporting the typical incident (Pi) and reflected (Pr) power during the infiltration stage*

In these tests, the temperature of the sample was brought from the initial value of 200 °C, achieved by means of the conventional resistive heating enabled by the reactor, to about 800 °C on the sample surface, exciting the reactor with 1000 W of MW power.

The pre-heating of the reactor to 200 °C is usually done in order to remove the possible residual humidity, which would interfere with the chemical reaction (4.1). Taking account of the inverse temperature profile characteristics of the MW heating, 800 °C on the sample surface corresponds to internal sample temperatures suited for the CVI process. Once this temperature was achieved, the MW power was reduced to about 850 W and the reactant gases were made to flow in the reactor, so activating the infiltration process. In this stage, the total gas pressure was kept to 150 $mbar$.

The infiltration shown in **Figure 4.13** lasted about 50 min. In this period, the MW power was slightly adjusted in a manual way, together with the position of the tuning stubs, in order to keep the desired surface temperature and a nearly critical coupling condition.

According to **Figure 4.13**, the heating of the sample from 700 °C to 800 °C took about 2.3 min, in good agreement with the data shown in **Figure 4.12**, where the same temperature interval is covered in about 2.8 min. Starting from the initial temperature of 200 °C, the infiltration conditions have been reached in about 5 min employing a MW power of 1000 W. The very fast heating of the sample represents a striking difference with respect to conventional CVI processes, in which the entire reactor chamber must be brought to the infiltration temperature and the thermalization of the sample requires a much longer period.

It is worth noting that the good agreement between the above theoretical and experimental heating times indicates that the doubts raised in recent literature [20] about the possibility to predict and control the EM and thermal behaviour of overmoded reactors appeared not justified, provided that great accuracy is dedicated to the design of the reactor and to the characterization of the dielectric properties of the material to process.

The results of a typical infiltration process of the Nicalon sample are reported in **Figure 4.14**, which shows the SiC grown on one of the central laminae of the multilayer preform, together with a scanning electron microscope (SEM) image of the most infiltrated region.

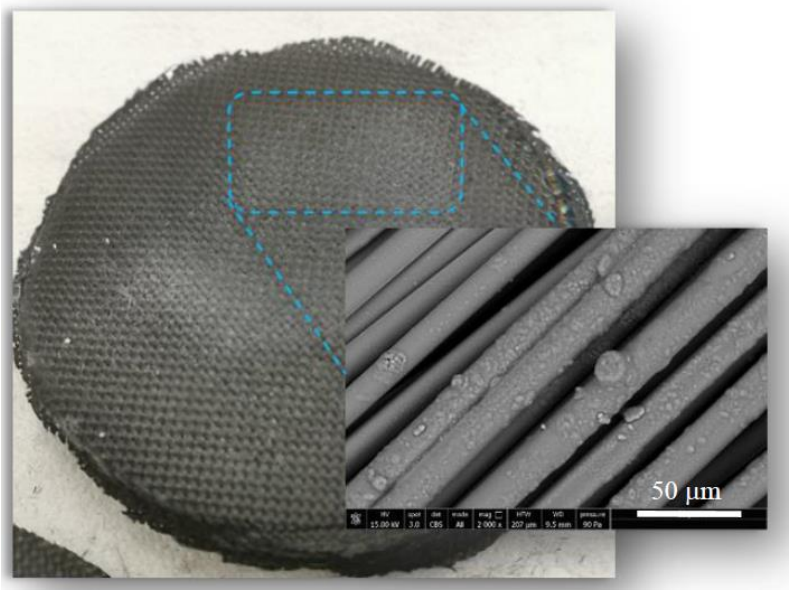

Figure 4.14 *- Result of a typical MW-CVI process, with the SiC infiltrated on one of the central laminae of a multilayer Nicalon preform (lighter color regions). The inset reports an SEM image, showing the SiC grown on the preform fibres and among them*

The analysis of the *SiC* infiltrated on the different laminae of the sample confirmed the presence of a hotter region in the central part of the sample, in agreement with the temperature distribution shown in **Figure 4.11**. Moreover, the decrease of the infiltrated *SiC* that is observed moving toward the most external laminae of the preform confirmed the inverse temperature profile predicted by the modelling and expected, in general, in the MW heating.

The SEM image shown in **Figure 4.14** evidenced the binding among the preform fibres due to the infiltrated SiC. A further discussion of the microscopic details of the infiltrated sample will be discussed into **Chapter 5**.

In the case of samples larger than those investigated in this work, better efficiencies are expected thanks to the most favourable ratio between the power dissipated in the sample and the power dissipated in the walls of the reactor cavity. On the other hand, the MW heating of samples larger than the employed wavelength is prone to scarcely homogenous temperature distributions. This inhomogeneous heating is exacerbated when the dielectric losses increase with the temperature.

Indeed, in this case a positive feedback mechanism is established, which can generate several hot spots. In the proposed reactor, the inhomogeneous MW heating can be mitigated either by distributing the MW power over the three excitation channels or by rotating the sample.

In general, the use of magnetron sources, characterized by a fixed-frequency emission, often dependent on the emitted power and on the ambient conditions, can represent a serious limitation in the achievement of the robust infiltration processing needed at industrial levels.

In this respect, the passage to fully controllable solid-state sources represent an ineludible step in the implementation of well-controlled and reproducible processing, necessary for high production yield and quality. From the point of view of the design of overmoded reactors, the use of solid-state sources makes less stringent the condition of overlapping consecutive modes and the use of a frequency tuning element, which is beneficial both for the energy efficiency and for the ease of construction.

Moreover, different resonance modes can be excited in a rapid sequence by means of tunable solid-state sources. In this manner, a more homogeneous MW heating can be obtained. The implementation of solid-state sources in the described MW-CVI reactor is the direction to which our current work is oriented.

4.4 Conclusions

In summary, an overmoded reactor cavity for MW-CVI of ceramic matrix composites at a pilot scale was designed, built in high-quality graphite, and tested. A two-step design was followed. First, the dimensions of the cavity were chosen on the basis of the spectral characteristics and of the expected energy efficiency, obtained by means of a general analysis. Then, a resonance mode enabling a high heating efficiency was identified through a rigorous modelling study.

Experimental tests on the reactor loaded with different samples showed that the critical coupling can be reached in a large variety of conditions. In the case of low-density Nicalon preforms, the power dissipated in the sample is greater than 60% of the power coupled to the reactor, despite the aging of the cavity walls due to the many infiltration cycles. Thanks to this efficiency, typical SiC-fibre reinforced preforms having a volume of the order of 100 cm^3 can be heated up to about 900 $°C$ in 5 min, using 1 kW of MW power.

The proposed design method, whose general approach is substantiated by a good agreement between calculated and observed quantities, is expected to become an important tool in the design of overmoded reactors for different applications.

4.5 References

[1] R.J. Meredith, Introduction and fundamental concepts, in: Eng. Handb. Ind. Microw. Heat., IET, Stevenage, United Kingdom, 1998: pp. 1–16. https://doi.org/10.1049/PBPO025E.

[2] R.E. Collin, Introduction, in: Found. Microw. Eng., 2nd ed., Wiley-IEEE Press, New York, 2001: pp. 1–16.

[3] E.T. Thostenson, T. Chou, Microwave processing: fundamentals and applications, Compos. Part A Appl. Sci. Manuf. 30 (1999) 1055–1071. https://doi.org/10.1016/S1359-835X(99)00020-2.

[4] R.R. Mishra, A.K. Sharma, Microwave-material interaction phenomena: Heating mechanisms, challenges and opportunities in material processing, Compos. Part A Appl. Sci. Manuf. 81 (2016) 78–97. https://doi.org/10.1016/j.compositesa.2015.10.035.

[5] S. Das, A.K. Mukhopadhyay, S. Datta, D. Basu, Prospects of microwave processing: An overview, Bull. Mater. Sci. 32 (2009) 1–13. https://doi.org/10.1007/s12034-009-0001-4.

[6] Y. V. Bykov, K.I. Rybakov, V.E. Semenov, High-temperature microwave processing of materials, J. Phys. D. Appl. Phys. 34 (2001) R55. https://doi.org/10.1088/0022-3727/34/13/201.

[7] M. Oghbaei, O. Mirzaee, Microwave versus conventional sintering: A review of fundamentals, advantages and applications, J. Alloys Compd. 494 (2010) 175–189. https://doi.org/10.1016/j.jallcom.2010.01.068.

[8] R. Rosa, P. Veronesi, S. Han, V. Casalegno, M. Salvo, E. Colombini, C. Leonelli, M. Ferraris, Microwave assisted combustion synthesis in the system Ti-Si-C for the joining of SiC: Experimental and numerical simulation results, J. Eur. Ceram. Soc. 33 (2013) 1707–1719. https://doi.org/10.1016/j.jeurceramsoc.2013.03.005.

[9] D.A. Jones, T.P. Lelyveld, S.D. Mavrofidis, S.W. Kingman, N.J. Miles, Microwave heating applications in environmental engineering - A review, Resour. Conserv. Recycl. 34 (2002) 75–90. https://doi.org/10.1016/S0921-3449(01)00088-X.

[10] F. Marken, Chemical and electro-chemical applications of in situ microwave heating, Annu. Reports Prog. Chem. - Sect. C. 104 (2008) 124–141. https://doi.org/10.1039/b703986g.

[11] S. Singh, D. Gupta, V. Jain, A.K. Sharma, Microwave processing of materials and applications in manufacturing industries: A Review, Mater. Manuf. Process. 30 (2015) 1–29. https://doi.org/10.1080/10426914.2014.952028.

[12] A. Lazzeri, Cvi Processing of Ceramic Matrix Composites, in: N.P. Bansal, A.R. Boccaccini (Eds.), Ceram. Compos. Process. Methods, John Wiley & Sons, Hoboken, NJ, USA, 2012: pp. 313–349.

[13] I.M. Low, Advances in ceramic matrix composites: Introduction, in: I.M. Low (Ed.), Adv. Ceram. Matrix Compos., 2nd ed., Woodhead Publishing, Cambridge, UK, 2018: pp. 1–7. https://doi.org/10.1016/B978-0-08-102166-8.00001-3.

[14] B. Clauß, Fibers for Ceramic Matrix Composites, in: W. Krenkel (Ed.), Ceram. Matrix Compos. Fiber Reinf. Ceram. Their Appl., Wiley-VCH, Weinheim, Deutschland, 2008: pp. 1–19. https://doi.org/10.1002/9783527622412.

[15] R. Naslain, Design, preparation and properties of non-oxide CMCs for application in engines and nuclear reactors: An overview, Compos. Sci. Technol. 64 (2004) 155–170. https://doi.org/10.1016/S0266-3538(03)00230-6.

[16] D. Jaglin, J. Binner, B. Vaidhyanathan, C. Prentice, B. Shatwell, D. Grant, Microwave heated chemical vapor infiltration: Densification mechanism of SiCf/SiC composites, J. Am. Ceram. Soc. 89 (2006) 2710–2717. https://doi.org/10.1111/j.1551-2916.2006.01127.x.

[17] A.C. Metaxas, R.J. Meredith, Industrial applications and economics, in: Ind. Microw. Heat., IET, London, United Kingdom, 2008: pp. 296–319.

[18] S.Y. Foong, R.K. Liew, Y. Yang, Y.W. Cheng, P.N.Y. Yek, W.A. Wan Mahari, X.Y. Lee, C.S. Han, D.V.N. Vo, Q. Van Le, M. Aghbashlo, M. Tabatabaei, C. Sonne, W. Peng, S.S. Lam, Valorization of biomass waste to engineered activated biochar by microwave pyrolysis: Progress, challenges, and future directions, Chem. Eng. J. 389 (2020) 124401. https://doi.org/10.1016/j.cej.2020.124401.

[19] J. Sun, W. Wang, Q. Yue, Review on microwave-matter interaction fundamentals and efficient microwave-associated heating strategies, Materials (Basel). 9 (2016). https://doi.org/10.3390/ma9040231.

[20] G.S.J. Sturm, M.D. Verweij, A.I. Stankiewicz, G.D. Stefanidis, Microwaves and microreactors: Design challenges and remedies, Chem. Eng. J. 243 (2014) 147–158. https://doi.org/10.1016/j.cej.2013.12.088.

[21] T. Mitani, N. Hasegawa, R. Nakajima, N. Shinohara, Y. Nozaki, T. Chikata, T. Watanabe, Development of a wideband microwave reactor with a coaxial cable structure, Chem. Eng. J. 299 (2016) 209–216. https://doi.org/10.1016/j.cej.2016.04.064.

[22] G. Annino, M. Cassettari, M. Fittipaldi, M. Martinelli, Complex response function of whispering gallery dielectric resonators, Int. J. Infrared Millimeter Waves. 22 (2001) 1485–1494. https://doi.org/10.1023/A:1015038606997.

[23] G. Annino, M. Cassettari, M. Martinelli, Millimeter wave dielectric resonators, Transworld Research Network, Trivandrum, Kerala, India, 2004.

[24] A.C. Metaxas, Hazards, leakage and safety, in: Ind. Microw. Heat., IET, London, United Kingdom, 2008: pp. 277–294.

[25] High-frequency ELectro-Magnetic technologies for advanced processing of ceramic matrix composites and graphite expansion" (HELM), FP7-NMP.2011.4.0-1, GA n°. 280464, (n.d.). http://www.helm-project.eu/.

[26] A.C. Metaxas, Multimode oven applicators, in: Ind. Microw. Heat., IET, London, United Kingdom, 2008: pp. 130–150.

[27] H. Weyl, Über die Randwertaufgabe der Strahlungstheorie und asymptotische Spektralgesetze, J. Fur Die Reine Und Angew. Math. 1913 (1913) 177–202. https://doi.org/10.1515/crll.1913.143.177.

[28] D.A. Hill, Circular Cylindrical Cavity, in: J.W.& Sons (Ed.), Electromagn. Fields Cavities Determ. Stat. Theor., IEEE Press, New York, 2009: pp. 41–52. https://doi.org/10.1002/9780470495056.

[29] J.F. Dawson, T. Konefal, M.P. Robinson, A.C. Marvin, S.J. Porter, L.C. Chirwa, Field statistics in an enclosure with an aperture effect of Q-factor and number of modes, IEEE Int. Symp. Electromagn. Compat. 1 (2005) 141–146. https://doi.org/10.1109/ISEMC.2005.1513489.

[30] D. Kajfez, P. Guillon, Microwave resonators, in: Dielectr. Reson., 2nd ed., Noble Publishing Corporation, Atlanta, 1998: pp. 9–62. https://doi.org/1-884932-05-3.

[31] J.D. Jackson, Classical Electrodynamics, 2nd Editio, New York, 1975. https://www.wiley.com/en-us/Classical+Electrodynamics%2C+3rd+Edition-p-9780471309321.

[32] A. Cozza, The role of losses in the definition of the overmoded condition for reverberation chambers and their statistics, IEEE Trans. Electromagn. Compat. 53 (2011) 296–307. https://doi.org/10.1109/TEMC.2010.2081993.

[33] L.R. Arnaut, G. Gradoni, Probability Distribution of the Quality Factor of a Mode-Stirred Reverberation Chamber, IEEE Trans. Electromagn. Compat. (2012). https://doi.org/10.1109/TEMC.2012.2213257.

[34] P. Hallbjörner, U. Carlberg, K. Madsén, J. Andersson, Extracting electrical material parameters of electrically large dielectric objects from reverberation chamber measurements of absorption cross section, IEEE Trans. Electromagn. Compat. 47 (2005) 291–303. https://doi.org/10.1109/TEMC.2005.847391.

[35] O. Klein, S. Donovan, M. Dressel, G. Grüner, Microwave Cavity Perturbation Technique: Part I: Principles, Int. J. Infrared Millimeter Waves. 14 (1993) 2423–2457.

[36] D. Agrawal, Microwave sintering, brazing and melting of metallic materials, Adv. Process. Met. Mater. 4 (2006) 183–192.

[37] D. Ding, W. Zhou, B. Zhang, Complex permittivity and microwave absorbing properties of SiC fiber woven fabrics, (2011) 2709–2714. https://doi.org/10.1007/s10853-010-5140-x.

[38] T.A. Baeraky, Microwave measurements of the dielectric properties of silicon carbide at high temperature, Egypt. J. Sol. 25 (2002) 263–273. https://doi.org/10.1016/b978-1-59749-266-9.00017-5.

[39] H. Zhang, Y. Xu, J. Zhou, J. Jiao, Y. Chen, H. Wang, C. Liu, Z. Jiang, Z. Wang, Stacking fault and unoccupied densities of state dependence of electromagnetic wave absorption in SiC nanowires, J. Mater. Chem. C. 3 (2015) 4416--4423.

[40] H. Wang, L. Wu, J. Jiao, J. Zhou, Y. Xu, H. Zhang, Z. Jiang, B. Shen, Z. Wang, Covalent interaction enhanced electromagnetic wave absorption in SiC/Co hybrid nanowires, J. Mater. Chem. A. 3 (2015) 6517--6525.

[41] G. Chollon, R. Pailler, R. Canet, P. Delhaes, Correlation between microstructure and electrical properties of SiC-based fibres derived from organosilicon precursors, J. Eur. Ceram. Soc. 18 (1998) 725–733. https://doi.org/10.1016/S0955-2219(97)00177-5.

[42] E. Tan, Y. Kagawa, A. Dericioglu, Electromagnetic wave absorption potential of SiC-based ceramic woven fabrics in the GHz range, J. Mater. Sci. 44 (2009) 1172–1179. https://doi.org/10.1007/s10853-009-3257-6.

[43] R. Mo, X. Yin, F. Ye, X. Liu, L. Cheng, L. Zhang, Mechanical and microwave absorbing properties of Tyranno ZMI fiber annealed at elevated temperatures, Ceram. Int. 43 (2017) 8922–8931. https://doi.org/10.1016/j.ceramint.2017.04.030.

[44] T. Hu, X. Li, G. Li, W. Ying-de, J. Wang, SiC fibers with controllable thickness of carbon layer prepared directly by preceramic polymer pyrolysis routes, Mater. Sci. Eng. B. 176 (2011) 706–710. https://doi.org/10.1016/j.mseb.2011.02.024.

[45] H. Liu, H. Tian, Mechanical and microwave dielectric properties of SiCf/SiC composites with BN interphase prepared by dip-coating process, J. Eur. Ceram. Soc. 32 (2012) 2505–

2512. https://doi.org/10.1016/j.jeurceramsoc.2012.02.009.

[46] G. Annino, A. Cintio, R. D'Ambrosio, A. Lazzeri, Dielectric characterization of Si, SiC, SiC/SiC and C/SiC samples, in: 17th Int. Conf. Microw. High-Frequency Heating, AMPERE 2019, 2019. http://ampere2019.com/program/topics/.

[47] Archer Technicoat Ltd, Archer Technicoat Ltd, (n.d.). https://www.cvd.co.uk/.

[48] Schunk Carbon Technology, (n.d.). https://www.schunk-carbontechnology.com/en/products/technical-ceramics.

[49] W.E. Courtney, Analysis and Evaluation of a Method of Measuring the complex permittivity and permeability of microwave insulators, IEEE Trans. Microw. Theory Tech. (1970) 476–485.

[50] Schunk Carbon Technology, private communication, (n.d.).

[51] COMSOL Multiphysics, COMSOL Multiphysics, (n.d.). https://www.comsol.it/.

[52] JKRIZAY: Custom quartz and alumina fabrication, JKRIZAY: Custom quartz and alumina fabrication, (n.d.). http://www.jkrizay.com/.

[53] Unifrax, Unifrax, (n.d.). https://www.unifrax.com/.

[54] R.A. Waldron, The Theory of Waveguides and Cavities, Gordon and Breach Science Publishers, 1969.

[55] H.M. Altschuler, Dielectric Constant, in: E. M. Sucher and J. Fox (Ed.), Handb. Microw. Meas., Polytechnic Press of the Polytechnic Inst. Brooklyn, New York, 1963: pp. 518–548.

[56] G. Annino, M. Cassettari, I. Longo, M. Martinelli, Whispering Gallery Modes in a Dielectric Resonator: Characterization at Millimeter Wavelength, IEEE Trans. Microw. Theory Tech. 45 (1997) 2025–2034. https://doi.org/10.1109/22.644226.

Chapter 5

5. Design of a pilot-scale microwave heated chemical vapor infiltration plant: An innovative approach

A hybrid Microwave-assisted Chemical Vapor Infiltration (MW-CVI) pilot plant to produce silicon carbide-based Ceramic Matrix Composites was designed, built and setup, as a part of the European project HELM. Being different from the existing lab-scale MW-CVI equipment, this pilot plant was designed with the idea of a further industrial scale-up.

In order to enable the infiltration of the large samples of interest in industrial applications, the reactor was designed with the internal microwave cavity acting as an overmoded resonator at the frequencies of interest. The designed pilot plant allowed proper microwave heating of cylindrical samples of diameter doubled with respect to typical lab-scale preforms, with reproducible operating conditions in terms of transmitted/reflected power.

First infiltration trials resulted in an average reaction efficiency of 25 % with the desired inside-out silicon carbide infiltration. The main steps of the design and the results of the first infiltration tests are discussed in this Chapter.

5.1 Introduction

Ceramic Matrix Composites (CMCs) represent one of the latest and most promising solutions for high-temperature applications in strategic industrial sectors, such as transport and energy. Due to their exceptional properties such as high toughness, low density, and high thermal stress resistance, CMCs are suitable for applications requiring reliable operations under extreme conditions. Indeed, these materials are considered one of the strategic issues of the EC Research Road Mapping in Materials [1] and are among the topical priorities of the European Technology Platforms EuMAT [2].

Much development work has been done on non-oxide CMCs [3], particularly carbon (C) or silicon carbide (SiC) fibre-reinforced SiC based materials (C_f/SiC or SiC_f/SiC composites). This is because non oxide CMCs have attractive high temperature properties, such as creep resistance and microstructural stability, and excellent thermal stress resistance due to high thermal conductivity and low thermal expansion.

Non-oxide CMCs have also gained much industrial consideration for thermally loaded components in space applications such as propulsion systems or thermal protection systems [4–6], refractory materials for furnaces [7] and energy reactors [8,9], and ceramic brake systems [10]. They also have applications in antiballistic plates [11], gas burners, high-pressure heat exchangers [12], fuel and solar cells [13].

However, the potential for this type of materials is still hindered by: high cost, difficulty of processing and materials reliability. Thus, this calls for major research efforts to develop adequate industrial solutions and novel manufacturing processes of CMCs that can lead to significant reduction of the processing times, possibly continuous manufacturing processes and near to net-shaped products. In addition, improved control of temperature and thermal gradients can deliver renewed material microstructures and morphologies with enhanced technical performance and/or creation of unexpected new features. This also results in new market perspectives. Moreover, a better release of heating energy will lead to subsequent reduction of losses and will enable moving towards more sustainable manufacturing industry while reducing environmental impacts [14].

Depending on the different methods for developing the C or SiC matrix, the resulting SiC_f/SiC, C_f/C, C_f/SiC and C_f/C-SiC materials have different properties and manufacturing costs. Among all infiltration techniques, the Chemical Vapor Infiltration (CVI) technique best meets the quality requirements for the industrial production of CMCs [15–17]. This process allows the pre-coating of fibres with C, nitride boride (BN), or SiC [18], ensuring the activation of toughening mechanisms and protecting the fibres from oxidation [19,20]. The CVI technique is based on the principle of impregnating a porous body, consisting of an array of fibres (preform), by means of a mixture of precursor gases that reacts, decomposes, and precipitates the solid within the pore network of a heated substrate.

The CVI technique has three different variants. The first one is the Isothermal-isobaric (I-CVI), where the preform is heated very slowly to minimize the temperature gradient developed between the hot external surface and the inner part of the sample [21]. This technique presents the drawback of the “crusting” phenomenon, in which the gas inlet is stopped by the occlusion of surface pores. Consequently, it is necessary to stop the process to reopen the occluded pores by machining. This avoids a high residual porosity of the final composite but leads to lengthy process times (600−2000 h) to reach the final density [22]. To overcome this problem, an

approach based on the forced flow of the gases combined with a temperature gradient across the sample has been developed (F-CVI) [23] that improves homogeneity and efficiency. However, this approach presents difficulties to control the gas flow and manufacturing of complex geometries. Finally, the use of a Pulsed pressure process (P-CVI) allows the modulation of pressure, fastening the infiltration time and improving the densification rate as compared with I-CVI [24]. However, P-CVI has low efficiency in terms of chemical reaction and is generally used for the final densification of CMCs produced using the above-mentioned techniques.

Processing materials using high-frequency electromagnetic (EM) fields, such as microwave (MW), is considered a relatively new technology [25]. Although some processing applications have achieved industrial maturity in the 80s and are now considered as standard production methods, MW processing has mainly remained restricted to laboratory-scale research for most classes of materials [26,27]. A few published papers have demonstrated, at lab scale, that MW fields can be beneficial for the main processes involved in the production of SiC-based CMCs [21,28–30].

In comparison to the standard techniques in which the entire reaction chamber is heated to the temperature at which the chemical processes occur, the use of high-frequency EM fields to selectively heat the sample represents a cleaner, faster, and more efficient approach. In addition to the much lower thermal mass to be heated, the MW fields assisted processes are characterized by volumetric heating of the sample, whose speed is limited only by the available MW power and a controllable inverse temperature profile. These processes also prevent closure of premature pores, potentially allowing faster densification compared with the conventional CVI processes.

The ability of the EM waves to heat a material depends critically on its dielectric properties. Although essential in the design of a MW reactor, there is a lack of data about these properties owing to the extreme temperature conditions at which they must be determined and the requirement of specific composition and structure of the materials of interest. This situation is complicated by the strong variations showed by these quantities with respect to frequency and temperature, which makes the extrapolation of the available data questionable.

When the dielectric properties of a typical ceramic sample at the temperatures of the densification process are taken into account, the EM field distribution in the reactor is strongly deformed. Hence, the sample must be considered as part of the reactor to maximize the MW heating efficiency and minimize the EM field inhomogeneity. Such a design becomes particularly demanding when the reactor is intended for pilot-scale production in which the useful dimensions of the samples to be infiltrated are much larger than the employed EM wavelength.

Accordingly, the major difficulties preventing wide industrial application of EM-assisted techniques mainly include the lack of proper design methods of MW-CVI reactors that can effectively reproduce the processing of large samples. Moreover, this is exacerbated by the limited and approximated knowledge of the dielectric properties at the infiltration temperatures of interest.

Thus, this Chapter reports a contribution to the development of sustainable and economic production of SiC-based CMCs of industrial interest by means of MW-CVI processes at 2.45 GHz. It describes the design of a new hybrid conventional/MW-CVI pilot plant, built in the framework of the European HELM project [31], by using an innovative approach to achieve the homogeneous heating and the infiltration of relatively large samples, in view of further industrial scale-up of this technology.

5.2 Materials and Methods

5.2.1. CVI process

In CVI, silanes are generally used for producing SiC. In the present work, the well-known ceramic precursor CH_3SiCl_3, methyltrichlorosilane (MTS, Sigma-Aldrich, 99 % of purity), was employed. MTS was vaporized in a flow of hydrogen (used also as carrier gas) in a 1:10 ratio and introduced into the reactor, employing both MW and conventional heating, where it decomposed to SiC at temperatures 900–1200 °C [32]:

$$CH_3SiCl_{3(g)} \overset{H_2}{\leftrightarrow} SiC_{(s)} + 3HCl_{(g)} \qquad (5.1)$$

The reaction progress was monitored based on pH variation using a digital pH-meter (Process instruments CRONOS). This process involves in fact the formation of different intermediates and the competition between direct and inverse reactions [33]. Two main families of crystalline arrangement of SiC can be identified: α-SiC and ß-SiC. The first one is formed at temperatures greater than 1700 °C and has a hexagonal crystal structure similar to wurtzite. In comparison, ß-SiC has a cubic structure similar to the zinc blende and is formed at temperatures below 1700 °C [34]. Thus, the SiC produced by CVI is generally in the polymorphous form ß.

MTS is the ideal precursor for the production of high-quality ß-SiC using the CVI technique. This may be because the Si:C=1:1 ratio is the same as that of SiC. In addition, when MTS is the precursor in the production of SiC by CVI, hydrochloric acid (HCl) is released as a byproduct that can eliminate the deposition of pure Si crystals during the growth of SiC films or crystals [35]. The infiltration speed is also influenced by the presence of the carrier gas, H_2, which can facilitate the reduction of Si-Cl bonds on the growing SiC surface, thus, increasing the infiltration speed [36].

Different preforms based on SiC fibres were prepared and used for infiltration trials. Preliminary tests were performed using cylindrical preforms of 60mm of diameter and 5 ± 0.5mm of thickness with a round hole in the middle of 5mm diameter (SiC-1), provided by Archer Technicoat Ltd (ATL, Wycombe, England) company. After the optimization of the pilot plant, other infiltration tests were conducted using preforms based on a knitted multilayer system with polycarbosilane derived Si–C–O Nicalon NL-202 (Nippon Carbon, Tokyo, Japan) fibres.

Thirty disks measuring 100 mm in diameter were cut from the fibre cloth and stacked together to achieve a preform of 10 ± 0.5mm thickness (SiC-2). The images of SiC-based preforms prepared and tested are shown in **Figure 5.1**, while the starting data are reported in **Table 5.1**.

Table 5.1 *- Starting data on SiC-based preforms*

	***SiC* – 1**	***SiC* – 2**
Diameter [mm]	60	100
Thickness [mm]	5	10
Volume [cm^3]	14.032	94.985
Weight [g]	10.167	81.393
Density [g/cm^3]	0.500	0.856

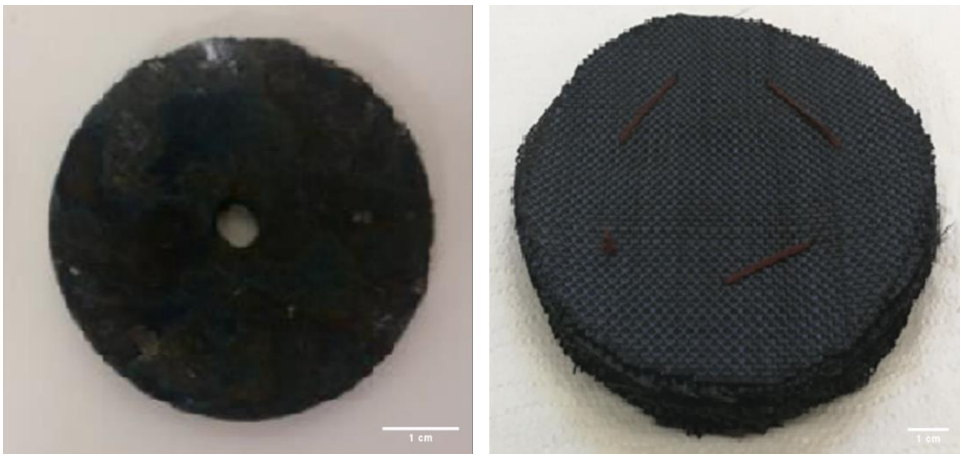

***Figure 5.1** - Preforms tested using MW-CVI process*

A sample holder system based on a high purity quartz structure (Momentive 214) shielded with disks made of mullite (Duraboard 1600 from Unifrax, Saronno, Italy) was used due to its low losses and to avoid contamination of the sample. **Figure 5.2** reports respectively the image of mullite disks, before and after the heat treatment, and the quartz sample holder, developed joining different cylindrical hollow tubes with a chair-like geometry. Specifically, the disks of mullite were heat treated at 350 °C for 24 h to completely burn the binder, which could absorb microwaves during the heating of the sample.

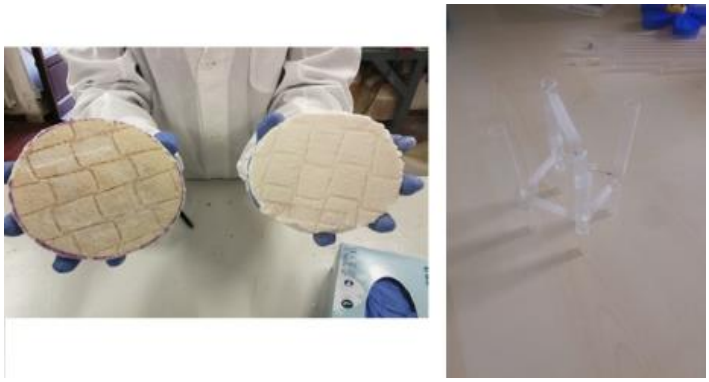

***Figure 5.2** - Mullite disks before/after binder removal (left); Quartz sample holder (right)*

NaOH solution (Sigma-Aldrich, Gillingham, UK), having pH=11, was used to neutralize the byproduct HCl, exiting to the scrubber.

5.2.2. High-temperature dielectric characterization

The dielectric properties of a series of SiC_f/SiC composites, provided by ATL, were investigated at 2.45 GHz for temperatures up to 1200 °C. The real and the imaginary parts of dielectric permittivity:

$$\varepsilon_r(T,d) = \varepsilon_r'(T,d) + i\varepsilon_r''(T,d) \qquad (5.2)$$

of the materials of interest have been measured as a function of temperature by means of a dedicated measurement system based on resonant cavity [37] developed following the approach described in [38]. A detailed description of the high-temperature dielectric characterization system, illustrated in **Figure 5.3**, will be published elsewhere.

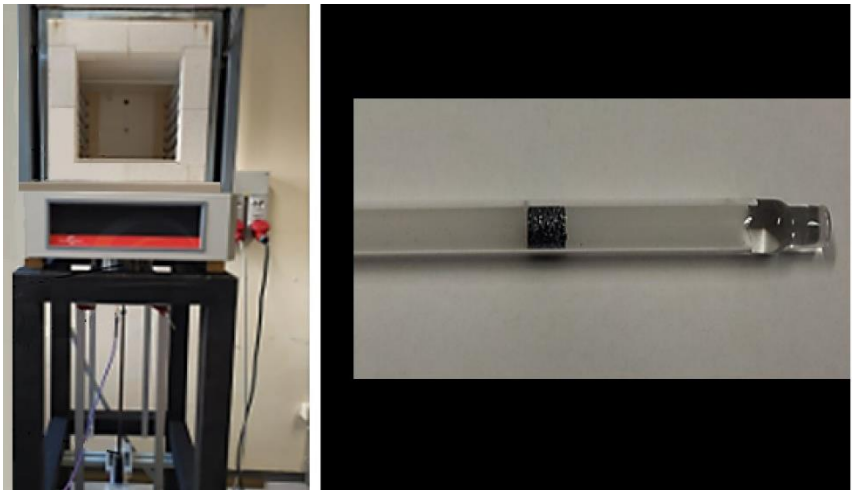

Figure 5.3 *- Left: View of the system for high-temperature dielectric characterization. Right: close-up view of a typical sample (dark region) and quartz sample holder (white/transparent regions) configuration*

The resonance frequency and the quality factor of the cavity loaded with sample and sample holder, heated by means of a furnace placed above the resonant cavity, were acquired from the resonance curves.

Thus, the complex dielectric permittivity of sample and sample holder was successfully determined. The passage from resonance figures (frequency and quality factor) to the dielectric properties is commonly based on the so-called "cavity perturbation" approach, which enables an analytical treatment of the data by means of calibration constants.

However, the accuracy of this approach depends on numerous factors that are difficult to control when the sample experiences a large temperature variation. Moreover, in some cases, the variation in these properties is so strong that it renders the calibration procedure doubtful. To avoid these uncertainties in our present work, the dielectric properties were extracted from the resonance figures based on a rigorous approach involving the numerical modelling of the EM field distribution, resonance frequency, and quality factor of the cavity loaded by the sample and sample holder. The finite-element software Comsol Multiphysics (COMSOL, Inc., Burlington, MA USA) was used for performing the analyses.

The real and the imaginary parts of the dielectric permittivity of three SiC_f/SiC samples with different density levels have been obtained for temperatures up to 900 °C, as shown in **Figure 5.4**:

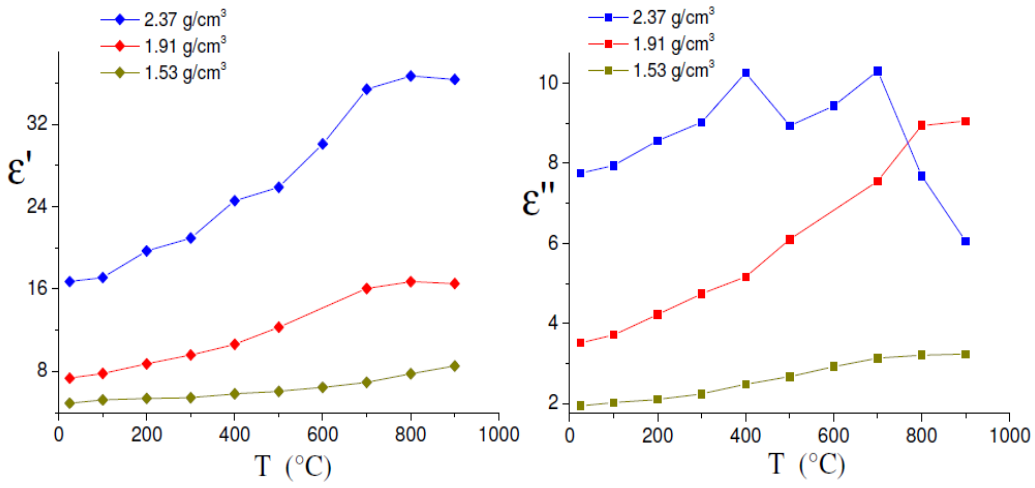

Figure 5.4 *- Real and imaginary parts of the dielectric permittivity of SiC_f/SiC samples*

5.2.3. Morphological characterization

The morphology of the infiltrated sample based on the SiC preforms was studied by stereomicroscopy using a Wild Heerbrugg M3 (Wild AG, Heerbrugg, Switzerland) and by field emission scanning electron microscopy (FESEM) using a FEI Quanta 450 ESEM FEG environmental field emission instrument (ESEM, FEI Company, Eindhoven, the Netherlands) equipped with an energy-dispersive spectrometer (EDS) for X-ray microanalysis (Bruker Nano GmbH, Berlin, Germany).

The EDS has a QUANTAX XFlash 6 | 10 Detector 6|10. The images obtained were used to study the morphology and measure the thickness of the deposits on flat substrates and around fibres, as well as to carry out compositional characterizations via the EDS detector.

5.3 Design of the pilot plant

A pilot plant was designed and built into the joint UNIPI – IPCF-CNR labs in Pisa where a hybrid conventional/MW heating system was used to tailor a suitable temperature profile in the preform to be infiltrated.

Different from existing lab-scale MW-CVI equipment, the design of this pilot plant has been carried out with the idea of a further industrial scale-up, avoiding any lab scale solution. This new approach faced certain complex engineering problems that were tackled successfully.

Moreover, since some ceramic materials may exhibit low dielectric losses at room temperature, the inner chamber of the reactor was designed to act as an overmoded resonator at the frequencies of interest.

In particular, the inner chamber and all the components exposed to high temperature and extreme chemical environment have been realized in conductive graphite. The final dimension of the cavity, as well as its EM behaviour, was determined using rigorous numerical modelling (Comsol Multiphysics software [39]).

5.3.1. Scheme and main components

The pilot plant was preliminarily built at High Wycombe (UK) in the ATL company and then set-up into the joint UNIPI – IPCF-CNR labs of Pisa, in collaboration with SAIREM IBERICA SL (now BEMENS - Barcelona Electromagnetic Energy Solutions S.L. - Castellbisbal, Barcelona, Spain) for the MW part.

The plant can be divided in 5 main parts: 1. General control cabinet; 2. Pumping system; 3. Scrubber tank; 4. Furnace; and 5. Microwave system. **Figure 5.5** shows the block diagram of the pilot plant, where each of the sections previously described is evidenced by a red rectangle with its corresponding number (left), and a general view of the final assembly (right).

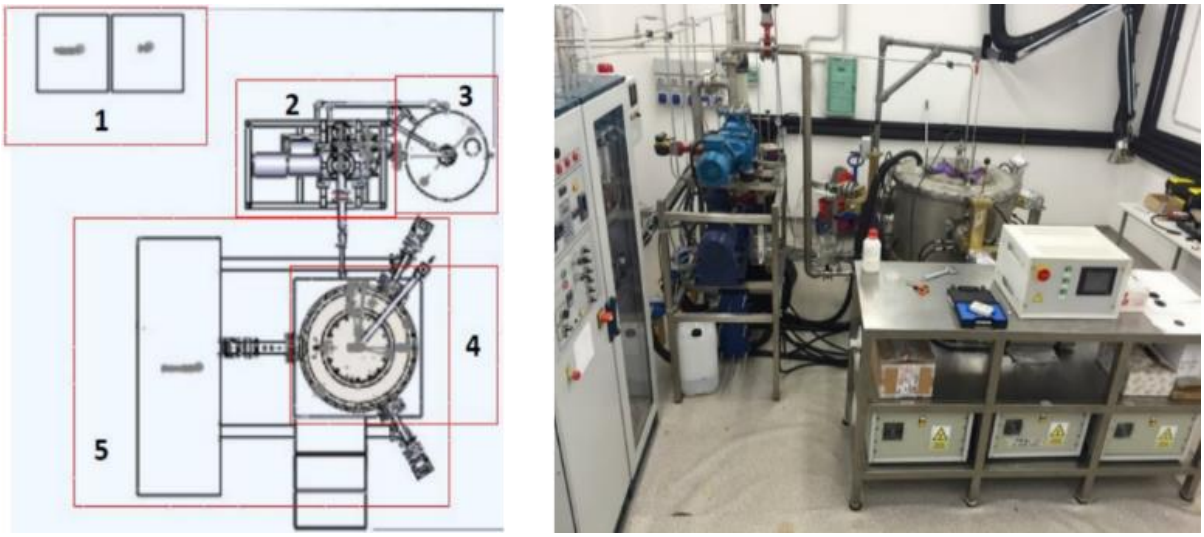

***Figure 5.5** - Block scheme of the MW-CVI pilot plant (left) and general view of the MW-CVI plant in Pisa, Italy (right).*

The pilot plant has been designed exploiting the previous experience of UNIPI [30], following the general scheme shown by **Figure 5.6**:

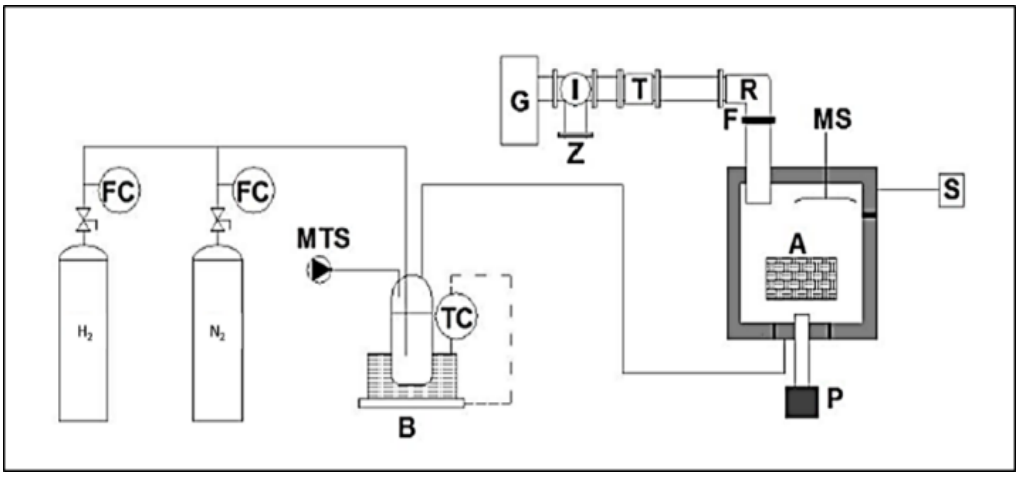

Figure 5.6 *- Schematic representation of the MW-CVI reactor (G: generator 2.45 GHz, 3 for 3 kW; I: three port circulator; Z: water cooled dummy load; T: auto tuner; R: connected transition; F: quartz window; A: applicator; MS: mode stirrer; P: pyrometer; S: scrubber system; B: bubbler; FC: feed controller; TC: temperature controller)*

The general control cabinet allows to set the operating process parameters (conventional heating temperature, operating pressure, reagents flows). Furthermore, inside the control cabinet, the MTS pressure tank connected to an evaporator is placed. At constant MTS mass flow, the tank allows the evaporation of the correct quantity of precursor.

The flow regulators of N_2, H_2, and purge flows (necessary for purging the flow system of MTS and the furnace) are placed inside the cabinet.

The pumping system consists of two pumps: a liquid ring pump for the main evacuation that can withstand a pressure of 50 mbar starting from normal external pressure (about 1 bar), and a booster pump that works from 50 mbar to 3 mbar. Two valves connected to two pumps are controlled automatically based on the parameters set onto the control cabinet.

The scrubber tank, which is a container filled with an alkalinized solution, can trap the by-products exiting the reactor.

The MW system consists of the general control apparatus and the three magnetrons, each emitting a maximum of 3 kW of MW power in the ISM band centred around 2.45 GHz.

Finally, the infiltration of the preform occurs in the furnace and the core of the plant. The inner chamber, where the preform is located, is made of conductive graphite shielded from the external stainless steel wall by an insulator inorganic fibrous material (allumino-silicate fibre blanket). The pyrometer connection is located on top of the stainless steel tube and leads to a transducer capable of converting the optical signal to an electrical one. The steel tube also contains the inlet of the reaction gases coming from a lateral flexible tube. The inlet of gases is on the fixed cover while the outlet is on the bottom of the reactor, precisely on the opposite side with respect to the other one.

5.3.2. Design of the MW reactor chamber and coupling system

Ceramic materials may exhibit relatively low dielectric losses at MWs, especially at the beginning of the densification process when their density can be very modest. In order to efficiently heat these materials, it is convenient to use a reactor chamber designed as a resonant cavity, having conducting walls electrically and thermally insulated from the external body of the reactor. In these resonant systems, the sample is heated via the multiple passages of the EM waves [26,40].

At the resonance conditions, the constructive interference among the waves passing through the sample leads to increased intensity of the field and increased efficiency of the MW heating process. However, this is limited to frequencies close to the resonance ones. The efficiency of the heating process can be further improved by using a high-conductivity material for the chamber walls. A mandatory condition that must be fulfilled by this material is its compatibility with the high reaction temperatures and the aggressive chemical environment.

On the basis of all these requirements, the material chosen for the construction of the MW-CVI reactor chamber was a high-conductivity graphite. The MW resistivity of this material was measured in the framework of the project HELM and was about 10 μΩ*m at 300 °C.

The design of a pilot-scale reactor for the infiltration of samples with linear dimensions of the order or larger than 100 mm, i.e., 4 times larger than the employed wavelengths, necessarily leads to a reaction chamber characterized by different modes resonating around 2.45 GHz (overmoded cavity). This is associated with several advantages, such as the absence of strict tuning requirements and achievement of a more uniform EM field inside the sample. On the other hand, the simultaneous presence of different resonance modes makes the actual EM field distribution on the sample less predictable.

In the design of an overmoded resonant cavity for MW-assisted processes, larger cavities enable denser resonance mode spectrum, which can lead to a more homogeneous average electric field on the sample. However, the volume of the cavity cannot be much higher than that of the sample, else the fraction of EM energy dissipated in the cavity walls increases at the expense of that dissipated in the sample.

Thus, a trade-off must be found in the reactor chamber size, which, in turn, requires a careful optimization of the reactor design taking into account realistic working conditions, particularly the dielectric permittivity of the sample as a function of T.

In the design of the MW-CVI reactor described in this contribution, the design of the reactor chamber was conducted with the help of a rigorous numerical modelling based on the Multiphysics software. The basic structure of the reactor chamber investigated by numerical modelling is shown in **Figure 5.7**.

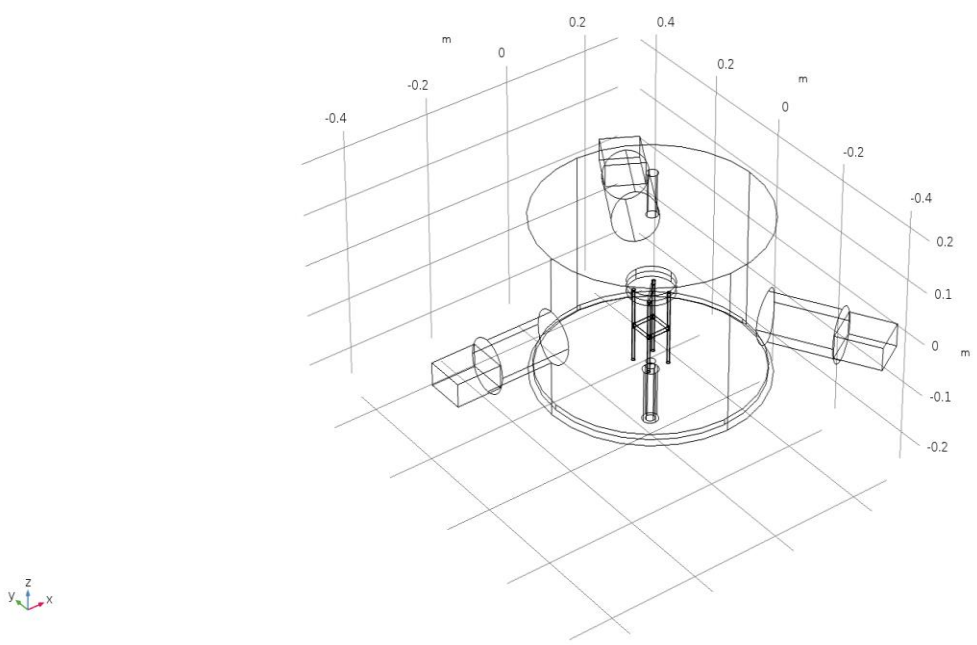

***Figure 5.7** - Model of the inner graphite chamber developed with Comsol Multiphysics*

It is composed of a cylindrical chamber, excited through three circular waveguides with 90mm inner diameter, entering in the cavity along its curve side. The circular waveguides are terminated by means of aluminum WR340 rectangular waveguides [41], connected to the magnetron sources. The rectangular waveguides are connected to the reactor by a cooled flange system, while coupling level between the single-mode waveguide and the resonant cavity is controlled using a 3-screw tuner [42].

In order to allow the MW passage and maintain the sealing in the reactor, three quartz windows (one for each waveguide) are located between the reactor flange and the end of the waveguide, and Viton O-rings are inserted to maintain the sealing.

After the flange system, the waveguides are made in graphite (same grade of the inner chamber) and have a little channel in the middle in order to decrease the conduction of heat from the chamber.

The reactor chamber includes a movable plate, placed close to its basis, which enables a frequency tuning of the resonance spectrum. In the numerical modelling, the presence of the inlet and the outlet of the reactant gases was included, as well as the presence of a 'chair-like' quartz sample holder and of a Duraboard disk, the latter being necessary to avoid a direct contact of the sample with the quartz rods.

The dimensions of the cavity were optimized by analysing, around 2.45 GHz, the EM field distribution in the sample, the linewidth of the resonance line, the coupling level of the incoming radiation to the cavity, and the fraction of the EM power dissipated in the sample. A detailed description of the design and optimization procedure is beyond the scope of this contribution and will be published elsewhere.

In view of the infiltration of samples with minimum diameter of about 100 and minimum thickness of 10 mm, a convenient choice for the cavity dimensions is 493mm inner diameter and 306mm inner height. The resulting structure is shown in **Figure 5.8**.

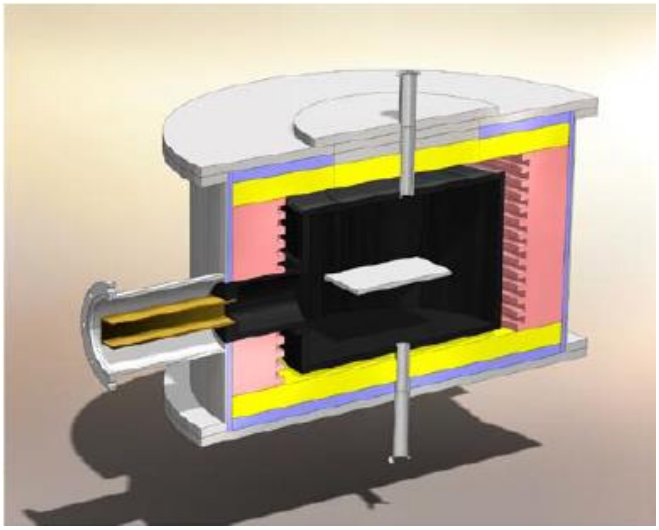

***Figure 5.8** - 3D design of the MW waveguide integrated in the CVI furnace (right) (Courtesy ATL).*

5.3.3. Cooling and flange system

A cooling system was introduced to keep constant the temperature of metallic flanges and the region connecting MW waveguides with the furnace at a temperature lower than the decomposition temperature of O-rings, thus avoiding issues related to overheating.

The parts of the pilot plant needed to be cooled were:

- Magnetron: when the plant works, the MWs flow along the waveguides into the reactor and could be reflected back due to mismatch of the source-cavity coupling level. Specifically, to avoid overheating of the magnetrons, a cooling system based on a brazed plate heat exchanger has been provided
- Pumping system: to guarantee adequate chilling to the liquid ring pump and avoid pump's oil vaporization
- Reactor lid
- Flange system

This cooling system provides water at 19 ± 1 °C (intermediate temperature between the value needed for magnetrons cooling and pumping system). Furthermore, the cooling system is equipped with pressure and temperature indicators for a continuous visual control during the processing.

During the set-up of pilot plant, certain tests were carried out by setting a MW power of 3 kW. It was observed that for each waveguide, there was an overheating in the side walls caused by the sum of two effects: the heat generated from MW and the heat developed by the inner part of the reactor (caused by the irradiation of the hot sample inside the reactor).

The combination of these two heat sources generated a heat flow that spreaded along the waveguides, in the opposite direction of the MWs, and contributed to increase the overall temperature of the walls. In order to keep flanges temperature constant and remove the heat generated during the infiltration, cooled flanges were designed and built.

Figure 5.9 shows the temperature trend, measured by means of a thermocouple positioned between the flanges, during the set-up test and first infiltration trials. It can be observed that

an uncooled flange system increased the temperature, while the cooled flange system maintained a constant temperature.

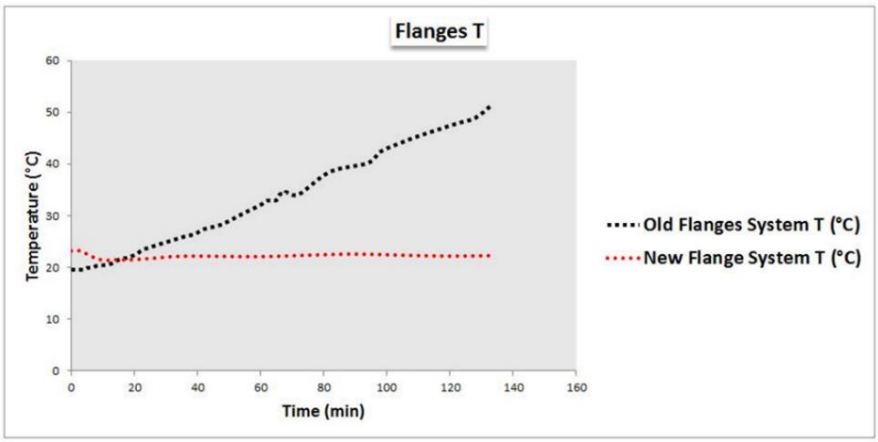

Figure 5.9 *- Temperature profile during set-up tests*

5.3.4. Scrubber tank

According to Eq. 5.1, the main byproduct of the reaction that occurs during the SiC infiltration is HCl, which is a gaseous, highly corrosive acid that must be properly neutralized. This neutralization occured in a scrubber tank filled with an alkalinized solution (based on NaOH) that can abate the by-products coming out from the reactor.

All the gas flows coming out of the furnace pass through the scrubber. The tank is equipped with a membrane that separates the liquid and the solid. The liquid portion is connected to the pump system for cleaning the vacuum vapours coming out of the reactor, avoiding pump damages. One connection lead to the shower for abatement of volatile acids. A tap on the bottom of the tank allows removal of liquid during the periodic maintenance operations. The level of the liquid in the tank must be controlled because the liquid can overcome membrane separation, causing the mixing of the liquid and solid.

5.3.5. Experimental procedure

The infiltration procedure can be divided into different steps. Once the preform and sample holder were located inside the reactor, the system was kept under vacuum at 4 mbar and 300 °C (reached using conventional heating) for 8 h to dehumidify the environment.

Then nitrogen was flushed for 10 min, followed by hydrogen for the same amount of time at the operating pressure. At this point, MW heating was started, setting the power necessary to reach the infiltration temperature and tuning it to minimize reflections from the cavity.

Finally, MTS was flown starting SiC deposition inside the preform. The pH-meter continuously monitored the pH of the solution inside the pump so that a fresh feed of NaOH solution is suctioned by the pump when this value was near to 8.

At the end of the reaction, the system was purged again with nitrogen for 2 h, and when the reactor cools down, it is opened allowing the detailed analysis of the sample.

5.4 Results and discussion

Preliminary tests were conducted to prove the compatibility of this technique for the production of SiC-based CMCs and verify the expected advantages of MW heating. These trials were carried out on SiC-1 preforms. Based on these first results, several optimizations were carried out to the pilot plant to further increase reaction efficiency, overcoming the issues observed. Other infiltration tests were repeated after the optimization of the pilot plant on SiC-2 preforms, assessing the scale-up of the technology.

5.4.1. Preliminary tests

Several infiltration trials were made to choose the best operating parameters, which remained constant among those tests (see **Table 5.2**). The operating pressure was chosen as the minimum level to avoid plasma formation. For each gas, the critical voltage value (or breakdown voltage) necessary to start plasma is a function of the pressure [43].

Table 5.2 *- Operating parameters for MW-CVI preliminary tests on SiC-1 preforms*

	$SiC-1$
Operating Pressure [mbar]	150
Infiltration Temperature [°C]	900 – 1000
MTS/H_2 ratio	1:10
MTS flow rate [kg/h]	0.06
H_2 flow rate [L/min]	1.40
Processing Time [min]	440
Starting density [g/cm^3]	0.498
Final density [g/cm^3]	0.718
MW Power input [kW]	3.3
MW Power reflected [kW]	2.2

To avoid plasma formation, a good compromise must be achieved between the operating pressure and the MW power necessary to reach the infiltration temperature in a specific gaseous environment. Considering the higher MW power level limit, nitrogen was preferred as inert gas instead of argon. The total MW power was obtained exciting the reactor chamber by means of two excitation channels. The total reflected power also took into account the cross-coupling between the two excitation channels.

Another point of importance regarded the fabrication atmosphere employed, which plays an important role on the resulting complex permittivity of the SiC matrix deposited [44]. Specifically, it was reported that the use of a hydrogen-based atmosphere leads to an almost stoichiometric SiC matrix, whereas an argon-based atmosphere leads to a carbon rich SiC matrix.

An important key parameter to compare MW-CVI with traditional CVI is the infiltration rate. Usually, this is defined as microns per hour of SiC deposited and is determined by SEM [45,46]. In this work, we determined the deposition rate V_{SiC} as follows:

$$V_{SiC} = \frac{P_f - P_i}{P_i} \frac{1}{t_{inf}} \qquad (5.3)$$

where P_f is the final weight of the sample, P_i is the starting weight of the sample, and t_{inf} is the infiltration time. The MTS flow is known to be important for the control of growing density [47]. Moreover, it is necessary to study the reaction efficiency as the ratio of effectively infiltrated SiC with respect to the theoretical amount that could be produced if all the MTS had reacted according to **Equation 5.1**.

The reaction efficiency measured among all the infiltration trials, and relative density increase together with relative deposition rate are reported in **Figure 5.10** and **Figure 5.11**, respectively:

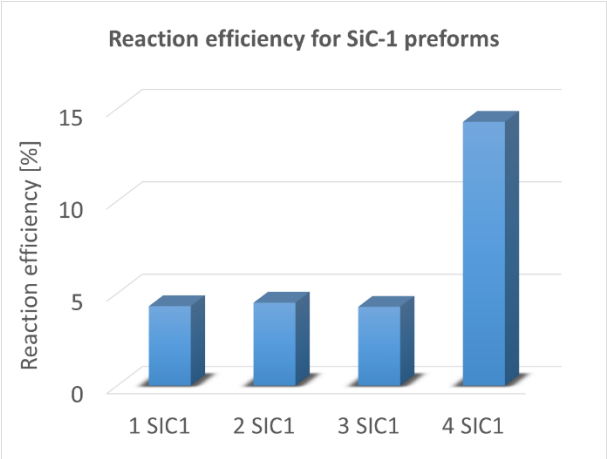

Figure 5.10 *- Reaction efficiency data after MW-CVI trials on SiC-1 preforms*

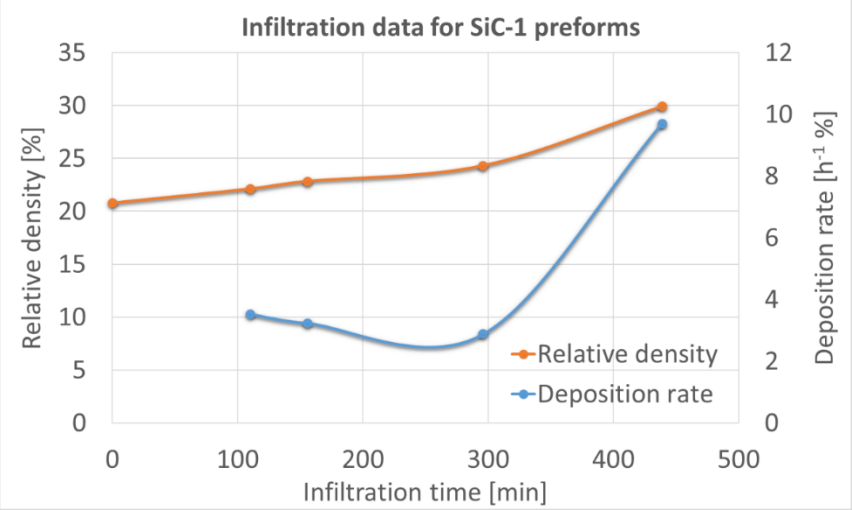

Figure 5.11 *- Infiltration data after MW-CVI trials on SiC-1 preforms*

Specifically, the relative density was determined from the increase in mass along different infiltration trials with respect to a reference value of 2.5 g/cm^3 for CVI-SiC$_f$/SiC [16,48]. A maximum reaction efficiency of 14 % was obtained among these infiltration trials. In the preliminary tests, the deposition conditions were not constant when trying to achieve the optimum performance of the system.

In particular, the increase in SiC infiltration corresponded to a rise in the dielectric properties of the sample, improving its MW absorption. The latter effect allowed to further reduce the operating pressure; hence, an increase was observed in the deposition rate.

The achievement of the expected inverse temperature profile has been proved from SEM-EDS analysis on external and internal regions of the samples due to the preferential presence of SiC on the latter one, as shown in **Figure 5.12**.

External surface

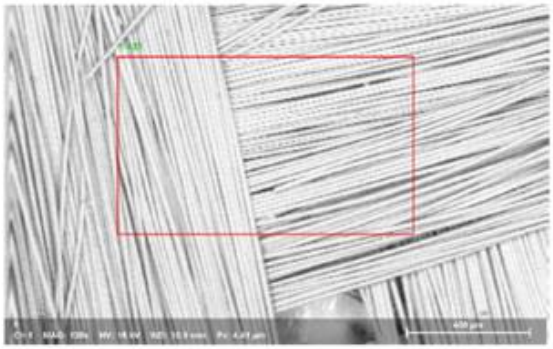

Element	At. No.	Netto	Mass [%]	Mass Norm. [%]	Atom [%]
Carbon	6	1319	24.14	23.06	36.71
Oxygen	8	3788	22.25	21.26	25.40
Silicon	14	55642	58.28	55.68	37.90
		Sum	**104.67**	**100.00**	**100.00**

Internal surface

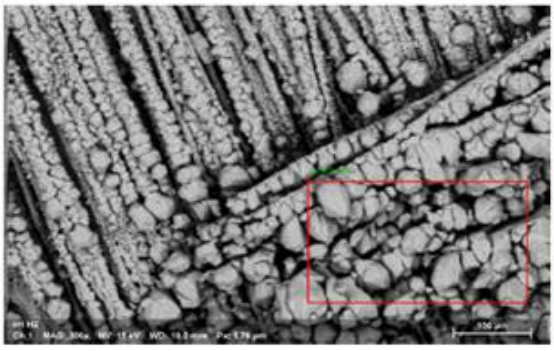

Element	At. No.	Netto	Mass [%]	Mass Norm. [%]	Atom [%]
Carbon	6	2405	46.62	46.95	66.92
Oxygen	8	177	1.62	1.63	1.75
Silicon	14	43163	51.05	51.42	31.34
		Sum	**99.29**	**100.00**	**100.00**

Figure 5.12 *- Image of infiltrated SiC-1 preforms (up); SEM-EDS analysis of external (bottom left) and internal (bottom right) regions*

The microanalysis performed showed results evidencing mainly the deposition of SiC, but there were also issues related to the formation of heterogeneous deposits on the samples. In particular, the white regions were ascribed to the formation of acicular silica due to the thermal degradation of SiC fibres used [49,50]. While the analysis of rainbow-like regions was related to the formation of a vitreous silica layer caused by high-temperature oxidizing plasmas in the reactor [51].

5.4.2. Optimization of the pilot plant

The pilot plant was further optimized to improve reaction efficiency, ensuring a finer control of the operating parameters with reproducible conditions in terms of transmitted/reflected power among different infiltration tests and overcoming the above-mentioned issues.

In order to adjust the operating pressure, a pressure control valve was inserted on the outlet line, providing a rapid and precise tuning of the reaction pressure. Another 2-color pyrometer equipped with a color video module (Dias Pyrospot DSR 10 N V, DIAS Infrared GmbH, Dresden, Germany) was added to monitor the temperature profile of the sample during infiltration trials and eventual plasma formation in the cavity.

Both sensors provided information on the surface temperature of the sample, which is lower than the internal temperature due to the inverse temperature profile enabled by the MW heating. In the following, the reported infiltration temperatures will refer to the sample surface.

Preliminary heating tests have been made to find the infiltration temperature and MW power needed to favour **Equation 5.1** without plasma and silica formation (770 °C–830 °C). In addition, the use of a Magic T, designed as a combination of WR340 rectangular waveguides and equipped with sliding stubs, was essential in reaching the critical coupling condition, in which all the incoming MW power was dissipated in the reactor loaded by the sample. The minimization of the power reflected by the reactor was indeed a prerequisite for the maximization of the MW heating process.

In the MW-CVI reactor, the Magic T system was inserted between the flanges surrounding the excitation channel and the rectangular waveguides. The gas sealing of the reactor chamber was guaranteed by a first quartz window mounted between the flanges of the reactor and the Magic T with the help of O-ring. An additional quartz window is inserted between the Magic T and the rectangular waveguide.

Figure 5.13 shows the typical EM field distribution in the reactor excited through one of its external waveguide, equipped with a magic T tuner [52], together with the temperature distribution on the sample surface obtained in stationary conditions.

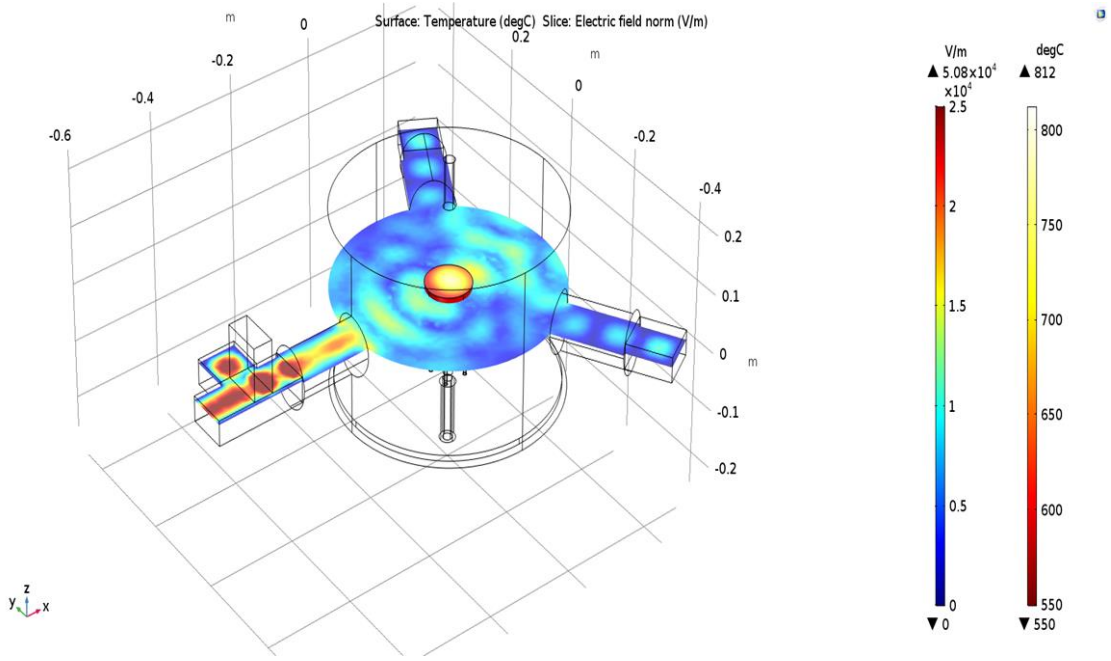

Figure 5.13 *- Electric field distribution in the plane of the sample and resulting thermal profile, as obtained by means of simulation with Comsol Multiphysics*

The numerical model leading to the results of **Figure 5.13** included the dielectric properties at variable T, as well as the relevant thermal quantities (specific heat and thermal conductivity), both measured in the framework of the HELM project. The employed MW power was set to 1200 W.

The numerical results showed that there was a difference of about 200°C - 250°C between the surface and inner temperature of the sample (as displayed in **Figure 5.14**), thus a reference surface temperature of 800 ± 30°C was considered valid for subsequent infiltration trials.

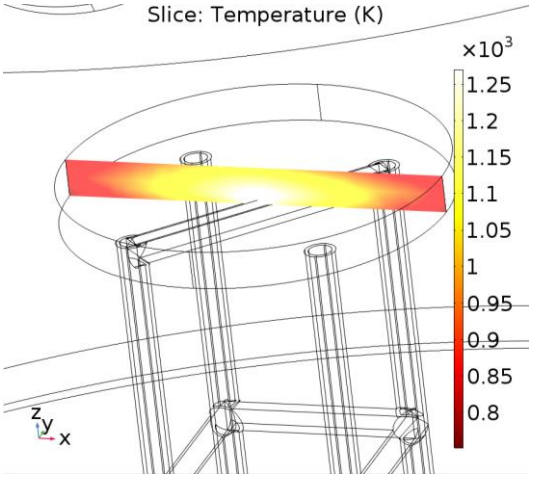

Figure 5.14 *– Slice of SiC-2 sample showing the inverse temperature profile established within the preform, obtained by means of simulation with Comsol Multiphysics*

Furthermore, previous MW heating tests carried out on 1°gen Nicalon fibre reinforced preforms showed marked oxidation phenomena above measured surface temperatures of 900°C thus showing the overcoming of their degradation resistance (> 1100°C) [53,54].

5.4.3. Final infiltration tests

Further infiltration trials have been made on SiC-2 preforms. The experimental procedure was changed based on the upgrades performed on the MW-CVI pilot plant. First the position of the sample on the sample holder was adjusted in order to be at a height corresponding to the median plane of the cavity using a cross-check control with the thermal camera installed. This allowed to verify eventual presence of deposits on the quartz windows which could hamper the thermal readings from the pyrometer during experimental trials.

Before infiltration trials, MW heating tests were performed based on a spectral analysis of the loaded cavity, as described in **Chapter 4**. Those measurements were obtained through reflection coefficients measurement with a Vector Network Analyzer (VNA) connected to the microwave channel of interest, given by a single-mode rectangular waveguide, by means of a coaxial cable-to-waveguide transition. A first positioning of Magic T stubs was then carried out to ensure the coupling with the mode of interest at the closer emission frequency of one of the available magnetrons. The choice of the volume mode of interest was based on the analysis of the results obtained from numerical modelling. Following, dehumidification of the cavity and leak tests have been carried out, then nitrogen and hydrogen were flushed into the cavity, in accordance with first trials.

MW heating tests have been realized in hydrogen atmosphere to evaluate the operating pressure window and the power necessary to reach the infiltration temperature while avoiding plasma formation. Finally, MTS was sent into the cavity starting SiC-deposition reaction. In this framework, several information regarding sample infiltration temperature, chamber temperature, operating pressure, transmitted/reflected MW power, have been systematically recorded to monitor the MW-CVI process. Before and after each infiltration the infiltrated sample was weighted in order to determine the variation of mass related to the infiltration step.

The results obtained from 5 h of different infiltration tests, using the same single port excitation scheme discussed before, resulted in improved reaction efficiency (see **Figure 5.15**), despite the increase in sample dimension, without plasma formation and a good compromise in terms of operating pressure (see **Table 5.3**).

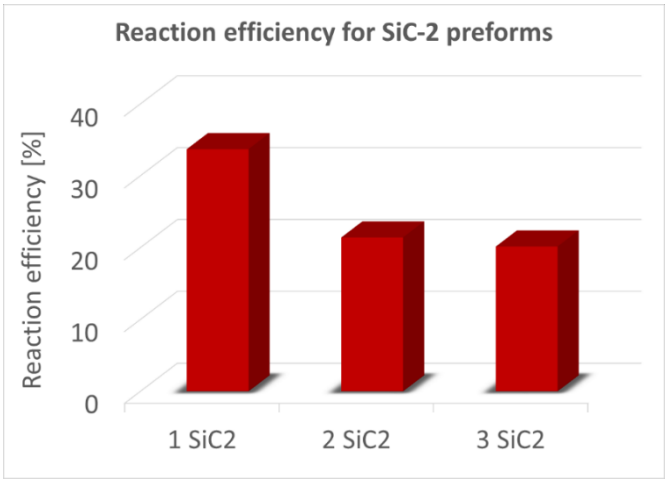

***Figure 5.15** - Reaction efficiency data after MW-CVI trials on SiC-2 preforms*

Table 5.3 *- Operating parameters for MW-CVI tests on SiC-2 preforms*

	SiC-2
Operating Pressure [mbar]	70
Infiltration Temperature [°C]	770 – 830
MTS/H_2 ratio	1:10
MTS flow rate [kg/h]	0.06
H_2 flow rate [L/min]	1.40
Processing Time [min]	300
Starting density [g/cm^3]	0.857
Final density [g/cm^3]	1.052
MW Power input [kW]	1.2
MW Power reflected [kW]	0

During the infiltration, the temperature of the sample surface was limited to about 770 °C–830 °C to take into account the inverse temperature profile and avoid partial degradation of the sample observed in the first infiltration tests.

In this case, a careful adjustment in the Magic T stubs configuration enabled the critical coupling condition along the whole infiltration process, which resulted in a high energetic efficiency. Such efficiency is confirmed by the observed deposition rate, reported in **Figure 5.16**, which suggests a potential reduction of total infiltration time with respect to I-CVI.

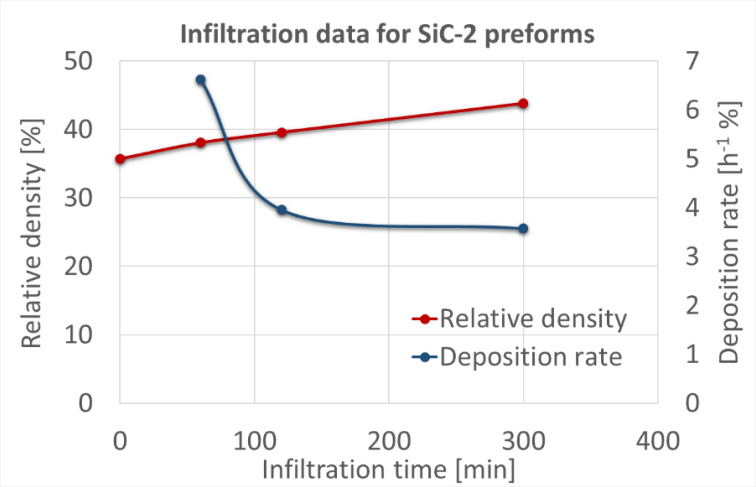

Figure 5.16 *- Infiltration data after MW-CVI trials on SiC-2 preforms*

During SiC-1 MW-CVI trials the operating pressure was reduced after the first runs thus achieving a higher deposition rate and chemical efficiency (as described in **Figure 5.10**). The purpose was to check how the increase in the complex permittivity affected the operating pressure. Differently, along SiC-2 infiltrations the operating pressure was increased as a safety measure to minimize plasma formation during first runs. Based on those results, more hours of infiltrations were needed to allow a reduction of the operating pressure.

SEM-EDS analysis (see **Figure 5.17**) confirmed a predominant infiltration of SiC on central laminae of the sample, as expected from the inverse temperature profile typical of the MW heating.

Figure 5.17 *- Image of the central laminae related to infiltrated SiC-2 preform; SEM image (inset)*

The similar values obtained for the deposition rates together with the higher reaction efficiencies suggested that the SiC deposition reaction (Eq. 5.1) was favoured with respect to the other secondary reactions. The typical heating dynamic obtained during the infiltration process is reported in **Figure 5.18** (left).

The curve refers to the temperature read with the thermal camera. It is composed by a rapidly increasing part, in which the infiltration temperature is reached on a time scale of few minutes, followed by a plateau region. The heating of the sample to about 800 °C of surface temperature in a few minutes by using about 1.2 kW of MW power is in close agreement with the results of the Multiphysics modelling.

The inset in the left part of **Figure 5.18** shows temperature distribution of the lateral sample surface. The right part of **Figure 5.18** reports the control panel of the three magnetron sources taken during these infiltration tests. Only magnetron 3 was in use, delivering 1.2 kW with no reflected power (critical coupling condition).

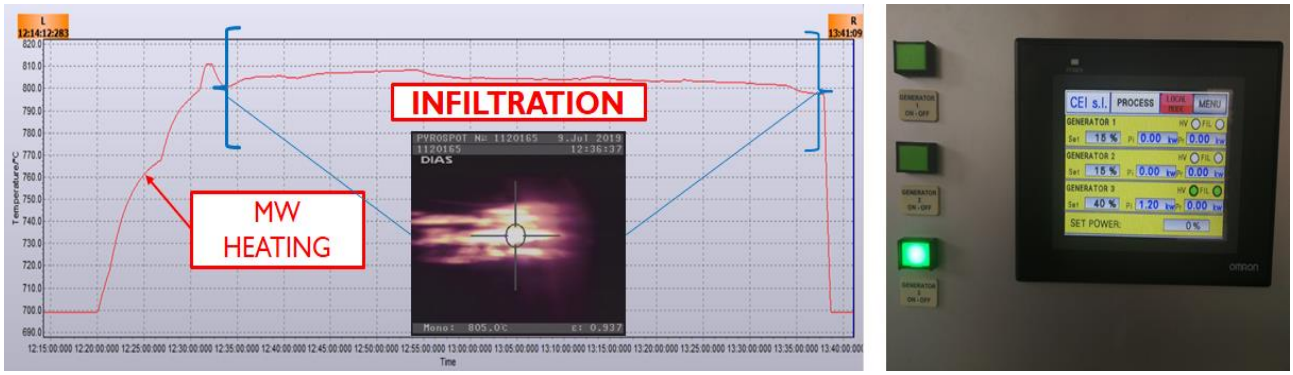

Figure 5.18 *- Thermal profile measured by the pyrometer (left); experimental values of the transmitted/reflected MW power during infiltration trials*

The very fast sample heating illustrated by **Figure 5.18** was the sharpest difference in comparison to the conventional CVI reactors, based instead on resistive heating. In the latter, a much longer thermalization time is necessary, both in the heating and the cooling stage, due to the much larger involved mass.

Moreover, the problem of external pores occlusion occurring in conventional reactor, forced to stop and repeat the infiltration process several times, thus further increasing the processing time.

In MW-CVI, the sample heating stage can be completed in few minutes by using a low MW power around 1 kW. A similar period was necessary for the sample cooling, as shown in the right part of **Figure 5.18**, due to the very efficient thermal irradiation towards the much colder reactor walls, which can be taken to a minimum T of about 200 °C, thus allowing a rapid opening of the reactor.

Finally, the much faster sample heating translated in a higher energy efficiency. On the other hand, a weakness of the MW-CVI process is still given by the limited temperature – and thus infiltration – uniformity, which will require further work to be mitigated.

5.4.4. Industrial scale-up

The MW-CVI reactor discussed in this work was designed with the goal to infiltrate SiC-based samples with diameter ranging from about 100mm–200mm and thickness from about 10mm to 20 mm. Although larger samples could be treated, a limited infiltration efficiency is expected in the external part of these samples.

A further scale-up of the reactor is thus necessary for samples with dimensions larger than about 200 mm. The size of the reactor should be commensurated to that of the samples and to its dielectric properties, in order to ensure that the majority of the MW energy is dissipated in the sample instead of the reactor walls, thus keeping a high efficiency.

This point can be mathematically formalized and will be discussed in a forthcoming publication. In general, the maximum size of samples that can be efficiently treated with MW-assisted processes is limited by the penetration depth of the microwaves in the samples [55].

A further scale-up to industrial level is currently under consideration for the treatment of relatively long CMC tubes.

5.5 Conclusions

In conclusion, a MW-CVI pilot plant has been designed and developed for the production of pilot-scale SiC-based CMCs samples. The objective of the plant was the production of SiC-based CMCs, as well as the identification of strengths and weaknesses of the MW-CVI at these production scales.

The infiltration tests confirmed the inverse temperature profile expected by the use of the MW heating. The obtained results demonstrated that an efficient MW-CVI process at 2.45 GHz, based on magnetron sources, can be achieved for SiC-based samples of linear dimensions of the order of 100 mm.

From the EM point of view, the MW-CVI reactor can reach the critical coupling conditions for a large class of samples, optimizing the use of the available MW power. Moreover, the analysis of the sample heating dynamics confirms that the majority of the MW power is effectively dissipated in the sample. As a result, a typical sample can be heated from the room T to the infiltration temperatures (around 1000 °C in the sample volume) in a few minutes, leaving the temperature of the cavity walls to much lower temperatures of the order of 300 °C.

During the infiltration process, the formation of hot spots in the sample and the appearance of plasma regions at relatively low operating pressures need to be taken care of. The latter can be particularly detrimental because they damage the sample surface and substantially alter the EM response of the reactor.

Both these problems can be mitigated by implementing an accurate control over the power and frequency of the EM radiation exciting the reactor. In this respect, the replacement of the most economic but much less controllable magnetrons with the fully controllable solid-state sources is expected to further improve the capabilities of the MW-assisted processes in terms of operating conditions, reliability, and automation. Work is currently underway in the upgradation of the MW-CVI pilot plant to solid-state sources.

5.6 References

[1] Baas A de. Research Road Mapping in Materials. Research*eu [Internet]. 2010; Available from: https://ec.europa.eu/research/industrial_technologies/pdf/research-road-mapping-in-materials_en.pdf.

[2] Jovanovic A. Roadmap of the European Technology Platform for Advanced Engineering Materials and Technologies. EuMaT Members Version [Internet]. 2006;27:147. Available from: http://eumat.eu/filehandler.ashx?file=3229.

[3] Clauß B. Fibers for Ceramic Matrix Composites. In: Prof. Dr.-Ing. Walter Krenkel, editor. Ceramic Matrix Composites: Fiber Reinforced Ceramics and their Applications. Weinheim: Wiley-VCH; 2008. p. 1–20.

[4] American Ceramic Society Bulletin. Ceramic matrix composites taking flight at GE Aviation. 2019; Available from: www.ceramics.org.

[5] Levy D. Ceramic matrix composites take flight in LEAP jet engine [Internet]. ScienceDaily. 2017. Available from: https://www.ornl.gov/news/ceramic-matrix-composites-take-flight-leap-jet-engine.

[6] F.W.Zok. Ceramic-matrix composites enable revolutionary gains in turbine engine efficiency. American Ceramic Society Bulletin. 2016;95:22 28.

[7] Filsinger D, Münz S, Schulz A, et al. Experimental assessment of fiber-reinforced ceramics for combustor walls. Journal of Engineering for Gas Turbines and Power. 2001;123:271–276.

[8] Snead LL, Nozawa T, Ferraris M, et al. Silicon carbide composites as fusion power reactor structural materials. Journal of Nuclear Materials [Internet]. 2011;417:330–339. Available from: http://dx.doi.org/10.1016/j.jnucmat.2011.03.005.

[9] Muroga T, Gasparotto M, Zinkle SJ. Overview of materials research for fusion reactors. Fusion Engineering and Design. 2002;61–62:13–25.

[10] Krenkel W, Heidenreich B, Renz R. C/C-SiC composites for advanced friction systems. Advanced Engineering Materials. 2002;4:427–436.

[11] Schuldies JJ, Nageswaran R. Ceramic matrix composites for ballistic protection of vehicles and personnel [Internet]. Blast Protection of Civil Infrastructures and Vehicles Using Composites. Woodhead Publishing Limited; 2010. Available from: http://dx.doi.org/10.1533/9781845698034.2.235.

[12] Sommers A, Wang Q, Han X, et al. Ceramics and ceramic matrix composites for heat exchangers in advanced thermal systems-A review. Applied Thermal Engineering [Internet]. 2010;30:1277–1291. Available from: http://dx.doi.org/10.1016/j.applthermaleng.2010.02.018.

[13] Bai F. One dimensional thermal analysis of silicon carbide ceramic foam used for solar air receiver. International Journal of Thermal Sciences [Internet]. 2010;49:2400–2404. Available from: http://dx.doi.org/10.1016/j.ijthermalsci.2010.08.010.

[14] Ibn-Mohammed T, Randall CA, Mustapha KB, et al. Decarbonising ceramic manufacturing: A techno-economic analysis of energy efficient sintering technologies in the functional materials sector. Journal of the European Ceramic Society [Internet]. 2019;39:5213–5235. Available from: https://doi.org/10.1016/j.jeurceramsoc.2019.08.011.

[15] Lazzeri A. Cvi Processing of Ceramic Matrix Composites. In: Bansal NP, Boccaccini AR, editors. Ceramics and composites processing methods. Hoboken, NJ, USA: John Wiley & Sons; 2012. p. 313–349.

[16] Coltelli M-B, Lazzeri A. Chemical vapour infiltration of composites and their applications. In: Choy K-L, editor. Chemical Vapour Deposition (CVD): Advances, Technology and Applications. CRC Press; 2019.

[17] Langlais F, Vignoles GL. Chemical vapor infiltration processing of ceramic matrix composites. In: Peter W.R. B, Carl H. Z, editors. Comprehensive Composite Materials II. Oxford: Elsevier; 2018. p. 86–129.

[18] Naslain RR. The design of the fibre-matrix interfacial zone in ceramic matrix composites. Composites Part A: Applied Science and Manufacturing [Internet]. 1998;29:1145–1155. Available from: http://www.sciencedirect.com/science/article/pii/S1359835X97001280.

[19] Lamon J. Chemical Vapor Infiltrated SiC/SiC Composites (CVI SiC/SiC). Handbook of Ceramic Composites. 2006;55–76.

[20] Kohyama A. Advanced SiC/SiC ceramic composites : developments and applications in energy systems. Ceramic transactions. 2002;144:3–18.

[21] Jaglin D, Binner J, Vaidhyanathan B, et al. Microwave heated chemical vapor infiltration: Densification mechanism of SiCf/SiC composites. Journal of the American Ceramic Society. 2006;89:2710–2717.

[22] Tai N -H, Chou T -W. Modeling of an improved Chemical Vapor infiltration Process for Ceramic Composites Fabrication. Journal of the American Ceramic Society. 1990;73:1489–1498.

[23] Binner J, Vaidhyanathan B, Jaglin D, et al. Use of electrophoretic impregnation and vacuum bagging to impregnate SiC powder into SiC fiber preforms. International Journal of Applied Ceramic Technology. 2015;12:212–222.

[24] Zhu Y, Schnack E. Numerical modeling chemical vapor infiltration of SiC composites. Journal of Chemistry. 2013;2013.

[25] Das S, Mukhopadhyay AK, Datta S, et al. Prospects of microwave processing: An overview. Bulletin of Materials Science. 2009;32:1–13.

[26] Thostenson ET, Chou T. Microwave processing : fundamentals and applications. Composites Part A: Applied Science and Manufacturing. 1999;30:1055–1071.

[27] Singh S, Gupta D, Jain V, et al. Microwave processing of materials and applications in manufacturing industries: A Review. Materials and Manufacturing Processes. 2015;30:1–29.

[28] Leonelli C, Veronesi P. Microwave Processing of Ceramic and Ceramic Matrix Composites. Ceramics and Composites Processing Methods. 2012;0:485–515.

[29] Karandikar PG, Aghajanian MK, Agrawal D, et al. Microwave assisted (mass) processing of metal-ceramic and reaction bonded composites. Mechanical Properties and Performance of Engineering Ceramics and Composites. 2007;27.

[30] Cioni B, Lazzeri A. Modeling and development of a microwave heated pilot plant for the production of SiC-based ceramic matrix composites. International Journal of Chemical Reactor Engineering. 2008;6:28.

[31] High-frequency ELectro-Magnetic technologies for advanced processing of ceramic matrix

composites and graphite expansion" (HELM), FP7-NMP.2011.4.0-1, GA n°. 280464 [Internet]. Available from: http://www.helm-project.eu/.

[32] Naslain R, Langlais F, Fedou R. The CVI processing of Ceramic Matrix Composites. Journal de Physique Colloques. 1989;50.

[33] Besmann TM, McLaughlin JC, Lin HT. Fabrication of ceramic composites: forced CVI. Journal of Nuclear Materials. 1995;219:31–35.

[34] Gary Lynn H. Properties of silicon carbide. Gary Lynn H, editor. Electronic Materials Information Service. London, United Kingdom: IET; 1995.

[35] Ge Y, Gordon MS, Battaglia F, et al. Theoretical Study of the Pyrolysis of Methyltrichlorosilane in the Gas Phase. 3. Reaction Rate Constant Calculations. The Journal of Physical Chemistry A [Internet]. 2010;114:2384–2392. Available from: https://doi.org/10.1021/jp911673h.

[36] Lee YJ, Choi DJ, Park JIY, et al. Effect of diluent gases on the growth behavior of CVD SiC films with temperature. Journal of Materials Science. 2000;35:4519–4526.

[37] Cintio A, D'Ambrosio R, Lazzeri A, et al. High temperature dielectric characterization of SiC-based Ceramic Matrix Composites. 10th International Conference on High Temperature Ceramic Matrix Composites – HT-CMC 10 [Internet]. 2019. p. 140. Available from: http://ht-cmc10.event-vert.org/wp-content/uploads/2019/09/Book-of-Abstracts-HT-CMC-10.pdf.

[38] Hutcheon R, Jong M de, Adams F, et al. A System for Rapid Measurements of RF and Microwave Properties Up to 1400°C. Part 2: Description of Apparatus, Data Collection Techniques and Measurements on Selected Materials. Journal of Microwave Power and Electromagnetic Energy. 1992;27:93–102.

[39] COMSOL Multiphysics. COMSOL Multiphysics [Internet]. Available from: https://www.comsol.it/.

[40] Bykov Y V., Rybakov KI, Semenov VE. High-temperature microwave processing of materials. Journal of Physics D: Applied Physics. 2001;34:R55.

[41] Meredith RJ. Engineers' Handbook of Industrial Microwave Heating [Internet]. Stevenage, United Kingdom: IET; 1998. Available from: https://doi.org/10.1049/PBPO025E.

[42] Griffin EJ. Design of 3-Screw Tuners. Electronics Letters. 1976;12:1–2.

[43] Husain E, Nema RS. Analysis of Paschen curves for Air, N2, and SF6 using the Townsend Breakdown Equation. IEEE Transactions on Electrical Insulation. 1982;EI-17:350–353.

[44] Yu XM, Zhou WC, Luo F, et al. Effect of fabrication atmosphere on dielectric properties of SiC/SiC composites. Journal of Alloys and Compounds. 2009;479:L1–L3.

[45] D'Angio A. Microwave enhanced chemical vapour infiltration of silicon carbide fibre preforms. University of Birmingham; 2018.

[46] Burgio F. Studio del processo CVI/CVD per lo sviluppo di compositi ceramici rinforzati a fibra lunga. Alma Mater Studiorum - Università di Bologna; 2011.

[47] Wei X, Cheng L, Zhang L, et al. Numerical simulation of effect of methyltrichlorosilane flux on isothermal chemical vapor infiltration process of C/SiC composites. Journal of the American Ceramic Society. 2006;89:2762–2768.

[48] Krenkel W. Ceramic Matrix Composites: Fiber Reinforced Ceramics and their

Applications. Krenkel W, editor. Weinheim, Deutschland: Wiley-VCH; 2008.

[49] Jaskowiak MH, DiCarlo JA. Pressure effects on the thermal stability of SiC fibers. NASA Technical Memorandum. 1986;0–17.

[50] Johnson SM, Brittain RD, Lamoreaux RH, et al. Degradation Mechanisms of Silicon Carbide Fibers. Journal of the American Ceramic Society. 1988;71:C-132-C-135.

[51] Owens W, Merkel D, Sansoz F, et al. Fracture Behavior of Woven Silicon Carbide Fibers Exposed to High-Temperature Nitrogen and Oxygen Plasmas. Journal of the American Ceramic Society. 2015. p. 4003–4009.

[52] Sorrentino R, Bianchi G. Passive microwave components. In: Kai C, editor. Microwave and RF Engineering. Chichester, United Kingdom: John Wiley & Sons, Ltd; 2010. p. 187–235.

[53] Bunsell AR, Piant A. A review of the development of three generations of small diameter silicon carbide fibres. Journal of Materials Science. 2006;41:823–839.

[54] Dicarlo JA, Yun H-M. Non-oxide (Silicon Carbide) Fibers. In: N.P. B, editor. Handbook of Ceramic Composites [Internet]. Boston, MA: Springer; 2005. p. 33–52. Available from: https://doi.org/10.1007/0-387-23986-3_2%0A.

[55] Metaxas AC, Meredith RJ. Industrial Microwave Heating. London, United Kingdom: IET; 2008.

Chapter 6

6. Latest developments & Conclusions

The results achieved, both in terms of the optimized performance of the MW heated cavity and efficiency of the MW-CVI process, were implemented to process high purity SiC fibre-reinforced preforms previously coated with a PyC interphase. These preforms have been prepared addressing some of the difficulties emerged in the previous chapters, as the strict operating conditions due to the limited oxidation resistance of 1°gen SiC-Nicalon™ fibres.

The increase of preforms electrical conductivity, due to the PyC coating deposited on SiC fibres, was addressed considering a preliminary slurry infiltration process in order to achieve favourable dielectric properties without plasma formation while keeping an acceptable MW-CVI process efficiency, both in terms of the MW heating and matrix deposition rate. In addition, the slurry infiltration process was evaluated to reach a preliminary consolidation and densification of the preform, without occluding surface pores, further reducing processing times.

Those tests have been carried out in collaboration with the Department of Metallurgy and Materials of the University of Birmingham, thanks to their considerable experience both on manufacturing technologies and MW-CVI processing of CMCs.

Finally, conclusions and future developments will be detailed based on the results obtained during all the PhD activity, with particular attention to the replacement of magnetrons with the new promising solid-state sources.

6.1 Introduction

The literature review performed on SiC_f/SiC manufacturing technologies in **Chapter 2**, showed that one of the major limits for conventional CVI processing was the significant residual porosity of the infiltrated material of about 10-20 % [1,2]. Two different levels of porosity are usually displayed by 2D preforms: intratow and intertow porosity [3]. Specifically, the matrix deposition rates of conventional infiltration technologies are significantly slowed down when trying to fill those pores in the last densification phase, leading to a huge increase of processing times (from days to weeks in some cases) [4]. Usually this phenomenon it is due to reaching of the minimum percolation threshold limit for transport, corresponding to a decrease of pores network size [5].

Common industrial approaches to overcome those difficulties are to employ hybrid or multi-stage approaches, filling most of those micro/macropores at the beginning thus reducing the residual porosity [6]. The purpose of these solutions is to complement the disadvantages of one technology reaching better performances.

As a matter of fact, the long processing times characteristic of CVI technology, due to the premature occlusion of surface pores, were addressed using together a PIP process that in turn, through the application of different polymeric matrix infiltration and pyrolysis cycles, is characterized by an improved ease of access into the porous structure but a lower quality of the deposited SiC matrix than the former (mostly amorphous with reduced thermo-mechanical properties) [7,8]. A high number of cycles (> 10) is usually necessary for the PIP process to reach an acceptable residual porosity [9], thus further increasing processing times. Moreover, the high pyrolysis temperatures of preceramic precursors (1250°C-1700°C), required to achieve a high quality SiC matrix, demand for the usage of high purity SiC fibres (Tyranno SA3™ or Hi-Nicalon Type S™).

Therefore, different preliminary strategies have been investigated to impregnate more efficiently fibre-reinforced preforms filling the large inter-bundle voids initially present. For instance, a hybrid CVI/Slurry infiltration/PIP process was employed showing a reduction of total PIP cycles (< 10) to achieve a residual porosity below 10 % (corresponding to density of 2,6 g/cm^3) [10].

The LSI process raised great industrial interest in the latest years also for SiC_f/SiC manufacturing, due to the high versatility, low processing times and residual porosity values (< 2%) [11]. The high market interest, especially into the aerospace sector, was proved by the commercialization of several turbine engines employing an increasing number of CMC components into the hottest sections. Main research efforts about this technology are dedicated to the further increase in turbine engine efficiency overcoming the current maximum working temperature limits [12].

Accordingly, major issues of the LSI process are based on the residual silicon content inside the matrix (10-15 % vol) and the high infiltration temperatures required (up to 1600°C). In particular, the high silicon content limits the maximum operating temperatures close to 1400°C (silicon melting point). Moreover, even high purity SiC fibres are attacked by unreacted silicon during the LSI-process in a solution and precipitation process [13]. Therefore, several research activities are being dedicated to study protective coatings as well as reducing the amount of unreacted silicon and free carbon which would compromise the resulting CMC thermo-mechanical properties [14].

Some of the problems above reported for the LSI process could be also addressed complementing the latter with one additional manufacturing route. For instance, the amount of precursor and liquid silicon was reduced preliminary infiltrating the preform using a slurry infiltration process. It was shown that the addition of a SiC powder, blended with the resin precursor or into a slurry prior to the impregnation phase, led to high density with closed pores of the resulting composite [15].

Another fundamental component of a CMC material is the interface/interphase region, which plays a critical role into the resulting composite mechanical behaviour [16]. Commonly employed interphases for SiC fibre-reinforced CMCs are based on a PyC, nitride boride (BN) or multi-layer coatings [17]. Pre-treatments of the SiC fibres are also performed to tailor the fibre-matrix interphase bonding [18]. Despite of the reduced oxidation resistance of PyC coatings (they degrade above 500°C), improved performance and lifetimes have been reported in literature with respect to BN [19], therefore a PyC coating was chosen to perform additional trials using the MW-CVI process.

A further limitation encountered in the first part of this work was related to the usage of 1°gen SiC-Nicalon™ fibres, that are oxidized above temperatures of 1100°C [20,21]. Due to their considerably lower cost, preforms reinforced with those fibres were considered to make first trials in order to identify the best operating conditions and confirm the expected benefits of a MW assisted process for pilot-scale preforms, as described in **Chapter 5**. The reduced oxidation resistance required a fine tuning of the MW power density deposited on the material with the operating pressure, which was obtained carefully designing the MW cavity as described in **Chapter 4**.

In the following trials 3°gen SiC Hi-Nicalon Type S™ fibres were employed due to their improved creep and oxidation resistance up to 1400°C [22]. Together with the other 3°gen SiC fibres families, their improved performance was achieved thanks to the reduction in the free carbon and oxygen content (< 1 % wt) with a stoichiometric Si/C ratio and higher processing temperatures, resulting in larger grains and thus higher creep rates.

In addition, a preliminary slurry infiltration process was chosen to provide sufficient support to hold the sample shape together up to the initial consolidation and due to its suitability with the CVI process [23], since it does not reduce gas permeability into the preform.

6.2 Production of SiC_f/PyC/SiC composites by hybrid slurry infiltration and MW-CVI process

The purpose of this paragraph is to present the results obtained about the production of SiC_f/PyC/SiC pilot-scale samples, using a preliminary slurry infiltration process to consolidate and slightly densify the preform to be further infiltrated by MW-CVI technology.

6.2.1. Preform preparation and preliminary heating/infiltration tests

The preform has been prepared stacking 20 layers of 2D fabrics based on Hi-Nicalon Type S™ fibres with cylindrical shape, having a diameter of 10 cm each. The fabrics were preliminary coated with a PyC interphase of about 0,5 μm thickness through CVD process by ATL company[31].

Following, the coated fabrics were impregnated with a $\beta - SiC$ based slurry and subsequently stacked reaching a thickness of 10 ± 0,05 mm (see left side of **Figure 6.1**), prior to be consolidated through a vacuum bagging step (see right side of **Figure 6.1**) and dried.

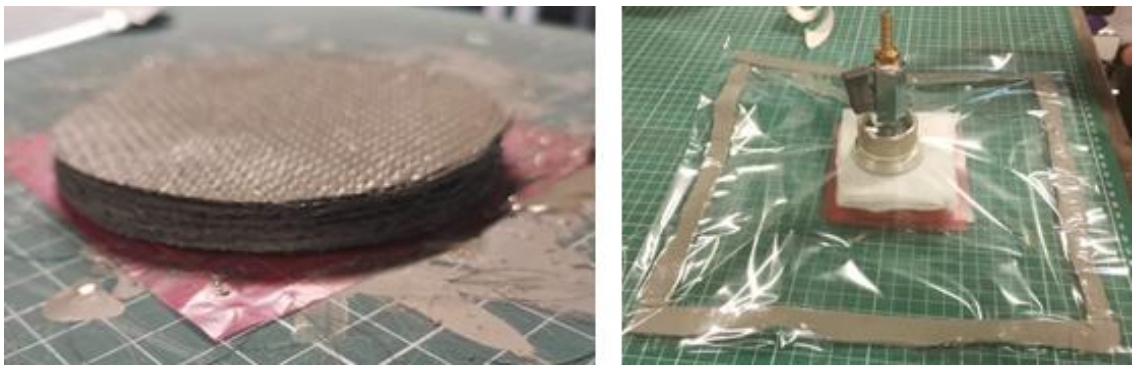

Figure 6.1 *- Slurry impregnated Hi-Nicalon Type S fibre fabrics (left) and vacuum bagging preparation (right)*

Preform preparation was carried out at the Department of Metallurgy and Materials of the University of Birmingham. The specifics of the sample are reported in **Table 6.1**:

Table 6.1 *– Hi-Nicalon Type S preform specifics*

Data on Hi-Nicalon type S preforms			
Diameter [**mm**]	*Thickness* [mm]	*Weight* [g]	*Density* [g/cm^3]
100±0,05	10±0,05	77,8	0,991

A simple resistivity measurement using a digital multimeter tester allowed to measure a significant decrease of surface electrical resistivity (see **Figure 6.2**) of the processed sample with respect to the previous 1°gen SiC-Nicalon™ reinforced preform, suggesting a conductive

[31] https://www.cvd.co.uk/

electrical behaviour. This result could hamper the MW penetration depth leading only to a surface heating and eventual plasma formation.

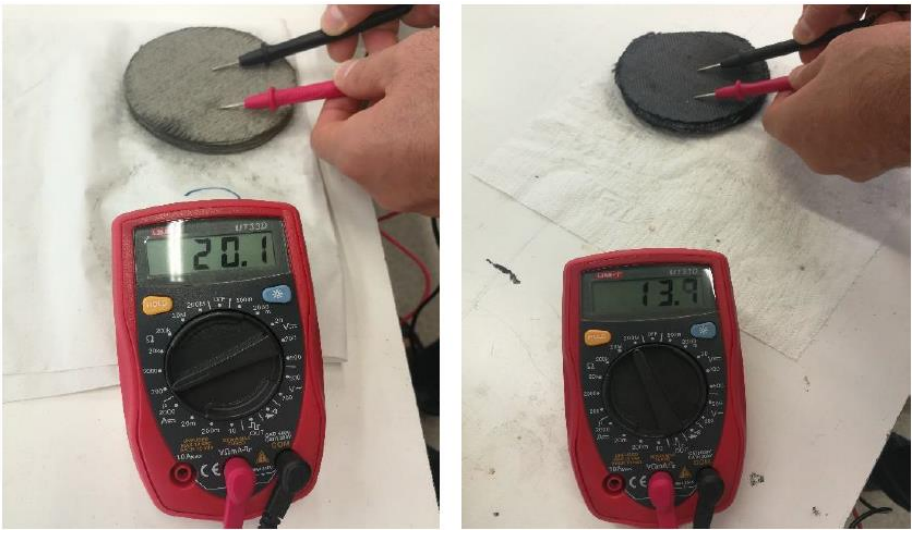

Figure 6.2 *– Electrical resistivity measurements on Hi-Nicalon Type S (left) and Nicalon (right) samples*

Therefore, first heating tests were needed in order to assess MW heating efficiency and the absence of plasma formation phenomena establishing the operating pressure window. Initially the reflected power from the applicator was around 80% then, due to an increase in material dielectric properties, the source-applicator coupling was improved and the infiltration temperature was quickly reached as shown in **Figure 6.3**.

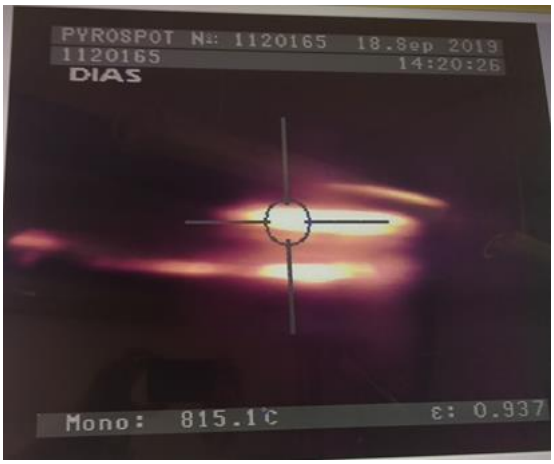

Figure 6.3 *- Thermo-camera image at the infiltration temperature*

Once the reagents were introduced into the MW chamber, the SiC infiltration reaction started. A careful tuning of the MW power was necessary during this phase, due to the change of dielectric properties and reflected power levels, to keep the infiltration temperature almost constant. A first mass increase of the treated preform was observed as reported in **Table 6.2**:

Table 6.2 *– Treated preform data after MW-CVI first trial*

Sample data after MW-CVI first trial			
$m_f\ [g]$	$d_f\ [g/cm^3]$	$\eta_{SiC}\ [\%]$	$t_{inf}\ [min]$
80,349	1,023	13,65	70

Where m_f, d_f are the resulting mass and density of the treated sample while η_{SiC} was the reaction efficiency obtained after the infiltration time t_{inf}.

The sample did not show any visible iridescence due to plasma formation or heterogeneous deposit on the surface caused by thermal degradation of the fibres, despite of the much higher preform electrical conductivity. Moreover, similar operating conditions (reported in **Table 6.3**) were applied confirming the flexibility of the MW-CVI process for different SiC-based preforms.

Table 6.3 *– Preliminary MW-CVI processing conditions*

Preliminary MW-CVI operating conditions				
$\boldsymbol{P}$ $[\boldsymbol{mbar}]$	$T_{chamber}$ $[°C]$	T_{inf} $[°C]$	P_{in} $[kW]$	P_{ref} $[kW]$
120	250	800 - 820	1,80	0,95

Plasma formation was observed below 100 mbar, thus the higher operating pressure value reported above, always using the same single port excitation scheme. The main differences regarded the slightly higher operating pressure and MW power levels, although better coupling conditions were expected during next trials due to the infiltrated SiC increase, thus more favourable dielectric properties.

First tests showed that it was possible to properly heat and infiltrate also the reported sample, using the same single port excitation scheme previously employed, despite of the PyC coating.

6.2.2. MW-CVI processing

Further MW-CVI trials have been performed in the following steps in order to densify the preform and verify if/when a percolation limit of the matrix deposition rate would have been reached.

Due to the starting reduced amount of SiC, shorter trials have been carried out to check when the dielectric properties of the sample would have been resulted in more favourable coupling conditions.

After few runs critical coupling conditions were obtained and longer trials have been carried out to verify if the temperature profile remained stable along the process and the resulting reaction efficiencies. The reproducibility of processing conditions in terms of the MW power levels transmitted/reflected resulted almost equal with respect to the values employed in previous tests, confirming the robustness and flexibility of the design of the MW applicator (see **Figure 6.6**).

Moreover, the flexibility of different samples treatable using the MW-CVI pilot plant was confirmed by the measurements of the experimental spectra performed at the beginning and almost 20 hours of infiltration of the Hi-Nicalon Type S™ fibre reinforced preform with respect to the 1°gen Nicalon™ sample previously considered, as displayed in **Figure 6.4**:

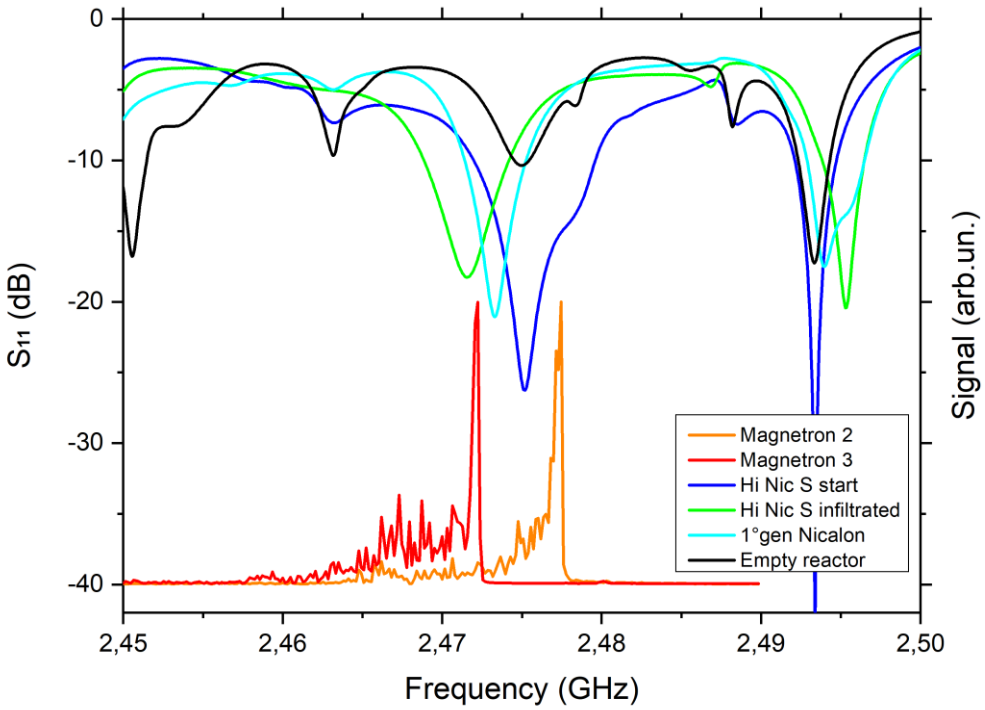

Figure 6.4 *- Comparison among the experimental spectra of the reactor loaded with a Nicalon sample, with a Hi-Nicalon Type S sample not infiltrated and after MW-CVI (left y axis), all placed on the quartz sample holder and the Duraboard disc. The spectra of two of the available magnetron sources, with amplitude and baseline arbitrarily normalized, are also shown (right y axis).*

Despite of the PyC coating presence, the starting spectrum of the Hi-Nicalon Type S™ sample remained into the operating frequency bandwidth with high coupling levels. The latter confirmed again the stability of the MW cavity designed with respect to the sample properties, varying along with the heating and the infiltration process, as proved by the low decrease of the resonance frequency of the experimental spectrum measured for the infiltrated preform in **Figure 6.4**. The good dielectric properties displayed by this sample could be also related with the preliminary SiC slurry infiltration process.

The operating conditions range applied during MW-CVI trials for the Hi-Nicalon Type S™ (Hi-Nic S) are reported in **Table 6.4**:

Table 6.4 *- Operating parameters for MW-CVI tests on Hi-Nic S preform*

	Hi – Nic S
Operating Pressure [mbar]	120
Infiltration Temperature [°C]	790 - 840
MTS/H_2 ratio	1:10
MTS flow rate [kg/h]	0,060
H_2 flow rate [L/min]	1,400
Processing Time [h]	18,516
Starting density [g/cm³]	0,991
Final density [g/cm³]	1,499
Average Reaction efficiency [%]	13,862
MW Power input [kW]	1,125 – 1,375
MW Power reflected [kW]	0

The higher operating pressure value resulted in a lower average reaction efficiency of 13,86%, although in the latest trials it was possible to further decrease the operating pressure due to the expected increase of material dielectric properties with density.

The relative density increase (with respect to a reference density value of 2,5 g/cm^3) together with the deposition rate V_{SiC} measured along the various trials, are reported in **Figure 6.5**:

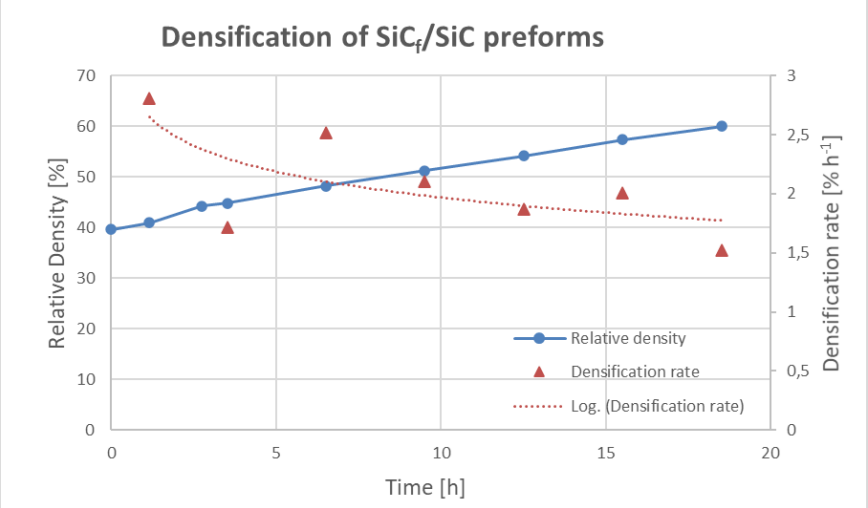

***Figure 6.5** -Infiltration data after MW-CVI trials on Hi-Nic S preforms*

The latest five trials were continuously conducted for 3 hours each, resulting in a typical temperature profile as shown in **Figure 6.6**.

In the latest trials it was possible to observe a constant increase of the relative density thus a prediction of the remaining infiltration hours t_{miss} can be derived by:

$$t_{miss} = \frac{\Delta M_f}{M_i} * \frac{1}{\overline{V_{SiC}}} \quad [h] \qquad (6.1)$$

Where ΔM_f is the SiC mass to be infiltrated to reach the reference density value, M_i is the current mass of the infiltrated preform, while $\overline{V_{SiC}} = 0{,}020\ h^{-1}$ is the average densification rate along the latest five trials. Provided to verify the constant densification rate hypothesis in the end, using **Equation 6.1** it resulted that 30 hours of MW-CVI were still needed to reach the desired density, for a total processing time of about 50 hours.

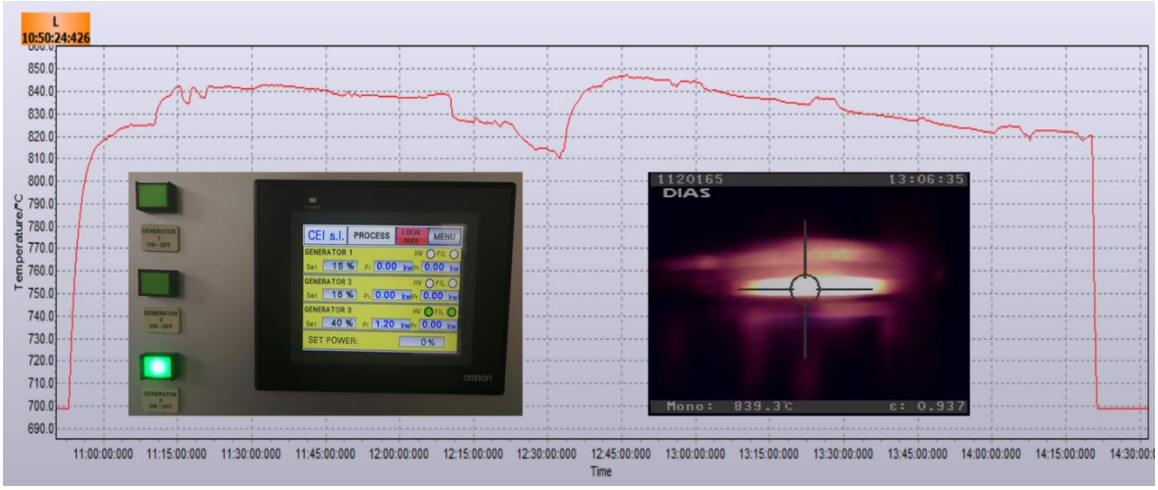

***Figure 6.6** – Temperature profile during MW-CVI run; the left inset reports the MW power levels used during the process while the right inset show a thermo-camera image*

6.2.3. Analysis of the infiltrated preform

After MW-CVI runs, the infiltrated preform was analysed to confirm the expected benefits from a MW assisted process. At first the sample appeared quite delaminated (see **Figure 6.7**) after all the trials due to the initial too high interlaminar distance which could not be filled just using MW-CVI.

Figure 6.7 *– Delaminated preform after MW-CVI runs*

SEM-EDS analysis were carried out on both the external and inner laminae. On the top layer there was not any presence of infiltrated $\beta - SiC$ while the intertow porosity, checking material cross-section, was completely filled with fine grained (~ 5 μm) SiC (see **Figure 6.8**).

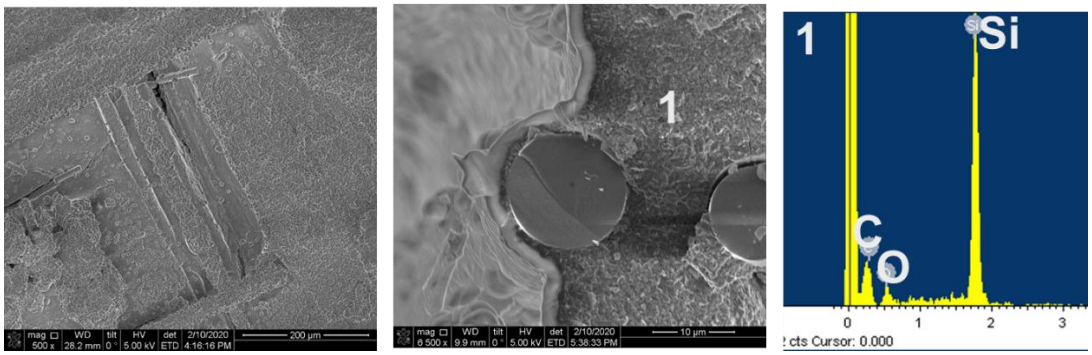

Figure 6.8 *– SEM-EDS analysis of the top layer with focus on cross-section view (mid) and local EDS analysis (left)*

Similar analysis performed on the 10th lamina layer displayed a considerable content of infiltrated SiC, confirming the presence of the desired reverse temperature gradient as shown in **Figure 6.9**.

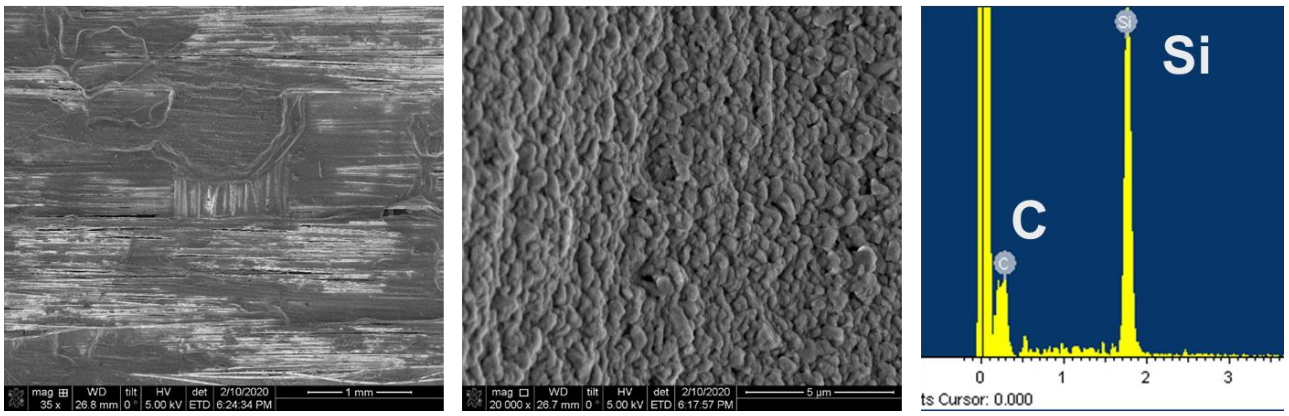

Figure 6.9 *- SEM-EDS analysis of the mid layer (left) with focus on the infiltrated regions (mid) and local EDS analysis (right)*

The thickness of the single fabric layer was around ~ 200 μm, although a gap of about 400 μm was present after the delamination of the preform which could not be appropriately filled, improving the interlaminar bonding strength.

Future work should be oriented in preliminary reducing the interlaminar distance between single fabric layers avoiding the deconsolidation of the preform. Further MW-CVI trials will be then needed to reach the final density value verifying the correctness of the constant deposition rate of the matrix or an eventual law change up to a threshold limit.

The reason to be of the MW-CVI process is the inside-out infiltration pattern, thanks to the volumetric MW heating mechanism, which should allow to reach higher densities and thus lower residual porosity values with respect to conventional manufacturing technologies. This mechanism, together with the evaluation of the resulting total processing time, will be the object of further investigations on similar preforms.

The possibility to reach critical coupling conditions with high MW heating efficiencies into the overmoded resonant applicator designed still proves the high potential of the MW-CVI technology. In addition, the reproducibility of the operating conditions among different runs was an important step in order to make further analysis on the dependence from the infiltration temperature, pressure, reagents flow ratios on the reaction efficiency.

An ineludible step in any industrial application is the automation of the process. Although the most convenient from the economical point of view, magnetron sources are prone to several drawbacks mostly related to the incoherent nature of their EM emission which cannot be controlled in phase and frequency, as well as to the relatively short wavelength.

The above described drawback can be overcome by the replacement of the high-power magnetrons with sources based on solid state amplifiers with LDMOS transistors, providing a large frequency tunability and very good spectral purity of the emitted waves, in which both the frequency and the phase can be carefully controlled. Such a solution is becoming more and more appealing also from the economical point of view thanks to the recent development of high-power transistors, also at the kW power levels necessary for the MW-CVI process, and thus it is the direction to where this work is oriented.

6.3 Conclusions

The design of the MW-CVI pilot plant used along the whole PhD activity, unlike other existing lab-scale equipment, has been carried out with the idea of a further industrial scale-up using an innovative approach to achieve the highest energy efficiency for a large variety of CMC samples with dimensions of industrial interest. This new approach has faced some complex engineering problems which have been tackled in an original way.

In particular, the inner chamber and all the components exposed to high temperature and extreme chemical environment have been realized in conductive graphite, addressing both the problems derived from the harsh operating conditions of the process and efficiency of the MW heating. The appearance of plasma regions at the very low-pressure values necessary for CVI was another detrimental problem for the efficiency of the chemical process, which requires a fine tuning of the operating pressure in the specific gaseous environment of the MW heated chamber. Moreover, this pilot plant can use a combination of conventional and MW heating in order to tailor a suitable temperature profile in the preform to be infiltrated.

The possibility of achieving sufficient predictability and control of the EM behaviour of overmoded reactors loaded by relatively large samples has been strongly questioned recently. The results show, in fact, that a predictable and robust behaviour of a well-designed overmoded reactor can be achieved, definitely clarifying, for the first time to the author knowledge, that the use of overmoded reactors, necessary for industrial applications, is not hindered by their continuous EM spectrum.

Consequently, the heating dynamic of the sample was determined with good accuracy up to very high temperatures, thanks to the above discussed results and to the accurate determination of the dielectric properties of the sample as a function of the temperature and the density, which was conducted in the framework of the research activities. This demonstrates the possibility to predict with good accuracy both the EM and thermal behaviour of the reactor along with the whole heating and infiltration process.

The tuning of a specific temperature profile is critical to control the inside-out SiC deposition in order to achieve a stoichiometric SiC matrix. Inside this work, the main goal was to prove the scalability of the MW-CVI technology granting the desired infiltration of the matrix with the highest energy and chemical efficiency. Indeed, a detailed characterization of the deposits was missing and would have improved our understanding of the process, thus it will need to be properly addressed to confirm the adopted operating conditions.

The design of this pilot plant resulted in a robust MW heated reactor, where CMCs can be quickly heated to the infiltration temperature with reproducible operating conditions, reduced processing times and high chemical reaction efficiencies. The inside-out densification pattern for the pilot-scale samples treated has been confirmed through morphological investigations showing the high potential of this technology for the development of a continuous process.

6.4 Future developments

The MW-CVI reactor studied during this PhD activity displayed several potential advantages for the manufacturing of SiC-based CMCs with respect to conventional technologies. The high flexibility usage for different reinforcements and material dielectric properties range was one of the main achievements obtained, thanks to the careful design of the MW cavity. The latter point was also proven during the last trials, where a further step ahead was carried out using a PyC coating on SiC fibres.

This result could open possibilities for the manufacturing of C_f/SiC composites, strongly widening the market possibilities of the MW-CVI process, which possess a major share into the CMCs market due to the considerably lower cost of carbon fibres. A SiC pre-infiltration step, using for instance the slurry infiltration process employed in the last part of research activities, could help improving the resulting dielectric properties reducing eventual plasma formation and arcing phenomena.

Due to the transparent MW behaviour of BN, it would be interesting also to evaluate its effect on the resulting EM behaviour of the material into the MW-CVI process. In addition, a study about the dependence of the coating thickness on the MW absorption properties could help finding the best compromise resulting in optimal MW absorption properties and desired pseudo-ductile fracture behaviour of the CMC.

In order to have a clearer insight on material behaviour, novel NDE characterisation technologies based on 3D imaging data have been continuously developed and improved. Innovative algorithms for generating robust and accurate meshes can be used for the prediction of macro-structural properties of composites [24].

One of the latest solutions to retrieve those kinds of information is Micro-computed tomography (Micro-CT), which is able to create cross-sections of a physical object recreating a virtual 3D model without destroying the original object. Efficient AI-based tools have been developed successfully for woven SiC-fiber composite preforms [25–27], building realistic numerical models of woven fabrics that preserve the prescribed weaving pattern and that are free of interpretation, which makes them compatible with further numerical simulations. This technique can be also applied to determine the initial porosity of the preform to follow the densification field along the MW-CVI process [28].

The rapidly growing technology of generation of MW energy by solid-state semiconductor sources is making a revolutionizing impact on the entire field of MW power engineering [29]. Thus, the recent advances achieved by this technology led us to analyse its usage for the MW-CVI process. The reasons behind this choice lie in the rapid and precise control of the signal frequency, as well as a more stable and reproducible distribution of the EM field [30], with the important possibility, from an industrial point of view, to automate the whole infiltration process, which in turn opens further new possibilities to this technology [31]. Solid-state MW transistors can also provide 10 times longer lifespans than magnetrons, ensuring significantly higher reliability and a reduced cost per working hour.

One of the major deficiencies of magnetron tube-based MW sources is their lack of fine control over frequency, power and the phase of the emitted wave, which prevent the implementation of closed-loop control aimed at the minimization of the power reflected by the MW reactor. On the contrary, with solid-state MW energy sources, forward and reflected power levels can be easily

adapted with closed-loop controls thanks to the inherent and precise control over the solid-state source emissions in terms of frequency, power and phase [32,33].

These sources, now available also at the kW power levels necessary for MW-CVI, are frequency agile and capable of operating either at a single fixed frequency or in a frequency sweep mode that can cover the entire ISM band. The very short response time of the solid-state microwave generators and the possibility to pulse their output power can open unexplored possibilities in which the temperatures of the product can be rapidly controlled, avoiding hot spots and limiting the occurrence of plasma phenomena, thus reducing the risk of damage occurring due to overheating. Moreover, the solid-state generators can be connected to the reaction chamber (MW cavity) via standard coaxial cables, minimizing the space requirements.

The heating of the sample with solid state sources is expected to improve the uniformity of the sample temperature, with the additional possibility to dynamically adjust the EM field in the reactor without involving any moving metal part. Moreover, the benefits expected from the use of coherent multifrequency sources could be maximized by means of rigorous and detailed numerical modelling activities of the MW-CVI reactor loaded by the sample of interest, using FEM based software as COMSOL Multiphysics.

Accordingly, solid-state sources are the ideal choice for a well-controlled and reproducible reaction, which translates to higher energy efficiency and better product quality. In fact, thanks to the possibility to precisely select the operating frequency and so the mode granting the highest uniformity of the EM field, we will also be able to choose the best location of the sample inside the MW cavity and to predict the effects due to different sample dimension and geometry granting an easier industrial scale up of the MW-CVI technology.

6.5 References

[1] Lamon J. Chemical Vapor Infiltrated SiC/SiC Composites (CVI SiC/SiC). Handb. Ceram. Compos. 2006;55–76.

[2] Langlais F, Vignoles GL. Chemical vapor infiltration processing of ceramic matrix composites. In: Peter W.R. B, Carl H. Z, editors. Compr. Compos. Mater. II. Oxford: Elsevier; 2018. p. 86–129.

[3] Chen ZR, Ye L, Lu M. Permeability predictions for woven fabric preforms. J. Compos. Mater. 2010;44:1569–1586.

[4] Kinney AJH, Breunig TM, Starr TL, et al. X-ray Tomographic Study of Chemical Vapor Infiltration Processing of Ceramic Composites. Science (80-.). 1993;

[5] Sheldon BW. The control of gas phase kinetics to maximize densification during chemical vapor infiltration. J. Mater. Res. 1990;5.

[6] Kopeliovich D. Advances in the manufacture of ceramic matrix composites using infi ltration techniques. In: Low IM, editor. Adv. Ceram. Matrix Compos. Introd. 2nd ed. Cambridge, UK: Woodhead Publishing; 2018. p. 79–108.

[7] Ortona A, Donato A, Filacchioni G, et al. SiC-SiCf CMC manufacturing by hybrid CVI-PIP techniques: Process optimization. Fusion Eng. Des. 2000;51–52:159–163.

[8] Nannetti CA, Riccardi B, Ortona A, et al. Development of 2D and 3D Hi-Nicalon fibres/SiC matrix composites manufactured by a combined CVI-PIP route. J. Nucl. Mater. 2002;307–311:1196–1199.

[9] Motz G, Schmidt S, Beyer S. The PIP - process: Precursor Properties and Applications. In: Krenkel W, editor. Ceram. Matrix Compos. Fiber Reinf. Ceram. their Appl. Weinheim, Deutschland: Wiley-VCH; 2008.

[10] Nannetti CA, Ortona A, Pinto DA, et al. Manufacturing SiC- Fiber- Reinforced SiC Matrix Composites by Improved CVI/Slurry Infiltration/Polymer Impregnation and Pyrolysis. J. Am. Ceram. Soc. 2004;

[11] Ortona A. Ceramic Matrix Composites: Reaction Bonded. In: Nicolais L, editor. Wiley Encycl. Compos. [Internet]. 2nd ed. Hoboken, New York: John Wiley & Sons; 2012. p. 271–274. Available from: https://onlinelibrary.wiley.com/doi/abs/10.1002/9781118097298.weoc031.

[12] Corman G, Upadhya R, Sinha S, et al. General Electric Company: Selected Applications of Ceramics and Composite Materials. In: L. M, E. S, editors. Mater. Reserch Manuf. Cham, Switzerland: Springer; 2016. p. 59–91.

[13] Mainzer B, Kelm K, Watermeyer P, et al. How to tame the aggressiveness of liquid silicon in the LSI process. Key Eng. Mater. 2017;742 KEM:238–245.

[14] Mainzer B, Frieß M, Roder K, et al. Development and characterisation of phenolic resin based liquid silicon infiltrated SiC/SiC composites with SiNx fibre coating. Mater. Sci. Forum. 2015;825–826:224–231.

[15] DiCarlo J, Bansal NP. Fabrication Routes for Continuous Fiber-Reinforced Ceramic Composites (CFCC) [Internet]. Mater. Sci. 1998. Report No.: NASA/TM-1998-208819. Available from: https://ntrs.nasa.gov/citations/19990009073.

[16] Chawla KK. Ceramic Matrix Composites. Compos. Mater. Sci. Eng. 4th ed. Birmingham,

AL, USA: Springer; 2019. p. 251–295.

[17] Lamon J. Influence of Interfaces and Interphases on the Mechanical Behavior of Fiber-Reinforced Ceramic Matrix Composites. Ceram. Matrix Compos. [Internet]. John Wiley & Sons, Ltd; 2014. p. 40–64. Available from: https://onlinelibrary.wiley.com/doi/abs/10.1002/9781118832998.ch3.

[18] Kanazawa S, Yamazaki N, Kishi T, et al. Influences of heat treatments on the strength properties of amorphous SiC fibers. Adv. Compos. Mater. [Internet]. 2019;28:491–506. Available from: https://doi.org/10.1080/09243046.2019.1595837.

[19] Rebillat F, Lamon J, Guette A. Concept of a strong interface applied to SiC/SiC composites with a BN interphase. Acta Mater. 2000;48:4609–4618.

[20] DiCarlo JA, Yun H-M. Non-oxide (Silicon Carbide) Fibers. In: Bansal NP, editor. Handb. Ceram. Compos. Boston, MA: Springer US; 2005. p. 33–52.

[21] Le Coustumer P, Monthioux M, Oberlin A. Understanding Nicalon® fibre. J. Eur. Ceram. Soc. 1993;11:95–103.

[22] Sha JJ, Hinoki T, Kohyama A. Thermal and mechanical stabilities of Hi-Nicalon SiC fiber under annealing and creep in various oxygen partial pressures. Corros. Sci. [Internet]. 2008;50:3132–3138. Available from: http://dx.doi.org/10.1016/j.corsci.2008.08.003.

[23] Binner J, Vaidhyanathan B, Jaglin D, et al. Use of electrophoretic impregnation and vacuum bagging to impregnate SiC powder into SiC fiber preforms. Int. J. Appl. Ceram. Technol. 2015;12:212–222.

[24] Ayadi A, Nouri H, Roger F, et al. X-ray computed tomography from assessment of mechanical properties and monitoring damage. JEC Compos. Mag. 2017;54:63–66.

[25] Bénézech J, Couégnat G. Variational segmentation of textile composite preforms from X-ray computed tomography. Compos. Struct. 2019;230.

[26] Perrot G, Couégnat G, Ricchiuto M, et al. Image-Based Numerical Modeling of Self-Healing in a Ceramic-Matrix Minicomposite. Ceramics. 2019;2:308–326.

[27] Mazars V, Caty O, Couégnat G, et al. Damage investigation and modeling of 3D woven ceramic matrix composites from X-ray tomography in-situ tensile tests. Acta Mater. 2017;140:130–139.

[28] Morales-Rodríguez A, Reynaud P, Fantozzi G, et al. Porosity analysis of long-fiber-reinforced ceramic matrix composites using X-ray tomography. Scr. Mater. 2009;60:388–390.

[29] Werner K. RF Energy Systems: Realizing New Applications. Microw. J. [Internet]. 2015;58:22–34. Available from: https://www.microwavejournal.com/articles/25583-rf-energy-systems-realizing-new-applications?v=preview.

[30] Mallah F und, GmbH MT. Fricke und Mallah Microwave Technology GmbH - Solid State Microwave Generator.

[31] Korpas P, Wieckowski A, Krysicki M. Effects of applying a frequency and phase-shift efficiency optimisation algorithm to a solid-state microwave oven. 2014 20th Int. Conf. Microwaves, Radar Wirel. Commun. MIKON 2014. 2014;2–5.

[32] Yakovlev V V. Effect of frequency alteration regimes on the heating patterns in a solid-state-fed microwave cavity. J. Microw. Power Electromagn. Energy. 2018;52:31–44.

[33] Yakovlev V V. Frequency control over the heating patterns in a solid-state dual-source

microwave oven. 2015 IEEE MTT-S Int. Microw. Symp. IMS 2015. 2015;1–4.